A study of the soil pattern, properties and hydrology of a mole and tile-drained, loess-mantled downland in Southland, New Zealand

---

A thesis

submitted in partial fulfilment

of the requirements for the Degree of

Doctor of Philosophy

at

Lincoln University

by

Kirstin Ella Deuss

Lincoln University

2022

Abstract of a thesis submitted in partial fulfilment of the requirements for the Degree of Doctor of Philosophy

A study of the soil pattern, properties and hydrology of a mole and tile-drained, loess-mantled downland in Southland, New Zealand

by

Kirstin Ella Deuss

Dissected, loess-mantled terraces (downlands) are a dominant component of the soil-landscape in Southland, New Zealand and commonly contain soils with dense subsoils that impede drainage. Consequently mole and tile drainage systems, which removes excess soil moisture, are widespread. Alongside agronomic benefits, mole and tile drainage creates problematic secondary effects, including altered stream hydrographs, contaminant transfer into surface water and possible modification of soil properties. Today, water quality and quantity management rely heavily on environmental modelling. Models of soil – water interactions are informed by knowledge of soil hydraulic properties and processes, which is gained from a variety of disciplines, including pedology, soil physics and hydrology. Understanding the properties and processes relevant to mole and tile-drained, slowly permeable loess soils is, thus, criticical for reliable simulations of their water dynamics. Concerningly, this understanding remains elusive. There is a need to better understand the variability in soil properties that regulate water storage, movement and connectivity, as well as the intrinsic and extrinsic controls on water flow pathways. These research gaps were addressed by characterising and monitoring a small, mole and tile-drained basin on a typical Southland sheep farm.

Surveying of the soil and loess mantle found vertical differentiation of soil properties was due to contemporary pedogenesis, and soil features inherited from buried loess sheets were important sources of heterogeneity in water-regulating soil properties. Catchment side slopes had greater soil variation relative to the interfluves. Buried loess sheets, which had been exhumed by hillslope procceses, were contributing to the subsoils on the basin slopes whereas the soils on the interfluves were formed solely into the uppermost loess sheet. The findings confirm that understanding the soil-geomorphology of loess-mantled downlands is important for improving soil – landscape models, characterising soil spatial variability and producing more accurate soil maps.

Ground penetrating radar (GPR) was effective at identifying and mapping mole channels, thus allowing drainage density to be quantified and the mole network to be characterised. It demonstrated that the mole networks had non-systematic patterns and most likely were multi-generational. Ground truthing during the GPR survey showed mole channels were in good condition even after 30 + years without maintenance.

From a survey of soil hydraulic properties it was apparent that the mole fracture network created when moles were installed had not persisted. The finding has implications for hydrological and water quality modelling, as preferential flow via the fracture network is commonly considered to be the major route for rapid water and contaminant transfer into moles. Mole channels were not found to influence soil properties directly; however, it was discovered that surface saturated hydraulic conductivity (K_{sat}) was controlled by antecedent soil moisture state in parts of the landscape where perched water tables (PWT) persisted. This was hypothesised to occur by priming of the macropore network when capillary rise from a PWT removed air pockets, signalling a potential indirect influence of drainage systems on K_{sat}.

A water balance analysis refuted a common assumption of negligible deep drainage in slowly permeable loess, with or without artificial drainage. Deep drainage varied between events as well as seasonally and occurred via piston flow through the fragipan and underlying loess mantle. Runoff (tile and overland flow) responses to rainfall events could be discriminated by thresholds of precipitation volume and/or intensity, depending on antecedent soil moisture state (dry or wet). Infiltration-excess overland flow was the most common form of surface runoff, consistent with the low surface infiltration rates estimated from infiltration experiments. A corollary is that shifts in the distribution of precipitation intensity with climate change could change the overland flow component of the water balance of this landscape. Tile flow from small events was predominantly sourced from the interfluves and upper hollow. As events became larger, the source area expanded until most of the catchment was contributing to tile flow. When considering the mitigation of contaminant transfers to surface water, winter and spring should be be key time periods, and the upper hollow and interfluves key locations, on which to focus.

Soil moisture spatial patterns appeared to be influenced by both PWTs and the artificial drainage network and were not well predicted by the topographic wetness index (TWI). In the dry soil moisture state, upslope areas were hydrologically disconnected. With increasing catchment wetness, hydrological connectivity expanded from the lower hollow to the PWTs at the mid- to

upper hollow, and eventually up to the interfluve PWTs. Once the hydrological connection between the lower hollow and interfluve had been established, the catchment had completed its transition into the wet state, and the interfluve PWT and mole network became the primary regulator of tile flow. The transition from dry state to wet state soil moisture conditions took about two weeks and began at the lower catchment hollow. Only rainfall periods with exceptional precipitation volumes and intensities connected the slopes, and only when all other parts of the catchment were saturated. There was no evidence that natural interflow, either as matrix or preferential flow, led to hydrological connection. Surface-sourced preferential flow to the tile drain occurred when the soil was in the dry state, but the flux was hydrologically insignificant.

The thesis highlights:

- The need for significant sources of soil variation associated with loess stratigraphy to be represented in soil classification and mapping.
- That, while there was no un-drained control in the experimental set-up, the effects of the artificial drainage network appear to be profound and must be considerd in hydrological-contaminant modelling. And finally,
- That several common assumptions about flow pathways (i.e., mole channel fracture networks, negligible deep drainage, significant natural interflow, insignificant overland flow) in artificially drained, low permeability loess may be inappropriate and, consequently, their use in modelling in support of management and mitigation needs careful evaluation.

Keywords: Loess, fragipan, soil stratigraphy, multisequal soils, soil variability, ground-penetrating radar, mole channel, tile drain, artificial drainage, soil moisture, soil properties, water flow pathways, soil water balance, event-based runoff analysis, overland flow, tile flow, deep drainage, saturated hydraulic conductivity, hydrological connectivity, perched water table

This thesis is dedicated to the memory of my mother, Dr. Gabrielle Josephine Myra Deuss,

who taught me that through determination, perseverance and kindness, we can achieve great things.

Acknowledgements

To my mentors, colleagues, friends and family, who have provided me with guidance, assistance and encouragement during this four-year PhD adventure. Your time, energy and love has enabled me to achieve a lifelong personal goal; to be a scientist and to do science. Without you all, this thesis would not exist. In particular, I would like to acknowledge:

The funders of this project, Manaaki Whenua Landcare Research (MWLR) and Environment Southland (ES), whose financial and technical support gave me the opportunity to pursue an exciting and challenging PhD research project which satisfied my desire to learn as much about as many things as I could.

My supervisory team: Peter Almond, Sam Carrick, Henry Chau, Carol Smith and Crile Dosher. Thank you for giving me the freedom to challenge myself and learn more than I could ever have imagined. Peter especially, for your encouragement, constructive criticism, kind words, interesting conversations and for sharing your knowledge and going out of your way to create opportunities for me to learn, grow, and network. And Sam, for being so kind and generous with your time and support.

Regan Strang and Rachael Miller, who welcomed me and my sensors and probes onto their farm and worked around me and my solar panel-mounted deer posts for over three years. Thank you for your cooperation, assistance, interest, and enthusiasm. I will always have a deep connection to that little drainage basin and will probably never stop thinking about its mysterious flow pathways, stratigraphy and water chemistry.

Nigel Beale, thank you for your mentorship in the world of electronics, sensors, data logging and programming, and for your creativity, attention to detail, and perfectionism that resulted in the development of a world-class catchment hydrology monitoring network which ran smoothly with next-to-no malfunctions for the length of my studies.

Lawrence Kees, thank you for encouraging me to follow my science dreams and giving me so many opportunities to do so. For being my reliable PA, for bringing me coffees and lunch and a fully charged 12V battery on ‘those’ days in the field. For breaking rules in the name of science. For teaching me how to use so many different types of power tools and equipment. For turning a

blind eye to the fridge and freezer full of soil samples and water contaminated with *E. coli* and *Campylobacter*…

Tim Ellis, for your assistance in negotiating funding with ES, your quirky, intelligent and encouraging messages of support, and for your advice and constructive criticism of my work. Becky Goodsell and Tapuwa Marapara, thank you for being young role models and showing me that my dream was possible. For your chats, support, encouragement, empathy, understanding and advice on all things related to the world of the early-career scientist.

The entire Soil Science Department at Lincoln University. Such a fantastic group of passionate, kind and intelligent people. You have made the last four years of my life an absolute pleasure. I particularly would like to thank Roger Cresswell, for not only for being so kind, helpful and expeditious as a lab manager, but also for your cherished friendship. Amal, thank you for looking out for my mental health, dragging me away from my desk and to the gym. Carol, Judith and Josh for creating opportunities for us to learn so much at the Soil Judging Competitions. "The dream" soil judging team – Julie, Louisa and William – thank you for being SO enthusiastic and SO passionate about soils, geology, science, and the world and for sharing some of the most fun times across NZ and Australia. I must especially thank Zach Simpson, for the time and effort he put into teaching so many of us how to effectively use R.

To my flatmates; Tom, Camilla and Randel. Thank you for sharing these personally-, nationally- and globally eventful past four years with me. For supporting, empathising and encouraging me throughout my PhD journey.

John Triantafilis, thank you for surrounding me in much-needed positivity and reassurance during the Dark Days of the Dark Age that was the last six months of my thesis write-up. For the time you invested into kick-starting my writing, and for teaching me how to take constructive criticism constructively.

My siblings, for sharing life's highs and lows with me, for being there for me no matter what and for making sure that we are always in touch. My dad, for teaching me to have high standards and for giving me the support and opportunities in life that continue to allow me to achieve my goals. Finally, I would like to thank my darling mother, for watching over me always and for sending me butterflies when I need them the most ♡

Table of Contents

List of Tables

List of Figures

List of Plates

List of Acronyms and Abbreviations

AC	Air capacity
AD	Anno Domini
APSIM	Agricultural Production Systems simulator
ASCE	American Society of Civil Engineers
ASMD	Antecedent soil moisture deficit
AWC	Available water capacity
BEST	Beerkan Estimation of Soil Transfer parameters
BP	Before present
c	Clay
CEC	Cation exchange capacity
CNr	Carbon-nitrogen ratio
CoV	Coefficient of variation
DBD	Dry bulk density
DC	Direct current
DD	Deep drainage
DEM	Digital elevation model
dSS	Divergent side slope
DTD	Downslope travel distance
ENE	East-Northeast
ET	Evapotranspiration
FC	Field capacity
GDP	Gross domestic product
GNSS	Global navigation satellite system
GPR	Ground penetrating radar
GPS	Global Positioning System
GW	Groundwater
GWT	Groundwater table
HRT	Hydrograph response time
HS	Head slope
ID	Identification
IN	Interfluve
IQR	Interquartile range
K_s; K_{sat}	Saturated hydraulic conductivity
lHO	Lower hollow
MAP	Mean annual precipitation
Masl	Metres above sea level
mbs	Metres below the surface
mHO	Mid-hollow
MIT	Minimum inter-event time
MPor	Macroporosity
MS	Multispectral
NA	Not applicable
NASS	National Agricultural Statistics Service
NIR	Near-infrared
NIWA	National Institute of Water and Atmospheric Research
NR	No runoff
NS	Nose slope
NZ	New Zealand

NZSC	New Zealand Soil Classification
NZVD	New Zealand Vertical Datum
OC	Organic carbon
OF	Overland flow
P	Precipitation
PC	Principal component
PCA	Principal component analysis
PD	Particle density
Pd	Precipitation duration
Pi	Precipitation intensity
Por	Porosity
PR	Phosphorus retention
pSS	Divergent side slope
PTF	Pedotransfer function
Pv	Precipitation volume
PVC-U	Unplasticised polyvinyl chloride
PWT	Perched water table
Qavg	Average flow rate
Qmax	Maximum flow rate
R	Runoff
R ratio	Runoff ratio
RAW	Readily available water content
Rd	Flow duration
RTK	Real-time kinematic
s	Sand
SD	Standard deviation
SMD	Soil moisture deficit
SS	Subsurface lateral flow
SSE	South-southeast
STF	Spectrotransfer functions
SW	Shallow water
SWAT	Soil & Water Assessment Tool
TDR	Time-domain reflectometry
TF	Tile flow
TIR	Thermal infrared
TN	Total nitrogen
TWI	Topographic wetness index
uHO	Upper hollow
UK	United Kingdom
UP	Underpass
US	United States
USDA	United States Department of Agriculture
VIS-C	Visible-colour
Vt	Total discharge volume
VWC	Volumetric water content
WSW	West-southwest
z	Silt
θ_v	Soil volumetric moisture content
θ	Hillslope angle

Chapter 1

Introduction

1.1 Setting the scene: a short history of Southland, New Zealand

One of the earliest written accounts of Southland's suitability for agriculture was provided in 1844 by Frederick Tuckett, who spent roughly 7 days in mid-winter surveying the land around Aparima and Bluff in southern New Zealand. He noted swampland, peat bogs, vegetation indicative of poor quality soil, short days and frequent rain capable of significantly reducing the number of days in which one could work the land. In summary, as quoted by the Southland Times, he described the region as "a mere bog, utterly unfit for human habitation" ("Invercargill - Southernmost city in the world", 1900). Tuckett had accurately identified the two major limitations to agricultural productivity in Southland: impeded drainage, and nutrient-deficient soils. However, as understanding of the New Zealand environment grew and agricultural technology advanced, methods capable of overcoming the natural limitations of soils brought Southland into prominence as a region with great agricultural potential. Implementation of some key land management practices prompted expansive land development and increases in land productivity. One hundred years later, Southland had transformed into one of the most prosperous farming regions in New Zealand (Kellaway, 1970).

The Southland landscape has been dramatically altered, both physically and functionally, since the arrival of humans. Vast areas of indigenous scrub and forests have been cleared by both Māori and Europeans over the past 800 years (MfE & StatsNZ, 2015b, 2016). Prior to human settlement, wetlands covered over 450,000 hectares of Southland (Figure 1-1). Over the subsequent 160 years, approximately 90 % of those wetlands were eradicated through the installation of drainage ditches and subsurface drainage channels (MfE & StatsNZ, 2015b, 2016). Artificial drainage systems now remove the water rapidly from the soil and discharge it into streams and rivers, which have been straightened and confined within stop-banks to control flows and maximise productive land area (Ellis et al., 2018). Poorly drained soils that have formed in loess, a wind-transported sediment of silt sized particles, underlie extensive parts of Southland. With drainage, these soils form some of the region's most productive agricultural landscapes (Manaaki Whenua - Landcare Research, 2022).

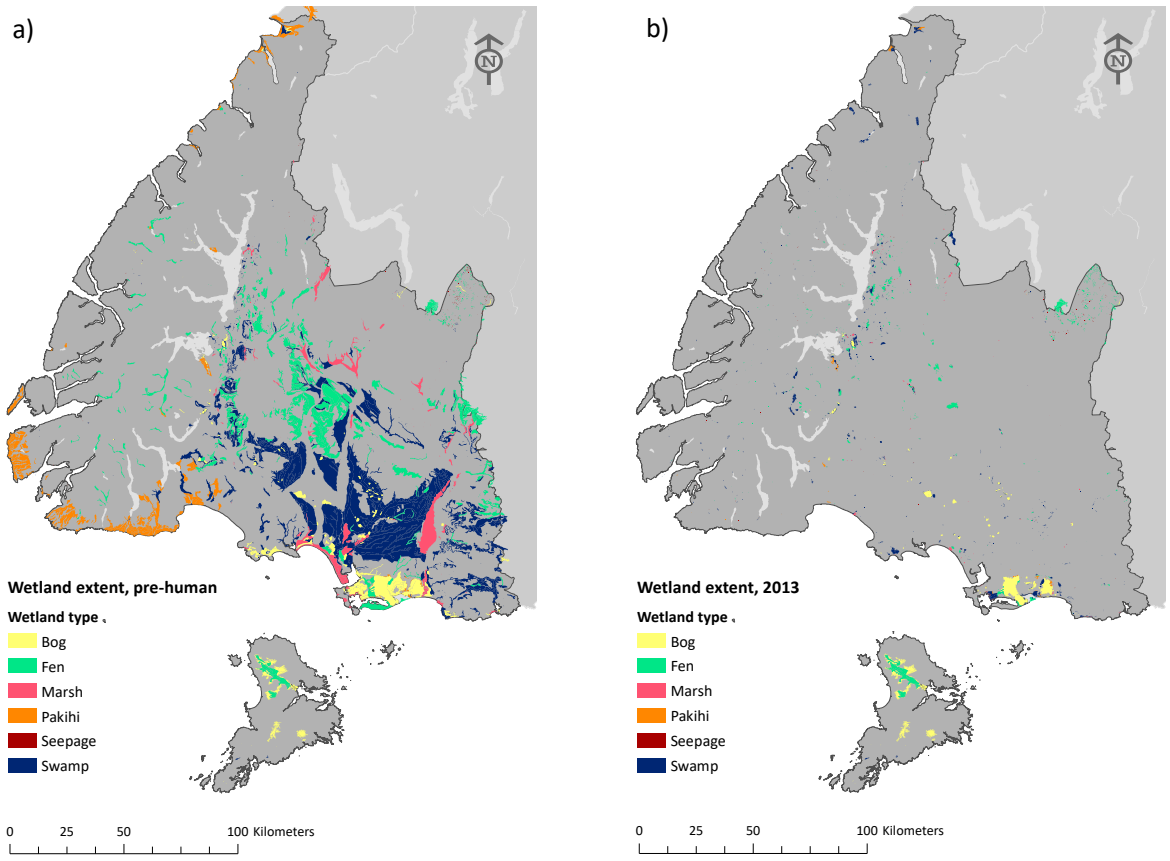

Figure 1-1. Estimated wetland coverage, by wetland type, across Southland (encapsulated within the dark grey area), showing a) wetland extent pre-human settlement (ca. 1000 AD; source: MfE & StatsNZ, 2015b) and b) post-human settlement (2013; source: MfE & StatsNZ, 2016).

1.2 Southland in the 21st Century

Southland has a population of around 100,000 (as of June 2014), of which 30 % live rurally (Moran et al., 2017). From the late 19th Century until the mid-1980's, sheep farming dominated rural Southland, with total stock numbers for the region peaking at over 9 million (Environment Southland, 2014). Today, sheep farming (including mixed sheep and beef) occupies 56% of developed land in Southland (Moran et al., 2017). Over the past 35 years, dairy farming has grown from relative insignificance to become one of Southland's most significant industries. On the Central Plains (section 2.1) today, dairy, sheep-and-beef, and sheep farming together make up over 70 % of the total land use, by area, with dairy alone occupying 45 % (Pearson & Couldrey, 2016). The Southland economy is heavily reliant on agriculture, which contributes 22 % of regional GDP (Moran et al., 2017). Southland's agricultural industry is also nationally significant, contributing 5 % of New Zealand's national GDP in 2012 (Moran et al., 2017).

1.3 Problem statement

Dissected, loess-mantled terraces are the dominant component of the Southland soil-landscape (J. Schmidt et al., 2005). Significant areas of these loess-derived soils have dense subsoils that impede drainage through the profile, causing ephemeral water-tables which 'perch' on the dense subsoil. As a result, subsurface artificial drainage systems are widespread across Southland, with an estimated 75% of the lowland being artificially drained (Pearson, 2015). However, despite the spatial predominance of these drained soil-landscapes there has been little research quantifying their hydrological pathways and dynamics, and no explicit recognition of the complex loess-stratigraphy associated with these landscapes. Such features may control important variability in the soil hydraulic properties that regulate water storage and movement.

As more has been learnt about the important ecosystem services provided by natural soil-landscapes, it has become clear that, alongside the agronomic benefits, subsurface drainage creates problematic secondary effects. Subsurface drainage alters the partitioning of fluxes amongst water balance components and influences streamflow event hydrographs, which need to be accounted for by hydrological and nutrient-loss models (King et al., 2014; Rahman et al., 2014). They also provide a direct route for contaminant transfer into surface waters, may alter patterns of soil moisture variability and possibly even modify soil properties (Messing & Wesström, 2006; Monaghan et al., 2016; Oliver et al., 2005; Øygarden et al., 1997; Schottler et al., 2014; Shipitalo et al., 2004; Williams et al., 2019). Despite the known problems linked to mole and tile drainage, information regarding the extent, characteristics, and longevity of these networks is limited.

Today, effective catchment management (e.g., freshwater allocation and contaminant mitigation) relies strongly on predictive modelling tools, such as Overseer (Wheeler et al., 2003) for nutrient management, and the NZ Water Model (NIWA, 2018) for catchment hydrology. Such models are informed by knowledge of soil physical and hydraulic properties and processes. At present there are few studies, at scales beyond experimental plots, to develop and validate the accuracy and reliability of model simulations in mole and tile-drained landscapes.

This PhD research attempts to provide new knowledge of the characteristics of loess-mantled landscapes with thin loess sheets in which soils with dense subsurface horizons form; the artificial subsurface drainage networks that are commonly used to counter the problems of low permeability; as well as the effects of these artificial drainage systems on the soil and catchment hydrological behaviour.

1.4 Aims, objectives and thesis structure

There is a gap in our understanding of the intrinsic and extrinsic controls on the spatial variability of soil hydraulic properties and soil hydrological behaviour in low permeability loess landscapes in which mole-tile drainage has been installed. The aim of this research is to provide a foundational understanding of the hydrological functioning of artificially drained landscapes formed in loess. This study focuses on a small, artificially drained basin formed in a loess-mantled downland landscape, typical of the Central Plains in Southland, New Zealand.

The specific objectives of this thesis are:

1) To characterise the spatial distribution of soils within a dissected loess landscape and determine whether multisequal soils are an important component of these landscapes, and if their recognition as distinctive taxa would improve characterisation of soils in a way that would facilitate better soil and environmental management,

2) To characterise a mole and tile drainage network (i.e., drain depth, orientation, location, integrity, connectedness, density) that is likely to be representative of similar artificial drainage systems across slowly-permeable loess soils in Southland,

3) To quantify the direct and indirect influence of mole drainage channels on soil hydraulic properties, as well as the influence on the overall soil moisture regime classification,

4) To construct a water balance and examine the temporal variability in runoff pathways, quantify runoff generation controls and thresholds and characterise and quantify groundwater recharge at event-based time scales, and

5) To qualitatively analyse the soil moisture, perched water table and runoff dynamics in order to identify mechanisms of hydrological connectivity in artificially drained landscapes.

This thesis is structured into eight chapters, following the thesis-by-papers style. Each chapter has been written with the intention of being submitted as either a journal article or short communication. Following this format, the literature review and methodology components of the

thesis are dispersed within the relevant research chapters. To ensure continuity and comprehensiveness for the purpose of thesis coherency, some content is included in each research chapter that will be removed prior to journal submission (e.g. chapter cross-referencing) or condensed for journal paper submission.

Following this introductory chapter, Chapter 2 provides a literature review that includes a description of the general study area, including the geology, geomorphology, climate, soils, and environmental concerns. The following research chapters deal with each of the specific thesis objectives as follows: Chapter 3 (Objective 1), Chapter 4 (Objective 2), Chapter 5 (Objective 3), Chapter 6 (Objective 4) and Chapter 7 (Objective 5). Finally, the key results are synthesised, and conclusions and future research suggestions are presented in Chapter 8.

Chapter 2

Southland's soil-landscape and the influence of mole and tile drainage

2.1 Geography

Southland (Murihiku in Te reo Māori), made up of the south-western portion of the South Island and Stewart Island, is the southernmost region in New Zealand and covers an area of 3.2 million hectares (Figure 2-1). Approximately 40 % of the region has been developed for human use, with the remainder under indigenous vegetation, and largely made up of inaccessible, mountainous terrain. Mountains to the north and west are drained by four major river systems, which flow through terraces, rolling downlands and alluvial flats toward the southern coastline. The extensive, low-lying components of Southland comprise three geographically and climatically distinct areas: the Waiau Basin, the Waimea Plains and the Southland Plains (Grant, 2008; Macara, 2013). The Southland Plains are often further classified into the Central Plains and the Eastern Plains, which are characterised by the ancestral floodplains of their major rivers (Aparima, Oreti and lower Mataura). While no official definition exists, the Central and Eastern Plains are sometimes delineated by the Oreti River (Rekker, 1998). A more appropriate physiographic boundary, however, may be the Makarewa River, as it separates two, clearly distinct, radiometric (or gamma-ray) signatures, which reflect parent material differences in loess and alluvium as estimated by concentrations of the radioelements potassium, uranium and thorium in the near surface (Figure 2-2). This study was centred on a Quaternary downland in the Central Plains (as defined using the Makarewa River boundary), 30 km north-west of Invercargill. The Central Plains encompass the downlands and plains of the Aparima and lower Oreti catchments, and are bound by the Longwood Ranges and Takitimu Mountains to the east and the Taringatura and Hokonui Hills to the north.

2.2 Geology

Southland's underlying geology is diverse and includes several of New Zealand's major Paleozoic to Mesozoic basement rock units: the Takaka, Brook Street, Dun Mountain-Maitai, Murihiku and Caples terranes, and the plutonic rocks of the Median Batholith. Outcrops of these basement rocks occur in high country and mountainous areas, which dominate the peripheral regions. In the broad, low-lying areas of central and southern Southland, surface exposure of older

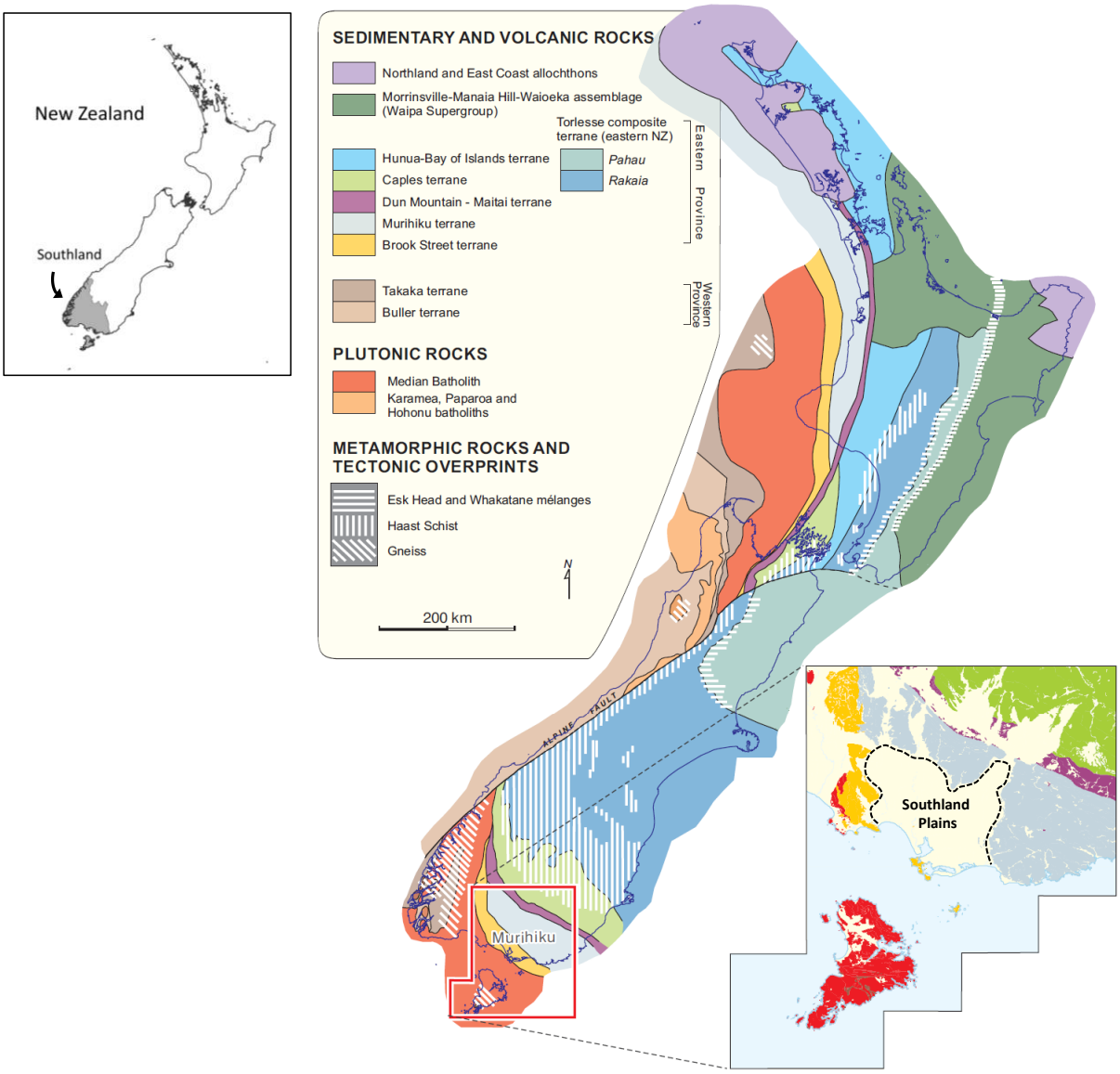

Figure 2-1. Map showing the location of the Southland region (grey shaded area) in New Zealand (top left) and the basement rocks of New Zealand (right), including the sedimentary and plutonic rocks that underlie the southern South Island. The inset shows a close up of the Southland Plains (area within dashed line), where the basement rocks are covered by Quaternary gravels of both alluvial and marine origin (pale yellow). Adapted from Turnbull and Allibone (2003).

rocks is limited by an extensive blanket of Cretaceous to Cenozoic gravels and windborne sediments (Cahill, 1995).

2.3 Geomorphology

The landscape of Southland has been sculpted by climatically-driven geomorphological processes of the Quaternary period. In brief, successive glaciation and deglaciation in the

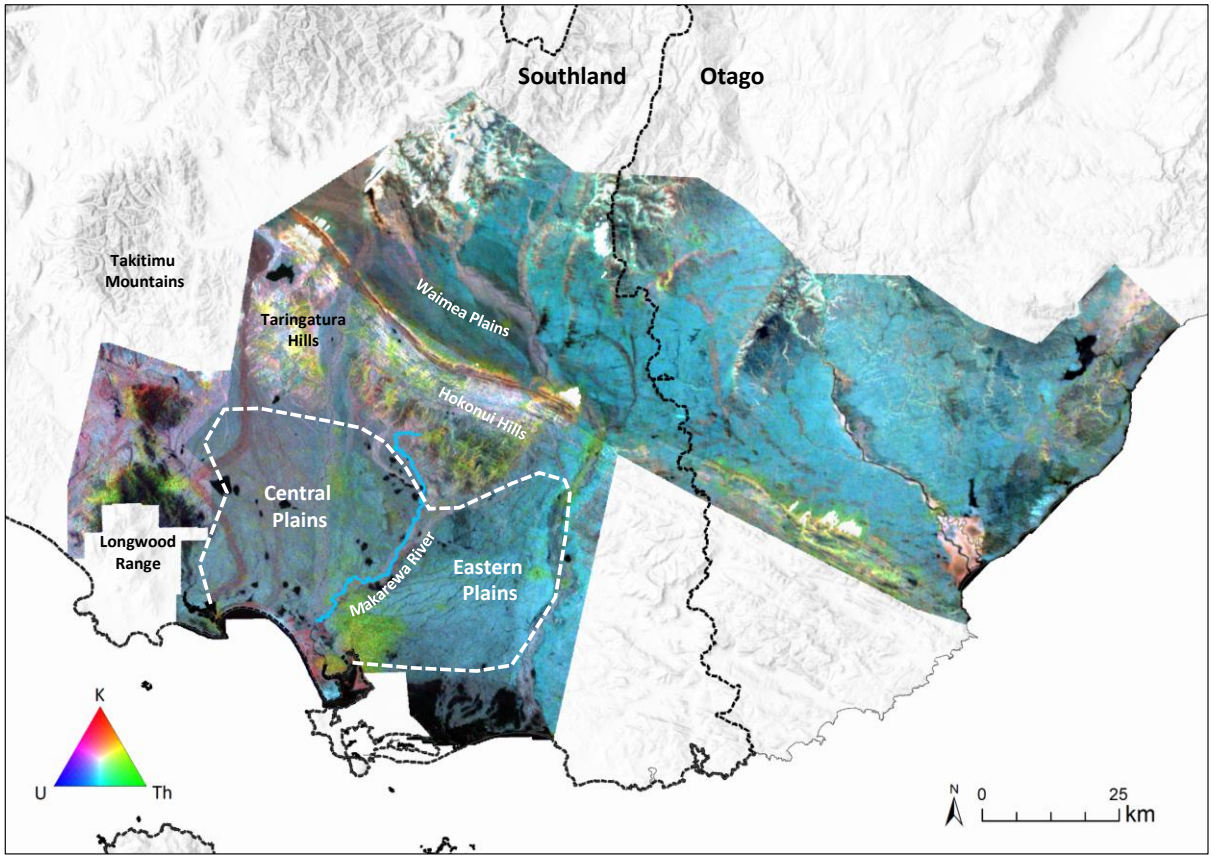

Figure 2-2. Radiometric map of Southland and Otago (New Zealand Petroleum & Minerals, 2020), showing relative concentrations of the radioelements potassium (K; red), uranium (U; blue) and thorium (Th; green) in the near-surface. Black colours are low in all elements; white colours are high in all elements. Overlain are some of the prominent geographical features of Southland, including the Central Plains and Eastern Plains (encompassed within the dashed line and separated by the Makarewa River).

mountainous headwaters of all of Southlands major rivers triggered the formation of expansive alluvial plains and terraces (Raeside, 1964). The cold, dry and windy climate during glacial periods facilitated the transport of abundant silt from the sparsely vegetated floodplains towards older, elevated surfaces where the aeolian deposits formed sheets of loess. During interglacial periods, sediment load decreased, rivers incised, loess deposition slowed and the warmer and wetter climate increased rates of pedogenesis. Characteristic to the loess-derived soils was a compact, low permeability subsoil termed a fragipan (Kemp & McIntosh, 1989). A process of concomitant loess deposition and upbuilding pedogenesis (Almond & Tonkin, 1999; Lowe et al., 2008) followed by topdown pedogenesis repeated with each glacial cycle, creating a mantle of loess sheets, each containing a fragipan. Following the last glacial period, alterations in atmospheric circulation have seen the Southland climate through three periods of distinct vegetation and climate (McGlone & Bathgate, 1983). Since the most recent climatic period began, ca 7,000 years B.P., a cool, humid

climate has sustained wetland ecosystems, which formed on terraces as a result of water perching above the modern fragipan, and in more permeable, low-lying areas as a result of high water tables (McGlone & Bathgate, 1983; Robertson et al., 2018). On the terraces, dissection and hillslope formation have exhumed the thin, buried loess sheets and contemporary pedogenic processes have been overprinted to form polygenetic soils with complex subsurface stratigraphy (Bruce, 1996).

Quaternary gravel terraces mantled in loess are widespread throughout the low-lying areas of Southland, and especially on the Southland Plains. Loess deposits over 1 m thick form gently-rolling to undulating topography along the terraces of present day and Pleistocene floodplains. Thinner layers of loess (mostly ≤ 50 cm) also cover deposits of late Pleistocene alluvium on large areas of Southlands alluvial plains (Bruce et al., 1973).

2.4 Present-day climate

Southland lies within the latitudes of southern westerly winds and receives most of its weather from the west and south-west. Rainfall is evenly distributed throughout the year in the Southland Plains, and dry spells longer than two weeks are uncommon (Macara, 2013). Annual rainfall averages between 900 – 1100 mm on the Central Plains, which are subject to a rain shadow effect from the Longwood Ranges (Macara, 2013). Southland's climate is temperate, with daily average air temperatures ranging from 4 ˚C in winter (July) to 15 ˚C in summer (January; Macara, 2013). Maximum air temperatures over 25 ˚C occur on average less than 12 days per year and frosts are common across Southland in the winter months (Macara, 2013). The Southland Plains experience approximately 1600 – 1700 sunshine hours per year (Macara, 2013). Seasonal variation in sunshine hours is predominantly due to the declination of the sun, with daylight hours ranging between 8.5 hours at the winter solstice and 15.75 hours at the summer solstice. Penman calculated mean evapotranspiration varies from 5 – 13 mm per month in June, to 125 – 130 mm per month in January (Macara, 2013).

2.5 Soils

Approximately 700,000 hectares, or 20 % of the total regional area, has been mapped for its soil distribution (Figure 2-3), with a focus on the lowland areas (Manaaki Whenua - Landcare Research, 2022). Over 80 % of the mapped area comprises just three soil orders (NZSC; Hewitt, 1998): Brown (46 %), Gley (18 %) and Pallic (17 %).

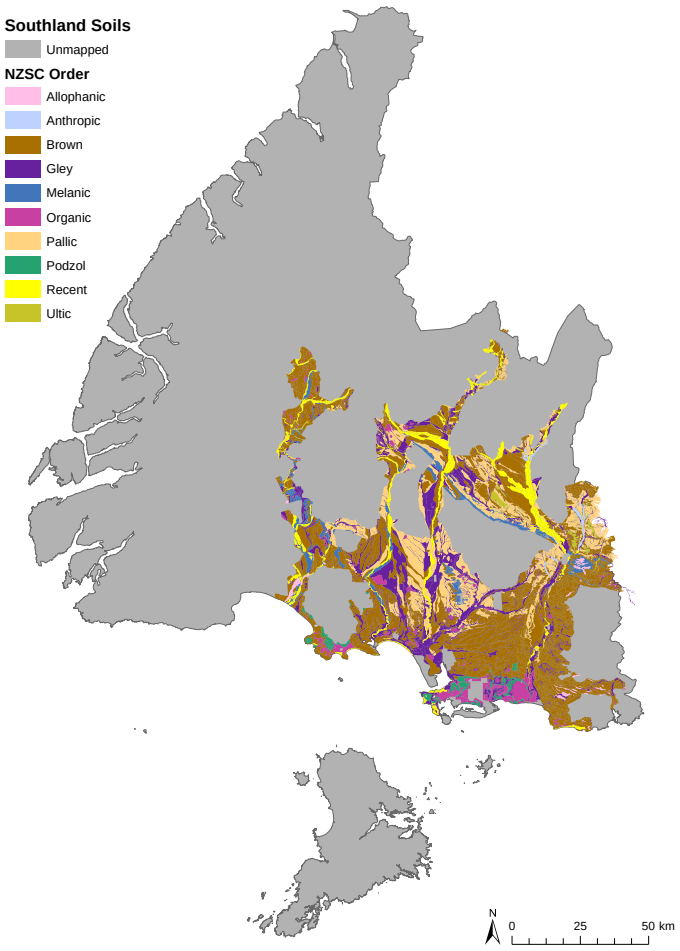

Figure 2-3. Mapped soil orders of Southland, following the New Zealand Soil Classification (NZSC). Source: S-Map Soils Database, Manaaki Whenua - Landcare Research (2022).

Brown soils cover around 330,000 hectares, occurring predominantly on flat to rolling areas of Southland, as well as some steeplands (Manaaki Whenua - Landcare Research, 2022). They occur where the climate is moist (i.e., mean annual precipitation [MAP] > 1000 mm) and where drought is uncommon. The parent material of Brown soils is predominantly siliceous quartzo-feldspathic sedimentary rocks and/or their derivatives, such as loess and alluvium (Hewitt et al., 2021). Brown soils have relatively stable, grey-brown topsoils and yellowish-brown subsoils as a result of high amounts of dispersed secondary iron and aluminium oxides. They have good drainage and are rarely waterlogged, and no poorly drained or very poorly drained soils are included in the soil order (Hewitt, 1998). They have low to moderate base saturation, which reflects the leaching environment in which they form, and moderate to high phosphate retention.

Gley soils make up around 130,000 hectares of Southland, and occur in low parts of the landscape where water tables are high or where water accumulates in topographically convergent areas or above impermeable subsurface horizons (Manaaki Whenua - Landcare Research, 2022). Both Gley and Pallic soils, along with Organic soils, made up a large component of Southlands original wetland extent (MfE & StatsNZ, 2015a). They form predominantly in mineral parent materials, commonly alluvium or colluvium, and are characterised by poor or very poor drainage status. Gley soils are often saturated for prolonged periods of time, such that oxygen content is low (anaerobic) and reducing conditions occur. As a result, they are characterised by greyish matrix colours and redox segregations of iron and manganese oxides which form large mottles, concretions and pans (Hewitt, 1998). Because of their low-lying position in the landscape, Gley soils are often fertile, as they form a landscape sink for nutrient-laden water runoff from upslope areas. The moisture status of Gley soils limits rooting depth and trafficability, so for agricultural use, these soils are almost always artificially drained. Once drained, they form productive agricultural land

Pallic soils cover around 120,000 hectares of the Southland landscape, and have predominantly formed on rolling hills and terraces of the plains and downlands (Manaaki Whenua - Landcare Research, 2022). They are common on the Waimea Plains and downlands north of Gore where MAP is 600 – 900 mm, and also on the Central Plains, where MAP is 900 – 1100 mm (Macara, 2013; Manaaki Whenua - Landcare Research, 2022). Pallic soils often experience moisture deficits in summer and moisture excess in winter and spring. Loess forms the parent material of most of Southland's Pallic soils, which are generally fine-textured, and have pale coloured subsoils because of low of secondary iron oxide contents (Hewitt, 1998). Pallic soils often contain a dense fragipan, which restricts water and root penetration and leads to the formation of perched water tables in winter. As a result, these soils commonly exhibit redoximorphic features such as grey veins and mottles. Soil material is strongly dispersive and prone to slaking, particularly in the subsoil, and topsoils are sensitive to compaction. Pallic soils are generally weakly weathered and leached, with low phosphorus retention. Like Gley soils, for agricultural use, Pallic soils are very often artificially drained, especially on the Central Plains, where the climate is moist (Pearson, 2015). Drained Pallic soils form some of Southlands most productive agricultural landscapes.

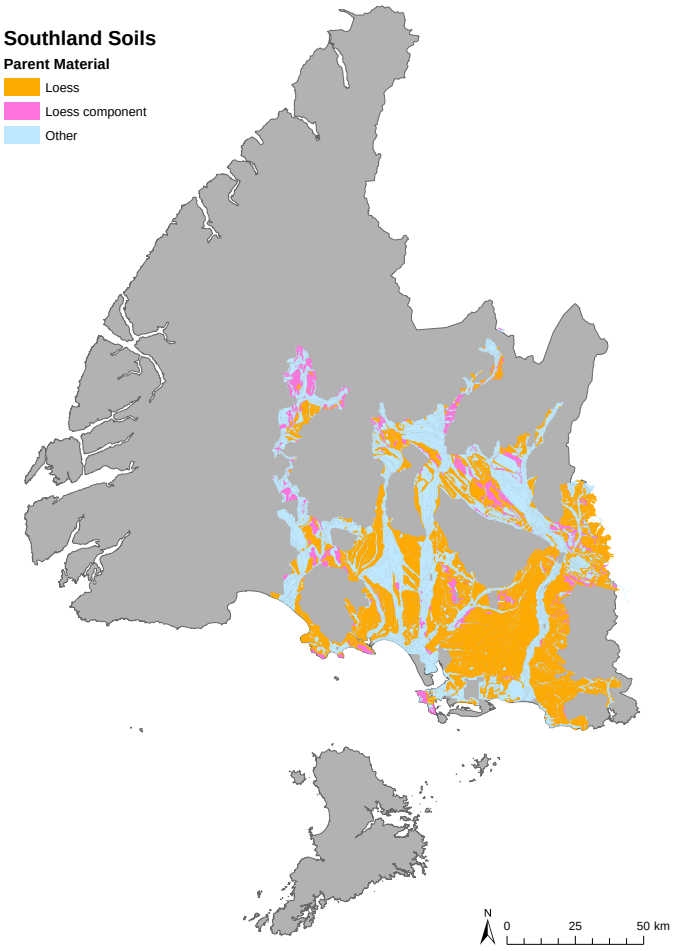

Figure 2-4. Parent material of mapped soil in Southland. Source: S-Map Soils Database, Manaaki Whenua - Landcare Research (2022).

2.6 Loess

Loess is widespread throughout Southland, occurring on all types of topography and with no identified altitudinal limit (Bruce et al., 1973). Loess is the primary parent material for 45 % of all of Southlands soils, and forms a component of the parent material in a further 8 % of soils (Figure 2-4) (Manaaki Whenua - Landcare Research, 2022). The stratigraphy (i.e., the nature of the layering) of the loess deposits is similar throughout the region (Churchman & Bruce, 1987), although their thickness varies. The thickest and most extensive loess deposits are found on the terraces and rolling downlands. In the Central and Eastern Plains, the average thicknesses of the loess mantle is two to four metres (Bruce, 1973a). During periods of loess accumulation, the most significant source of loess was the floodplains of Southland's major rivers, whose headwaters reside in the mountains of western and northern Southland. Two main loess provinces (north/east and

south/west) were originally described within Southland, along with a number of smaller, more localised sources (Bruce, 1973a; Raeside, 1964; Wood et al., 1956). Intermixing of loess between these provinces is limited by the physical barrier formed by the uplands of the Southland Syncline (i.e., the Hokonui Hills), except for gorges through which the major rivers transect. Loess in northern and eastern Southland (i.e., the Waimea and Eastern Plains) and into the Clutha District of southern Otago is derived from the metamorphic rocks of Otago (ie., the Haast Schist; Figure 2-1; (Bruce, 1973a)), and shows higher proportions of thorium and uranium relative to potassium (i.e., cyan colours in Figure 2-2) which is consistent with the radiometric signature of its parent rocks. This loess was transported by north westerly winds down the Waimea Plains and northerly winds down the Clutha valley. Loess in the south and west is more variable in its mineralogical composition and has higher proportions of potassium and uranium relative to thorium (i.e., magenta colour in Figure 2-2), consistent with the radiometric signature of its tuffaceous greywacke parent rocks (Bruce, 1973a; Hewitt et al., 2021; McIntosh, 1994). This loess was transported by westerly or south-westerly winds and deposited in the Waimea Basin, and the Central and Eastern plains and downlands.

Where loess layers are thin, current soil development traverses across more than one loess sheet (Morrison, 1978). These soils are termed 'multisequal' or 'polygenetic' soils, as current pedogenic processes are being super-imposed on 'buried' soil horizons which were formed in a previous cycle of soil formation (Figure 2-5a). Where loess is thicker, soils are more often 'unisequal' or 'monogenetic', with current pedogenesis confined to the single, uppermost loess layer that has not undergone a previous cycle of soil formation (Figure 2-5b). Features of Southland's polygenetic subsoils may include clay increases, cutans and signs of disintegration (Churchman & Bruce, 1987).

2.7 Poorly drained soils

Soils may experience drainage limitations as a result of either high groundwater tables (due to a low-lying position in the landscape), or inherent physical properties, which restrict the transmission of water through their mass (low permeability). Poorly drained soils lose water so slowly that they remain at, or close to, saturation for significant periods of the year. In high rainfall regions, excess soil moisture is likely to be one of the most important limiting factors for land productivity. The rate of gas diffusion in saturated soil zones is insufficient to meet the oxygen needs of growing roots (Lynch et al., 2012), while the restricted volume of aerated soil limits the

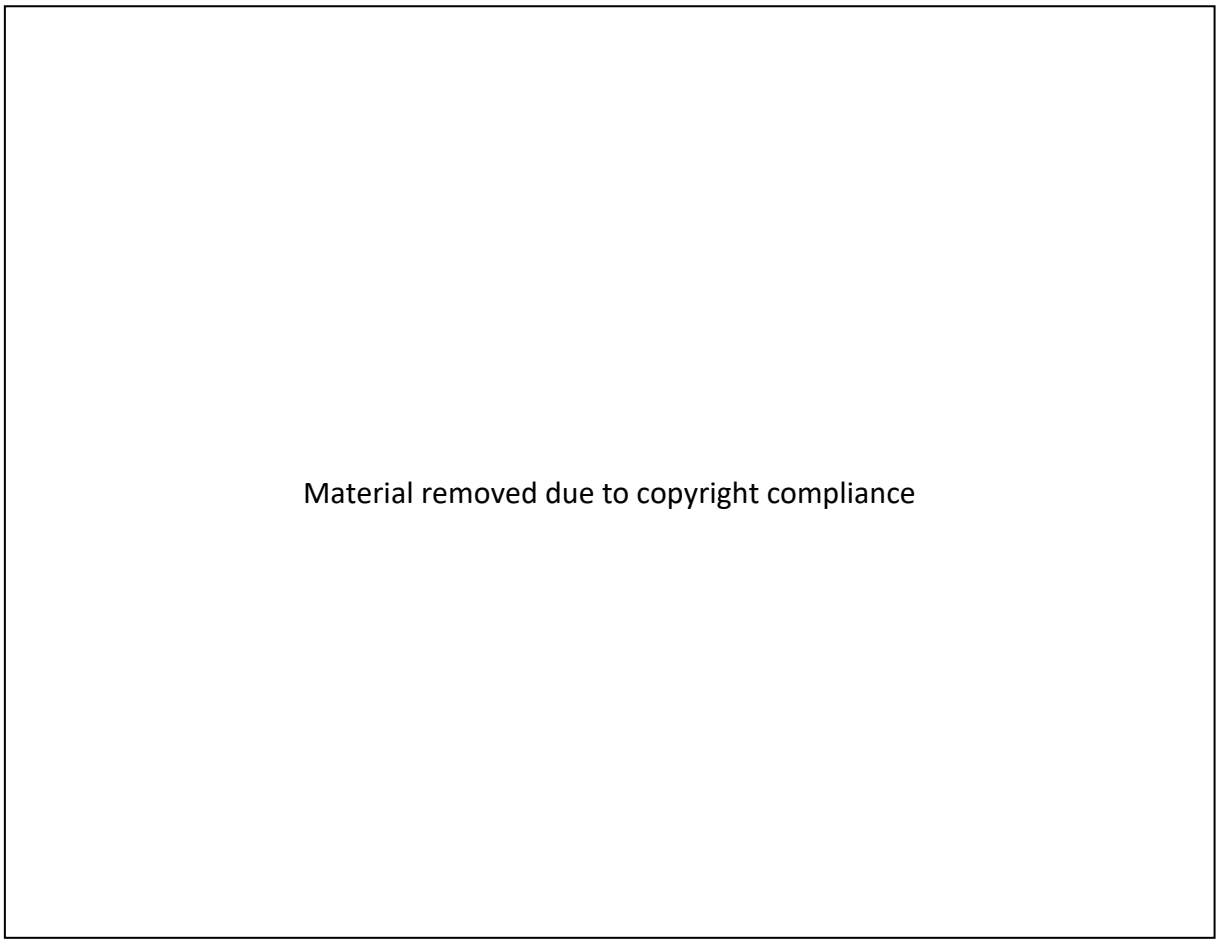

Figure 2-5. Where loess sheets are thick (a), soils formed in them (i.e., the top 1 m) tend to be unisequal or monogenetic, which means they are formed entirely in the uppermost loess sheet and its transported and deposited facies. Underlying paleosols are separated from the surface soil by a small thickness of unweathered, intervening sediment. Where loess sheets are thin (b), the soils formed in them may be multisequal (composite/polygenetic), and include subsoil horizons inherited from the paleosols of buried loess sheets, which themselves may be overprinted by contemporary pedogenesis. Image modified from Morrison (1978).

capacity for root uptake of nutrients and water (Arduini et al., 2019; Stevens & Prior, 1994; Zhou & Lin, 1995). As such, prolonged moisture-excess will reduce the growth, development and health of many agricultural and horticultural plants. Furthermore, as the soil gets closer to saturation, soil shear strength is reduced, with significant consequences for land trafficability (Houlbrooke et al., 2021; Hu et al., 2021). For fine textured soils especially, operating heavy machinery in waterlogged conditions is challenging and can cause severe structural damage to the soil. Stock carrying capacity is also reduced, and pugging can lead to soil compaction and physical damage to plants (Drewry et al., 2008; Drewry & Paton, 2000), as well as concerns for animal welfare (Ministry for the Environment & Ministry for Primary Industries, 2021). Consequently, the time available for working and grazing the land is reduced on soils prone to long periods under excess-moisture.

In New Zealand, around 25 % of soils under high producing grassland and cropland are classified as imperfectly, poorly, or very poorly drained (Manaaki Whenua Landcare Research, 2018; Ministry for the Environment, 2020a). Overall, 31.5% of high producing land has slowly permeable subsoils, with a significant proportion of these soils having some degree of periodic saturation (Manaaki Whenua Landcare Research, 2000). In Southland, almost 40 % of the mapped soil area is classified as very poorly or poorly drained, and a further 15 % is classified as imperfectly drained (Table 2-1; Manaaki Whenua - Landcare Research, 2022). Soil drainage limitations are considerably relevant to the Central Plains in Southland, with 55 % of the area's soils classified as poorly drained, and almost 75 % classified as between imperfectly and very poorly drained (Manaaki Whenua - Landcare Research, 2022).

2.8 Mole and tile Drainage

Poorly drained soils are managed through the installation of drainage systems. There are various types of artificial drainage systems and the most effective system depends primarily on the topography, the soil properties and the causes of the poor drainage (Bowler, 1980). Soils with slowly permeable subsoils can be efficiently drained by means of subsurface drainage, which involves the installation of a network of drainage pipes at depths of generally ≤ 1 metre below the surface. These pipe drains, commonly termed 'tile drains', are buried in ditches, which are backfilled with permeable material to facilitate transport of water into the pipes. Tile drainage effectively lowers both perched and true groundwater tables, by gathering excess soil water and discharging it rapidly into local canals or waterways (Smedema et al., 2004). The effective area of a tile drain or open ditch is often increased by installing mole channel networks. Mole channels are unlined channels, generally around 45 cm deep, created by pulling a blade and attached plug through the soil behind a tractor (Figure 2-6). Their installation fractures the soil, creating a network of cracks that radiate out from the mole channel towards the soil surface (Leeds-Harrison et al., 1982; Youngs, 1985). They are suitable only in soils not prone to slaking and must be installed under specific soil hydrological conditions (Bruce, 1972). The optimum soil conditions for installation facilitate the formation of a stable mole channel and promote the fracturing of the soil above the mole. Such conditions generally occur in late spring or early summer, when the subsoil is at approximate field capacity, but the topsoil is dry enough to both fracture the upper soil, and give mechanical traction for the tractor (Bowler, 1980). Additionally, the mole drains should not carry water in their first season post installation, to avoid siltation and collapse (Bowler, 1980). Because installation conditions and soil properties are so variable, it is not possible to give an

Table 2-1. The ten most areally abundant S-Map soil families of Southland, in order of greatest coverage area (hectares). These 10 soil families represent approximately 50% of the total area of mapped soils in Southland. Source: Manaaki Whenua - Landcare Research (2022).

Rank	Family	Area (ha)	Drainage Capacity	NZSC	%
1	Waikiwi	71,000	Moderately well	BFT	10.0
2	Pukemutu	51,700	Poor	PPJX	7.3
3	Woodlands	39,800	Imperfect	BFM	5.6
4	Claremont	37,500	Poor	PPX	5.3
5	Makarewa	34,100	Poor	GOT	4.8
6	Eureka	31,700	Poor	GOA	4.4
7	Braxton	21,500	Poor	GOT	3.0
8	Balmoral	17,700	Well	BOA	2.5
9	Mokotua	16,000	Imperfect	BOMA	2.2
10	Heretaunga	15,900	Well	BOP	2.2
Total		**336,900**			**47**

absolute value for the serviceable lifetime of mole drainage. Under ideal soil and installation conditions estimates of 5 – 7 (McPhillips, 1979) and 10 – 15 (Bowler, 1980) years have been provided, although examples exist of functional mole systems that are around 25 years old (Bowler, 1980). Conversely, on less suitable soils, or under suboptimal installation conditions, the lifespan is limited to between one and five years (Bowler, 1980; McPhillips, 1979).

Mole and tile drainage is extremely prevalent in agricultural regions around the globe, especially in the UK, Europe and NZ, on both flat land and hillslopes (Feick et al., 2005; Hill et al., 2018; Manderson, 2018; USDA NASS, 2017). Subsurface drainage as a means of improving land productivity in Southland dates back to around the beginning of the 20th century (Critchfield, 1954), and is commonplace to this day. There is limited published research quantifying the benefits of mole and tile drainage in New Zealand pasture systems, which, through increasing soil aeration, are reported to include; enhanced germination, root growth and yields, improved bearing capacity (which supports higher stocking rates, heavier machinery, and increased periods in which farmers can work the land) and reduced land-surface erosion (due to a decrease in saturation periods that generate surface runoff; King et al., 2015; Robinson et al., 1987). It is likely that, in pasture systems, the main benefit of mole and tile drainage is the improvement in soil strength and bearing capacity. In a study on silt loam over clay soils in south Otago, Scott (1963) found that mole and tile drainage alleviated the pasture yield depressions following intensive winter sheep grazing practices (i.e., ca 150 ewes ha^{-1}) by around 10 %; however, where winter grazing was not practiced, they found that drainage offered no benefit to pasture production. In low-permeability clay loam soils of south-

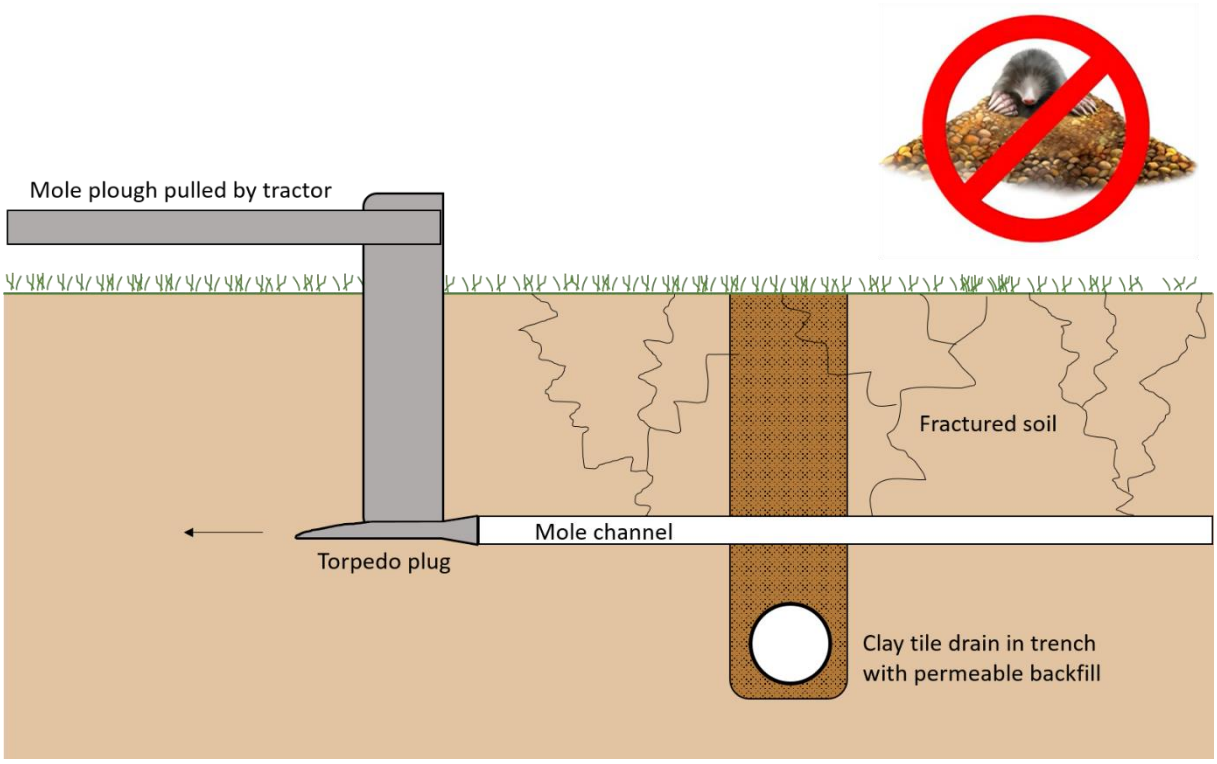

Figure 2-6. Mole channel installation. A tractor pulls a mole plough through the soil, which creates an unlined channel. The plough is pulled across the pre-installed tile drain to connect the mole channel hydrologically to the tile drain. The term 'mole' channel is presumably named after the mammal of the same name; however, mole animals are not involved in artificial subsurface drainage in Southland, as they are not found in New Zealand.

west England, Tyson et al. (1992) found that after five years, the benefits of installing mole and tile drainage on beef production were modest, and resulted in annual dry matter yield increases of 3 % for pasture and annual liveweight gain increases of 11 % per hectare. The liveweight gain increases were attributed to a five day increase in the length of the grazing season as a result of drainage. Armstrong (1986a) also found that drainage increased the length of the grazing season: by 19 days in spring, and 28 days in autumn.

Artificial drainage installation is an unregulated activity in New Zealand, and little data is available on the type, density, and distribution of these systems. Mole and tile drainage is particularly widespread on the Southland Plains; however, detailed maps of these systems are limited to a handful of properties and no information about associated mole channels is available. Work by Pearson (2015) provides an idea of the likelihood of artificial subsurface drainage being present in a given area, and suggests that artificial subsurface drainage may cover approximately 75 % of agricultural land in Southland; however, this is yet to be calibrated. While aerial images can provide insight into the spatial extent of surface drainage (e.g. drainage ditches; Ewans, 2016),

information regarding the spatial extent of subsurface drainage is much more difficult to obtain once the surface scars from installation have healed over. This is particularly true for mole channels, which lack the discernible outlet characteristic of tile drains.

2.9 Environmental concerns

At least 43 % of New Zealand's agricultural land fails to meet the minimum environmental objectives set by regulatory bodies for freshwater nitrate concentrations (Snelder et al., 2020). Contamination of surface and groundwater are a dominant environmental concerns in contemporary Southland and many of the region's freshwater monitoring sites do not meet the New Zealand national limit guidelines (Ministry for the Environment, 2020b) for nitrogen, phosphorus, sediment or *E. coli* (Moran et al., 2017; Norton et al., 2019; Quinn et al., 2010; Williamson et al., 2010). Nitrogen and phosphorus availability are limiting elements required for photosynthesis, but their oversupply in freshwater systems leads to eutrophication (excessive plant and algal growth) and, during the subsequent biomass decomposition, oxygen depletion that may threaten aquatic ecosystems (Carpenter et al., 1998). Excessive sediment in the water column blocks light required for photosynthesis and smothers aquatic ecosystems (Davies-Colley, 2013). Freshwater incidence of enteric bacterial pathogens such as *E. coli* and *Campylobacter* are a risk to human health, with Campylobacteriosis the most commonly reported disease in New Zealand (Ministry of Health, 2012). Sheep are a known source of both *E. coli* and *Campylobacter* contamination of freshwater, and have been implicated in significant community outbreaks of Campylobacteriosis (Bartholomew et al., 2014; Gilpin et al., 2020; Moriarty et al., 2011).

In agricultural landscapes, the primary pathways for contaminant transfer to surface water are overland flow and subsurface flow, including via tile drainage (Barkle et al., 2021; Monaghan et al., 2016; Oliver et al., 2005). Artificially drained agricultural landscapes have come under particular scrutiny within the past few decades for their contribution to freshwater contamination (Grangeon et al., 2021; Scott et al., 1998; Thornley & Bos, 1985; VanderZaag et al., 2010). The rapid removal of excess water by the drainage network reduces the residence time of water within the soil, and decreases the opportunity for mobilised contaminants to be transformed and/or assimilated by the soil. As a result, concerning levels of nutrients, sediment and faecal bacteria may be found in tile drain discharge (Gramlich et al., 2018; Royer et al., 2006; Scott et al., 1998). Transfer of nutrients or pesticides out of the agricultural system is also economically wasteful for farmers (Robinson et al., 1987). In addition to contaminant transfer, subsurface drainage systems

have also been shown to alter the partitioning fluxes amongst water balance components, and influence streamflow event hydrographs in agricultural catchments (King et al., 2014; Rahman et al., 2014).

2.10 Accounting for mole and tile drainage in environmental modelling

Understanding the interactions between water and soil, from the profile scale to the catchment scale, is critical for understanding both current and future landscape responses to climate and land use. Today, decision making processes to guide water quality and quantity management rely heavily on environmental modelling (Lin, 2003). Models are used to quantitatively extrapolate or predict rainfall-runoff responses, nutrient and contaminant transport, impacts of land use change, and many other environmental responses (Beven, 2012). An example of a widely applied model in New Zealand includes the OVERSEER model, which predicts farm scale nutrient losses and requires information on soil properties, including bulk density, saturated hydraulic conductivity, clay content, texture and drainage class (Overseer Support, 2020; Wheeler et al., 2003). Overseer is additionally employed by New Zealand's regional governing bodies, who use it to impose nutrient limits in an attempt to manage diffuse nutrient pollution (Freeman et al., 2016). There is an acute recognition, however, that its effective and socially-acceptable implementation is limited by gaps in our understanding in a number of areas, such as: catchment-scale dynamics; knowledge of historic and current land use practices (such as artificial drainage systems); and local and site-specific data (Parliamentary Commissioner for the Environment, 2018).

Modelling is a necessary tool for the management of water quality and quantity because 1) direct measurement must capture large-scale variation in space, time and context, which quickly becomes prohibitively expensive, and 2) the processes that determine the movement, storage and state of water are inherently complex, and are generally not represented by the limited measurement techniques we have available to us (Beven, 2012). Those available measurements therefore require extrapolation in order to be applied to areas and time scales (e.g., the future) for which we do not have measurements.

There are several hydrological models that include a tile drain component, including, among others, SWAT, HYDRUS-2D/3D and Overseer. Most of these models simulate tile drainage using steady-state flow equations, such as the Hooghoudt, Töksoz-Kirkham, and Ernst equations (Qi & Qi, 2017), which require information about the lateral and vertical hydraulic conductivity of the soil, the soil depth, the drainage network depth and spacing, and the water table position. Koch et

al. (2013) showed that incorporating tile drainage into the SWAT model significantly modified the simulated stream flow constitution, and that the proportion of tile flow contributing to stream flow was strongly dependent on the extent of tile drainage within the various catchments. They suggested that a significant improvement in model quality would arise through more accurate mapping of tile-drained areas. Qiao (2014) simulated tile drainage using the HYDRUS 2D/3D model and tested it against flow measurements from experimental plots. They found that the model simulations performed well on a weekly scale, but predicted water flow poorly at the daily scale. They suggested that soil processes not accounted for by the model, such as the dynamics of frozen soil in winter and desiccation-induced soil cracking in the summer, may have explained some of the discrepancy between simulated and observed data. Tile drainage can be accounted for in nutrient budgeting by the OVERSEER model, and requires information about the proportion of the block that is artificially drained, the drain spacing and depth, subsoil clay content and depth to the slowly permeable layer (Wheeler, 2018). If drain spacing is not known, default values of 20 m for dairy/cattle and 60 m for sheep are used.

Models of soil - water interactions are informed by knowledge of soil physical and hydraulic properties and processes. Such knowledge is gained from a variety of disciplines, including traditional pedology, soil physics and hydrology, the integration of which is necessary for linking phenomena that occur at point-, pedon-, catena-, and catchments scales (Lin, 2003; Lin et al., 2006). Key to this bridging of scales are detailed analyses of landscape heterogeneity (e.g., spatial and temporal soil variability) that can answer the question of 'why' such heterogeneity exists (McDonnell et al., 2007). In the loess-derived soils of Southland, for example, does the variable genesis of multi- and unisequal soils impart a signature on soil properties that are of relevance to hydrological functioning? Such information is a critical component of accurate soil mapping which, in turn, inform catchment-scale models.

Models are challenged when they do not align with reliable data, prompting reassessment of the assumptions, governing equations and paramaterisation on which a model is based (Beven, 2012). Reliable measurements, therefore, play a critical role in testing and developing our understanding of key hydrological processes and those properties that are responsible for their regulation.

2.11 Summary

Southlands agricultural sector contributes significantly towards the New Zealand economy, owing in part to extensive mole and tile drainage. This practice has brought great improvements in

agronomic productivity but has also contributed towards deterioration of regional freshwater quality. Mitigation will require an interdisciplinary, integrated approach that will rely on understanding the hydrological response dynamics of these important agricultural landscapes. Research areas identified as key to the development of such an holistic understanding in Southland include:

- Controls on soil-landscape heterogeneity
- The extent and characteristics of artificial drainage networks
- Soil hydraulic properties in artificially drained landscapes
- Water fluxes and their controls in artificially drained landscapes
- Spatiotemporal dynamics underpinning landscape contributions to freshwater recharge

The following research chapters will further develop and define these ideas as specific research objectives and/ or questions, before attempting to address them by way of experimental analysis.

Chapter 3

Characterisation of the vertical and lateral subsurface heterogeneity in loess soils using qualitative (morphological) and quantitative (k-means) techniques

3.1 Abstract

Landscapes formed in loess may have complex subsurface stratigraphy that produces distinctive patterns of soil variability related to the exhumation of buried loess sheets on hillslopes. Hillslope soils may be composite, including subsoil horizons inherited from paleosols of buried loess sheets. Additionally, the paleosols themselves may be overprinted by contemporary pedogenesis (welded soils). However, identifying paleosol-derived horizons has an element of subjectivity, and even when identified correctly, their relevance to characterisation of soil pattern and properties is subject to debate. In this study, a dissected, loess-mantled downland with multiple thin loess sheets was surveyed using auger boring and soil pit methods in order to develop a conceptual understanding of the landscape evolution and the nature of the loess sheet exposure within the soil mantle. In addition, soil samples were collected (n = 66) from five depths and each sample was characterised by 17 physical, hydraulic and chemical soil attributes (i.e., sand, silt, clay, particle density, dry bulk density, porosity, macroporosity, air capacity, saturated hydraulic conductivity, field capacity, readily available water content, available water content, organic carbon, total nitrogen, carbon-nitrogen ratio, cation exchange capacity and phosphorus retention). Principal component analysis (PCA) was conducted on the attribute dataset in order to test the robustness of qualitative soil description and classification in identifying the most important sources of attribute variability. Additionally, the *k*-means algorithm was employed to assess how well an objective, quantitative method of horizon classification aligned with qualitative horizon designation. Results of the detailed soil stratigraphic study indicated that drainage basin hillslopes cut across four buried loess sheets that had been laid parallel to a flat-lying alluvial gravel. Soils on the interfluves formed entirely in the uppermost loess sheet (unisequal), while hillslope soils were multisequal, comprising upper soil horizons formed in mobile colluvial material overlying paleosol horizons of buried loess sheets. The PCA results indicated that morphologically-assigned soil horizons following traditional classification methodology was able to capture the most significant variation in soil attributes, especially with regard to the Ap, A/B, Bw horizons (i.e., the vertical anisotropy of soil) and a 2B horizon, which corresponded to the alluvial gravels. The deeper subsoil of all soils was occupied

by a horizon of fragic qualities (dense and brittle). On the interfluves this horizon manifested as a Bx horizon formed in the uppermost loess sheet, whereas in composite soils on hillslopes it included horizons inherited from paleosols in buried loess sheets. The PCA showed that the Bx horizon and the subsoils of composite soils were less clearly discriminated using morphological methods. The *k*-means clusters reflect sensible groupings that are easily explained by pedogenic processes and gave almost equivalent results to the conventional morphological horizon designation, with $k = 6$ able to identify the Ap, A/B, Bw and 2B, as well as some, but not all, of the morphologically described soil stratigraphy in the loess. Vertical anisotropy, resulting from top-down pedogenesis, appeared to be the dominant effect in these soils; however, the hydraulic properties were also influenced by loess stratigraphy. These results demonstrate that subjective (qualitative/morphological) horizon designation is effective at partitioning variability in important soil properties. Qualitative and quantitative methods of horizon designation identify greater complexity in the side slopes of the catchment relative to the interfluves, demonstrating that a more refined understanding of the soil-geomorphology of loess-mantled downlands may lead to better soil-landscape models, more accurate soil maps and better characterisation of soil variability.

3.2 Introduction

Loess-mantled landscapes are found across the planet, including in important agricultural regions of North and South America, Central Asia, China, Europe and New Zealand (Catt, 2001; Pye, 1984, 1995). Allocation of limited freshwater resources, as well as their contamination by nutrients, sediments and pathogens are major concerns in these landscapes (Gates et al., 2011; Langer et al., 2020; Lin & Wei, 2006; O'Geen et al., 2002; Reuter et al., 1998). The management of freshwater relies heavily on environmental models to simulate the water balance, the scale and source of contaminants, the mechanism of contaminant transport and the effect of mitigation strategies or land use change (Koch et al., 2013; Leng et al., 2020; Qiao, 2014; Wheeler et al., 2003). Accurate mapping of soil variability is essential information for upscaling soil hydraulic information from the pedon to the catchment scale and producing appropriate models of landscape hydrology for land management applications (Lin, 2003). Incorporating well-resolved soil spatial variability can significantly improve simulations of spatial and temporal soil moisture patterns (Lin et al., 2006).

Loess mantles often contain multiple buried loess sheets of variable depositional age, with complex soil stratigraphy that has developed through phases of upbuilding pedogenesis during glacial periods and top-down pedogenesis during interglacial periods (Alloway et al., 2018; Almond & Tonkin, 1999). Patterns of soil variability may be produced in loess landscapes depending on the interaction between loess sheet thickness and relief (Hughes et al., 2010). Where loess sheets are thick and relief is small, the surface soil may be formed entirely in the uppermost loess sheet and its transported and deposited facies. In such cases, soils will have relatively low variability and can be considered as a unisequal, or single parent material, soil catena (Milne et al., 1936; Webb & Burgham, 1997). Where loess sheets are thinner, or relief is greater the hillslopes may crosscut buried loess sheets and their associated paleosols, increasing the degree of complexity of the soil pattern. In this circumstance, the upper solum forms in a colluvial biomantle (Borella et al., 2016; Johnson, 1990; Johnson et al., 2005) that overlies horizons inherited from paleosols of varying character. The latter may be overprinted by contemporary topdown pedogenesis, forming welded (Ruhe & Olson, 1980) or composite (Morrison, 1978) soils. This is a situation akin to a multiple parent material soil catena (Milne et al., 1936) involving multisequal (polygenetic) soils.

Traditional semi-detailed and detailed soil survey represents soil variability by way of the spatial distribution of soil taxa, e.g. soil series, defined at lower categories of hierarchical soil classification

systems. Soil series or taxonomic equivalents rely heavily on soil morphological properties for their definition, including the kind, and sequence, of horizons (Soil Science Division Staff, 2017). In loess landscapes, multisequal soils, whose subsoils show inheritance of paleopedological features of buried loess sheets, are sufficiently morphologically, physically, chemically and mineralogically distinct that they may warrant definition as separate soil series (Jacobs & Mason, 2007; Negri et al., 2021; Olson, 1997 ; Presley et al., 2010; Ruhe, 1956).

In New Zealand, loess is a common soil parent material (Jochen Schmidt et al., 2005), and soils with a loess a component cover approximately 60 % of the country (Bruce et al., 1973). Loess mantles with a thickness of at least one metre cover over 10% of the country's land surface (McCraw, 1975), and these are commonly multi-layered (Almond & Tonkin, 1999; Bruce, 1973a; Hughes et al., 2010; Roering et al., 2004). However, no soil maps in loess landscapes explicitly recognise associations of unisequal and multisequal soils resulting from thin loess sheets, or differential erosion and exhumation of buried loess sheets on hillslopes. This may be because much of the loess soil-landscapes form in a thick upper loess sheet (Webb & Burgham, 1997) where multisequal soils are rare. However, in the loess-mantled downlands of Southland, there are multiple thin loess sheets and composite (polygenetic soils) have been recognised (Bruce, 1996).

In this study we investigate the morphology and spatial distribution of soils on a loess-mantled downland in Southland where the relief is often greater than the combined thickness of the loess mantle. In such a landscape the likelihood of multisequal soils on hillslopes is high. The aim is to characterise the spatial distribution of soils to determine if 1) multisequal soils are an important component of the soil-landscape and 2) if their recognition as distinctive taxa would improve characterisation of soils in a way that would facilitate better soil and environmental management. To achieve our aim we first characterise the loess stratigraphy and develop a conceptual model of how loess sheets may outcrop on hillslopes. We use this understanding to define soil horizons that capture the soil stratigraphy and multisequal nature of soils when present. We then apply multi-variate statistical techniques to examine how morphologically defined horizons partition the variability of a suite of accessory properties. Lastly, we use the quantitative evaluation of morphologically defined horizons to assess if multisequal soils warrant recognition as distinct taxa that should be recognised within soil mapping units. The study sits within a larger project aiming to characterise the variability of soils and their influence on the hydrology of a mole and tile-drained agricultural landscape on the loess-mantled downlands. Accessory properties were selected accordingly.

3.3 Methods

3.3.1 Study area

The study site was located on a gently dissected, loess-mantled downland 30 km north-west of Invercargill (46°14'02" S 168°11'27" E) in Southland, New Zealand (Figure 3-1 & Figure 3-3). Climate in the area is temperate, and long-term average annual precipitation is 1,244 mm (Thornbury; NIWA, 2021). The site is a 3.95 ha zero-order unchanneled basin, with elevation ranging between 39 – 46 metres above mean sea level (NZVD 2016), and slope varying from 0.2° on the interfluves, to 7.9° on the basin side slopes. The basin comprises a primary hollow, aligned ENE, and a secondary hollow, aligned WSW (Figure 3-3), which drain east into the Waianiwa Stream. Native vegetation was cleared in the late 1800's and the site has since been predominantly used for sheep grazing. The soils across the catchment are mapped as uniform Argillic-fragic Perch-Gley Pallic (NZSC; Hewitt, 1998), or Aeric Kandiaqualf soils (USDA; Soil Survey Staff, 2014) of the Pukemutu soil family (Manaaki Whenua Landcare Research, 2022). These soils are characterised by the presence of a fragipan surface at between 60 and 90 cm depth, which restricts drainage.

A 4-metre digital elevation model (DEM) for the area was derived from Real Time Kinematic (RTK) GPS survey using a Leica Viva GS15 GNSS antenna coupled with a Leica CS15 field controller. The GPS data were cleaned to remove obviously erroneous points. Empirical Bayesian Kriging (from the ArcGIS Geostatistical Analyst toolbar) was used to generate the DEM. This interpolation method was able to handle the multiple coincident data points by assigning the mean value of the coincident points to their respective locations (Esri, 2021).

3.3.2 Loess deposits in Southland

The most well-known loess deposit in Southland is the Stewarts Claim Formation, a 6 metre stack of aeolian sediments overlying Waikaka Quartz Gravels (Wood et al., 1956). A complete section of the loess formation is exposed in a hillside at a disused gold mining site ("Stewarts Claim"), 4.5km east of Waikaka on the Southland-Otago regional boundary. This type section was described in detail by Bruce (1973a), who identified four to five major loess sheets, the upper boundary of each buried sheet being defined by a paleosol (Figure 3-2). The loess members were termed Yellow A, Yellow B, Brown A, Brown B, and Brown C, in order of increasing depositional age. The paleosols at the surface of each buried loess sheet did not usually comprise a

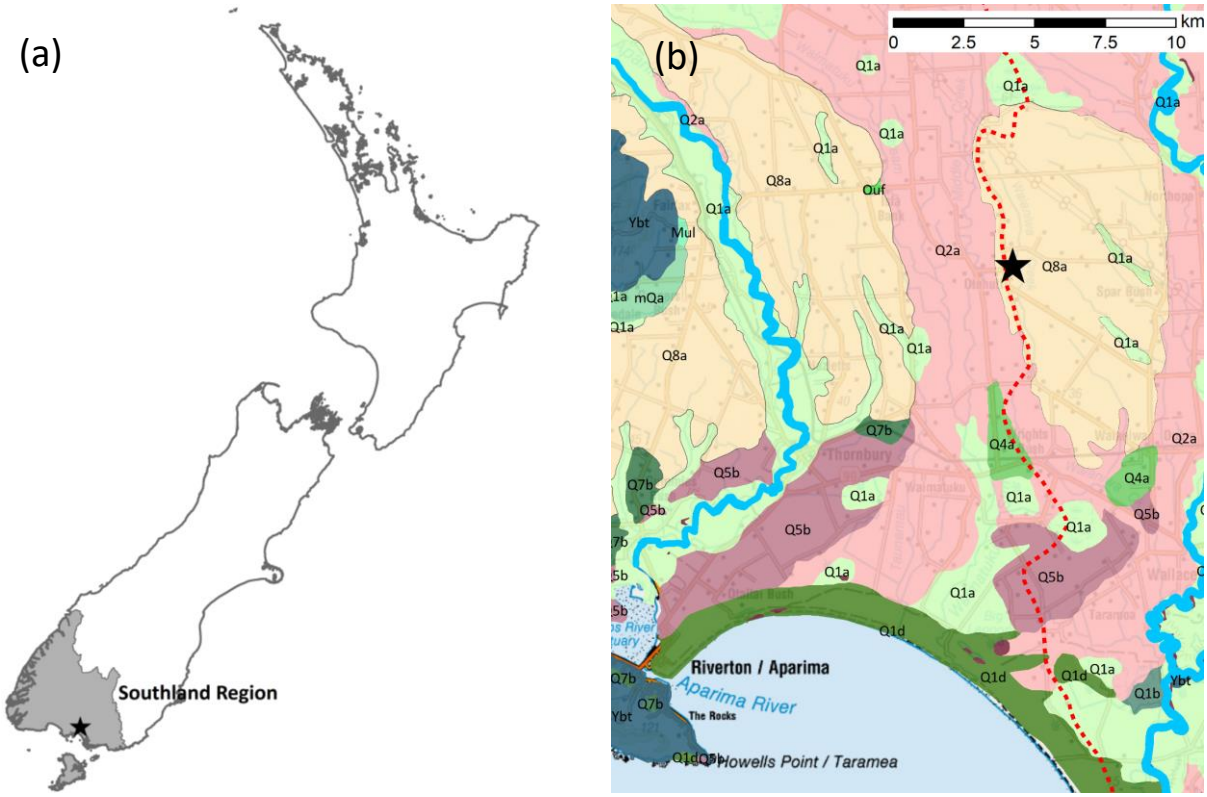

Figure 3-1. The field site (black star) as it lies (a) within the Southland Region of New Zealand and (b) relative to the underlying geology, specifically the Quaternary gravels (Q), which are shown by their relative age from youngest (Q1) to oldest (Q8); numbers refer to inferred marine oxygen isotope stages. The field site is located on the western edge of a loess-mantled glacial outwash terrace (Q8a; mid-Pleistocene; Turnbull & Allibone, 2003), which forms a section of the boundary (dotted red line) between two of the region's major watersheds, the Aparima to the west and the Oreti to the east.

complete solum, but instead resembled the fragic horizon of the subsoil in modern day soils and often had a platey structure. Bruce hypothesised that the A, A/B and B horizons of each loess sheet were eroded before deposition of the successive layer of loess, a process he termed "pedosphere stripping". On rolling downlands underlain by gravels, pedosphere stripping is indicated by a discontinuous line of small quartz pebbles found at paleosol surfaces, presumably sourced from higher elevation gravel exposures.

The Yellow loess member is the uppermost loess sheet and has as average thickness of two metres, with a 1-3 m range (Bruce, 1973a). It is often divided into Yellow A and Yellow B loess members, separated by a minor paleosol. The paleosol is sometimes difficult to distinguish, in which case it is mapped as an undifferentiated Yellow loess member. Yellow A represents the

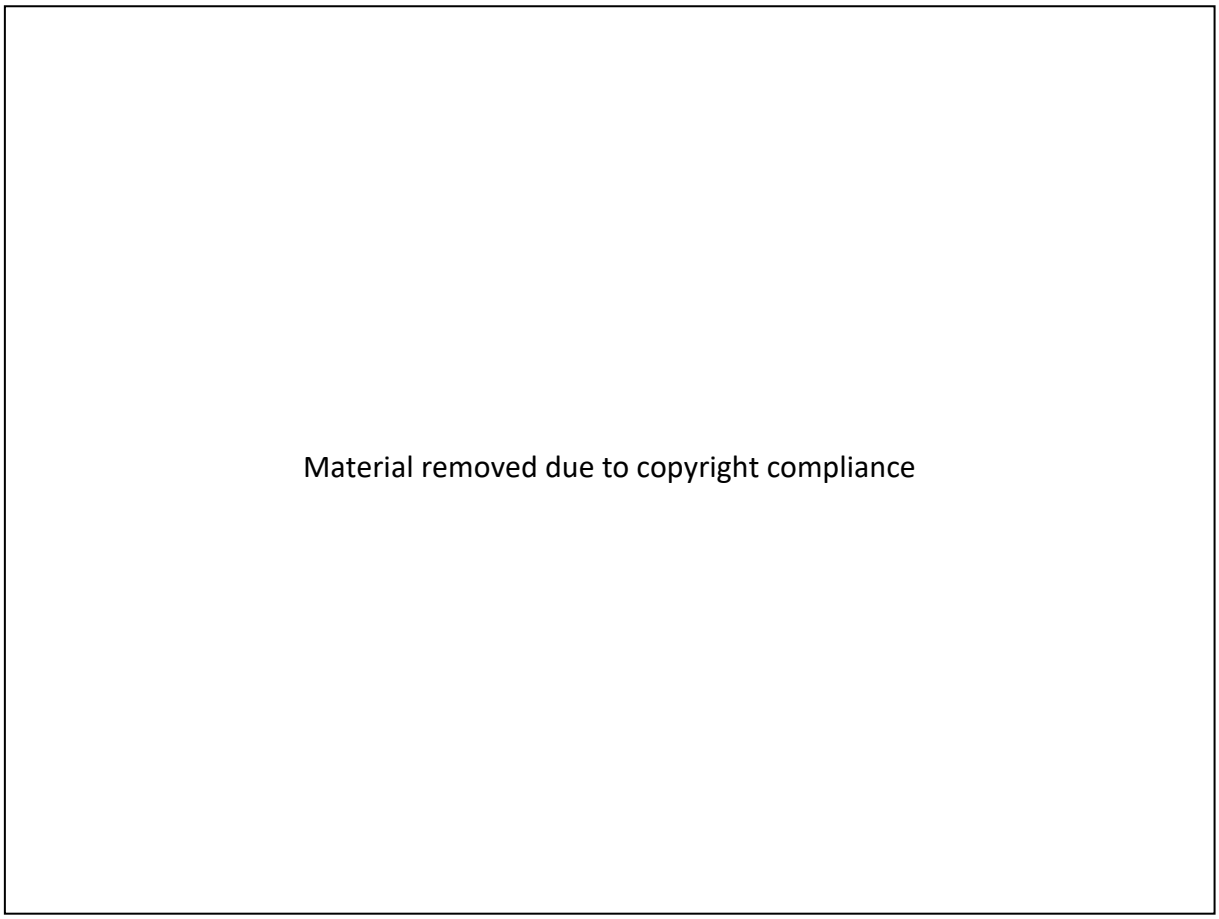

Figure 3-2. Description of the Stewarts Claim Formation (left) by Bruce (1973a), with all loess members displayed in an upper downlands section (right), near Romahapa. The tape has been placed on the Brown A loess member. Platey/blocky structure of paleosols and anastomosing of gammate colour patterns in horizons immediately above paleosols was noted by the surveyor. Photograph by Q. Christie, sourced from Bruce (1973b).

contemporary surface soil. A typical morphological feature of Yellow A is the dense subsoil, which is often associated with fragic horizons in Pallic soils, or firm horizons in Brown soils.

Yellow B is similar in structure, compaction and colour to the overlying dense subsoil of Yellow A, but in regions with wetter climates it has a prominent, strongly mottled "orange" horizon at its base. Gleying extends down vertical gammate fissures, which arise in the Yellow A and anastomose in the orange horizon. The orange horizon is likely to have evolved due to the impermeable nature of the underlying Brown Loess, and it presents a reliable marker for differentiating the younger Yellow Loess Members from the older Brown Loess Members.

The three Brown Loess Members present similar morphology and have an identical sequence of horizons, which are characterised by structure and compaction. It is the repetitive nature of the morphology that supports the characterisation of three distinct loess layers within the Brown Loess

Members. Commonly, the break between the layers may additionally be marked by a discontinuous layer of quartz pebbles. Brown C is much more weathered than both Brown A and B and is generally only found at the base of the thickest deposits on the highest surfaces. Brown A and B have an average thickness of 1.2 m, and Brown C is generally less than one metre thick.

This stratigraphy is exposed in many sites throughout Southland, although in most places the sequence is incomplete, with the lower brown members often missing. A complete sequence has previously been identified 25 km north-west of the field site at Raymonds Gap (46° 5'17.45"S, 167°54'54.62"E; Bruce et al., 1973).

3.3.3 Loess mantle investigation & soil description

Nineteen auger bores (Figure 3-3) were drilled by hand auger through the loess to the underlying gravels (≤ 4.5 m). The sites were chosen to cover the eastward draining basin in detail. Additional points were sampled to the north of the basin, crossing the interfluve and connecting with a deep road cutting across the interfluve that exposed the loess and underlying gravel. The soil extracted from each auger drilling was logged according to depth (cm) and described, where possible, for matrix colour (Munsell Colour Charts), redoximorphic features, texture and consistence following Milne et al. (1995). From this information, horizons were designated for the full depth of the drilling using the horizon notation of Milne et al. (1995). The underpass exposure was also described. Loess sheets were identified on the basis of buried soils that showed analogous sequences of horizons to the surface soil (excluding the A horizon), specifically the presence of a strongly redox-mottled clay-rich horizon with or without Mn nodules over a more uniformly coloured brittle horizon (Btg/Bxg). Loess sheets were labelled from L1 to L*n*, with L1 being the uppermost sheet. Depths were referenced to the surface elevation (derived from the DEM). Elevation of loess sheet boundaries relative to the vertical datum were used to interpolate between drill sites in order to develop a conceptualisation of the loess stratigraphy and surface topography of the underlying gravels.

Six soil pits, indicated in Figure 3-3, were excavated in August 2018, each adjacent to a previously described auger drilling site. Two pits were located on the interfluve (IN) at the highest point of the basin. Further pits were located on the head slope (HS) of the main basin, the north-facing planar (pSS) and slightly divergent (dSS) side slopes, and a nose slope (NS) separating the

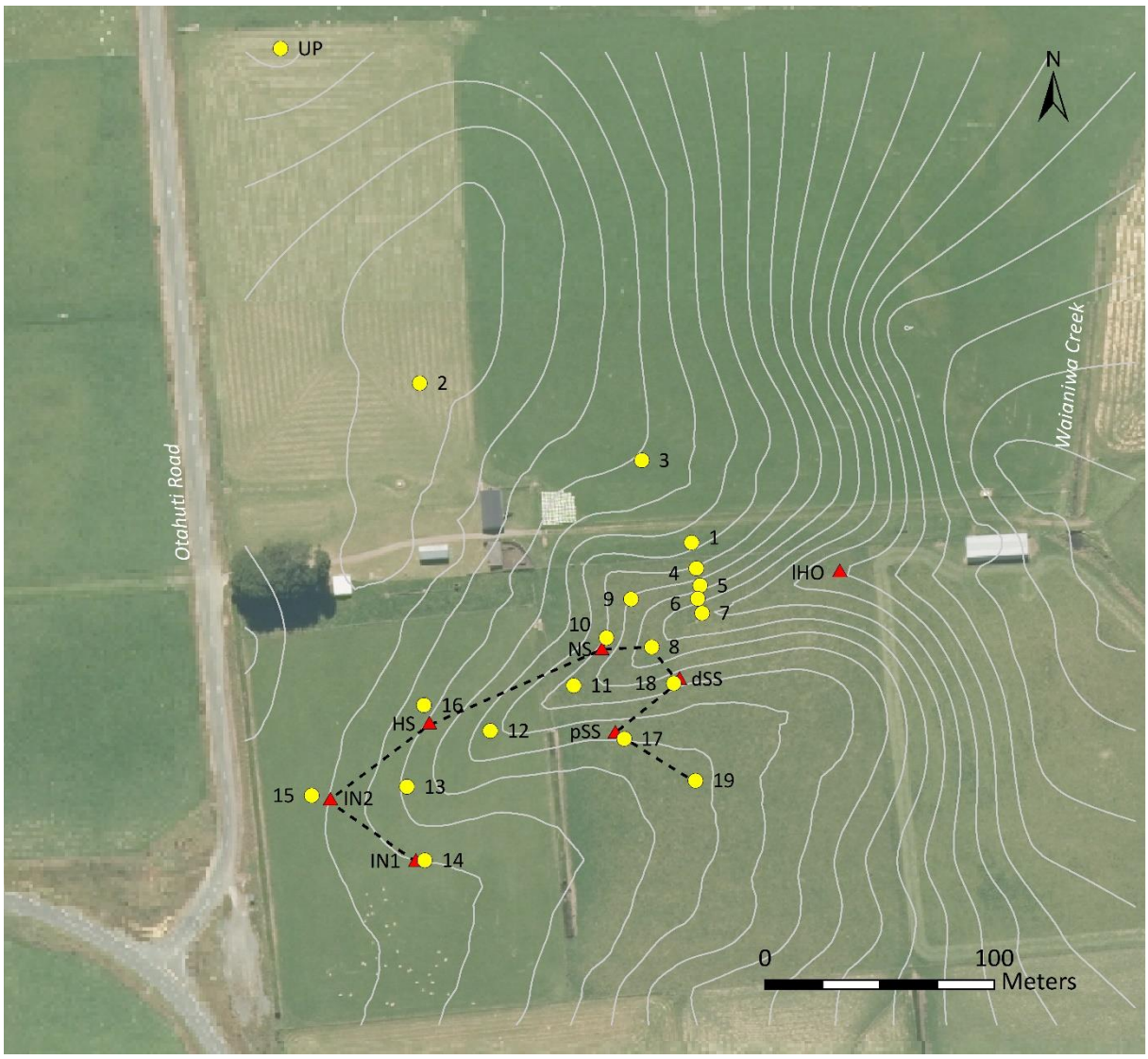

Figure 3-3. Study site image showing the location of the soil pits (red triangles) and auger bores (yellow circles). Soil pits are labelled according to their landscape position: IN1 and IN2 sit on the catchment interfluves; HS is on the northern side of the head slope of the main basin; pSS is on a north-facing planar side slope; dSS was on a slightly divergent side slope with north-west aspect; NS was on a nose slope that separated the south-west oriented main basin from a north-west trending secondary basin. The lowest soil pit was in the hollow (lHO) at the mouth of the basin. Loess stratigraphy revealed by auger bores (1 to 19), is complemented by a deep exposure on the sides of an underpass excavated through the interfluve at UP after the aerial photo was taken. The gully transect is identified by the dashed black line. Contour lines of 0.5 m interval are also displayed; however, the accuraccy of the DEM north of site 2 is low and there is no DEM data for west of Otahuti Road. The terrace edge follows the road and is c. 15 m higher than the plains to the west.

south-west oriented main basin from the north-west trending secondary basin. One profile per pit were described to 100 cm following Milne et al. (1995) and Hewitt (1998). A seventh pit, not located on the auger transect, was excavated at the basin hollow (lHO). Using the conceptualisation of loess stratigraphy developed from the auger survey, the soil profile horizons could then be designated the ID of the loess sheet in which they had formed (i.e., L1 – L*n*, etc.). A transect (Figure

3-3) was selected that combined sites with both auger and soil profile descriptions and could capture the subsurface morphology of the eastward-draining basin. Information on the stratigraphy of the underlying gravels was obtained from local bore logs owned by the Southland Regional Council.

3.3.4 Soil description, sampling and analyses

Samples (two cores [7.5 cm depth x 10 cm diameter and 3 cm x 5 cm] and one bagged sample) were collected from depths of 15, 30, 45, 60 and 75/85 (dependent on the depth of the fragipan) cm down each of the 12 profiles located on the transect. Extra samples were collected from pSS at depths of 67.5 and 90 cm. The 13th profile, located at lHO, was only sampled at 15 and 45 cm. The samples were analysed for the physical, hydrological, and chemical properties shown in Table 3-1. These properties are expected to be correlated with physically and morphologically defined soil horizons. For example, organic carbon provides an indication of the humified organic matter characteristic of an A horizon; sand, silt and clay content vary according to vertical gradients of weathering and clay translocation; and porosity, dry bulk density and K_{sat} reflect the vertical gradients of bioturbation, and structure grade and type.

In order to compare the qualitative soil descriptions with the quantitative data, samples collected from 15 and 30 cm were assigned Ap and A/B notation, respectively (independent of the loess sheet), reflecting their morphologically assigned horizon notation. Samples taken from B horizons in the uppermost loess sheet (L1) were separated into Bw and L1 (Bx). All other samples were identified by the loess sheet in which they had formed (i.e., L1 – L*n*, etc.), with most of these horizons satisfying diagnostic criteria of fragipans/brittle B horizons (Bx). Where relevant, samples that appeared to come from the highly weathered Quaternary gravels were labelled 2B to identify the change in lithology. These designations recognised the most important qualitative information by capturing the morphological variation related to contemporary soil processes and the paleopedological features inherited from buried loess sheets forming the lower solum of multisequal soils on some hillslope elements.

3.3.5 Principal component analysis

A total of 66 data points containing information on the physical, hydraulic and chemical data collected from each depth within each of the 13 soil profiles were used to conduct a principal component analysis (PCA). PCA attempts to increase interpretability by reducing the

Table 3-1. The physical, hydrological and chemical attributes analysed from each of 66 samples taken from 13 soil profiles. The abbreviation used to describe each attribute is also given, as well as the method used for analysis.

Soil Property	Attribute	Abbr.	Method
Physical	Sand (%)	s	(Claydon, 1989)
	Silt (%)	z	(Claydon, 1989)
	Clay (%)	c	(Claydon, 1989)
	Particle density (g cm^{-3})	PD	(Gradwell & Birrell, 1979)
	Dry bulk density (g cm^{-3})	DBD	(Gradwell & Birrell, 1979)
	Porosity (%)	Por	(Gradwell & Birrell, 1979); 0 kPa
	Macroporosity (%)	MPor	(Gradwell & Birrell, 1979); 0 to -5 kPa
	Air capacity (%)	AC	(Gradwell & Birrell, 1979); 0 to -10 kPa
Hydrological	Saturated hydraulic conductivity (mm h^{-1})	K_{sat}	(Fernández-Gálvez et al., 2021)
	Field capacity (%)	FC	(Gradwell & Birrell, 1979); -10 kPa
	Readily available water content (%)	RAW	(Gradwell & Birrell, 1979); -10 to -100 kPa
	Available water content (%)	AWC	(Gradwell & Birrell, 1979); -10 to -1500 kPa
Chemical	Organic carbon (%)	OC	(Leco, 2003) and (Metson et al., 1979)
	Total nitrogen (%)	TN	(Leco, 2003) and (Metson et al., 1979)
	Carbon-Nitrogen ratio	CNr	Calculation
	Cation exchange capacity (cmol[+] kg^{-1})	CEC	(Blakemore et al., 1987)
	Phosphorus retention (%)	PR	(Saunders, 1965)

dimensionality within a dataset and identifying linear combinations of the original variables that describe the greatest proportion of the variation in the dataset. These linear combinations are assigned as new variables, or principal components. The data were scaled in R (R Core Team, 2019) by subtracting the variable mean and dividing by the standard deviation. PCA was carried out on the scaled data using the 'prcomp()' function from the 'stats' package (version 4.0.4). The efficacy by which morphologically defined horizons discriminated the quantitative soil properties was assessed by plotting samples identified by their corresponding soil horizon in PC biplots.

3.3.6 K means clustering

K-means clustering was conducted on the same 66 data points used in the PCA. The *k*-means algorithm is an unsupervised machine learning technique that aims to find the optimal clustering of *n* observations into *k* groups. Squared Euclidean distance is used as a measure of dissimilarity to minimise total within-cluster variation, such that each observation then belongs to the *k* cluster with the nearest mean or cluster centroid. The *k*-means algorithm was employed here to produce

objectively defined clusters using soil physical, chemical, biological and hydrological data. The cluster soil vertical distribution was then compared with the morphologically defined soil horizons. The soil physical, hydrological, and chemical properties were scaled individually using JMP version 10 software (SAS Institute Incorporated, 2012) into $k = 3$, $k = 4$, $k = 5$ and $k = 6$ clusters.

3.4 Results

3.4.1 Loess stratigraphy

The depth of the loess to the underlying Quaternary-age gravels ranged from 4.3 m on the interfluves (auger 15; Table 3-2) to 0.7 m on the south facing side slope below the convergence of the two basin axes (auger 6; Appendix A.1), which was also the steepest slope within the basin. The loess mantle was also thin (0.8 m) on the nose slope (auger 10; Table 3-2) between the two basin gullies and in the lower parts of the hollow (0.8 m; auger 7; Table 3-2), although it got progressively thicker moving up the hollow.

Up to five thin loess sheets were identified in the thickest deposits (Figure 3-4), which showed morphological consistency with the five loess sheets described by Bruce (1973a) in other areas of Southland (i.e., Yellow A [L1], Yellow B [L2], Brown A [L3], Brown B [L4], Brown C [L5]). The underpass provided the best exposure of the loess mantle although all five loess sheets were not preserved (Plate 3-1). Loess sheets were distinguishable in the exposure by the repetition of a couplet comprising a mottled/concretion-rich horizon overlying a fragic horizon. Platy structure was observed within the concretion rich zone at the surface of L4 (Plate 3-1). The underlying gravels were highly weathered and of a similar colour in the UP exposure to the loess mantle. All five loess sheets were identifiable on the interfluves, but their presence in other parts of the catchment varied according to landform and depth of the loess (Table 3-2).

The relief on the surface of the gravels was more subdued than that of the ground surface (Figure 3-4). Logs of local bores obtained from the Southland Regional Council pointed towards the presence of an aquitard between approximately 28 and 32 masl, which explained the presence of groundwater in a well just 8 m below the highest part of the landscape (the interfluves; a), and also the artesian nature of a bore (b) located in the lowest part of the landscape (by the Waianiwa Stream; c). It is probable that the unconfined aquifer provides baseflow for the Waianiwa Steam. This information was included in the conceptualisation, as it was of relevance for the wider study.

Table 3-2. Summary of soil stratigraphy characteristics at each of the eight auger sites along the gully transect. The associated soil pit ID is shown in brackets. Loess (L) sheets are labelled from 1 to 5. Apparent re-worked loess (rwL) from one, or more, younger loess sheets is also identified; for example, rwL1/L2 describes re-worked loess sheet 1 over a buried soil formed in loess sheet 2.

Auger Bore ID (Site ID)	14 (IN1)	15 (IN2)	16 (HS)	10 (NS)	8	18 (dSS)	17 (pSS)	19
Landform	Interfluve	Interfluve	Head slope	Nose-slope	Hollow	Divergent side slope	Planar side slope	Interfluve
Depth to fragipan (Bx)	0.60 m	0.60 m	0.70 m	0.40 m	NA	0.80 m	0.60 m	0.65 m
Depth to gravels	3.29 m	4.27 m	2.55 m	0.83 m	0.90 m	1.33 m	2.58 m	3.01 m
Number of loess sheets	4-5	5	4-5	2-3	1	3	3-4	5
Loess sheets in top 1 m	L1	L1	rwL1/L2?	rwL1/L4/ L5	rwL	rwL1/ rwL4/L5	rwL1/L2/ L3	L1
Loess sheet of the subsoil	L1	L1	L2?	L4 and L5	NA	L5	L2 and L3	L1

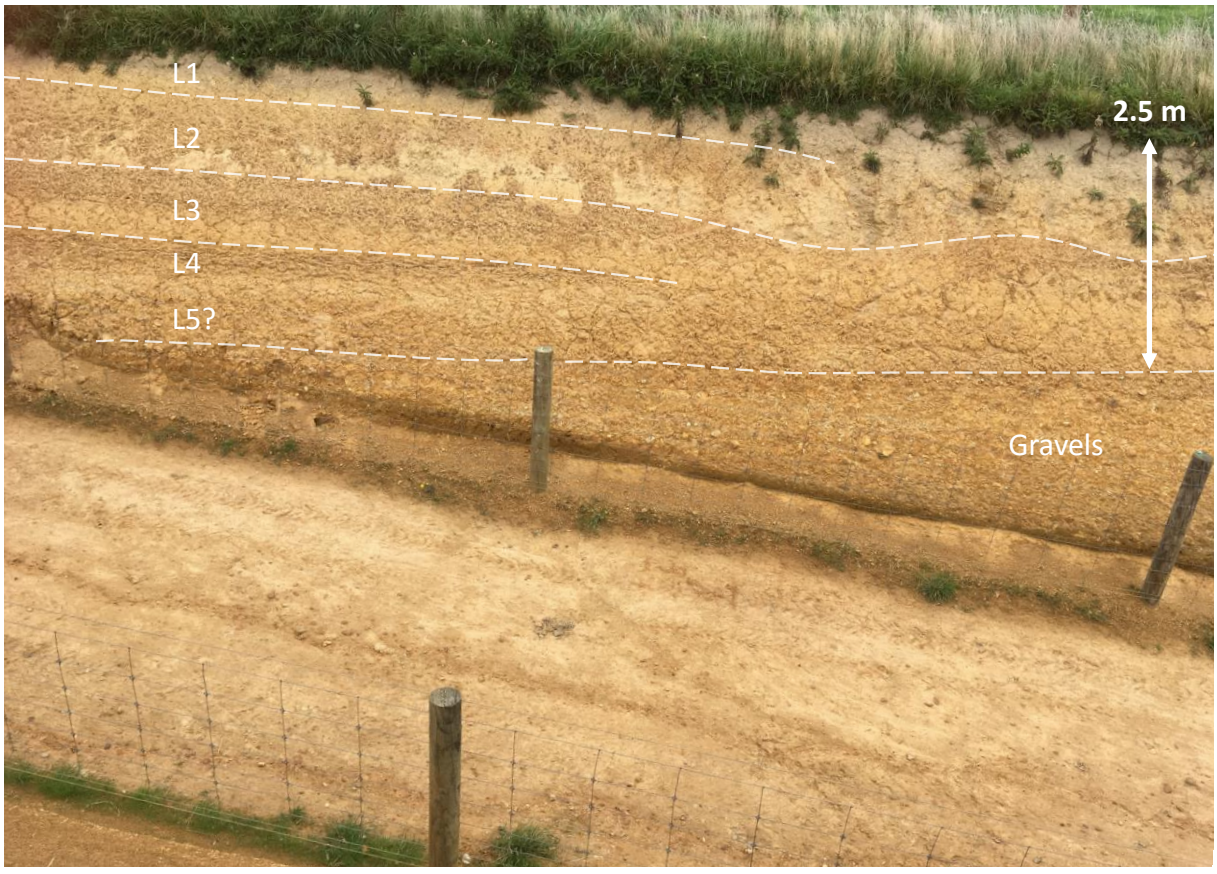

Plate 3-1. Exposure cut into the western terrace edge during construction of a road underpass (UP). The description for UP was for the profile under the 2.5 m arrow. Platy structure appears to make up the surface of L4. Highly weathered gravels can be seen at the base of the exposure and they are overlain by c. 2.5 - 3 m of loess. Stratigraphy is apparent in the loess mantle (L1 – L5), identified by the dashed lines.

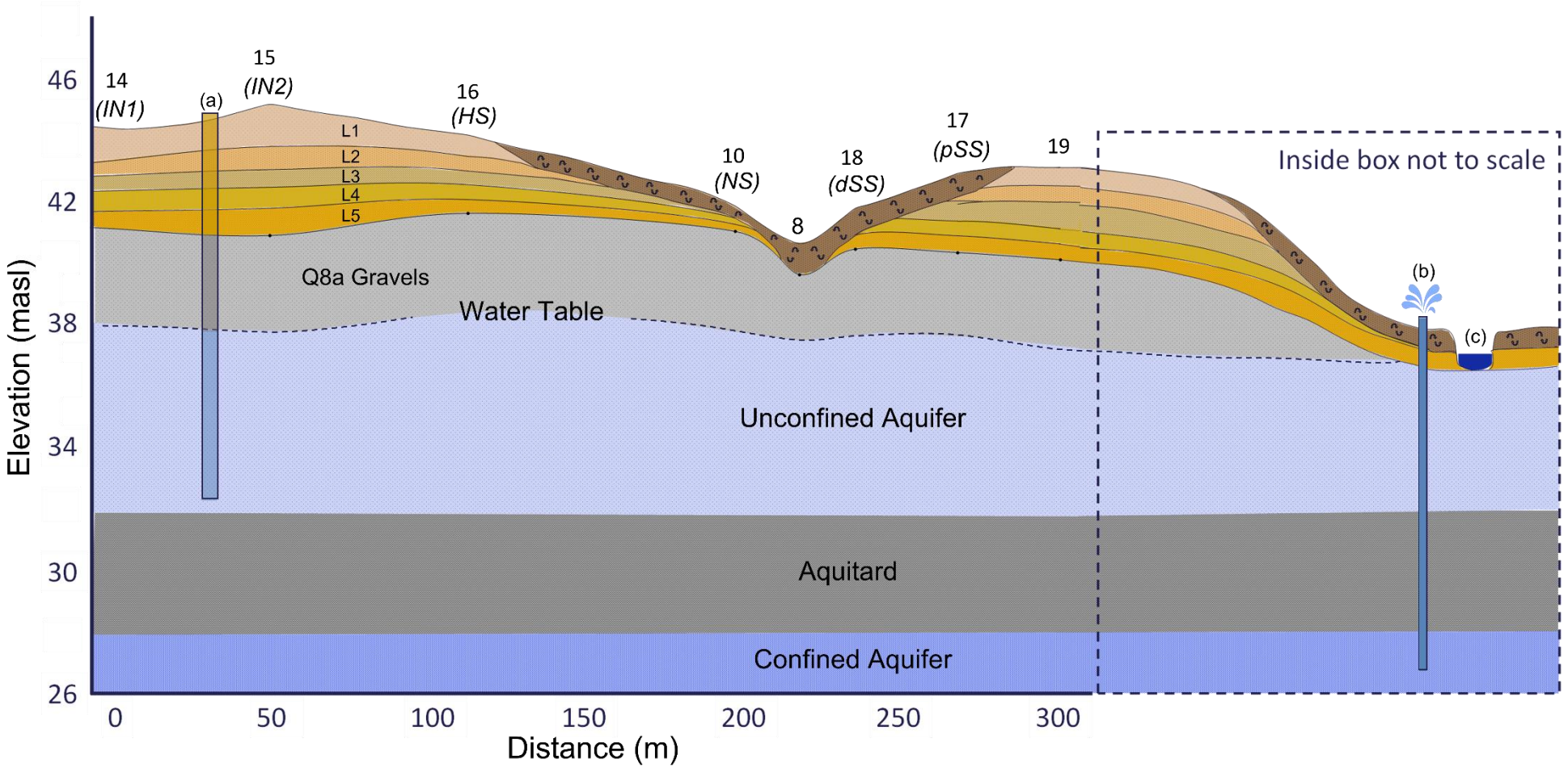

Figure 3-4. Scaled conceptualisation of the loess stratigraphy underlying the drainage basin, developed from information obtained from 19 auger drillings, 8 profile descriptions and bore log data analysis. The position of the cross-section transect in the landscape is indicated in Figure 3-3. The basin hollow drains into the Waianiwa Stream (c); displayed with vertical, but not horizontal accuracy (inside dashed square). Five loess sheets (L1 – L5) overly Quaternary (Q8a) gravels. Overlying the hollow is a colluvial biomantle (brown layer, rotating arrows). The relative positions of eight drilling sites are indicated on the surface, including augers 14 (soil pit IN1), 15 (IN2), 16 (HS), 10 (NS), 8, 18 (dSS), 17 (pSS) and 19. The relative position of an open concrete well (a) is also shown, as well as an artesian bore (b).

3.4.2 Soil profile descriptions (top 100 cm)

Surveying of the soil to 100 cm identified an association of imperfectly-drained Mottled Fragic Pallic (PXM) soils generally located around the periphery of the drainage basin, and imperfectly-drained Mottled Firm Brown (BFM) soils, generally located on the slopes adjacent to the basin axis (NZSC; Hewitt, 1998). Soils changed from Mottled Orthic Brown (BOM) soils in the lower basin hollow to Mottled Fragic Pallic (PXM) in the head of the basin hollow. A tile drain was installed in the lower to mid hollow, and was overlain by an anthropogenic mix of predominantly topsoil mixed with subsoil material.

Photographs of one profile from each of the seven pits are shown in Plate 3-2, as well as the soil sample location and its associated horizon ID. On the hillslopes and interfluve, topsoil depth averaged 25 cm, whereas in the floor of the hollow it extended down to 55 cm below the surface. Most of the surveyed area contained a dense and brittle fragipan, the surface of which ranged in depth between 40 and 90 cm (i.e., the nose slope [NS] and divergent side slope [dSS], respectively). No fragipan was evident in the base of the lower hollow; however, beneath the tile drain, the soil was dense and clayey.

With respect to the loess stratigraphy identified from auger surveying (Figure 3-4), soils on the interfluve (IN1 and IN2) were formed in the uppermost loess sheet and shared similar morphology (Plate 3-2a and b). Their fragipan, formed in the same loess sheet, was dark and had a weathered and irregular surface. The soil at the head slope (HS) had a bright orange fragipan whose upper boundary was highly occluded, which was labelled as buried loess sheet L2 based on how the inferred loess stratigraphy intercepted the hillslope (Plate 3-2c). Soils on the slopes (pSS, dSS and NS) appeared to be formed in a colluvial biomantle of reworked loess from L1 and possibly underlying loess sheets over a fragipan formed in *in situ* older loess sheets (Figure 3-4). The fragipans formed in older loess sheets had smooth and abrupt upper boundaries, and, with the exception of the shallow profile on nose slope, tended to be deeper than on the interfluves (Plate 3-2d – f). The hollow was primarily composed of reworked deposits (Plate 3-2g).

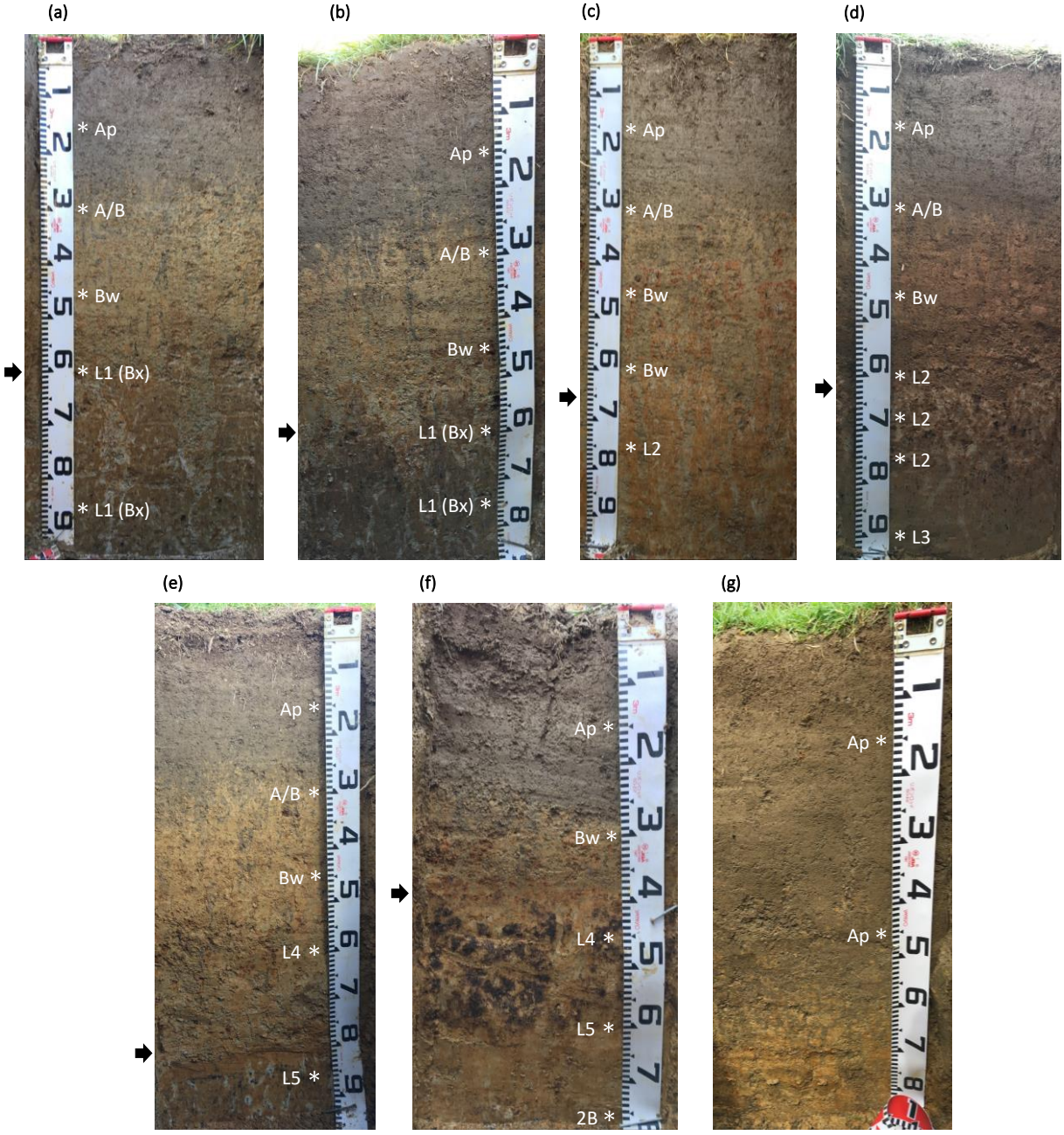

Plate 3-2. Soil profiles from the highest to the lowest part of the study site, including sites (a) IN1, (b) IN2, (c) HS, (d) pSS, (e) dSS, (f) NS and (g) lHO. The arrows show the surface of the fragipan, if present. The sampling points for each profile are represented by an asterisk, with each point labelled according to the loess sheet in which it presides, based on information obtained from the auger survey of the loess stratigraphy. The Ap and A/B (topsoil) horizons are labelled separately from any loess sheet and the L1 is separated into a weathered B (Bw) and a fragic B (Bx) horizon. The 75 cm deep sample collected from lHO appeared to be the weathered surface of the gravels (2B).

3.4.3 Soil physical, hydrological and chemical properties

The morphologically defined horizons partitioned some of the variation in soil physical, hydrological and chemical properties, which often showed consistent trends with depth (Figure 3-5, Appendix B). All horizons contained low sand (s) content, which ranged from a median of 4.5 % in the L3 horizon, to 9.5 % in the L4 horizon. Silt (z) decreased with increasing age of the parent material, ranging from a median of 66.5 % in the topsoil Ap and A/B to 38.5 % in the 2B. Contrariwise, clay (c) content was lowest in the topsoil (27 %) and progressively increased with increasing age of the parent material (2B, 52.5 %). Particle density (PD) was lowest in the Ap (median 2.62 g cm^{-3}), and progressively increased until the L1 (Bx; median 2.73 g cm^{-3}), below which point it did not shift significantly. The dry bulk density (DBD) was lowest in the Ap and 2B, with equivalent medians of 1.17 g cm^{-3}, and highest in the L3 (median 1.46 g cm^{-3}). Porosity (Por) ranged from 46.4 % to 56.8 % and was highest in the L5 and Ap horizons and lowest in the L3 horizon. Macroporosity (MPor) was highest in the A/B and Bw, with median values of 8.78 and 8.06 % respectively. The Ap had a median MPor of 6.63 %, with the lowest MPor found in the L5 (3.61 %). Similarly, air capacity (AC) was highest in the A/B (9.74 %), and lowest in the L5 (3.86 %). The median values for saturated hydraulic conductivity (Ks) generally decreased with depth and increasing age of the parent material, ranging from 22 mm h^{-1} in the A/B horizon to 0.22 mm h^{-1} in the 2B horizon, but were slightly higher in the A/B than the Ap. The 2B horizon had significantly higher field capacity (FC; 51.7 %) than all other horizons, with the Ap and L5 having the next highest values (median 45.7 and 46.8 %, respectively). The lowest median FC values were found in the A/B and Bw and were 40.1 % and 40.7 %, respectively. Readily available water content (RAW) was highest in the Ap (median 11.7 %) and decreased progressively to the L1 (Bx) (median 6.0 %) below which it remained relatively constant. There was a large variation in RAW among the L1 (Bx), L2, L4 and L5 horizons. Available water content (AWC), conversely, had the highest median values in both the Ap and 2B (25.8 and 22.1 %, respectively), and lowest in the L2 (13.7 %). Both organic carbon (OC) and total nitrogen (TN) showed similar distribution patterns, decreasing between the Ap (OC = 3.12 %; TN = 0.29 %) and the L1 (Bx) (OC = 0.37; TN = 0.05 %), with the remaining horizons fairly consistent with the L1 (Bx). The carbon-nitrogen ratio (CNr) was highest in the Ap, A/B and Bw (medians = 11, 12 and 11.5, respectively), and lowest in the L3 and 2B (medians = 7.5 and 8, respectively), with the remaining horizons showing large variation.

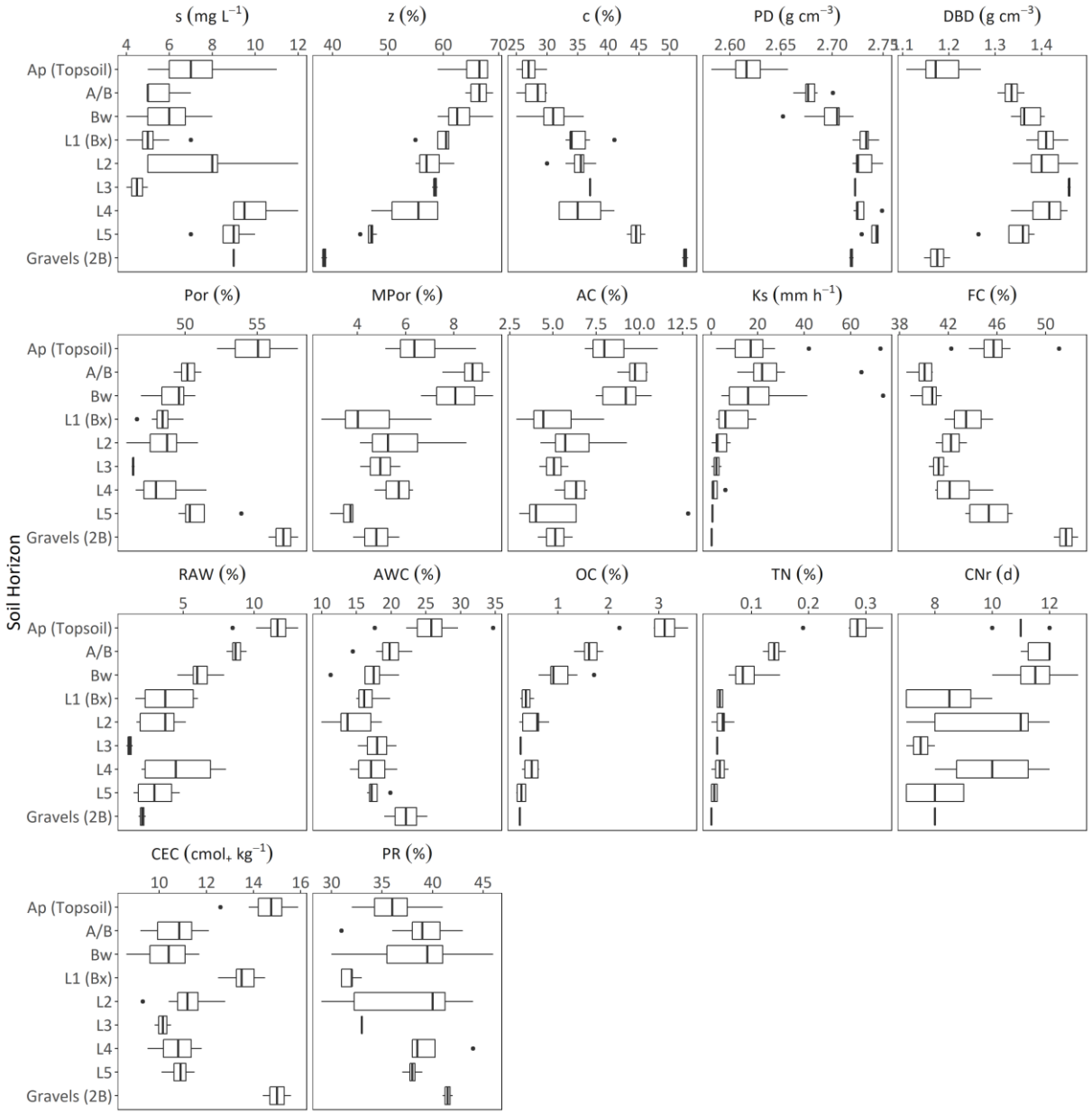

Figure 3-5. Soil property variation in each of the soil horizons and loess sheets identified through qualitative description techniques. Refer to Table 3-1 for details of variable abbreviations.

Cation exchange capacity (CEC) was notably higher in the Ap, L1 (Bx) and 2B (medians = 14.8, 13.5 and 15 cmol[+] kg^{-1}, respectively), relative to the remaining horizons (median range between 10.2 and 11.2 cmol[+] kg^{-1}). Phosphorus retention (PR) was highest in the 2B (median = 41.5 %) and lowest in the L1 (Bx) (median = 32 %). There was considerable variation in PR in the L2.

3.4.4 Principal component analysis

In order to select the optimal number of components from the principal component analysis (PCA), the Kaiser criterion (Kaiser, 1960) was employed, which rules that any principal component associated with an eigenvalue of magnitude greater than one may be retained. The PCA produced four components with eigenvalues >1 which together accounted for 87 % of the total variance (Table 3-3). The first and second component accounted for 46 and 24 % of the total variance, respectively, while the third and fourth components explained 11 and 6 % of the total variance, respectively. OC (0.35), TN (0.34) and RAW (0.34) had large positive loadings on the first component, while PD (-0.34) had a large negative loading. To a lesser extent, DBD (-0.29), AWC (0.27), Por (0.26) and c (-0.26) also contributed to PC1. Conversely, FC (0.47) and CEC (0.35) had the largest positive loadings on the second component, while MPor (-0.35) had the largest negative loading. The CNr (-0.27), AC (-0.27), Z (-0.26) and Por (0.27) also contributed, albeit to a lesser extent, towards PC2. The largest loadings on the PC3 were PR (-0.60) and sand (-0.45), with silt (0.36), AC (-0.27) and c (-0.25) also contributing. Sand (0.45) and Ks (-0.51), and to a lower degree clay (-0.31) had the largest loadings for PC4.

Large overlaps exist in the multivariate space among the morphologically derived morphological horizon classes (Figure 3-6). In the plane of PC1 and PC2, topsoil, A/B and Bw horizons were well discriminated from each other and from all other horizons (Figure 3-6a). Topsoil horizons had distinctly high scores on PC1, as a result of high OC, TN, RAW and low PD. A/B and Bw horizons were discriminated by lower PC1 scores (Bw < A/B), but also negative scores on PC2 resulting from higher MPor and lower FC and CEC. The remaining (subsoil) horizons clustered and overlapped around negative values of PC1 (higher PD, DBD and clay) and near zero to positive values of PC2. The 2B horizon was discriminated from the other subsoil horizons by higher PC2 scores (high FC and CEC, low MPor).

Only L1 (Bx), L3, L4, and 2B were separated from the large cluster of all other horizons centred on the origin of the PC3 – PC4 plot (Figure 3-6b). L1 (Bx) and L3 overlapped in the quadrant of

Table 3-3. Principal component analysis of the measured soil physical, hydrological and chemical properties. The loadings considered most important for each principal component are highlighted in boldface.

Principal component	**PC1**	**PC2**	**PC3**	**PC4**
Eigenvalue	7.770	4.091	1.944	1.008
Proportion of Variance	0.457	0.241	0.114	0.059
Cumulative Proportion	0.457	0.698	0.812	0.871
Eigenvectors/loadings				
Organic carbon (OC)	**0.346**	0.050	0.028	0.151
Total nitrogen (TN)	**0.342**	0.080	0.054	0.151
Particle density (PD)	**-0.338**	-0.055	-0.066	-0.108
Readily available water capacity (RAW)	**0.336**	-0.040	0.030	0.146
Dry bulk density (DBD)	**-0.294**	-0.234	0.159	0.167
Available water capacity (AWC)	**0.270**	0.224	0.043	-0.020
Porosity (Por)	**0.262**	**0.267**	-0.202	-0.226
Clay (c)	**-0.257**	0.234	**-0.250**	**-0.313**
Silt (z)	0.237	**-0.260**	**0.355**	0.116
Air capacity (AC)	0.219	**-0.268**	**-0.267**	-0.215
Carbon-Nitrogen Ratio (CNr)	0.202	**-0.271**	-0.182	0.160
Saturated hydraulic conductivity (Ks)	0.180	-0.202	-0.058	**-0.514**
Macroporosity (Mpor)	0.178	**-0.349**	-0.239	-0.203
Cation exchange capacity (CEC)	0.171	**0.350**	0.130	-0.138
Field Capacity (FC)	0.062	**0.470**	-0.029	-0.087
Sand (s)	-0.022	0.171	**-0.445**	**0.564**
Phosphorus retention (PR)	0.005	-0.087	**-0.595**	0.093

high PC3 scores (reflecting lower PR and higher silt) and negative PC4 scores (reflecting higher Ks). In contrast, L4 generally had negative PC3 scores but high PC4 scores whereas 2B had negative PC3 and PC4 scores. Negative PC3 scores relate to high PR and low silt content. PC4 scores are strongly influenced by Ks such that they decrease as Ks increases.

3.4.5 *K* means clustering

For k = 3 in the k-means clustering analysis the three clusters occurred in a consistent depth sequence in soils across all landscape positions (Figure 3-7a). Cluster 1 corresponded to Ap horizons, cluster 2 to A/B and Bw horizons, and cluster 3 to the horizons designated as Bx horizons, buried loess sheets, or lithological discontinuities. When four clusters were prescribed (k = 4), clusters 1 and 2 remained unchanged from k = 3 while cluster 3 of k = 3 lost individual horizons of the nose slope and planar sideslope to the new cluster 4 (Figure 3-7b). A five-cluster partition (k = 5) retained clusters 1 and 2 intact, but the previous cluster 3 shrunk in favour of an enlarged cluster 4 and a new cluster (cluster 5). The new cluster 4 included the upper part of L2 in

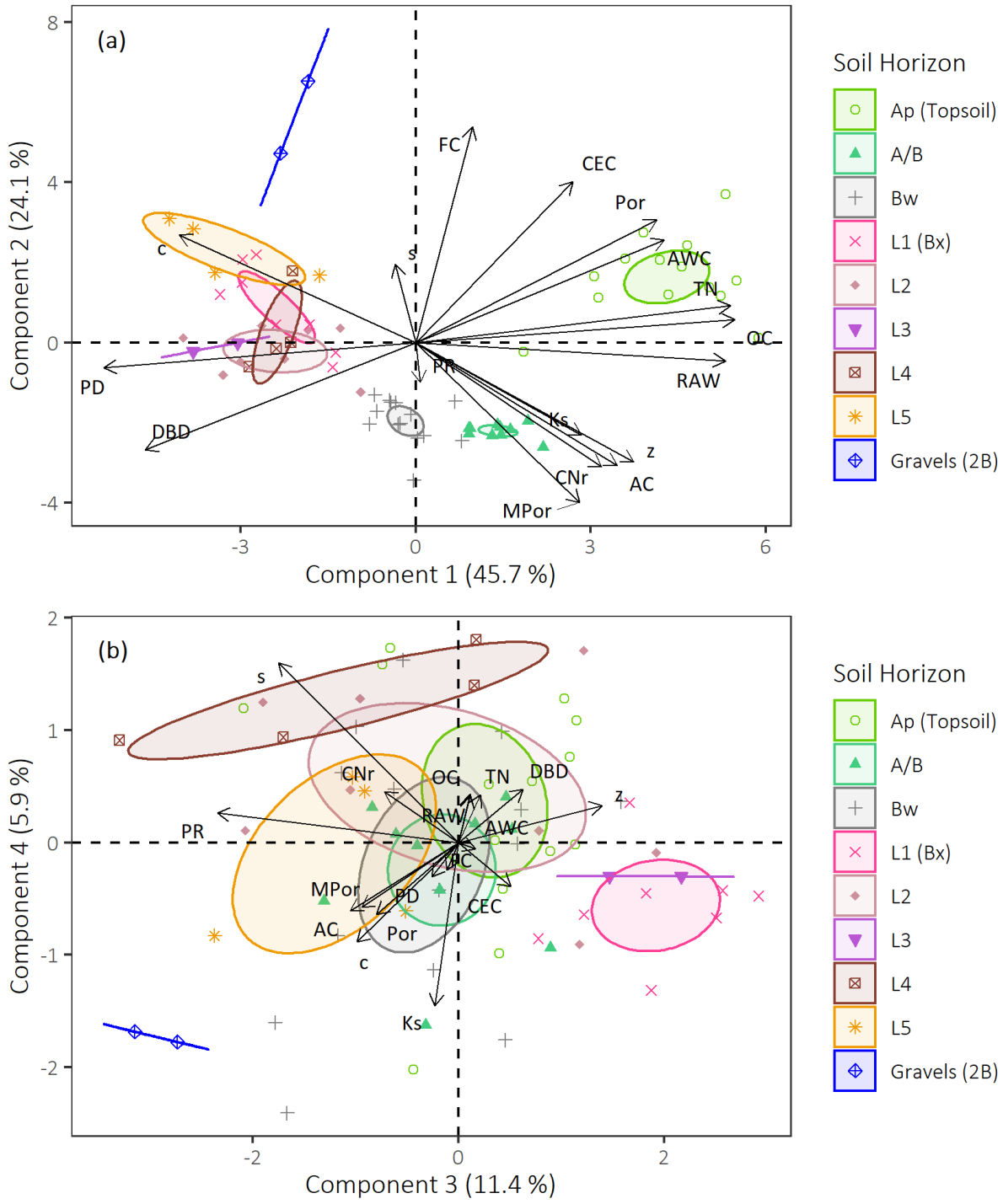

Figure 3-6. PCA biplot showing the loadings on (a) PC1 and PC2 and (b) PC3 and PC4 for each measured soil property, including OC (organic carbon), TN (total nitrogen), PD (particle density), RAW (readily available water capacity), DBD (dry bulk density), AWC (available water capacity), Por (porosity), c (clay), z (silt), AC (air capacity), CNr (carbon-nitrogen ratio), CEC (cation exchange capacity), MPor (Macroporosity), Ks (saturated hydraulic conductivity), FC (field capacity), s (sand) and PR (phosphorus retention). The points are individual samples plotted against where their attributes locate them in the PC biplot and coloured by soil horizon grouping (as identified from soil profile descriptions). The 95 % confidence ellipses are also shown for each grouping. The arrows represent the original attributes, with their direction representing the correlation between the attribute and the principal component, and the length the contribution of the attribute to the principal component.

the profiles on the planar sideslope, while cluster 5 (two individuals) corresponded to 2B in the base of the profile at the nose slope (Figure 3-7c). When a sixth cluster (k = 6) was prescribed, it formed as a split of previously stable cluster 2, occupying the upper depths of that pre-existing cluster (Figure 3-7d).

The mean cluster values for each soil attribute are displayed in Table 3-4. For k = 3 (Table 3-4a), cluster 1 had the highest mean values of OC (3.14 %) and TN (0.29 %), as well as the highest silt (66.1 %) and Por (55.1 %) but the lowest clay (26.7 %) and DBD (1.17 g cm^{-3}). Cluster 2 had the highest mean values for MPor (8.4 %), Ks (22.1 mm h^{-1}) and PR (38.8), but the lowest CEC (26.7 %). Cluster 3 had the highest mean values of clay (38 %) and DBD (1.39 g cm-3) but lowest MPor (4.8 %), Ks (4.3 mm h^{-1}), OC (0.38 %) and TN (0.04 %).

When considering the attribute means of clusters at k = 4 and k = 5 (Table 3-4b and c, respectively), the results of these clusters can be consolidated by considering k = 6 (Table 3-4d), because cluster 3 divided into clusters 4 and 5, while cluster 2 divided into clusters 2 and 6. At k = 6, cluster 3 had the highest mean values for DBD (1.42 g cm^{-3}) and the lowest mean values for Por (47.8 %), while cluster 5 had the highest mean values for clay content (52.5 %) and Por (56.8 %), and the lowest mean values for silt content (38.5 %), DBD (1.17 g cm^{-3}), and Ks (0.2 mm h^{-1}). Cluster 4 had mean values of silt (49.6 %), clay (40.8 %), DBD (1.36 g cm^{-3}), Por (50.2 %), and Ks (2.4 mm h^{-1}) intermediate to clusters 3 and 5. Cluster 6 had higher mean values for Ks (23.3 mm h^{-1}), RAW (8.4 %), OC (1.64 %) and TN (0.14 %) relative to cluster 2 (Ks = 20.6 mm h^{-1}, RAW = 5.8 %, OC = 0.89 % and TN = 0.08 %).

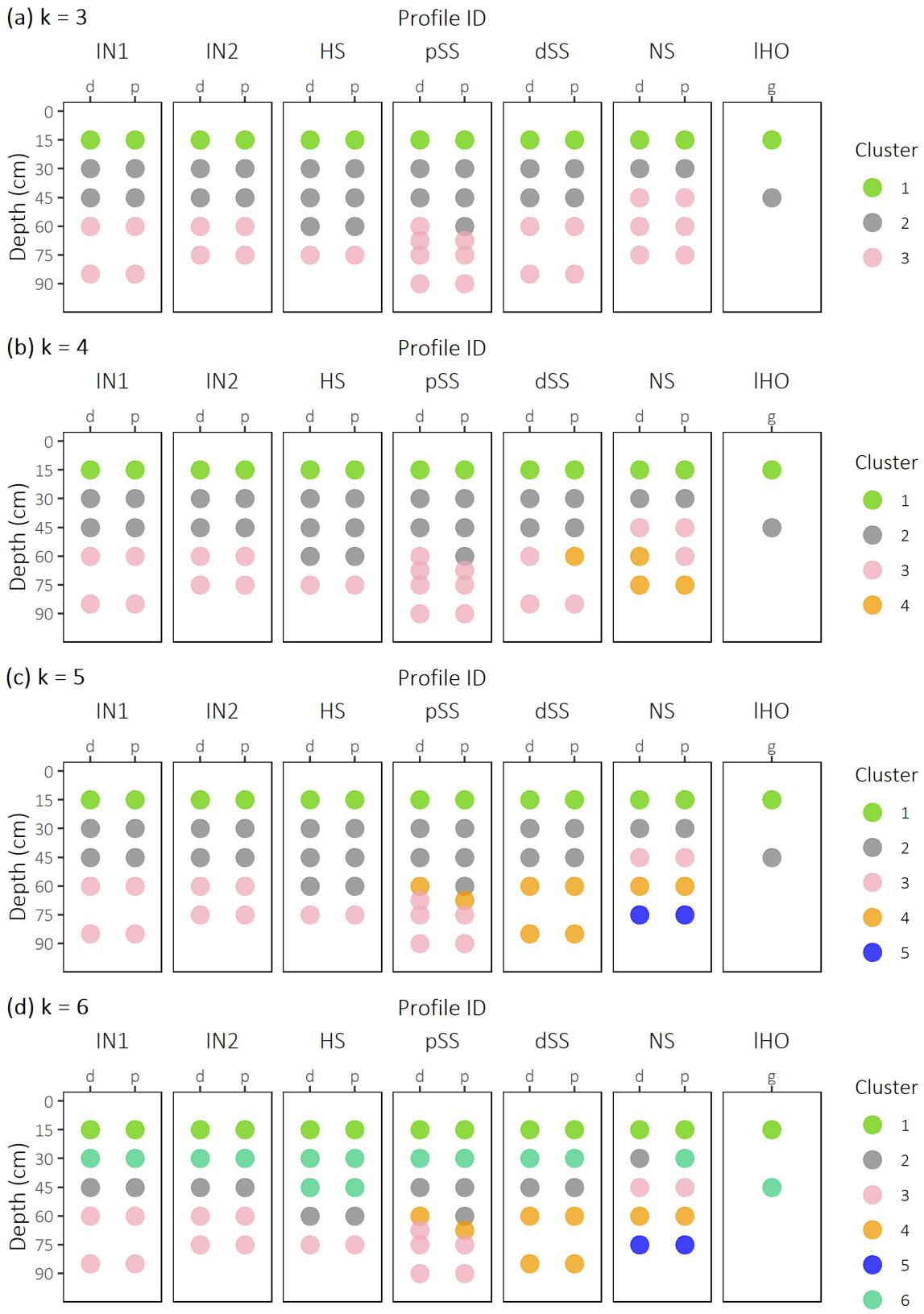

Figure 3-7. The resulting clusters of the k-means cluster analysis for (a) k = 3, (b) k = 4, (c) k = 5 and (d) k = 6 clusters. Each of the 66 points are coloured by the cluster it belongs to for a given value of *k*, and are plotted relative to the landscape position of the soil pit (i.e., IN1, IN2, HS, pSS, dSS, NS and lHO) and profile (i.e., pit side 'd' or side 'p') from which they were taken, as well as the depth (cm).

Table 3-4. Table of attribute means for each of the clusters identified for each value of *k*, including the number of points making up each cluster. Refer to Table 3-1 for details of variable abbreviations.

	Cluster	*n*	s	z	c	PD	DBD	Por	MPor	AC	Ks	FC	RAW	AWC	OC	TN	CNr	CEC	PR
a) *k* = 3	1	*13*	7.2	66.1	26.7	2.62	1.17	55.1	6.5	8.3	20.6	46.1	11.8	26.3	3.14	0.29	10.8	14.8	35.6
	2	*26*	6.1	63.8	30.1	2.69	1.35	49.7	8.4	9.3	22.1	40.4	7.2	18.1	1.30	0.11	11.6	10.6	38.8
	3	*27*	7.2	54.8	38.0	2.73	1.39	49.2	4.8	5.5	4.3	43.8	3.4	16.9	0.38	0.04	8.8	12.0	36.0
b) *k* = 4	1	*13*	7.2	66.1	26.7	2.62	1.17	55.1	6.5	8.3	20.6	46.1	11.8	26.3	3.14	0.29	10.8	14.8	35.6
	2	*26*	6.1	63.8	30.1	2.69	1.35	49.7	8.4	9.3	22.1	40.4	7.2	18.1	1.30	0.11	11.6	10.6	38.8
	3	*23*	6.8	56.9	36.3	2.73	1.41	48.3	4.8	5.2	4.9	43.1	3.5	16.1	0.39	0.04	8.8	11.7	35.0
	4	*4*	9.8	42.8	47.5	2.73	1.24	54.8	4.9	7.5	0.6	48.1	2.7	21.3	0.37	0.04	9.0	13.3	41.3
c) *k* = 5	1	*13*	7.2	66.1	26.7	2.62	1.17	55.1	6.5	8.3	20.6	46.1	11.8	26.3	3.14	0.29	10.8	14.8	35.6
	2	*26*	6.1	63.8	30.1	2.69	1.35	49.7	8.4	9.3	22.1	40.4	7.2	18.1	1.30	0.11	11.6	10.6	38.8
	3	*17*	5.9	59.1	35.0	2.73	1.42	47.8	4.7	5.1	5.6	42.6	3.6	15.9	0.41	0.04	8.9	12.1	33.5
	4	*8*	9.6	49.6	40.8	2.74	1.36	50.2	5.0	6.5	2.4	44.3	3.2	17.7	0.37	0.04	8.9	10.9	39.9
	5	*2*	9.0	38.5	52.5	2.72	1.17	56.8	4.8	5.1	0.2	51.7	2.1	22.1	0.25	0.03	8.0	15.0	41.5
d) *k* = 6	1	*13*	7.2	66.1	26.7	2.62	1.17	55.1	6.5	8.3	20.6	46.1	11.8	26.3	3.14	0.29	10.8	14.8	35.6
	2	*12*	5.8	62.2	32.0	2.71	1.37	49.5	8.2	9.1	20.6	40.6	5.8	17.0	0.89	0.08	11.3	10.3	38.1
	3	*17*	5.9	59.1	35.0	2.73	1.42	47.8	4.7	5.1	5.6	42.6	3.6	15.9	0.41	0.04	8.9	12.1	33.5
	4	*8*	9.6	49.6	40.8	2.74	1.36	50.2	5.0	6.5	2.4	44.3	3.2	17.7	0.37	0.04	8.9	10.9	39.9
	5	*2*	9.0	38.5	52.5	2.72	1.17	56.8	4.8	5.1	0.2	51.7	2.1	22.1	0.25	0.03	8.0	15.0	41.5
	6	*14*	6.3	65.3	28.4	2.68	1.34	50.0	8.5	9.5	23.3	40.1	8.4	19.1	1.64	0.14	11.9	10.8	39.4

3.5 Discussion

3.5.1 Loess stratigraphy

The results of the qualitative descriptions of auger and profile horizonation demonstrate that loess and soil stratigraphy, paleopedology, geomorphic history and current morphometry are important ingredients to conceptualising and portraying the soil pattern. The auger survey of loess stratigraphy indicated that the drainage basin hillslopes cut across up to four thin buried loess sheets that had been laid parallel to the gravel surface (Figure 3-4). Similar to the exposure described by Bruce et al. (1973) at Raymonds Gap, 25 km north-west of the field site, the combined thickness of L1 and L2 (i.e., the Yellow loess member of the Stewarts Claim Formation) was generally less than 2 m, with the overall thickness generally within 4 m. Platy structure, which is a feature of the paleosols of Brown loess members (Bruce, 1973a; Leamy et al., 1973) was observed at the surface of L4 in the UP (Plate 3-1), as well as in buried loess sheets L3 (i.e., Brown A) and L5 (i.e., Brown C) at dSS and pSS, respectively (Appendix A.2).

Soils on the interfluves appeared to have formed entirely in the uppermost loess sheet (unisequal), which displayed in-situ degradation of the fragipan. In contrast, hillslope soils had more complex soil stratigraphy. Their upper soil horizons appeared to have formed in mobile colluvial material, sourced from exhumed upslope loess sheets by, for example, erosional processes and soil creep driven by tree turnover and bioturbation (Hughes et al., 2009; Roering et al., 2004). Their subsoils comprised paleosols overprinted by contemporary, topdown pedogenesis. These hillslope soils appeared to be multisequal/composite soils formed in multiple thin, buried loess sheets.

Unlike the landscapes of the US Midwest (Olson, 1997), where there are broad hillslope zones underlain by a single loess sheet, the study site showed a clear partition between the interfluve (soils formed in L1) and the hillslopes (composite soils with any one of four loess sheets forming the subsoil). These results show how the outcropping of thin, buried loess sheets may influence the morphology of the soil profile, information that is important for understanding the soil pattern in these landscapes and may be relevant for developing conceptual landscape models.

3.5.2 Principal component analysis (PCA) of soil attribute variation

Principal component analysis revealed that the morphologically defined horizons are meaningful with respect to the suite of physical, chemical and hydraulic soil properties. This

suggests that the qualitative method of horizon designation can be a robust method for determining the most significant variation down the soil profile, especially with regard to the Ap, A/B, Bw (the shallower and younger soil horizons) and 2B (a change in lithology). While the modern fragipan and buried loess horizons were not well-differentiated by variability in the measured soil attributes, they were distinguished by PC1 as different from the Ap, A/B and Bw. This suggests that there is not a large difference between the fragipan and buried loess sheets in terms of the morphological groupings of measured soil physical, hydraulic and chemical properties, but that they are together substantially different from their overlying horizons. It is worth noting that the variability of the deep subsoil horizons is likely to be low relative to the vertical variability of the upper horizons engendered by topdown pedogenesis. As such, it is possible that more detailed discrimination of the buried loess members may be enabled, by excluding the A, A/B, and Bw horizons from the PCA. Moreover, it is possible that differentiation could be achieved by incorporating supplementary properties into the PCA such as those relating to soil mineralogy or colour (i.e., value, chroma and hue).

PC1 primarily reflects vertical differentiation resulting from gradients of bioturbation and carbon inputs, weathering and clay translocation (Walker & Green, 1976) induced by contemporary topdown pedogenesis. OC and TN are sourced from the soil surface and generally decrease with depth, explaining why samples collected from the Ap (topsoil) horizon had the highest PC1 loadings, whilst the A/B, Bw, and all other horizons had respectively lower PC1 loadings. Furthermore, organic matter has very low particle density, which helps to explain why deeper and older horizons were associated with the lowest PC1 loadings. Additionally, larger clay content in the subsoil occurs as a function of wetting and drying cycles, with perched water tables causing weathering of silt into clay, and illuviation of weathered clay from within the topsoil (Ray, 1963), explaining the positive silt and negative clay loadings associated with PC1. Fragipans are usually overprinted with illuvial clay (Schaetzl & Thompson, 2015), while subsurface clay may also be inherited from buried loess sheets which were themselves at one point in time weathering at the land surface (Kemp & McIntosh, 1989).

PC2 was able to explain some of the variation associated with the deeper horizons including paleosol horizons that were undifferentiated by PC1. High positive loadings for field capacity (FC), porosity (Por) and cation exchange capacity (CEC) and negative loadings for macroporosity (MPor) suggest that PC2 is describing some aspect of the soil water regime, potentially a function of compaction under loading, as well as weathering and clay mineralogy. Horizon 2B stood out

with the highest PC2 scores, its distinctiveness explained by the fact that its lithological dissimilarity produced high values of FC and CEC and low values for Mpor. This distinctiveness may be explained by the weathering of the coarse clasts, whereby their disintegration and the illuviation of clay may lead to high water holding capacities. The deeper loess sheets had lower PC2 scores than the 2B but higher scores than the A/B and Bw. This is a logical result, as the deeper loess sheets are likely to be compacted or to have lost porosity from clay illuviation. The A/B and Bw could be discriminated from all other horizons by having the lowest PC2 scores, indicating that they are less influenced by compaction. Interestingly, the Ap horizon was unable to be differentiated from the deeper loess sheets on the PC2 axis, which is somewhat unexpected, as one would expect the Ap horizon to be significantly less compact relative to the deeper loess. High organic matter in non-compacted A horizons generally improves structure, increases macroporosity, and consequently decreases field capacity in silt loam soils (Chaney & Swift, 1984; Franzluebbers, 2002). As such, a non-compacted Ap would be expected to be associated with the lowest PC2 values, which was not observed here and points towards surface compaction of the Ap, presumably from sheep treading or machinery. Supporting this inference is that the soil type under investigation is known to be susceptible to soil structural degradation through land management practices (Hu et al., 2021).

PC3 and PC4 were able to discriminate some of the deeper and older horizons, specifically L1 (Bx), L3 and 2B on PC3 and L4 and 2B on PC4. High positive loadings for silt and negative loadings for phosphorus retention indicate that the PC3 axis reflects the degree of weathering, while large negative loadings for saturated hydraulic conductivity on PC4 suggest that it is describing the hydraulic properties. These results suggest that inclusion of different loess sheets in composite soils on hillslopes had demonstrable effects on soil properties including some important for the movement of water. However, these components together only described 17.3 % of the variation in the measured soil attributes, which demonstrates that vertical anisotropy (e.g., vertical gradients of organic matter addition, bioturbation, redox potential, compaction and eluviation/illuviation) dominates the variability.

Overall, the PCA results show that the morphological approach to soil horizon designation was able to partition most of the variation in the measured soil properties. Many of the loess sheets ended up clustering together; however, this is possibly to be expected given that they are buried, they have undergone an interglacial weathering cycle, and they have been compacted under an overburden. Although vertical anisotropy, resulting from top-down pedogenesis, appears to be the

dominant source of variability these soils, hydraulic properties of the subsoil are influenced by soil stratigraphic inheritance.

3.5.3 Unsupervised *k*-means clustering of soil attributes to identify key soil horizons

The results of *k*-means clustering showed that a quantitative approach can be used to objectively classify soil samples into soil horizon classes, giving almost equivalent results to a conventional qualitative soil description. The vertical anisotropy of soils was captured in the results of $k = 3$, which broadly identified the topsoil, upper subsoil, and lower subsoil. Despite few data points within each cluster, the *k*-means algorithm using $k = 6$, generated sensible clusters that were easily related to the Ap, A/B, Bw and 2B, as well as some, but not all, of the morphologically described stratigraphy in the loess.

Comparison of the *k*-means clusters showed that the Ap horizon was always well-resolved by cluster 1, with all points collected from 15 cm clearly distinguished as a unique and persisting cluster for all values of *k* between $k = 3$ to $k = 6$ (Figure 3-7a - d). Furthermore, the alignment of cluster 1 with the Ap horizon was consistent with the large cluster 1 *k*-mean value for OC content and low PD. This is consistent with the morphological characterisation of an A horizon, whereby soil colour is used to indicate a higher organic matter content relative to underlying horizons.

The A/B horizon was also well resolved when $k = 6$ and specifically by cluster 6, while the Bw horizon was well resolved by cluster 2. The *k*-means for OC and TN were much higher for cluster 6 than cluster 2, which reflected the transitional nature of the A/B and the incorporation of organic material from above. This is consistent with the qualitative determinants for A/B horizon designation, which state that pieces of A horizon should be incorporated into a B horizon (Milne et al., 1995). It is worth noting that cluster 6 (i.e., A/B) at the head slope (HS) extended down to 45 cm, indicating that, objectively, this depth increment was more like an A/B horizon and less similar to the Bw it was qualitatively classified as. Re-inspection of the profile images of HS (Appendix A.2) suggest that the A/B could in fact be qualitatively considered as extending to 50 cm (i.e., fingers of Ap material extend to 50 cm), indicating that the objective *k*-means approach was identifying human-error in the qualitative approach. Conversely, the 45 cm depth at lHO in the infilled hollow was partitioned into cluster 6 (i.e., A/B), despite being described on morphological grounds as an Ap horizon and despite having high organic matter, as indicated by its dark colour (Plate 3-2g). On the biplot of PC1 and PC2, this sample (i.e., Sample 66 in Table C-1; Appendix C) can be seen as corresponding closely along the PC1 axis with points grouped as

A/B horizon, and as intermediate to the Ap and A/B groupings on the PC2 axis. This result suggests that, despite the dominance of organic matter colouring at 45 cm, the other soil attributes, specifically TN, PD, clay (c) and dry bulk density DBD are more associated at this depth with a transitional horizon, and a bias of qualitative assessment whereby colour is over-empahsised. Residing in a topographically convergent zone, the soil at lHO likely has an over-thickened (60 cm) Ap horizon as a result of transport of the topsoil to the site by cultivation. It is interesting to note that the deeper part of the Ap horizon, which corresponds to the original A horizon before over-thickening appears now more similar to an A/B horizon. This transition may be capturing the response hypothesised by Almond and Tonkin (1999) as being a characteristic of upbuilding pedogenesis whereby surface horizons take on more of the character of subsoil horizons (but with some legacy) as they become progressively removed from the soil surface by land surface aggradation.

On the interfluves, cluster 3 resolved the L1 (Bx). At all other sites, clusters 3 and 4 together resolved the L1 (Bx) and the buried loess, although there was no unique association of each cluster with horizons or groups of horizons (loess sheets). There was a large difference between these two clusters in the *k*-means of sand (s), z and c, with the resulting particle size distribution of cluster 3 corresponding to a clay loam texture class, and cluster 4 to a loamy clay. Textural differences are used as indicators of changes in horizons and also changes in loess sheets, so it is reasonable to deduce that the breakdown of cluster 3 at k = 3 into clusters 4, 5 and 6 at k=5 and k = 6 is due to differences in horizons. Cluster 3 incorporated the buried loess sheets L2 at HS (Plate 3-2c), L2 and L3 at pSS (Plate 3-2d), and L4 at NS (Plate 3-2f), while cluster 4 was associated with L5 at both NS and dSS, but was also associated with L4 at dSS. A lack of a unique association of loess sheets with k-means clusters could be simply a result of *k* being smaller than the identified number of buried loess sheets; however, increasing *k* caused breakdown of the well-resolved and meaningful clusters, including the Ap horizon, suggesting more clusters began to differentiate within-horizon detail. A larger sample size may remove the overfitting problem and produce greater coherence of k-means clusters and loess sheets. Additionally, it is possible that the measured soil attributes could not resolve the subtle differences in soil morphology between the buried loess sheets.

The within-pit inconsistency at site pSS, at depths of 60 and 67.5 cm, where different clusters occurred at each depth at the distal and proximal exposures is probably attributable to a wavy horizon boundary, as evident in Plate 3-2d. It is possible that the 2D description of the soil horizon here inaccurately represented the 3D variability of the soil continuum.

Finally, the 2B horizon was well resolved by cluster 5 for $k \geq 5$, which was described by changes in silt and clay content (low and high, respectively), decreasing DBD and increasing Por. The stark lithological contrast may have influenced these properties directly or indirectly via influences on soil water movement or weathering (Lai et al., 2022).

The changes in clustering between $k = 3$ to $k = 5$ are restricted to profiles located on the hillslopes (i.e., pSS, dSS, and NS) and involve the partitioning of cluster 3 (lower subsoil), while the cluster centroids for the interfluve and head slope do not change. This suggests that with increasing k, clusters are being identified in the deeper layers of the side slopes, which is consistent with the identification of buried loess sheets at these sites using morphological techniques. These are subtle effects when compared with the overall profile anisotropy; however, they may have relevance for water storage and movement in these landscapes. These horizons separate out before the A/B, indicating that they are more important in terms of attribute variability than is the A/B.

More detailed discrimination of the buried loess sheets may have been achieved by considering other soil attributes. Codified soil colour (Evans & Franzmeier, 1988) and redox attributes might be appropriate additional attributes to consider, as they relate to wetting and drying cycles, one of the main drivers of pedogenesis in this climate (Bruce, 1983; Johnson et al., 1990). Moreover, sequences within the Southland loess deposits have previously been described in terms of their characteristic colour profiles (Bruce, 1973a).

Implementing the *k*-means algorithm method shown here removes some of the subjectivity in the traditional approach to soil horizon classification, but it requires a large amount of data that can be time-consuming and expensive to collect. New technologies, including visible and near-infrared (vis-NIR) spectroscopy and electrical conductivity sensing, can provide rapid and more cost-effective prediction of important soil physical and chemical attributes such as sand, silt, clay, carbon and CEC, while spectrotransfer functions (STFs; using different attributes of measured spectral reflectance) have been shown to have similar accuracy as pedotransfer functions (PTFs; using easily measurable basic soil properties) in the estimation of soil hydraulic properties such as the water retention curve and saturated hydraulic conductivity (Knadel et al., 2015; Santra et al., 2009; Zhao et al., 2021; Zhao et al., 2018). By reducing time and cost associated with data collection, these technologies enhance the viability of quantitative methods, such as *k*-means, as a tool for soil variability mapping.

S-Map, the digital soil map for Aotearoa New Zealand (Lilburne et al., 2004), maps the study area at a nominal scale of 1:50,000 as a simple mapping unit (the Pukemutu_6a.1 soil sibling). The sibling level of the NZ Soil Classification is defined on soil depth, soil texture profile, topsoil stoniness, drainage class, and functional horizons (Webb & Lilburne, 2011). Functional horizons are defined based on stone content, texture, structure size, and consistence (Webb & Lilburne, 2011). Principal component analysis was able to differentiate a number of subsurface horizons along the PC1, 2 and 3 axes, which appeared to reflect the soil water regime, degree of weathering, and hydraulic conductivity. The *k*-means clustering identified subsurface horizons on the slopes (clusters 3 and 4) that were differentiated by texture and saturated hydraulic conductivity. Variation between the morphologically and quantitatively assigned horizons in soil water regime, texture and hydraulic conductivity would indicate that, relative to the interfluves, soils on hillslopes are sufficiently different that distinct siblings should be recognised. That they are not may reflect a conceptual bias amongst pedologists in how soil variability is structured in loess-mantled landscapes. A more refined understanding of the soil-geomorphology of loess-mantled downlands may, therefore, lead to more accurate soil maps and characterisation of soil variability, which is essential information for upscaling soil hydraulic information from the pedon to the catchment scale and producing appropriate models of landscape hydrology.

3.6 Conclusions

The soil pattern across the loess-mantled downlands of Southland is influenced by hillslopes of small drainage basins crosscutting multiple thin loess sheets. Soils on the interfluves appeared to have formed entirely in the uppermost loess sheet (unisequal soils) while, on hillslopes, multisequal soils comprise an upper solum formed in mobile colluvial material overlying *in situ* pedogenically altered buried loess sheets (composite soils). Quantitative analysis of a suite of soil chemical, physical and hydraulic properties confirmed that the multisequal nature of hillslope soils was relevant to understanding soil spatial variability. PCA showed that vertical differentiation of soils by topdown pedogenesis was the dominant driver of heterogeneity. However, other factors likely related to the legacy of pedogenesis in buried loess sheets and burial-related consolidation were important for understanding subsoil variability.

Quantitative classification by the k-means algorithm produced clusters that corresponded closely with morphological soil horizons. When k was small (k= 3) the clusters corresponded with the first order vertical sequence of horizons characteristic of Pallic Soils: an organic-rich A horizon; a porous, lower OC, A/B horizon and upper (Bw) subsoil; and a dense, low permeability fragipan. As the prescribed number of clusters was increased, differentiation of the Bx horizon occurred that discriminated those formed in the upper loess sheet from those of paleosol origin or of contrasting lithology (loess vs gravel). The differences occurred in properties important for soil water movement and storage (field capacity, saturated hydraulic conductivity).

Current soil mapping at 1:50,000 does not recognise the variability revealed by the detailed qualitative and quantitative analysis of the present study, mapping the area as a simple mapping unit (single taxon). A more refined understanding of the soil-geomorphology of loess-mantled downlands may lead to better soil-landscape models, more accurate soil maps and better characterisation of soil variability, which are essential for upscaling soil hydraulic information from the pedon to the catchment scale and producing appropriate models of landscape hydrology.

Chapter 4

Identification, characterisation and mapping of a mature mole channel and tile drain network using Ground-Penetrating Radar (GPR)

4.1 Abstract

To expedite the removal of excess soil moisture and improve land productivity, slowly permeable agricultural soils are often drained using mole channel and tile drainage systems. It is often assumed that mole channels deteriorate with time, so maintenance often involves re-moling every couple of years. Little is known about the nature and longevity of these potentially complex mole networks, and there is no conventional method for mapping 'legacy' mole channels. This study aimed to test whether ground-penetrating radar (GPR) could be used to identify, map and characterise a typical mole and tile network in a small agricultural basin in a loess-derived Pallic Soil in Southland, New Zealand. The research questions were as follows: (1) can GPR be used to identify and map mole channels and a tile drain in a loess-derived soil? (2), do mole channel networks have high densities and complex design characteristics in areas where re-moling is practiced? (3) can multi-generational mole channels in slowly-permeably, loess-derived soils maintain a high degree of connectivity for 30 years? Results showed that GPR successfully located mole channels and a tile drain, showing high lateral precision, accuracy, and utility for mapping. However, accurate resolution of the vertical positioning required advanced signal processing, which may also enable characterisation of additional subsoil properties relevant to mole network longevity. The mole network was complex in terms of its design and had a high density of interconnected, multidirectional mole channels (1.6 m m^{-2}) which appeared to have been developed over several generations of mole ploughing. Moreover, the 30 + year old mole channels showed a high degree of connectivity and great structural integrity. Soil depth to the fragipan appeared to control longevity of the mole network, and moles that were formed in shallow fragipans appeared to have disintegrated. Visual observations provided no evidence for persistence of a soil fracture network induced at the time moles were installed; however, root growth and worm burrowing into the mole channels suggest that they are hydraulically connected to the surrounding soil through natural macropores. These results have significance for understanding catchment-scale hydrodynamics, especially considering that the life span of these artificial drainage networks has been shown to be considerably longer than previous estimates for this soil type (7 – 10 years).

4.2 Introduction

To expedite the removal of excess soil moisture, slowly permeable agricultural soils are often drained using mole channel and tile drain systems. This management practice is, therefore, essential to improving and maintaining land productivity in poorly drained agricultural regions across the world, including Europe, the US, Asia, the UK, Australia, and New Zealand (Feick et al., 2005; Hill et al., 2018; Manderson, 2018; USDA NASS, 2017). Mole channels are artificial unlined tunnels formed with a mole plough, which comprises a cylindrical foot attached to a vertical tyne, followed by a cylindrical expander. The act of pulling the mole plough through the soil behind a tractor results in a channel, with a usual diameter of 5 – 10 cm, and a depth of 0.4 – 0.6 m (Smedema et al., 2014). Mole channels are installed such that they traverse the slopes on either side of a tile-drained hollow, or, the area between adjacent tile drains, and intersect the tile drain permeable backfill. This practice is used in combination with tile drains as it provides an economic method of connecting wider areas of the landscape to the tile drain, extending its effective area, and is especially suitable in soils of low hydraulic conductivity (Jha & Koga, 1995; Ritzema, 1994).

The design of tile drain networks is often systematic, with specific design patterns (e.g., rectangular and herringbone) commonly employed on flat terrain, and tiles installed along drainage hollows in hillslope areas (Figure 4-1; Allred et al., 2020). Mole drains are shallower and more closely spaced (2 – 3 m) than tile drains (20 – 30 m), and are generally aligned with the slope of the land, provided the gradient is gentle enough to avoid the erosion and blow-outs associated with steep (> 3 %) terrain (Parkinson & Reid, 1986; Smedema et al., 2014). However, the practice of mole ploughing is site-specific, requires local practical experience, and has a subjective element in the network design, indicating that there are likely to be large variations in network patterns and densities (Farmers across Southland - New Zealand, personal communication, November 27 - 29, 2018; Jha & Koga, 1995).

Mole channels are commonly assumed to have a limited lifespan, beyond which they deteriorate and collapse, so it is common practice to re-mole every 3-10 years (Armstrong, 1986b; Robinson et al., 1987; Smedema et al., 2014). However, there are examples of mole channels that have remained functional for over 20 years (Bowler, 1980; Smedema et al., 2014) and, therefore, these multi-generational networks have the potential to be intensive and complex. While the literature

Figure 4-1. Common design patterns of tile drain systems include (a) rectangular, (b) herringbone, and (c) random (e.g., along hillslope hollows). Image taken from Allred et al. (2020).

provides examples of methods for mapping tile drains, there is little or no literature that has attempted to map, or characterise, artificial mole channel drainage networks.

Traditionally, tile drains are located using tile probes and/or trenching equipment; however, for mapping purposes these methods are unsuitable, as their implementation is inefficient and, in the case of trenching, significantly disturbs the soil (Koganti et al., 2021). Furthermore, there are no established methods for locating mole channels which, once installed, may be very difficult to identify as they lack the discernible outlet and installation 'scars' of tile drains (e.g., as observed in aerial imagery). Given the installation of mole channel and tile drainage systems is an unregulated activity in most countries, information regarding their true extent and characteristics is scarce. Most drainage maps only consider estimates of the areal extent of land that is modified by drainage or the likelihood that land is (densely) drained whilst ignoring information about their design characteristics, specific density metrics and longevity (Feick et al., 2005; Manderson, 2018; Pearson, 2015).

It is now well-established that, alongside direct improvements in soil moisture conditions, mole channel and tile drainage creates problematic secondary effects, including increased stream flow and stream bed erosion, altered patterns of soil moisture variability, contaminant transfer into

surface waters and possibly even the modification of soil properties (Messing & Wesström, 2006; Monaghan et al., 2016; Oliver et al., 2005; Øygarden et al., 1997; Schottler et al., 2014; Shipitalo et al., 2004; Williams et al., 2019). The ultimate influence of a mole channel and tile system will depend, in part, on the characteristics of the system itself. Therefore, to understand and mitigate the impacts of mole and tile drainage on soil and catchment hydrology and water quality in agricultural landscapes, knowledge of the drainage system characteristics, extent and longevity is required.

One potential approach to the study of mole channel characteristics and extent is the use of non-invasive, non-destructive methods such as ground-penetrating radar (GPR). GPR is an active proximal sensing technique that directs short pulses of electromagnetic (radio) energy into the subsurface from a transmitting antenna (Figure 4-2). The waves propagate as they travel downward and partially reflect off buried discontinuities (i.e., boundaries between materials of different permittivities), returning to the surface where they are picked up by a receiving antenna and identified as peaks in amplitude (Allred et al., 2008). The elapsed time between the emission of the radar pulse and the reception of the reflected wave is measured and converted to depth below the ground surface. The radar wave amplitude and two-way travel time is displayed as a signal trace and, when the GPR antennae are moved along a transect, multiple traces side-by-side produce a radargram, or two-dimensional image (e.g., Figure 4-2).

Coupled with centimetre-level precision Real-Time Kinematic Global Positioning System (RTK-GPS) information, GPR data can be used to produce detailed, two- or three-dimensional maps of subsurface features (Allred et al., 2018). Antenna frequency is inversely related to both the radar signal penetration depth and minimum detectable object size, so high frequencies (i.e., $\geq$ 250 MHz) are likely to be required for detection of small and shallow objects such as mole channels (Allred et al., 2008). Radar signal penetration depth is also influenced by soil electrical conductivity, which is a function of the soil water content, porosity, clay mineralogy and content, salinity, and the amount of iron oxide, sulphates and carbonates present (Kuang et al., 2012). Certain soil types may, therefore, be more or less appropriate than others for this technique.

GPR has previously been used to identify and map lined tile drainage channels (i.e., clay pipe and corrugated plastic tubing) in a variety of soil types, where the dielectric permittivity of the air

Figure 4-2. Principles of ground-penetrating radar (GPR) coupled with high-precision RTK-GPS. Tx = transmitting antenna; Rx = receiving antenna. The radar wave amplitude and two-way travel time is displayed as a signal trace and, when the GPR antennae are moved along a transect, multiple traces side-by-side produce a radargram, or two-dimensional image. Modified after https://scantech.ie/scantech-about-gpr.html.

or water inside the tile drain channel contrasts with that of the surrounding soil (Allred et al., 2004; Allred & Redman, 2010; Karásek & Nováková, 2020; Koganti et al., 2021). The tunnel system burrows of the channels' mammalian namesake, the mole, as well as those of gophers have also been mapped, in high detail, by GPR (Allroggen et al., 2019; Saey et al., 2014). GPR, therefore, has considerable potential for artificial mole channel drainage mapping purposes.

The aim of this research was to characterise (i.e., depth, orientation, location, integrity, connectedness, density), using GPR techniques, the mole channel networks on a typical sheep farm with slowly-permeable, loess-derived soils in Southland, New Zealand, including their deterioration over a 30+ year period. The research questions were as follows: (1) can GPR be used to identify and map mole channels and a tile drain in loess-derived soil? (2) what are the characteristics of a mole drainage system constructed from repeat episodes of moling? (3) how persistent are mole channels in Southlands loess-derived Pallic Soils?

4.3 Methods

4.3.1 Study area

The study catchment has been described previously in Chapter 3, section 3.3.1. In brief, the soil is classified as an Argillic-fragic Perch-Gley Pallic Soil (S-Map; Hewitt, 1998), or an Aeric Kandiaqualf (USDA), and contains a slowly-permeable fragipan. Soil texture across the catchment is uniformly silt loam, and grades towards silty clay at 80 cm below the surface. A mole channel and tile drainage system was installed at the site sometime before 1990 and, as of the commencement of this study (2018), was over 30 years old (Landowner, personal communication, February 21, 2018). Details of the drainage network were limited to the knowledge that a tile drain was located in the primary hollow, but no information was available regarding the mole channel network, or the maintenance of the network prior to 1990. No modifications have been made to the drainage network by the farmer within the past 30 years.

4.3.2 Identifying drainage channels along transects

Ground-penetrating radar (GPR) was used to locate both the mole channels and tile drain at the field site. The GPR unit used was the Leica DS2000 (also known as IDS Opera Duo), with a dual frequency antenna including high (700 MHz) and low (250 MHz) frequency for both shallow (<3 m) and deep (<5 m) target location, respectively. The DS2000 (Plate 4-1a) is a commercial utility locating device designed for real-time identification of subsurface features, with perpendicular and broadside antennae orientation, 400 kHz sampling frequency, an acquisition speed of 10 km h^{-1}, a scan rate per channel of 512 samples per scan at 381 scans s^{-1}, and a scan interval of 42 scans m^{-1}. The GPR was connected to a Leica Viva GS15 GNSS antenna for high-precision, real-time kinematic (RTK) spatial positioning (Plate 4-1b).

The GPR unit was first used along the western interfluves of the study area on 5 April, 2018 to determine if mole channels could be identified along two north-south orientated transect lines (A-B and C-D in Figure 4-3). The propagation velocity was set to 10.0 cm ns^{-1}. Additionally, the basin hollow was surveyed along a zigzag transect that followed the full length of the hollow (a section of which is represented by E-F in Figure 4-3) on 23 June, 2018 to identify the tile drain.

Plate 4-1. (a) Testing the ground-penetrating radar (GPR) device coupled with real-time kinematic (RTK)-GPS at the field site on a beautiful Southland evening. (b) GPR surveying of the mole channels in 10 x 10 m plots at high-resolution. The high-precision Leica Viva GS15 GNSS antenna is shown mounted directly over the radar. Real time reflections are shown on the screen and their locations recorded manually as a GPS coordinate at the apex of each reflector.

4.3.3 Ground truthing of mole channels and tile drain reflections

To ground truth the GPR scans of transects A-B and C-D, three sites were excavated where regular diffractors were observed on the radargram during surveying, suggesting regularly-spaced mole channels. Deeper GPR reflections in the hollow, indicative of the tile drain, were ground truthed using a one metre long, thin soil probe, which was pushed into the soil until it hit the clay pipe. More detailed ground truthing of the tile drain occurred during installation of a tile flow meter at the catchment outlet when the soil around the tile drain was excavated.

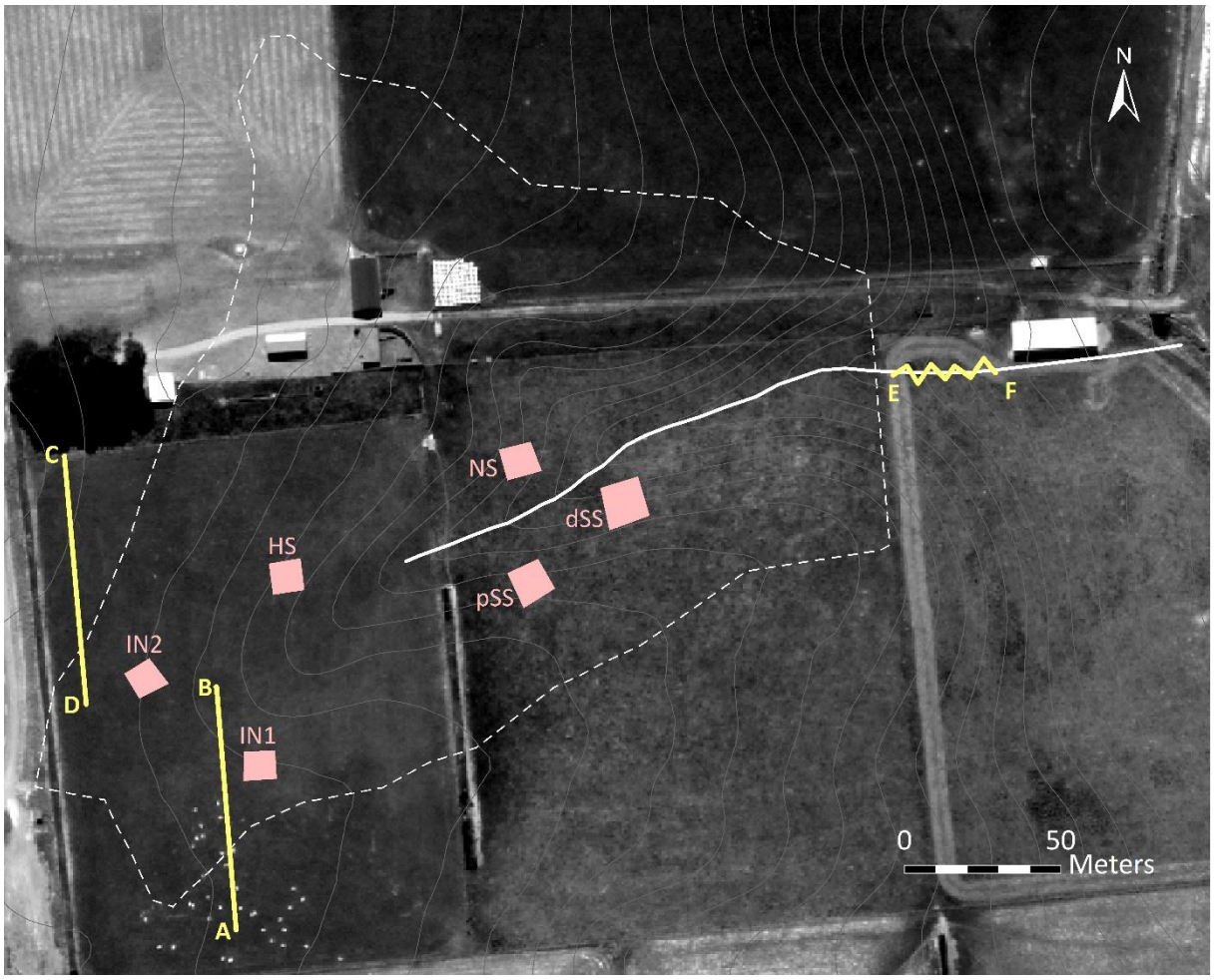

Figure 4-3. The field site drainage basin, showing the watershed (dashed line), and 0.5 m contour lines (dark grey). Transect lines A-B and C-D (yellow lines) were located on the interfluves to detect mole channels. Transect line E-F followed the hollow to locate the tile drain (solid white line). The six mole channel survey plots (pink squares) are shown on the interfluves (IN1 and IN2), the headslope (HS), the nose slope (NS), and the planar and divergent side slopes (pSS and dSS, respectively).

4.3.4 High resolution, small scale surveys of mole channel networks

Six areas within the 3.9 ha drainage basin were chosen for high-resolution mole channel mapping (Figure 4-3). The six sites were chosen to represent the slope, TWI and landscape element distributions within the drainage basin and were located on the interfluves (IN1 and IN2), head slope (HS), planar side slope (pSS), divergent side slope (dSS) and nose slope (NS).

Table 4-1 shows the depth to the fragipan, particle size distribution at 45 cm (i.e., the common depth of mole channel installation), and mean saturated hydraulic conductivity (K_{sat}) between the surface and the mole network (i.e., 0 – 45 cm) for each of the surveyed sites. At each site the GPR device was used to survey plots of 10 x 10 m in directions approximately parallel and transverse to the fence line between the two paddocks. The transect spacing was 0.35 m. GPS coordinates were manually recorded in real-time at the apex of each hyperbola (Figure 4-2). The coordinate dataset was then displayed on ArcGIS for 2-D visual interpretation of the mole channels. Mole channel density was estimated by visually linking the data points that formed apparently continuous channels and summing their total lengths (m) within the plot area (m^2).

Table 4-1. Depth (cm) to the fragipan surface, particle size distribution (%) as measured at 45 cm below the surface, and mean saturated hydraulic conductivity between 0 and 45 cm (K_{sat}; mm h^{-1}) for each of the six surveyed sites, including on the interfluves (IN1 and IN2), head slope (HS), planar side slope (pSS), divergent side slope (dSS), and nose slope (NS). * = point measurement at 45 cm; ¥ = mean of three measurements at 15, 30 and 45 cm.

Site	Depth to fragipan (cm)	Sand (%)*	Silt (%)*	Clay (%)*	K_{sat} (mm h^{-1}) ¥
IN1	60	5	63	32	21.8
IN2	60	7	65	29	29.0
HS	70	7	65	28	24.1
pSS	60	5	61	35	35.3
dSS	80	6	61	34	12.7
NS	40	9	59	32	8.8

4.4 Results

4.4.1 Mole channel and tile drain identification

Clear and regular diffractors were present on the high frequency (700 MHz) radargram during ground-penetrating radar (GPR) surveying of the interfluve transects (surveyed in April 2018). Along Transect A-B, multiple distinctive hyperbolic signatures were evident at an apparent depth of ca 0.5 m, indicative of the transverse crossing of multiple mole channels (i.e., perpendicular to the channel direction; Plate 4-2). For example, in Plate 4-2a between 20 and 30 m, there are six distinctive hyperbolic shapes. Continuous flat reflections were also observed at approximately the same apparent depth, along transect C-D, indicating the longitudinal overpass of a single mole channel (i.e., running above and parallel to the channel direction; Plate 4-3). For both transects, the resolution of the diffractions was more variable in the low frequency (250 MHz) radargram (Plate 4-2b and Plate 4-3b) and, because they were generally less informative for identifying mole channels, we did not analyse them further.

Ground truthing confirmed that the radargram hyperbola of the high frequency antennae (700 MHz) was identifying mole channels with high lateral accuracy and precision (i.e., within ca 5 cm; Plate 4-4a). The depth of the mole channels was between 40 and 50 cm. Moreover, the mole channels were in remarkably good condition, despite their age of over 30 years (Plate 4-4b). Fine roots could be seen growing inside the mole channel and material from the Ap horizon above had been transported by worm burrowing into the channel. Soil structure was also evident in the walls of the mole channel. No cracks or fissuring were visible between the mole channels and the soil surface.

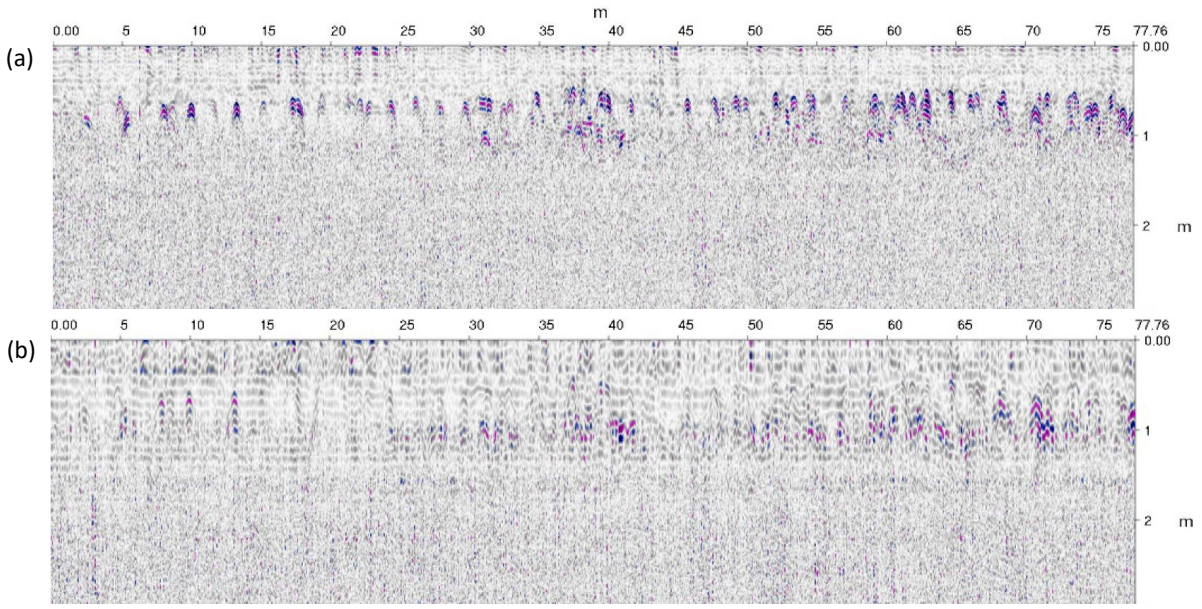

Plate 4-2. Radargram produced using ground-penetrating radar (GPR) along the 77.76 m transect A-B on the interfluve. Data shown are from (a) the high frequency antenna (700 MHz) and (b) the low frequency antenna (250 MHz). Multiple distinctive hyperbolic signatures are evident at an apparent depth of ca 0.5 m, and were indicative of the transverse crossing of multiple mole channels (i.e., perpendicular to the channel direction).

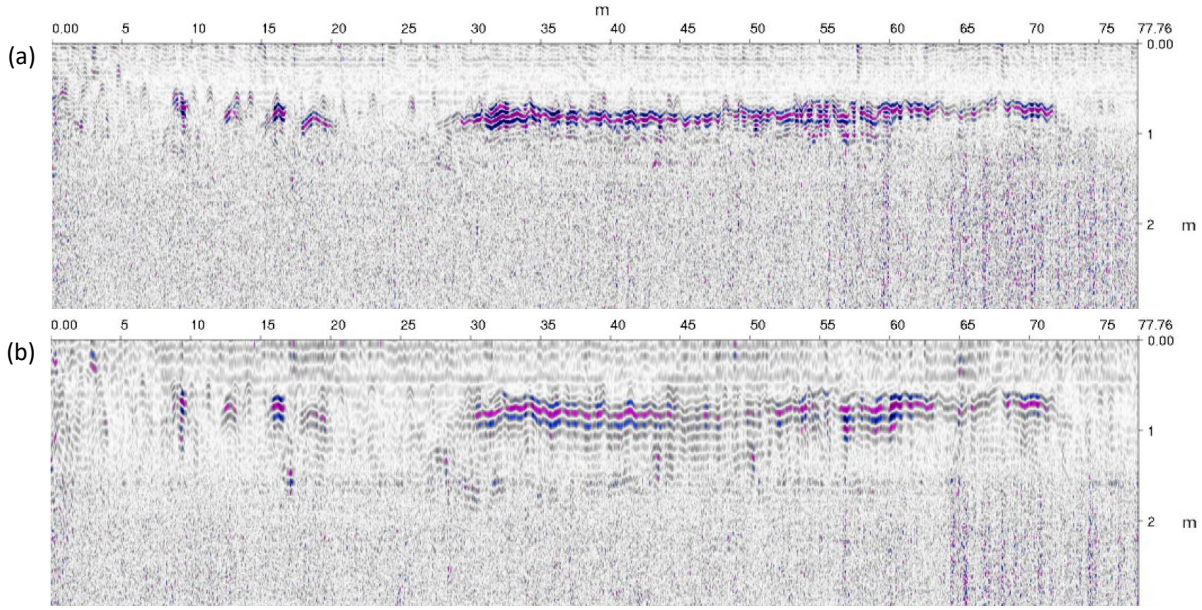

Plate 4-3. Radargram produced using ground-penetrating radar (GPR) along the 77.76 m transect C-D on the interfluve. Data shown are from (a) the high frequency antenna (700 MHz) and (b) the low frequency antenna (250 MHz). Continuous flat reflections are evident at an apparent depth of ca 0.5 m, and are indicative of the longitudinal overpass of a single mole channel (i.e., running above and parallel to the channel direction).

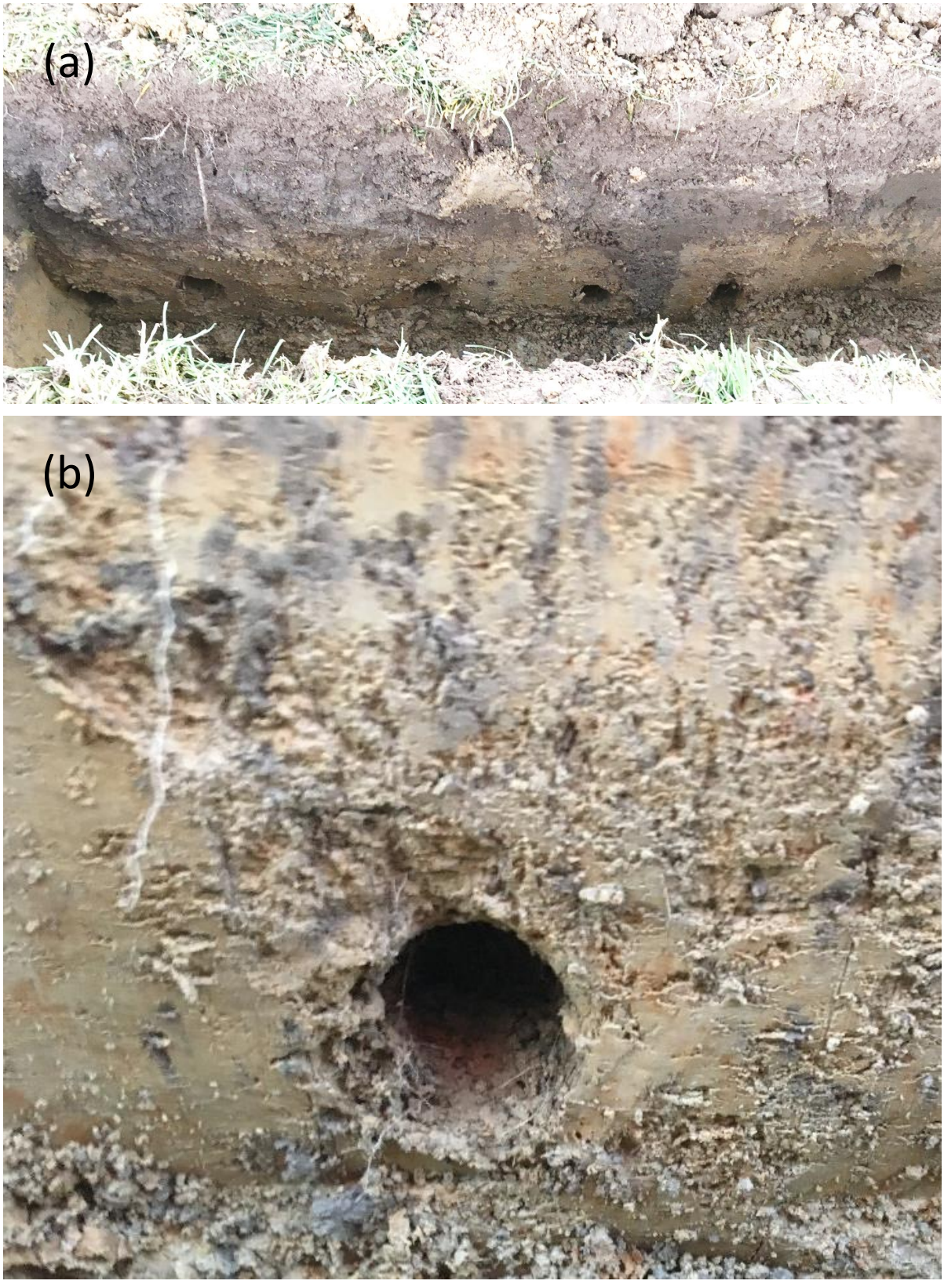

Plate 4-4. A trench (a) that was excavated at a location where the ground-penetrationg radar (GPR) radargram identified multiple distinctive hyperbolae, showing mole channels (5 cm diameter) located 40 – 50 cm below the surface. Upon close inspection (b), fine roots can be seen growing inside the cavity, as well as material from the Ap horizon above, apparently transported by worm burrowing. Soil structural units can also be seen forming the walls of the mole channel.

Along transect E-F (surveyed in June 2018), multiple distinctive hyperbolic signatures were evident in both the high frequency antenna (700 MHz) and low frequency antenna (250 MHz; Plate 4-5). The hyperbolae were at two apparent depths, 0.8 – 0.9 m and ca 1.2 m. The shallower reflections were, again, indicative of the transverse crossing of multiple mole channels, while the deeper were indicative of the transverse crossing of a tile drain running the length of the hollow.

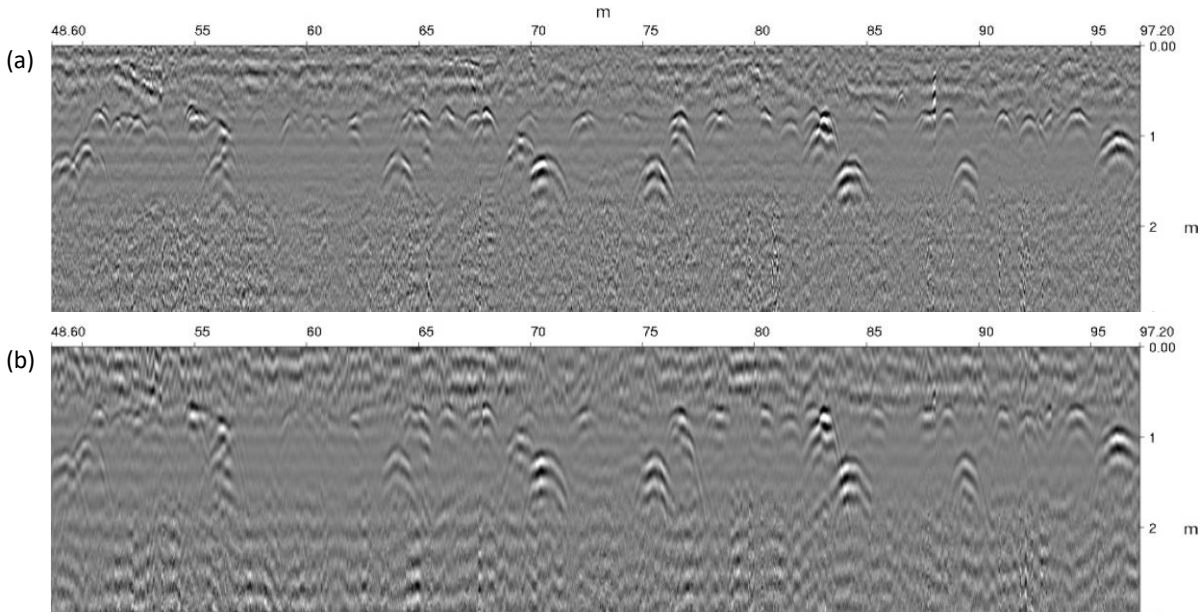

Plate 4-5. Radargram produced using ground-penertating radar (GPR) along the 48.6 m zigzag transect E-F of the field site hollow. Data shown are from (a) the high frequency antenna (700 MHz) and (b) the low frequency antenna (250 MHz). Shallow reflections were indicative of the transverse crossing of multiple mole channels, while the deeper were indicative of the transverse crossing of a tile drain running the length of the hollow

Ground-truthing using a one metre long, thin soil probe, confirmed the radargram hyperbola of the high frequency antennae identified the tile drain with good lateral accuracy and precision (i.e., within ca 5 cm). The depth of the tile channels was between 70 and 80 cm, demonstrating incoherence with the apparent depth (i.e., 1.2 m) portrayed in the radargram. The tile drain was constructed from multiple ca 30 cm long x 13.5 cm diameter clay pipes butted up against one another and was overlain by well-structured fill including topsoil material (Plate 4-6). The tile drain also appeared to be in good condition, despite its age of over 30 years.

Plate 4-6. The excavated, ca 13.5 cm diameter, tile drain at the catchment outlet could be identified from hyperbola reflections on the GPR radargram. The clay pipe was found at a depth of 70 – 80 cm and can be seen to be overlain by a well-structured fill, including topsoil.

4.4.2 Mapping the mole channel network and tile drain

A complicated network of closely spaced mole channels underlay all of the surveyed plots and, by extrapolation, the entire drainage basin. The channels were closely spaced, in some cases with as little as 30 cm between two more-or-less parallel drains. They ran in multiple orientations, but either trended perpendicular or parallel to the hillslope gradient or north-south and east-west on the flatter areas (Figure 4-4a-f & Figure 4-5).

At all of the surveyed sites, the reflectors were distinct, and their continuity was high. The only exception to this was noted at the nose slope (NS) between the primary and secondary hollow, where the soil depth to the fragipan was just 40 cm and the depth of loess to the underlying gravels was less than 90 cm. Here, the mole channel network appeared to have sustained some level of damage – with GPR reflections in half of the mapped area not indicating coherence of the drainage lines (Figure 4-4d).

By connecting the mapped mole channel points at each plot and calculating the total length of all of the mole channels present within each 100 m^2 plot, an average mole channel density of 1.6 m m^{-2} was calculated for the drainage basin.

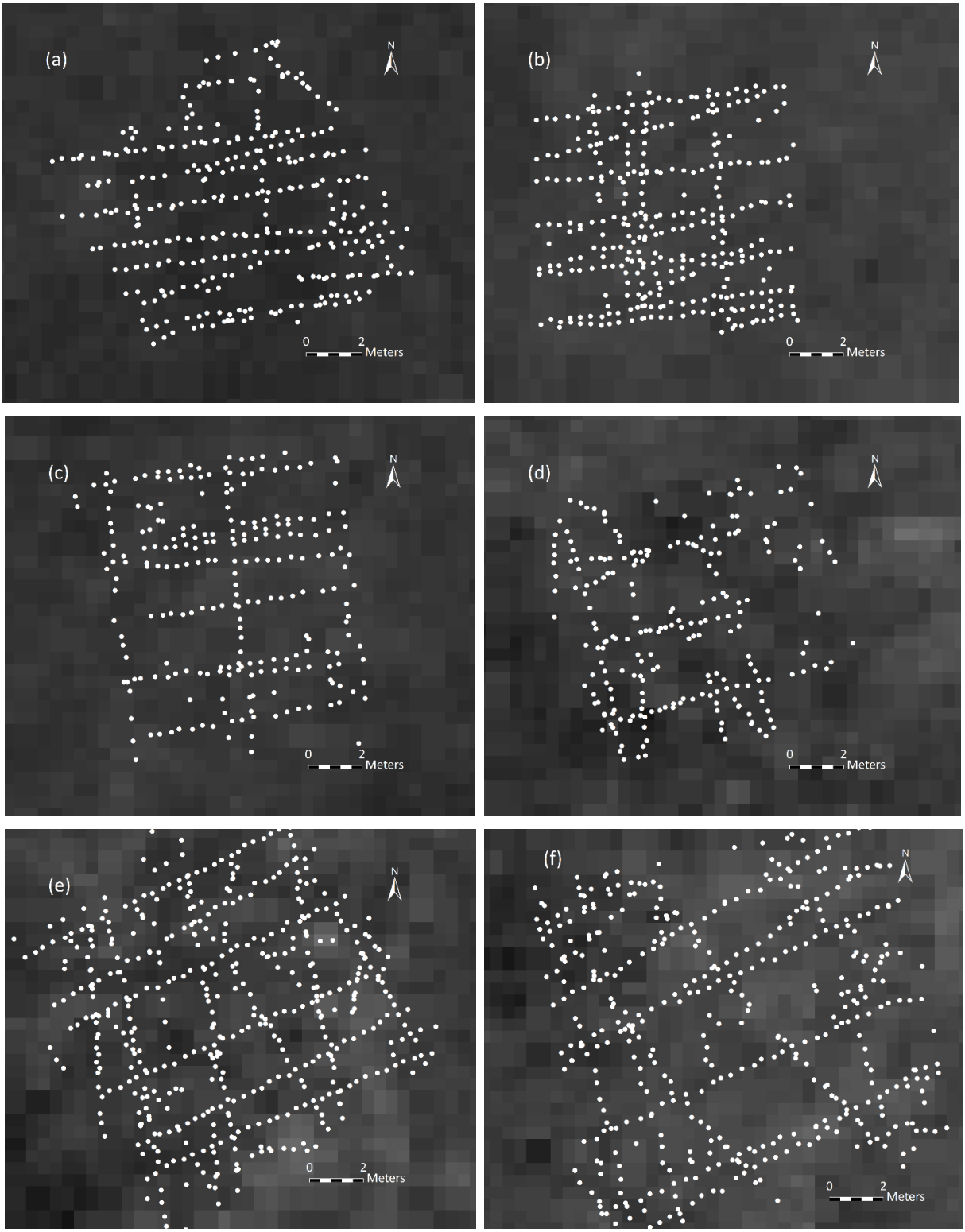

Figure 4-4. The six mole channel survey plots and the 2D-mapped radargram hyperbola axes, in close up, each showing a densely spaced mole channel network. The maps show (a) IN2, (b) IN1, (c) the headslope (HS), (d) the nose slope (NS), and (e) the planar and (f) divergent side slopes (pSS and dSS, respectively).

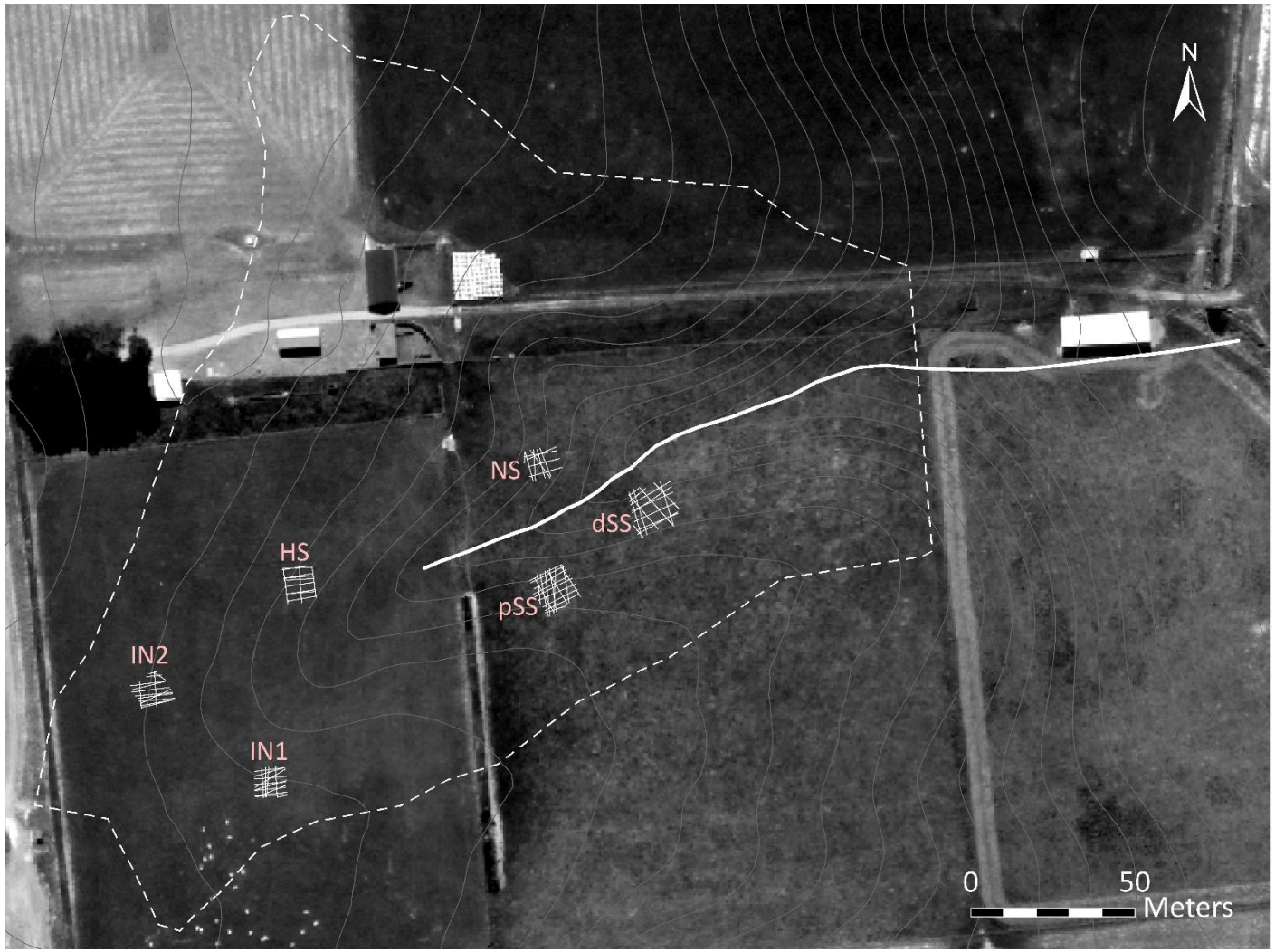

Figure 4-5. The mole network at each of the six survey plots, as well as the tile drain, extrapolated from the 2D-mapped radargram hyperbola axes. The mapped sites were on the interfluves (IN1 and IN2), the headslope (HS), the nose slope (NS), and the planar and divergent side slopes (pSS and dSS, respectively). The watershed boundary (dashed line), and 0.5 m contour lines (dark grey) are also shown.

4.5 Discussion

Hyperbolic signatures at an apparent depth of 0.4 – 0.5 m identified by the high frequency (700 MHz) antenna were shown by excavation to be a result of mole channels, thereby confirming that GPR, coupled with high precision RTK-GPS, can be used to identify and map these subsurface features. It is recognised that the method of manually recording GPS coordinates at hyperbolic GPR signatures is simplistic and relatively labour-intensive, and that post-processing software would have improved the efficiency, vertical accuracy and reliability of the results. For example, transects were surveyed on two different dates (i.e., mole identification on April 2018 and tile drain identification on June 2018), and while the horizontal position could be resolved with high accuracy and precision on both dates, the apparent depth was not, indicating the need for calibration of the dielectric constant. This could have been due to variation in soil moisture between the two dates (Ritzema, 1994), or, differences in soil properties between the hollow, where the tile drain was surveyed, and the interfluves and slopes, where the moles were surveyed. Advanced signal processing would also enable the extraction of additional information about the properties of the subsurface (e.g. depth of the fragipan surface or perched water tables) that may help to further characterise the mole network (Jol, 2008). However, this study provides evidence of the applicability of GPR for the purposes of mapping mole channel networks at plot and paddock scales. At larger scales (e.g., catchment), ground-based GPR may not be an efficient method for mapping mole channel networks and it may be worth considering alternative technologies. Unmanned aerial vehicles (UAVs) such as drones, combined with GPR, may have potential for increasing the efficiency of data collection, but this combination of technologies is in an early stage of development (Edemsky et al., 2021; Linna et al., 2022; Wu et al., 2019). Another technology that has shown promise in the mapping of tile drainage networks, and may have application in the use of mole network mapping, is visible-colour (VIS-C), multispectral (MS), and thermal infrared (TIR) imagery, also obtained by UAVs (Allred et al., 2020).

In the study area and presumably elsewhere in Southland the density of mature mole channel networks can be very high, and their orientation characteristics complex. In general, a two to four metre spacing for drainage lines (tiles and/or moles) is considered very closely spaced, and suitable for heavy soils of very low hydraulic conductivities (i.e., 0.4 mm h-1; Ritzema, 1994). Assuming that one generation of mole channels were installed in a parallel, rectangular pattern (Figure 4-1a), these spacings would equate to a density of between approximately 0.3 and 0.6 m m^2. The measured mole channel density at this field site (i.e., 1.6 m m^{-2}), can therefore be considered very

high. Multiple and very closely spaced (i.e., as little as 30 cm) mole channel orientations indicated that the network had been installed over several generations of mole-ploughing. These results are not unexpected, as it is common practice for mole channels to be re-ploughed every few years (Bowler, 1980; Smedema et al., 2014). In the Southland region where this study was conducted, estimates suggest that mole and tile drainage covers approximately 75 % of agricultural land (Pearson, 2015), so their influence on regional hydrology and water quality is likely to be significant.

The results demonstrate that multi-generational mole channels in loess-derived soils of Southland maintain a high degree of connectivity and good condition for up to 30 years or more. Long-term mole channel stability is influenced by installation conditions as well as several inherent soil factors (Spoor & Ford, 1987; Spoor et al., 1982). No information was available regarding the installation conditions of the mole network in the present study. Clay contents of > 45 % are considered particularly suitable for moling, whereas mole channels are unstable in soils with < 30 - 35 % clay (Ritzema, 1994; Tuohy, 2013). The soil clay content in the present study was between 28 and 35 % (Table 4-1), so it could be considered somewhat surprising that the drainage network appears to be highly stable. Clay mineralogy also has a significant influence on mole channel stability, with smectitic clays prone to channel collapse due to their shrink and swell properties (Ritzema, 1994; Spoor et al., 1982). Clay mineralogy was not determined at this field site; however, there was no visible evidence of significant shrink-swell behaviour (i.e., surface cracks during summer) over the course of the wider 3-year study. The apparent structural stability of the soils under investigation could be explained by the moderate phosphate retention (34 – 45 %), which was higher than that typical of other Fragic Pallic soils (22 %) mapped in S-map (Manaaki Whenua Landcare Research, 2022). This suggests that a greater degree of weathering has occurred at this site, as phosphate retention may be used as a measure of soil stabilising short-range-order oxy-hydroxides of aluminium and iron (Hewitt & Shepherd, 1997). Depth to the fragipan appeared to influence the longevity of the mole channel network in the present study. The nose slope (NS) was the only site where the mole network appeared to have sustained some level of damage – with GPR reflections in half of the mapped area not indicating coherence of the drainage lines. This was also the only site where the mole channels had been installed in the fragipan, due to its shallow surface (i.e., 40 cm). One of the conditions for fragic horizon designation is that the soil slakes when immersed in water (Milne et al., 1995). Structural stability on wetting is an additional factor that influences the lifespan of a mole channel (Ritzema, 1994), therefore the slaking property of

fragipans would suggest that mole channels installed in these horizons would be prone to dispersion and collapse (Bruce, 1972), explaining the observed results at the NS. As discussed by Bruce (1972), the key to the success of mole channel stability in loess soils is to install them in the lower B horizon, where the greatest weathering has occurred and to avoid the fragipan.

There was no visible evidence of a fracture network between the mole network and the soil surface, as would have been induced by soil displacement during mole channel installation. This secondary fracture network is considered to be a key functional element of the mole network through its facilitation of rapid, preferential flow between the soil surface and the mole channel, especially in soils with low hydraulic conductivity (Leeds-Harrison et al., 1982; Ritzema, 1994; Smedema et al., 2004). However, the observations of root growth and worm burrows into the mole channels, as well as the well-structured soil forming the channel walls suggest these channels are, nevertheless, likely to be well hydraulically connected to the surrounding soil. Furthermore, the soils under investigation are not heavy clay soils (i.e., clay ranges between 28 and 35 % at the depth of the mole network; Table 4-1) and the saturated hydraulic conductivity of the soil profile between the surface and the mole network (Table 4-1) is moderate (i.e., 4 – 72 mm h-1; Webb & Lilburne, 2011), which suggests that water movement into the mole channels is not significantly constrained by the soil properties. It is the satisfactory water entry into open and stable mole channels that determines the success of a mole drainage system (Ritzema, 1994), so these results suggest that, despite its age, the mole channel network can be considered a highly-connected (at least laterally) and functional artificial macropore network with the potential to regulate perched water tables and to modify soil hydrology (as demonstrated in Chapter 7).

Given that no modification has been made to the mole channel network within the past 30 years, these maps demonstrate the longevity of the mole channel network in slowly-permeable, loess-derived soils, provided the channels are installed in the weathered B horizon overlying the fragipan. Thirty years is considerably longer than previously reported estimates (7 – 10 years) of the longevity of mole channels in Argillic-fragic Perch-gley Pallic soils (Palmer et al., 2006), and the 10 – 15 years that Bowler (1976) estimated for mole drains in New Zealand soils. This work provides the first attempt at mapping and characterising mature, multi-generational mole channel networks in slowly permeable loess soils.

4.6 Conclusions

Ground-penetrating radar (GPR) was successfully employed to map and characterise the mole channel network and tile drain in a loess-derived Pallic Soil in Southland, New Zealand, showing high lateral precision and accuracy. The mole network was complex in terms of its design and had a high density of interconnected, multidirectional mole channels (1.6 m m^{-2}), which appeared to have been developed over several generations of mole ploughing carried out over 30 years ago. The mole channels demonstrated longevity, and ongoing functionality despite the soil being relatively low clay content (28 – 35 %), which is often considered unsuitable for long-term mole stability. Soil depth to the fragipan appeared to control longevity of the mole network, and moles that were formed in shallow fragipans appeared to have disintegrated. Visual observations provided no evidence for persistence of a soil fracture network induced at the time moles were installed; however, root growth and worm burrowing into the mole channels suggest that they are hydraulically connected to the surrounding soil through natural macropores. It is likely that these dense and highly connected 'legacy' mole channel networks are common in areas of similar soil types where mole and tile drainage is practiced, or has been practised within the past 30+ years. These results have significance for understanding catchment-scale hydrodynamics, especially considering that the life span of these artificial drainage networks has been shown to be considerably longer than previous estimates for this soil type (7 – 10 years). Further characterisation of these networks and mapping at broader spatial scales could provide important information pertaining to stream flow behaviour and the management of water quality.

Chapter 5

Soil hydraulic properties and moisture regime of a mature mole-tile drained loess-derived soil

5.1 Abstract

Installation of mole channels introduces secondary, vertical fracture networks, considered to be a key functional element of this type of drainage system. It is not clear how legacy installation effects, or the current mole network, influence soil physical and hydraulic properties when the mole channels are mature (30 + years), nor is it clear how important the consideration of mole and tile drainage is to current classifications of soil moisture regime. The aim of this chapter was to understand the direct and indirect influence of mature mole channels on soil properties and behaviour, and to assess the moisture regime of loess soils under long-term mole channel drainage. Surface and subsurface soil hydraulic and physical properties (i.e., saturated hydraulic conductivity [K_{sat}], dry bulk density, porosity, macroporosity and field capacity) were measured at mole-proximal and mole-distal sites to identify any influence due to the mole channel fracture network. The influence of antecedent volumetric water content (VWC) on surface K_{sat} was also examined. Finally, the soil moisture regime was characterized in terms of permeability and drainage class. No effect due to mole channel proximity was detected on surface and subsurface soil hydraulic and physical properties, demonstrating that mole channel longevity does not imply equivalent longevity of the mole fracture network. The results suggest that preferential flow to mature mole channels via artificial fractures was not an important hydraulic or contaminant transfer pathway at the study site. Surface K_{sat} appeared to be controlled by the antecedent soil moisture content, but only on the interfluves, where K_{sat} was significantly greater in wet state antecedent conditions than dry state antecedent conditions. This may have reflected a pore network with enhanced connectedness as a result of capillary rise above perched water tables, and the removal of entrapped air. Saturated hydraulic conductivity estimates provided a permeability classification consistent with that provided by the New Zealand Soil Classification; however, the assessment of drainage class varied with respect to the method used.

5.2 Introduction

Mole and tile drainage systems are generally installed in agricultural soils with low permeability and/or poor drainage due to an impeding layer, with the aim to reduce the amount of time under soil moisture excess. A key functional element of mole drainage is considered to be the secondary fracture network, which increases macroporosity and provides continuity of flow pathways between the soil surface and the mole network (Goss et al., 1983; Leeds-Harrison et al., 1982; Robinson et al., 1987; Youngs, 1985). The fracture network is a result of soil displacement during mole channel installation which, through shearing stress, leads to well-defined rupture planes that radiate from the mole channel to the soil surface (Figure 5-1) (Smedema et al., 2004). Fracture characteristics are dependent on the soil conditions during installation but, under ideal conditions, the cracks extend to a distance of approximately 0.3 m on each side of the blade slot, and have a width of between 5 and 60 mm (Leeds-Harrison et al., 1982; Youngs, 1985). Functionally, the fracture network facilitates rapid drawdown of perched water tables, as well as the direct, preferential flow of water between the surface and the mole channel (Bowler, 1980; Horne, 1985; Leeds-Harrison et al., 1982; Robinson et al., 1987; Scotter et al., 1979; Youngs, 1985). In the absence of the fracture network, the effectiveness of the drainage system is solely dependent on the natural hydraulic conductivity of the undisturbed subsoil (Leeds-Harrison et al., 1982; Scotter et al., 1979). How the fracture network influences soil physical and hydraulic properties is critical information for environmental models and land management decisions, of which these properties are a fundamental component. For example, flow through the fracture network may carry contaminants from the soil surface directly to the mole channels and, via the tile drain, into receiving surface waters (Hallard & Armstrong, 1992). Such knowledge is especially important in settings where mole drains are installed every 3 – 10 years, with the potential to result in dense and extensive mole networks (e.g., Chapter 4).

If the mole channel fracture network has a measurable effect on soil proximal to the drain location, density metrics (e.g., as calculated in Chapter 4) may enable the effect to be scaled to the entire drained area. Such an effect was demonstrated by Leeds-Harrison et al. (1982) who showed that surface infiltration rates above freshly installed mole channels were much greater than at mid-drain spacings. The effect was confined, almost totally, to the area directly above the mole drain, and was concluded to be a result of preferential flow through the secondary fracture network. They also showed that drainage response to precipitation by mole channels with an associated fracture network was more rapid, peak flow rates were greater, and hydrograph recession periods were

Figure 5-1. Diagramme showing the radial fracture network created by the mole plough during installation, forming cracks through which water flows preferentially from the ground surface. Image modified from Monaghan (2014).

shorter, all signs of fracture network flow. Goss et al. (1983) provided further evidence of the mechanically-generated macropore network, and highlighted that flow occurred predominantly through the slot left by the blade of the mole. Youngs (1985) proved, mathematically, that the fracture network enables a mole-drainage system to cope with higher rainfall rates and to produce more rapid water-table drawdowns. Robinson et al. (1987) showed that, despite the fractures being subject to the natural shrink/swell properties of clay, they do not close completely (within the monitored 5 year period), unless destroyed by the action of animal/machinery compaction. Scotter and Kanchanasut (1981) conducted dye studies above six year-old mole channels, and found that root and worm channels, in association with fracture planes, formed significant preferential flow pathways.

While much is known about the functional behaviour of the fracture network in newly-installed mole systems, there is little information about this functionality in mature (30 + year) mole systems. In the right soils, mole channels may have great longevity, maintaining their integrity and connectivity for 30+ years (e.g., Chapter 4, section 4.4.1). Whether the fracture network persists as long as the mole channels themselves in slowly permeable loess, or if they influence the soil physical

and hydraulic properties in a measurable way in mature (30+ year old) drainage networks, is unclear.

Even if the fracture network of mature mole networks no longer directly influences soil hydraulic properties, it is possible that mole channel drainage may still indirectly influence these properties. For example, lowered perched water tables reduce the antecedent soil moisture content at the onset of precipitation, so understanding whether or not there is an effect of antecedent moisture conditions on soil hydraulic properties is also necessary to understand the influence of subsurface drainage on these properties. A number of studies have investigated the influence of the antecedent soil moisture conditions on K_{sat}, with the results often demonstrating a negative correlation between antecedent volumetric moisture content and K_{sat} (Lin et al., 1998; Reynolds & Zebchuk, 1996; Zhou et al., 2008). To address the influence of mole channel drainage on key hydraulic properties such as K_{sat}, it is, therefore, also worth considering if there is an effect of the antecedent soil moisture content.

By rapidly lowering the perched water table, mole systems alter the soil's natural wetting and drying cycles, which are a key mechanism behind the development of soil structure. This occurs through the influence of wetting and drying on soil physical properties such as porosity and pore size distribution (Bodner et al., 2013; Pires et al., 2005). The high density of mole drainage (i.e., < 3 m spacing) likely results in a relatively even lowering of the perched water table, such that changes in wetting and drying behaviour are consistent between drain lines (Hillel, 1982). This means that, unlike soil fracturing, any changes in soil properties due to wetting and drying cycles are unlikely to be detected at the local scale of a mole channel, but may be detectable at scales relevant to soil classification and mapping.

With this in mind, it is imperative to understand whether current assessments of the soil moisture regime, which do not account for artificial subsurface drainage, sufficiently describe the hydrology of drained soils. In many classification schemes, assessment of the soil water regime requires consideration of both the potential of the soil to transmit water internally (i.e., soil permeability), and the actual rapidity and extent of water removal that controls the prevailing wetness (i.e., soil drainage; Milne et al., 1995; National Committee on Soil and Terrain, 2009; Schoeneberger et al., 2012).

The natural potential of a soil to transmit water is commonly quantified by assigning ranges of measured saturated hydraulic conductivity (K_{sat}, mm h^{-1}) to permeability classes. Permeability class boundaries vary among the different soil description systems around the world, and in New Zealand are recognized as slow (< 4 mm h^{-1}), moderate (4 – 72 mm h^{-1}), and rapid (≥ 72 mm h^{-1}) (Webb & Lilburne, 2011). The New Zealand Soil Classification (NZSC) recognizes 15 soil orders in level 1 of the classification, each of which are divided hierarchically into groups (level 2), subgroups (level 3), family (level 4) and sibling (level 5). Alongside a classification of soil-profile material, rock and texture, the identification of the 4th level soil family requires classification of the soil permeability, which is based on the slowest permeability horizon within the top 100 cm (Webb & Lilburne, 2011). Because of high spatial variability associated with K_{sat}, as well as the large cost associated with K_{sat} measurement, direct measures of K_{sat} are rare for NZ soils, so soil permeability is most often inferred from easily obtainable morphological characteristics, namely texture, structure (type, grade, and class) and soil consistence (Griffiths et al., 1999; Webb & Lilburne, 2011).

Drainage classes are also described qualitatively, through observations of water tables, landscape position and the assessment of soil morphological features (Vogeler et al., 2019). The relationship between soil morphology and the rapidity of water removal (Australian Soil Classification; National Committee on Soil and Terrain, 2009) or time periods under wet conditions (USDA; Schoeneberger et al., 2012) relies predominantly on observations of soil colour and reductimorphic features. In general, the greyer a soil horizon, and the closer the grey colours to the soil surface, the more poorly drained the soil. Reductimorphic features such as mottling and orange linings of root channels (i.e., through the oxidation of Fe^{2+} with aerobic conditions and subsequent precipitation of Fe^{3+}) indicates that the soil is subject to intermittent periods of anoxia throughout the year, while reddish or brownish colors and the absence of reductimorphic features indicates well-drained soils. Within the NZSC, information about the natural soil drainage is required for classification at all levels of the classification. In this instance, drainage class is based on morphologically defined soil horizons and their relative depth. Annual duration that the soil is above field capacity may also be used as an indication of soil drainage status. For example, in New Zealand, poorly drained soils may be described as those that experience 3-6 months above field capacity, while those that experience 1-2 months above field capacity are said to be imperfectly drained (Taylor & Pohlen, 1962; Vogeler et al., 2019).

The NZSC definition of soil moisture regime based on classification of natural soil morphological features does not take in to account artificial subsurface drainage, so it is important to understand whether this definition of soil moisture regime suffices in artificially drained landscapes. Therefore, the aim of this chapter was to understand the direct and indirect influence of mature (i.e., 30+ year) mole channels on soil properties, behaviour, and moisture regime.

The specific research questions and objectives of this chapter were as follows:

1) Does the landscape retain a fracture network induced when moles were installed that still influences soil hydraulic properties?

    - Quantify differences in surface saturated hydraulic conductivity (K_{sat}), as well as key subsoil hydraulic and physical properties, between 'mole-proximal' and 'mole-distal' locations at a range of depths.

2) Is saturated hydraulic conductivity dependent on antecedent soil moisture state (wet state versus dry state)?

    - Quantify the effect of soil moisture content on soil surface K_{sat}.

3) Are morphologically determined permeability and drainage classifications (as used in S-Map) meaningful in mole and tile drained, loess soils?

    - Classify the permeability and drainage class for a mole and tile-drained soil using spatial, temporal and point-scale measurements of soil hydraulic properties.

5.3 Methods

5.3.1 Study area

The study area has been previously described in Chapter 3, section 3.3.1. The soils were previously mapped as the Pukemutu_6a.1 soil sibling (Appendix D) within the Pukemutu soil family (Manaaki Whenua Landcare Research, 2022). These soils are Argillic-fragic Perch-Gley Pallics (S-Map; Hewitt, 1998), or Aeric Kandiaqualfs (USDA; Soil Survey Staff, 2014), and are characterised by the presence of a fragipan with an upper boundary between 60 and 90 cm depth. The permeability classification for Pukemutu soils is moderate in the topsoil (i.e., K_{sat} 4 – 72 mm h^{-1}) over slow (i.e., K_{sat} < 4 mm h^{-1}) in the subsoil, and their drainage classification is 'poor' (Manaaki Whenua Landcare Research, 2022). The texture was determined as silt loam grading to silty clay (Figure 5-2; Section 3.3.4.

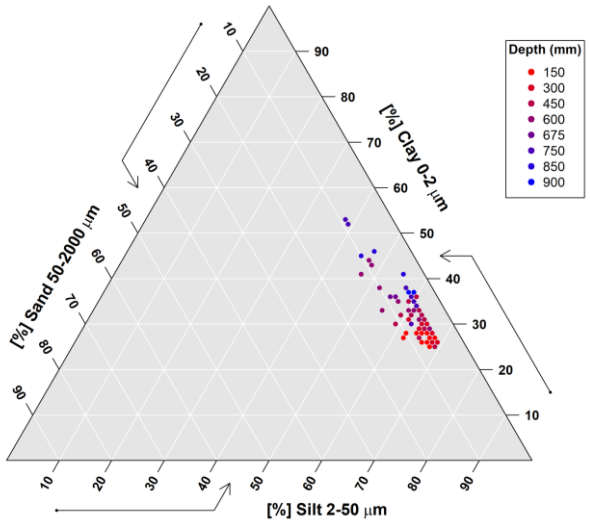

Figure 5-2. The soil particle size distribution by depth (mm), obtained from n=66 soil samples collected across the field site (Section 3.3.4).

5.3.2 Surface saturated hydraulic conductivity (K_{sat}) measurements

Six sites were selected to cover various landform elements across the drainage basin, including the interfluves (pits IN1 and IN2), head slope (HS), planar side slope (pSS), divergent side slope (dSS) and nose slope (NS). A map of the mole channel network at each pit location was obtained through ground penetrating radar (GPR) surveying, described in Chapter 4 (Figure 5-3).

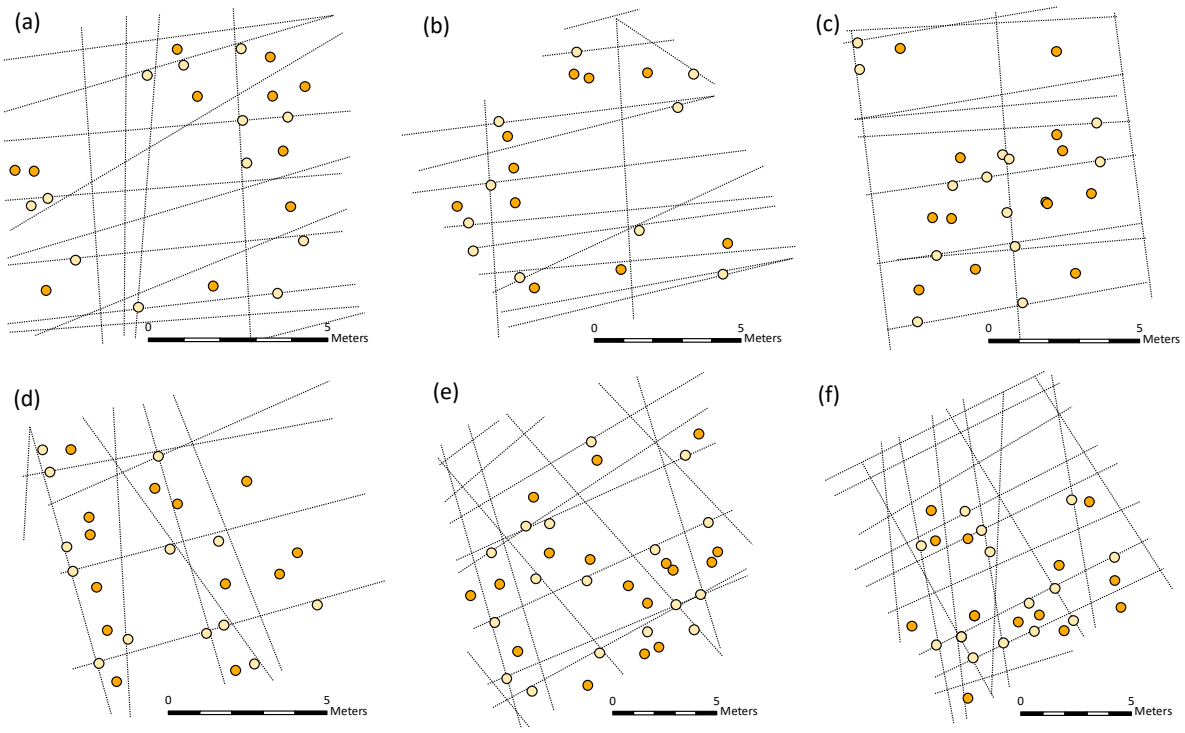

Figure 5-3. Measurement locations of surface saturated hydraulic conductivity (*Ksat*) at each of the surveyed sites (a) IN1, (b) IN2, (c) HS, (d) NS, (e) dSS and (f) pSS. Half the measurements were made proximal to (i.e., above; cream points) a mole channel (shown by the black lines), and half the measurements between the mole channels (i.e., orange points).

Surface saturated hydraulic conductivity (K_{sat}) was measured on six separate occasions at each site over the period between 29 March 2019 and 6 March 2020 (i.e., n = 144 total measurements). To identify potential variation in surface K_{sat} due to the mole-plough installation fissures, measurements were taken at two positions relative to the mole drain: directly above a mapped mole channel ('mole-proximal') and between mole channels ('mole-distal'; Figure 5-3). Mole-distal measurements were always 70 – 130 cm away from mole channel to ensure they were outside the zone of soil fracture (i.e., within 30 cm; Figure 5-1; Leeds-Harrison et al., 1982). Precise RTK-GPS (Leica Viva GS15 GNSS) was used to identify and stake out the measurement sites to ensure centimetre accuracy.

Measurement sites were prepared by trimming the grass back to the ground surface, and installing a single 30 cm diameter stainless steel ring 1 cm into the soil (Figure 5-4a). An automated infiltrometer (Ekanayake et al., 2019) was then set up inside the ring (Figure 5-4b) and used to measure infiltration rates following the Beerkan Estimation of Soil Transfer parameters (BEST) methodology (Lassabatere et al., 2013). An SM300 TDR soil moisture sensor (Delta-T Devices

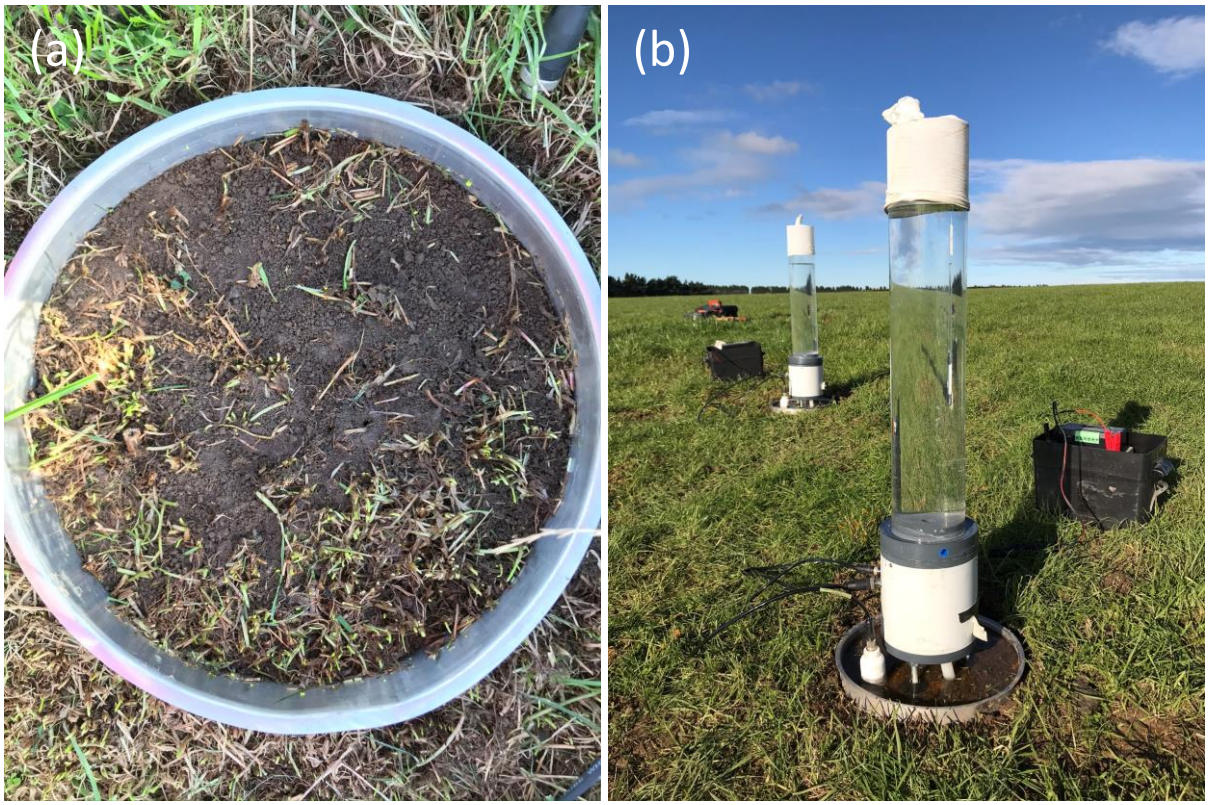

Figure 5-4. The automated infiltrometer setup, showing (a) the trimmed vegetation and (b) the device in action at the field site.

Ltd.) captured the real-time volumetric water content (VWC) for the top 0 – 5 cm increment inside the infiltrometer ring. Up to six measurements per site were recorded on each sampling date, with no measurements conducted more than once at any given location. Saturated hydraulic conductivity (K_{sat}) was determined from the three-dimensional, steady-state ponded flow using the Quasi Exact model of Fernández-Gálvez et al. (2019).

Soil surface K_{sat} was measured for two antecedent moisture states: the 'wet' state and the 'dry' state. The definition of 'wet' state and 'dry' state is developed and discussed in Chapter 6. To summarise, the soil was considered as being in the wet state when the antecedent soil moisture deficit (SMD) to 100 cm was < 7 mm and in the dry state when the antecedent SMD was > 7 mm. At 7 mm SMD, the equivalent volumetric water content (VWC) was ca 40 %. Therefore, each K_{sat} measurement was grouped based on its antecedent VWC into dry state (antecedent VWC < 40 %) or wet state (antecedent VWC > 40 %). Measurements of antecedent VWC were obtained from the TDR sensor installed 5 cm into the soil surface at the onset of K_{sat} measurement.

5.3.3 Subsurface soil description, sampling and analysis

A single pit was excavated at each of the six sites (i.e., IN1, IN2, HS, pSS, dSS, and NS) between 14 August and 14 September 2018, and was aligned such that two profiles could be assessed and sampled, one close to (within 30 cm) a mole channel (i.e., 'mole-proximal') and one distal to (spaced a maximum possible distance from; 70 to 130 cm) the mole channels (i.e., 'mole-distal'). Due to the low variability within each pit, only one profile per pit was morphologically described. Descriptions were carried out to 100 cm following Milne et al. (1995) and Hewitt (1998). A seventh pit was excavated at the basin hollow (lHO).

The soil sampling and analyses procedures are described in Chapter 3, section 3.3.4. In brief, two intact soil cores were collected from depths of 15, 30, 45, 60 and 75/85 cm (dependent on the depth of the fragipan) from each of the 6 pits (12 profiles). Extra samples were collected from pSS at depths of 67.5 and 90 cm. The samples were analysed for subsoil hydraulic and physical properties (i.e., K_{sat} [mm h^{-1}], dry bulk density [g cm^{-3}], porosity [%], macroporosity [%] and field capacity [%]). The analysis methodologies are described in Chapter 3 (Table 3-1).

5.3.4 PWT height between mole channels

To assess the relevance of variable perched water tables to the soil in this study (i.e., whether or not wetting and drying cycles are likely to vary with mole channel proximity), a numerical analysis of the spatial variability in perched water table height was conducted. The height of the water table that would prevail between drains of a certain separation and under a given rainfall regime can be estimated from the Hooghoudt equation (1937) when the K_{sat}, as well as the depth and spacing of the drainage channels is known (Hillel, 1982, pp. 262-264). This equation makes a number of assumptions, including that the soil is homogenous and of constant K_{sat}; that the drains are parallel and equally spaced; that the hydraulic gradient at each point beneath the water table is equal to the slope of the water table above that point; that Darcy's law applies; that an impervious layer exists at a finite depth below the drain; and that the supply of water from above is at a constant flux, q (Hillel, 1982, p. 262). These assumptions oversimplify the real conditions at the study site, nevertheless the equation can provide a useful indication of the magnitude of variation in perched water table height. At the midpoint between drains, the maximum height of the water table mound above the drain network (H_{max}) is obtained using:

$$H_{max} = \frac{qS^2}{8Kd_a} \qquad \text{Equation 5-1}$$

Figure 5-5. Model used to derive the Hooghoudt's equation. Image sourced directly from Hillel (1982).

where, q ([P-ET]/Δt) is the recharge flux (cm s^{-1}; where P is total precipitation, ET is total evapotranspiration and Δt is change in time [s]), S is the distance between drains (cm), K is the soil hydraulic conductivity (cm s^{-1}), and d_a is the height (cm) of the drain above the impervious horizon (Figure 5-5). The mole channel density (D) was estimated in Chapter 4 as 1.6 m m^{-2}, which equates to a parallel spacing (1/D) of ca 0.6 m. To assess the significance of mole drain spacing on the variable PWT in these soils, two different drain spacings were compared: 0.6 m (representative of the field system), and 10 m (an exaggerated, theoretical spacing). Values of K and d_a were obtained from soil sampling and description to estimate the likely values of H_{max}.

5.3.5 Soil moisture regime

Two different measures of the soil moisture regime were estimated for each site: permeability class and drainage class. Drainage class was considered based on both soil morphology and annual months above field capacity.

For classification of permeability, saturated hydraulic conductivity measurements were grouped into surface and subsurface horizons, with subsurface samples grouped by depth. For each site, the median K_{sat} was calculated for the surface and each subsurface horizon from either automated

infiltrometer measurements (surface; described above), or soil cores (subsurface). The overall soil profile permeability class was determined for each site using the K_{sat} of the slowest permeability horizon according to Webb and Lilburne (2011), and as shown in Table 5-1.

The months above field capacity were calculated using hourly data collected over three years. The data was split into three annual periods (i.e., 01/11/2018 – 31/10/2019; 01/11/2019 – 31/10/2020; 01/11/2020 – 31/10/2021). The total number of months above FC was calculated for each of the seven previously described sites (i.e., IN1, IN2, HS, NS, pSS, dSS and lHO) by summing the total number of hours above field capacity per annual period and multiplying by a conversion factor of 0.001369 (i.e., from hours to months).

5.3.6 Statistical analyses

Because the surface K_{sat} data did not meet the assumption of normality, a non-parametric Wilcoxon-Mann-Whitney test was used to determine if the median surface K_{sat} values for mole-proximal and mole-distal samples were significantly different at each site, as well as to test for significant differences in the median surface K_{sat} of the two antecedent soil moisture state groups (i.e., wet state and dry state). The 'two-independent sample comparison of means test with unequal variance' (Welch's t-test) was used to test for significant differences between the subsurface soil property means of mole-proximal and mole-distal samples for each depth. The Kruskal-Wallis test was used to determine if there were statistically significant differences in the K_{sat} values or months above FC between any of the monitored sites.

Table 5-1. Soil permeability class according to their values of the saturated hydraulic conductivity (K_{sat}), as defined by Webb and Lilburne (2011).

Soil permeability class	**K_{sat} (mm h^{-1})**
Rapid	> 72
Moderate	4 – < 72
Slow	< 4

Table 5-2. Definition key for soil drainage classes (Milne et al., 1995; Webb & Lilburne, 2011).

Drainage class	**Code**	**Definition**
Very poorly drained	VP	Peaty topsoil or Bg, Br, Cg, Cr < 10 cm from surface
Poorly drained	P	Bg, Br, Cg, Cr < 30 cm from surface or Bg, Br, Cg, Cr < 15 cm below topsoil
Imperfectly drained	I	Bg, Br, Cg, Cr within 30 to < 60 cm or Bw(g), C(g) < 30 cm from surface or Bw(g), C(g), Bw(f) < 15 cm below topsoil
Moderately well drained	MW	Bw(f), C(f) < 90 cm from surface or Bg, Br, Cg, Cr within 60 to < 90 cm or Bw(g), C(g) within 30 to < 90 cm
Well drained	W	Other

5.4 Results

5.4.1 Influence of mole channel proximity on key soil properties

A total of 144 surface K_{sat} measurements were recorded between March 2019 and March 2020. There were no significant differences (i.e., $p < 0.05$) in the median values of surface K_{sat} between the mole-proximal and mole-distal groups at any of the surveyed sites, with the exception of site pSS, where the median surface K_{sat} above the moles (i.e., 5.5 mm h^{-1}) was significantly larger ($p < 0.05$) than between the moles (i.e., 2.8 mm h^{-1}; Table 5-3). Median surface K_{sat} values for all sites were between 2.0 mm h^{-1} and 5.5 mm h^{-1}.

There were no significant differences (i.e., $p < 0.05$) between the mean values of the mole-proximal and mole-distal groups of each horizon for any of the measured subsoil hydraulic and physical properties (Table 5-4). The mean values between groups were very similar for all horizons and all attributes, with the main source of variation occurring between horizons and not between mole-proximity groups. The between-horizon variability was discussed in Chapter 3.

5.4.2 Influence of antecedent soil moisture on surface K_{sat}

Surface K_{sat} measurements showed larger variation and a greater number of larger K_{sat} values when the antecedent VWC was higher (Figure 5-6). The surface K_{sat} measurements were grouped according to whether their antecedent volumetric water content was in the wet state (i.e., > 40 % VWC) or dry state (i.e., < 40 % VWC). There was a significant difference ($p < 0.01$) in the median values of surface K_{sat} between the wet and dry antecedent moisture states (Figure 5-7).

Landform element appeared to be important to the influence of antecedent soil moisture on surface K_{sat} (Figure 5-8). At the interfluves, K_{sat} was significantly greater (i.e., $p < 0.01$) in the wet state than the dry state, with the effect apparent at both IN1 (wet state = 4.0 mm h^{-1}; dry state = 1.9 mm h^{-1}) and IN2 (i.e., wet state = 6.6 mm h^{-1}; dry state = 2.2 mm h^{-1}). However, there were no significant differences in K_{sat} between the two antecedent moisture content groups for any of the other landform elements.

Table 5-3. Summary surface K_{sat} statistics for each location (proximal or distal to a mole channel) and at each surveyed site. Statistical difference between the two group medians was calculated using the Wilcoxon-Mann-Whitney test, $p < 0.05$.

	n		Median K_{sat} (mm h^{-1})		Wilcoxon-Mann-Whitney test		
pit	Distal	Proximal	Distal	Proximal	Statistic	df	p_{adj}
IN1	*10*	*10*	2.1	2.7	43	1	0.63
IN2	*10*	*11*	3.7	3.4	43	1	0.43
HS	*10*	*10*	4.1	2.0	72	1	0.11
NS	*13*	*13*	3.5	2.5	91	1	0.76
dSS	*14*	*13*	2.9	4.6	68	1	0.28
pSS	*15*	*15*	2.8	5.5	60	1	0.03 *

Table 5-4. Results of the Welch's two independent samples t-test, showing the number of data points (*n*) for each attribute and location relative to the mole (i.e., proximal or distal), as well as the test statistic (t-statistic), the degrees of freedom (df) and significance of the adjusted p-value (p_{adj}).

		n		**Mean**		**t test**			
Attribute	Depth (cm)	Distal	Proximal	**Distal**	**Proximal**	statistic	df	p_{adj}	p_{adj} signif.
Saturated hydraulic conductivity (K_{sat}; mm h^{-1})	15	*6*	*6*	**29.6**	**12.9**	1.58	6.0	0.28	ns
	30	*6*	*6*	**15.1**	**31.4**	-2.20	6.4	0.34	ns
	45	*6*	*6*	**19.7**	**23.0**	-0.26	7.8	0.80	ns
	60	*6*	*6*	**8.5**	**6.5**	0.59	7.9	0.81	ns
	75/85	*8*	*8*	**2.1**	**4.1**	-0.81	8.0	0.95	ns
Dry bulk density (g cm^{-3})	15	*6*	*6*	**1.17**	**1.16**	0.48	9.0	0.79	ns
	30	*6*	*6*	**1.34**	**1.34**	0.41	9.2	0.72	ns
	45	*6*	*6*	**1.39**	**1.37**	1.10	10.0	0.50	ns
	60	*6*	*6*	**1.37**	**1.38**	-0.43	9.1	0.81	ns
	75/85	*8*	*8*	**1.39**	**1.38**	0.25	13.5	0.95	ns
Porosity (%)	15	*6*	*6*	**55.2**	**55.4**	-0.27	9.2	0.79	ns
	30	*6*	*6*	**50.0**	**50.1**	-0.36	9.2	0.72	ns
	45	*6*	*6*	**48.4**	**49.4**	-1.30	9.9	0.50	ns
	60	*6*	*6*	**49.7**	**49.4**	0.25	9.0	0.81	ns
	75/85	*8*	*8*	**49.1**	**49.4**	-0.20	13.3	0.95	ns
Macroporosity (%)	15	*6*	*6*	**7.0**	**5.9**	2.01	8.8	0.19	ns
	30	*6*	*6*	**8.5**	**8.8**	-0.80	7.5	0.72	ns
	45	*6*	*6*	**7.0**	**8.4**	-1.55	10.0	0.50	ns
	60	*6*	*6*	**7.6**	**6.2**	1.05	9.3	0.81	ns
	75/85	*8*	*8*	**4.4**	**4.2**	0.34	10.0	0.95	ns
Field capacity (%)	15	*6*	*6*	**45.9**	**47.2**	-2.35	7.2	0.19	ns
	30	*6*	*6*	**39.9**	**40.1**	-0.66	9.7	0.72	ns
	45	*6*	*6*	**40.1**	**40.2**	-0.27	7.8	0.80	ns
	60	*6*	*6*	**41.6**	**42.7**	-1.23	7.6	0.81	ns
	75/85	*8*	*8*	**44.3**	**44.4**	-0.06	13.9	0.95	ns

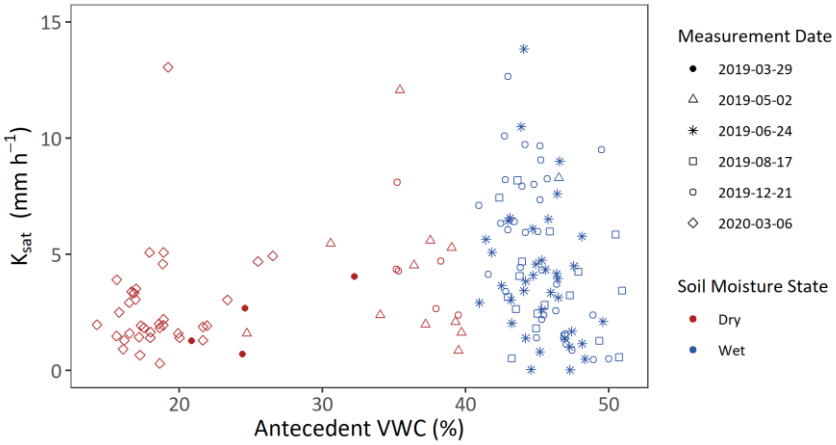

Figure 5-6. All 144 measurements of surface K_{sat} collected across the monitoring period and plotted against the antecedent volumetric water content (VWC; %) as recorded in the topsoil between 0 and 5 cm below the surface. The points are coloured by soil moisture state, which is classified as 'wet' when below 7 mm soil moisture deficit (SMD) and 'dry' when above 7 mm SMD. Different shapes represent the different sampling dates across the period.

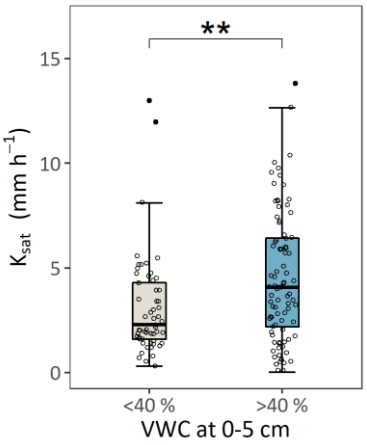

Figure 5-7. Distribution of all 144 surface K_{sat} data points, grouped by the antecedent soil moisture state (dry [i.e., < 40 %; cream] or wet [i.e., > 40 %; blue]), as measured the the soil surface (0 – 5 cm). Statistical difference between the two group medians was calculated using the Wilcoxon-Mann-Whitney test, $p < 0.01$.

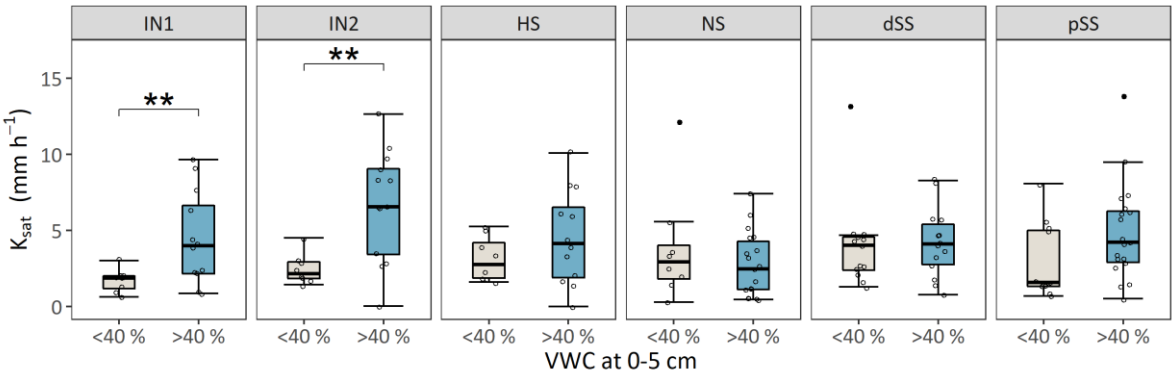

Figure 5-8. The distribution of all data points collected across the monitoring period at each of the six sites and grouped by the antecedent soil moisture state (dry [i.e., < 40 %; shown in cream] or wet [i.e., > 40 %; shown in blue]), presented as the antecedent volumetric water content as measured at the soil surface (VWC; 0 – 5 cm). Statistical difference between the two groups was calculated using the Wilcoxon-Mann-Whitney test, $p < 0.01$.

5.4.3 PWT height between mole channels

To estimate the maximum PWT height (H_{max}) using the Hooghoudt equation, q, was determined from the mean P (120 cm) and ET (70 cm) that occurred over a 12 month (i.e., Δt = 31,520,000 s) period (Chapter 6, Table 6-3). The K parameter was estimated from the mean subsoil K_{sat} from cores taken at 15, 30 and 45 cm (i.e., the soil profile between the surface and the mole network), which was 6.1 x 10^{-4} cm s^{-1}. The height of the mole network above the fragipan, d_a, was calculated as the average difference between the depth of the fragipan (Chapter 3, Table 3-2) and the depth to the mole network (45 cm), and was 20 cm. The two different drain spacings, S, were 0.6 m and 10 m, which resulted in an H_{max} of 0.06 cm and 17 cm, respectively.

5.4.4 Permeability class

There was a general trend of decreasing K_{sat} with depth for each of the sites, with the exception of the soil surface, which was notably lower than the proximate subsurface measurements (Table 5-5). No evidence of an influence on K_{sat} due to landform element was apparent at the surface (data not shown), nor any of the subsurface depths, with no statistically significant differences between any of the monitored sites (Kruskal-Wallis test; $p < 0.05$). For this reason, the median K_{sat} across all sites and depths was considered for permeability classification. With the exception of the soil surface, all measures of K_{sat} above 67.5 cm were between 4 and 72 mm h^{-1}; the permeability of the soil profile from 15 to 67.5 cm was classified as moderate (Table 5-1). Below 67.5 cm, all measures of K_{sat} were less than 4 mm h^{-1}; the permeability of the soil profile from 67.5 to 100 cm was classified as slow. The soil surface K_{sat} was less than 4 mm h^{-1}, so its permeability was classified as slow.

5.4.5 Drainage class

5.4.5.1 Horizon designation

The soil profiles on the interfluves (IN1 and IN2), as well as the head slope (HS) had similar horizon depths and designations (Figure 5-9), while the two pits on the side slopes (dSS and pSS) had slightly deeper fragipan surfaces. These five profiles all had a Bw(f) horizon located less than 15 cm from the base of the Ap horizon, therefore their drainage classification was Imperfectly Drained (Table 5-2). The soil profile at the nose slope (NS) was much shallower, with a Bx(g) horizon surface at 40 cm, and was also classified as Imperfectly Drained.

Table 5-5. Summary statistics of the catchment-averaged saturated hydraulic conductivity (K_{sat}; mm h^{-1}) measured at (a) the soil surface using the automated infiltrometer (BEST) method on six separate occasions and across six sites (i.e., IN1, IN2, HS, pSS, dSS, and NS), and (b) each depth (cm), using the soil core method.

	Depth (cm)	Method	IN1	IN2	HS	NS	dSS	pSS	**Median**
a)	Surface	Infiltrometer – BEST	2.2	3.4	3.6	3.7	4.1	2.5	**3.5**
b)	15	Core	19.1	40.9	14.7	14.6	3.5	34.8	**16.9**
b)	30	Core	23.5	22.6	41.5	11.3	19.9	20.7	**21.6**
b)	45	Core	22.8	23.5	16.1	0.5	14.7	50.4	**19.5**
b)	60	Core	6.2	17.2	6.2	0.6	3.8	7.1	**6.2**
b)	67.5	Core	-	-	-	-	-	1.7	**1.7**
b)	75	Core	-	10.8	5.6	0.2	-	0.4	**3.0**
b)	85	Core	3.2	-	-	-	0.6	-	**1.9**
b)	90	Core	-	-	-	-	-	2.3	**2.3**

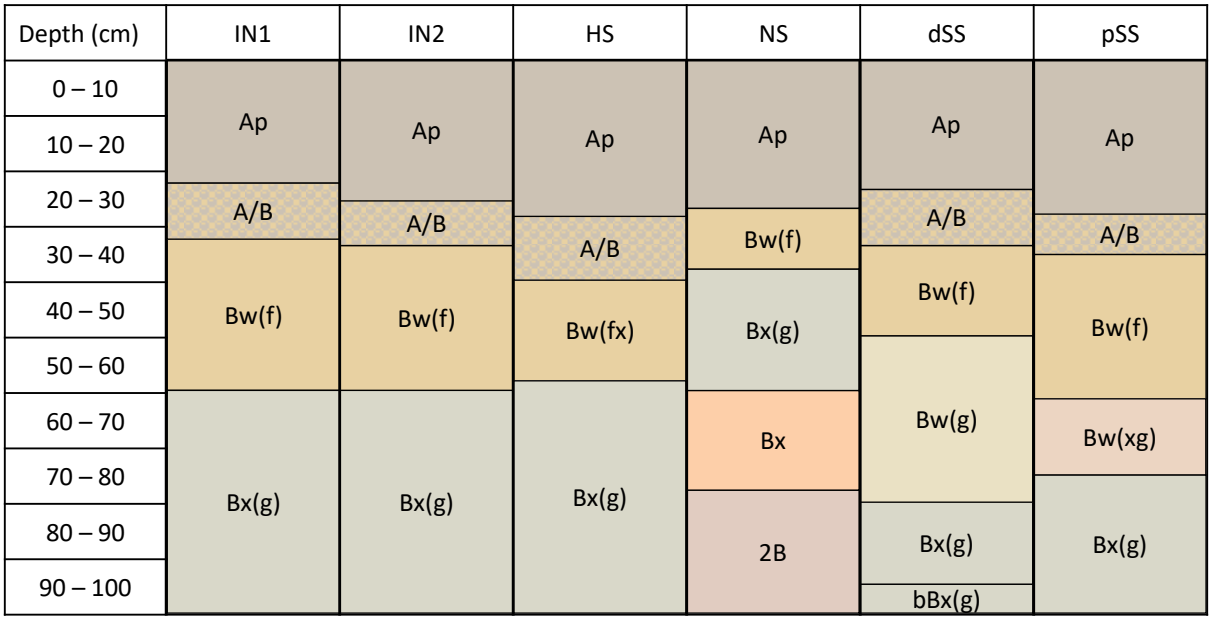

Figure 5-9. Summary of the soil horizon designations to 100 cm for the pits at each landform element, including on the interfluve (IN1 and IN2), at the head slope (HS), nose slope (NS), and divergent (dSS) and planar (pSS) side slopes.

5.4.5.2 Annual months above field capacity

All monitored sites were above FC for over 3 months of the year (i.e., poorly drained) and the variation among sites was small (<0.7 months) (Table 5-6). No influence of landform was apparent (Kruskal-Wallis test; $p < 0.05$).

Table 5-6. Months above field capacity (FC) for each monitored year and the mean ± standard deviation (SD) across the three years (2019, 2020 and 2021). Calculated by summing all the hours above FC.

	Pit	2019	2020	2021	**Annual Mean ± SD**
Months	**IN1**	3.4	2.6	3.2	**3.1 ± 0.5**
	IN2	3.7	3.0	3.5	**3.4 ± 0.4**
	HS	3.7	2.6	3.5	**3.3 ± 0.6**
	NS	3.8	2.8	3.4	**3.3 ± 0.5**
	dSS	3.8	2.3	3.5	**3.2 ± 0.8**
	pSS	3.9	3.1	3.6	**3.6 ± 0.4**
	lHO	4.3	3.6	3.5	**3.8 ± 0.4**

5.5 Discussion

5.5.1 The mature mole channel fracture network

More than 30 years from when mole channels were installed any remaining fractures in the loess-derived Pallic soil of our study site were not visible and had no discernible effect on spatial variability of the measured soil physical or hydraulic properties. Nevertheless, the moles themselves remained largely intact and functional (Chapter 4; Chapter 7).

Mole channels may influence the soil K_{sat} either directly through the associated fracture network that is induced during their installation (Leeds-Harrison et al., 1982), or, in theory, indirectly through their influence on wetting and drying cycles and associated soil structural changes (Bodner et al., 2013; Pires et al., 2005) and/or antecedent soil moisture content. The absence of higher K_{sat} rates inside, relative to outside, the zone of soil fracture, suggests that there are no significant differences in pore size distribution and pore connectivity between these areas. This is contrary to what was discovered by Leeds-Harrison et al. (1982) and Rycroft (1972) in freshly installed systems, where K_{sat} directly above mole channels was significantly higher than at points between mole channels. Similarly, in a study on the Tokomaru silt loam (also an Argillic-Fragic Perch-Gley Pallic), Scotter et al. (1979) found that the K_{sat} of undrained sites could not explain the high peak flow rates measured in the tiles of freshly mole and tile-drained sites, and concluded that mole drainage generated major, persistent changes in K_{sat}, particularly in the B horizon above the moles. The lack of evidence for a functional fracture network in the present study suggests that, after 30 + years, these artificial fracture flow pathways have been 'disconnected' from the mole network, either by extrinsic mechanisms, such as surface compaction, or intrinsic mechanisms, such as altered wetting and drying cycles (Bodner et al., 2013; Pires et al., 2005).

It must be considered that the zone of soil fracture may have been greater than that suggested by Leeds-Harrison et al. (1982) and Godwin et al. (1981) (i.e., 0.3 m), and may have in fact extended into the mole-distal sampling areas (i.e., 0.7 – 1.3m from a mole). If this were the case, it would imply that the sampling method was not capturing unfractured soil, given the close proximity of the mole channels to each other. In this case, the results would instead be representative of the variability present in the fractured soil. In terms of drainage response; however, there was no evidence of surface-sourced, rapid preferential flow at the study site (Chapter 6 and Chapter 7), so it is reasonable to conclude, on this basis, that the fracture network is not functional.

The very low surface K_{sat} values, and their low variability, could be indicative of surface compaction of the Pukemutu soil at this field site, which, under S-Map (Manaaki Whenua Landcare Research, 2022), are classified as having rapid topsoil and upper subsoil permeability (i.e., $K_{sat} \geq 72$ mm h^{-1}; Appendix D). Additionally, the topsoil (at 15 cm) had the lowest mean macroporosity (i.e., Distal = 7 %; Proximal = 5.9 %) of the entire profile, with the exception of the fragipan (i.e., Distal = 4.4 %; Proximal = 4.2 %). These results indicate structural damage at the soil surface – an interpretation that is supported by results from another study of Argillic-Fragic Perch-Gley Pallic soils, which showed that they are highly susceptible to surface compaction under sheep grazing (Drewry et al., 1999). Interestingly, however, Horne (1985) found that when the Tokomaru silt loam (NZSC; Hewitt, 1998) is mole and tile-drained, it is resilient to sheep pugging provided the water table is kept to below 20 cm from the soil surface, which was shown to be the case in Chapter 7 for the soils in the present study. Despite the water table remaining more than 20 cm below the surface at the present study site (Chapter 7) compaction appears to have occurred, which may reflect either soil, climate, management or mole drain network age effects. One site (the planar side slope; pSS) out of the six exhibited a significantly greater surface K_{sat} above, than between, the mole channels. However, there was no consistency in the results of the measurements when considering all of the sites together, with half the sites showing higher median K_{sat} values between the mole channels, and the other half showing higher median K_{sat} values above the mole channels. This suggests that the significant difference identified at site pSS was probably more likely a result of the natural variation in soil properties rather than due to an effect of the mole channel.

Notwithstanding disconnectivity as a result of surface compaction, the absence of an influence of mole channel proximity on any of the subsoil physical and hydraulic properties indicated that a fracture network was not active below the zone of compaction in this mature mole network. While the results do not allow deduction of the mechanisms involved in this apparent subsurface disestablishment of the fracture network, they do provide insight into one of the potential intrinsic mechanisms; alternate wetting and drying cycles. The high density of mole channels (1.6 m m^{-2}) at this field site were demonstrated, using the Hooghoudt equation, to result in a very evenly lowered perched water tables. Estimations of H_{max} demonstrated that, in the soil and climate under consideration, even a fairly wide spacing (i.e., 10 m) of mole channels would have very minor differences in the PWT height between the mole channels (i.e., 17 cm). At a spacing of 0.6 m, more in line with the system installed in the present study, the PWT height difference is effectively absent. Given such insignificant variation in water table height between the mole channels, any alteration

in wetting and drying cycles as a result of increased removal of excess water (i.e., lowering of the perched water table) by the drainage network would be similar both proximal and distal to the mole channels. Therefore, any effect on soil physical and hydraulic properties due to 30+ years of altered wetting and drying cycles is unlikely to be detected at the measurement scale used in this study, and either larger scale comparisons of drained with undrained sites, or measurements pre- and post-drainage are required.

These results demonstrate that great mole channel longevity does not imply equivalent longevity of the mole fracture network, which is widely considered to be a key functional element of these drainage systems (Goss et al., 1983; Leeds-Harrison et al., 1982; Robinson et al., 1987; Youngs, 1985). This may have implications for hydrological modelling, especially when considering the mechanisms of subsurface flow generation or the transport of surface-borne contaminants into drainage networks. Preferential flow via the fracture network is commonly considered to be the major route for rapid contaminant transfer in mole and tile-drained soils (Houlbrooke, Horne, Hedley, Hanly, & Snow, 2004; Monaghan & Smith, 2004; Snow et al., 2010); however, the results of this study do not support this assumption in the case of mature drainage networks. It is also worth noting that most studies on contaminant losses in drainage appear to be from young mole and tile systems, commonly less than 6 years old (Magesan et al., 1995, 1996; Magesan et al., 1994; Monaghan et al., 2002; Monaghan et al., 2005; Monaghan & Smith, 2003; Monaghan & Smith, 2004; Monaghan et al., 2016; Scotter & Kanchanasut, 1981). In mature (30 + year) mole networks it appears that the drainage system relies on the antecedent hydraulic conductivity of the subsoil. Caution needs to be applied when extrapolating contaminant-loss behaviour from young to mature mole systems.

5.5.2 Influence of antecedent moisture on surface K_{sat}

In situ surface saturated hydraulic conductivity appeared to be controlled by the antecedent soil moisture content at some parts of the catchment, specifically on the interfluves where K_{sat} was significantly greater in wet compared to dry antecedent conditions. These results contrast with those reported by Reynolds and Zebchuk (1996), Zhou et al. (2008) and Lin et al. (1998), who observed negative correlations between field-saturated hydraulic conductivity (K_{fs}) and antecedent volumetric water content (VWC). Zhou et al. (2008) ascribed this relationship to a drying-induced increase in soil macroporosity and enhanced expression of pedality, while Lin et al. (1998)

attributed the relationship to the shrink-swell processes characteristic of the vertic soils they were working with.

Why only the interfluves demonstrated a significantly higher K_{sat} under wet state antecedent conditions is uncertain. However, an obvious difference, potentially relevant to water movement, between the interfluves and all other sites is the persistence of a perched water table (PWT). The PWT persisted much longer at the interfluves that elsewhere in the study basin (Chapter 7 section 7.4.1). The increase in K_{sat} in the wet state may be an example of self-organisation of the preferential flow system, as proposed by Noguchi et al. (1999), Sidle et al. (2001), and Sidle et al. (2000). Self-organisation refers to the progressive connection and integration of conductive preferential flow pathways as the soil becomes wetter. These studies showed discrete macropores, lithic contacts, bedrock fractures, buried organic matter, and subsurface topography may all serve as 'nodes' of connectivity that become active with increasing soil moisture, facilitating the linkage (or self-organisation) of short macropore segments into complex networks. On the interfluves the persistence of a PWT may lead to thorough wetting of the pore network by capillary rise, keeping the upper layers near to saturation. This may in turn facilitate the removal of entrapped air (Fayer & Hillel, 1986; Gupta & Swartzendruber, 1964), which can break the connectivity of the pore network, and has been shown to influence both K_{sat} and soil moisture content (Carrick et al., 2011; Fayer & Hillel, 1986; Gupta & Swartzendruber, 1964; Linden & Dixon, 1976). Thus entrapped air may act as a 'node' that controls the connectivity of macropore networks, and the effective saturated hydraulic conductivity.

5.5.3 Soil moisture regime classification

Based on the K_{sat} measurements, the soil at the study site has a permeability classification of 'slow' (i.e., permeability of the slowest horizon to 100 cm), and a permeability profile of moderate over slow, both the same as the classifications given by S-Map to the soil sibling (Pukemutu_6a.1) mapped at the site (Manaaki Whenua Landcare Research, 2022; Webb & Lilburne, 2011). This suggests that the morphological characteristics (stoniness, texture, structure and soil consistence) used to estimate permeability remain useful in soils with mature mole drainage systems. If the assessments of permeability for S-Map were made on an undrained modal profile of the Pukemutu_6a.1 sibling then the similarity of permeability assessments described above would be consistent with the conclusion here that any effects of mole drainage on subsoil hydraulic characteristics (beyond the mole) has disappeared over 30+ years.

Consideration of the mole network in these soils is, however, still relevant to larger scale environmental modelling and land management. Because the moles are installed in the B horizon, the effective K_{sat} may be considered as the K_{sat} of the soil between the surface and the depth of the mole network. In the case of this field site, such consideration would not change the outcome of the classification for overall permeability, as the soil surface could be considered a major limiting layer, with it's median K_{sat} of 3.5 mm h^{-1}. As previously discussed, this very low surface K_{sat} is likely to be a result of surface compaction, suggesting that if the surface permeability can be improved through management practices, these mole and tile-drained soils could potentially be considered as "moderately permeable" if the effective depth is restricted to between the surface and the depth of the mole network. When fitted with mole and tile drainage, the permeability class of soils should therefore be considered for both above the drainage network (relevant for subsurface runoff) and below the drainage network (important for understanding flows to groundwater).

Drainage classification based on soil morphology was Imperfectly Drained at all landscape positions. This is in disagreement with the classification of Poorly Drained given by the NZSC for the Pukemutu_6a.1 soil sibling (Manaaki Whenua Landcare Research, 2022; Webb & Lilburne, 2011). Contrastingly, all of the monitored sites in this study had a mean annual duration of over three months above field capacity, which, according to the NZSC, placed them into the classification of Poorly Drained (Bruce, 1972; Taylor & Pohlen, 1962; Vogeler et al., 2019), despite the presence of the mole and tile drainage system. According to these results, soil morphology-based interpretations of drainage imply better drainage than that demonstrated by even a mole and tile-drained example of the Pukemutu_6a.1 sibling. It is important to note, however, that the time above FC was calculated by summing the total number of hours that the soil was above field capacity across each year, so this is a pessimistic assessment of wetness and does not imply that the soil was above FC for three consecutive months.

5.6 Conclusions

A mechanically-induced fracture network associated with mole channel installation was not distinguishable in mature (30 + year) mole networks installed in the loess-derived Pallic soils with fragipans in this study, despite great longevity of the mole channels themselves. This was demonstrated in this study, where no direct effects due to mole channel proximity (i.e., the zone of soil fracture) was detected on surface and subsurface soil hydraulic and physical properties. The results demonstrate that great mole channel longevity does not imply equivalent longevity of the mole fracture network, which is widely considered to be a key functional element of these drainage systems. The results have implications for hydrological and water quality modelling as preferential flow via the fracture network is commonly considered to be the major route for rapid water and contaminant transfer in mole and tile-drained soils. Surface K_{sat} appeared to be controlled by the antecedent soil moisture content, but only on the interfluves, where K_{sat} was significantly greater in wet state antecedent conditions than dry state antecedent conditions. It is hypothesised that the persistence of perched water tables may lead to thorough wetting of the pore network by capillary rise, facilitating the removal of pockets of air and resulting in a more well-connected pore network.

Mole and tile drainage, either through legacy effects of its installation or its current operation, had no effect on current assessment of permeability class (slow) for the Pukemutu_6a.1 soil sibling. Based on annual duration above field capacity the soil was considered poorly drained, which is consistent with the NZSC classification. However, field soil morphology descriptions of drainage class were not consistent with the NZSC classification, and resulted in classifications of imperfectly drained soils.

Chapter 6

Water balance analysis of runoff and deep drainage pathways in mole and tile-drained slowly permeable loess soils

6.1 Abstract

Understanding water flow pathways is necessary for the sustainable management of agricultural landscapes. Soils modified through the installation of mole and tile drainage systems are agriculturally important; despite this, our understanding of flow processes in these modified soils remains elusive, particularly with regard to runoff and its spatial and temporal, as well as intrinsic and extrinsic, controls. Moreover, deep drainage is often considered negligible, but there are insufficient empirical studies available to support this assumption. The aim of this research was to quantify the spatiotemporal variability and controls of runoff and deep drainage in a mole and tile-drained, loess-mantled downland in Southland, New Zealand. It was achieved by monitoring climate, soil water dynamics and runoff fluxes over a two year period, and using a water balance approach, combined with event-scale analysis of precipitation, soil moisture and runoff characteristics. Runoff occurred predominantly in winter and spring, with tile flow greatest in winter and overland flow greatest in spring. Deep drainage was shown to constitute an important temporally variable flow pathway, particularly in winter. It was activated by excess soil moisture and appeared to occur uniformly across the landscape via piston flow. Soil moisture governed the runoff response to precipitation characteristics; precipitation volume and instensity thresholds discriminated event runoff response depending on antecedent soil moisture state (dry or wet). Infiltration-excess overland flow was the most common form of surface runoff, and saturation-excess was rare. Tile flow was predominantly sourced from the interfluves and upper hollow, and the source area expanded as event size increased; however, events of the magnitude required to activate the side slopes occurred infrequently. The area of the hollow fitted with the tile drain was not identified as a key tile flow- or deep drainage-contributing area. The results of this study demonstrate that the common assumption of negligible deep drainage may be inappropriate when modelling flow pathways in slowly permeable loess, with or without artificial drainage. They also point towards a hydrologically sensitive landscape that demonstrates a highly non-linear response to variations in precipitation intensity, such that a shift in the distribution of precipitation intensity with climate change could make dramatic changes in the components of the water balance (i.e. more OF). Finally, the results identify winter and spring as key seasons and the interfluves and

upper hollow as key areas of the landscape that could be targeted for mitigating surface water contamination from mole and tile-drained loess landscapes.

6.2 Introduction

Artificially drained agricultural landscapes make up almost 200 million hectares globally (International Commission on Irrigation and Drainage, 2017). Approximately 2.5 million hectares are estimated to be drained in New Zealand alone, equivalent to 18.4 % of multiple use agricultural land (Manderson, 2018; Statistics New Zealand, 2020). Subsurface drainage improves land productivity, predominantly by modifying water flow pathways to reduce the time under moisture-excess, subsequently improving crop growth and land trafficability (Fausey & Schwab, 1969; King et al., 2015). Alongside the considerable agronomic benefits of subsurface drainage, however, are environmental and hydrological consequences, which challenge the sustainable management of these landscapes. For example, several studies have demonstrated concerning levels of nutrients, sediment and faecal bacteria in tile drain discharge, which is rapidly transported to surface water bodies, and may contribute to water quality deterioration (Gramlich et al., 2018; Royer et al., 2006; Scott et al., 1998). Subsurface drainage systems have also been shown to alter the partitioning of fluxes amongst water balance components and influence streamflow event hydrographs in agricultural catchments, which are important considerations for the development and calibration of hydrological and nutrient-loss models (King et al., 2014; Rahman et al., 2014).

Loess landscapes are are often drained by mole and tile drain systems when used for agricultural production. As a consequence of low fragipan permeability, these landscapes can experience ephemeral saturation of the soil profile, which may trigger saturated subsurface lateral flow (SS) and saturation-excess OF (McDaniel & Falen, 1994; McDaniel et al., 2008). Loess landscapes are found in important agricultural regions of New Zealand, North and South America, Central Asia, China, and Europe (Catt, 2001; Pye, 1984, 1995). In New Zealand, large areas of deep loess deposits occur in the south and east of the South Island (J. Schmidt et al., 2005). In the Southland region alone, Pearson (2015) estimated ca 1.4 million hectares, including loess soils, was drained using artificial drainage systems such as mole and tile drainage.

It is well-known that mole and tile drainage modifies water flow pathways and reduces soil water residence times (Armstrong, 1986b; Armstrong & Garwood, 1991; Blann et al., 2009; Goss et al., 1983; Schilling et al., 2012; Smith & Monaghan, 2003). There remain, however, significant gaps in our understanding of the hydroclimatic drivers of runoff and deep drainage responses, especially in mole and tile-drained soils with fragipans. Quantification of water flow pathways has been identified as a major challenge, especially at the catchment scale (Singh et al., 2021), and is,

therefore, one of the major limitations in understanding contaminant fluxes from agricultural landscapes (Sharpley et al., 2015). Water balance studies provide a relatively simple means of quantitatively evaluating the redistribution of water in time and space, and enable the computation of an unknown water balance component from the difference between the known components (Sokolov & Chapman, 1974).

Of particular interest is quantifying the relative importance, and controls, of the runoff (R) and deep drainage (DD) components of the water balance in mole and tile-drained landscapes. Pathways by which precipitation (P) inputs may leave a landscape include evapotranspiration (ET), overland flow (OF), deep drainage (DD), subsurface lateral flow (SS), and subsurface artificial drainage networks such as tile flow (TF; Figure 6-1). Plot-scale studies of mole and tile-drained soils demonstrate that tile flow may constitute a significant component of the water balance, with most losses occurring in winter and spring (Monaghan et al., 2002; Monaghan & Smith, 2004; Monaghan et al., 2016). When assessed as the portion of annual P, OF tends to be a less significant R pathway in artificially drained landscapes, as the drainage network reduces the likelihood of the soil achieving the water content threshold for saturation-excess (Klaiber et al., 2020; Robinson et al., 1987). However, overland flow may still occur when the rate of precipitation exceeds the capacity of the soil to infiltrate water, termed 'infiltration-excess' or 'Hortonian' (after Robert E. Horton) overland flow. Therefore, even in drained soils where saturation-excess mechanisms of overland flow are reduced, overland flow may still be an important pathway for phosphorus and sediment, and may remain the dominant pathway for *E. coli*, especially in winter and spring (Monaghan et al., 2016; Smith & Monaghan, 2003).

Studies addressing vertical DD to groundwater under mole and tile drainage are scarce and, consequently, this flow pathway is much less well understood. Assumptions have been made that higher drainage densities result in lower volumes of deep drainage (Environment Southland; Hughes et al., 2019, pp. 44-45; Rissmann et al., 2016), so the need for studies to back up such assumptions is paramount. Water balance simulations at the profile scale indicate that fluxes to groundwater may remain an important component of the water balance after the installation of drainage systems (Horne & Scotter, 2016; Vogeler et al., 2021); however, few data exist that quantify DD experimentally and at the catchment scale. Plot scale studies are prone to over- or underestimation of flow pathway contributions when upscaling to the level of a catchment (Gomi et al., 2008; Joel et al., 2002; Kirkby, 2002), so there is a need for catchment scale experimental quantification of the water budget in artificially drained landscapes.

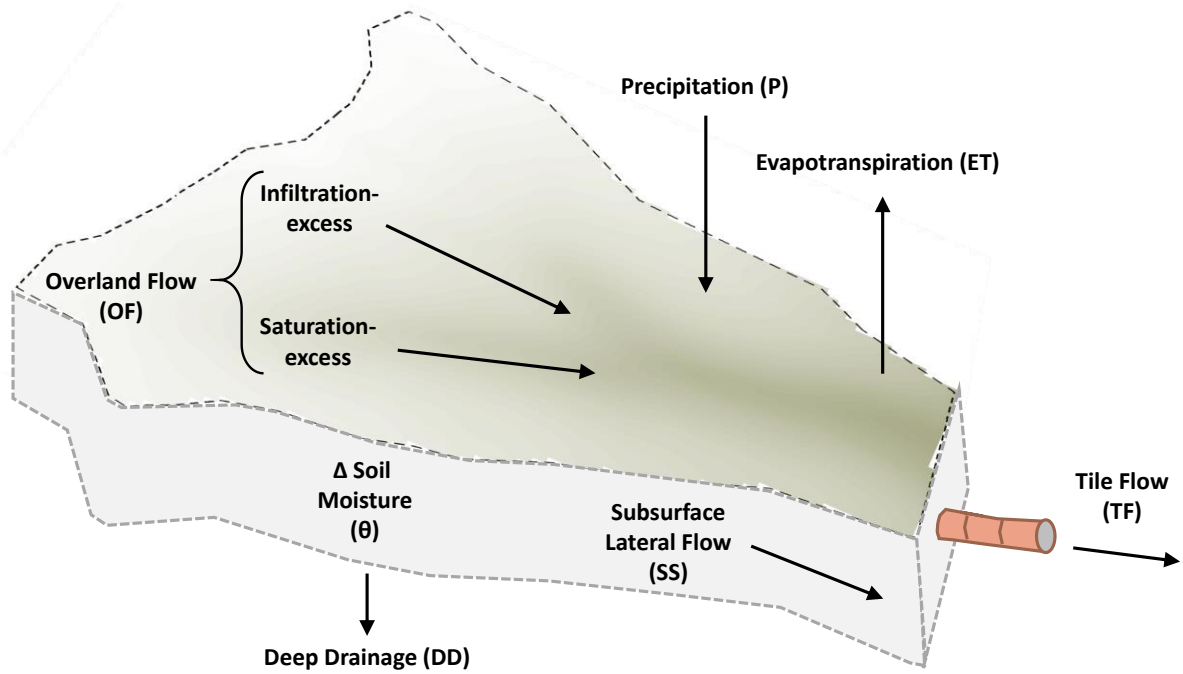

Figure 6-1. Conceptualisation of the catchment water balance components including inputs of precipitation (P) and outputs of evapotranspiration (ET), change in soil moisture ($\Delta\theta_V$), deep drainage (DD) and runoff (R). R is defined by the sum of two flow pathways, including overland flow (OF) and tile drain flow (TF).

Importantly, loess soils with high density fragipans are often assumed to have little DD to groundwater (Huang et al., 2020; Huang et al., 2017; Poulsen, 2013), especially where loess is thick (i.e., >1 m; Catt, 2001). Some studies, however, suggest that DD to groundwater may occur between the prismatic structural units that form the fragipan (Day et al., 1998; Lin & Wei, 2006; Parlange et al., 1989; Scotter et al., 1979), or, alternatively, may occur in gullies and other topographic lows as 'focussed infiltration' (Gates et al., 2011; Huang et al., 2019; Lin & Wei, 2006). While several studies have attempted to experimentally quantify the water budget of mole and tile-drained loessial soils, they have predominantly been undertaken at the plot scale, and commonly assume negligible deep drainage (Monaghan et al., 2002; Monaghan et al., 2016; Smith & Monaghan, 2003). The knowledge gap in the contribution of these landscapes to groundwater recharge is an important limitation of land-surface recharge models, which are a critical tool in water quality management, water resource allocation and climate and land use change assessment (Thorley & Ettema, 2007).

Of particular importance to hydrological modelling at the catchment scale, is identification of the triggers and controls that govern the runoff responses. Runoff generation in all landscapes is predominantly determined by the exceedance of precipitation and soil water content thresholds (Detty & McGuire, 2010a; Farrick & Branfireun, 2014; Saffarpour et al., 2016; Wilson et al., 2017; Zumr et al., 2015). Precipitation intensity and volume, as well as antecedent soil moisture deficit have been identified as important drivers for triggering runoff in drained and undrained landscapes (Hardie et al., 2010; Kokulan et al., 2019; Williams et al., 2019); however, the relative significance and magnitude of these thresholds varies with soil-landscape and land use, and few studies have addressed the triggers and controls involved in rainfall-runoff responses in artificially drained loess landscapes. Event-scale analysis of water balance components allows spatial and temporal patterns of regulation of runoff responses to be examined, including runoff triggers and controls on runoff volume. Those patterns can provide insight into the processes involved in how precipitation is distributed among different flow pathways (Kokulan et al., 2019; Macrae et al., 2019).

The aim of this research was to characterise quantitatively, where possible, the temporal variability of deep drainage and runoff as a basis for understanding potential transport pathways to water bodies in mole and tile-drained, loess-mantled landscapes. It was achieved by monitoring catchment meteorology, soil water dynamics and runoff fluxes over a two year period, and constructing a water balance. The specific research questions and objectives were as follows:

1) What is the rate of DD and how does it depend on other components of the water balance?
    - Using a water balance approach estimate deep drainage by difference and relate to the groundwater table dynamics.
2) What are the triggers of runoff (tile and overland flow) and the controls on runoff volume?
    - Relate event-scale precipitation, soil moisture and runoff flow characteristics.
3) What are the key source areas of tile flow?
    - Relate event-scale tile flow characteristics to the perched water table (PWT) across different landscape elements.

6.3 Methods

6.3.1 Study area

The study area (Plate 6-1) was previously described in Chapter 3, section 3.3.1. In brief, the study site was a 3.95 ha zero-order unchanneled basin, located on a loess-mantled downland 30 km north-west of Invercargill in Southland, New Zealand. Loess deposits, up to 4 m thick on the interfluves, overlay highly weathered glacial outwash gravels (Q8a; mid-Pleistocene; Turnbull & Allibone, 2003). Climate in the area is temperate, with average summer temperatures of 15.7 °C and average winter temperatures of 7.6 °C (Environment Southland, 2018). The long-term average annual precipitation is 1,244 mm, measured in Thornbury, 10 km south-east of the field site (NIWA, 2021). Rainfall is evenly distributed throughout the year, and dry spells longer than two weeks are uncommon (Macara, 2013). Mean annual Penman-calculated potential evapotranspiration is 772 mm at Invercargill Airport, 22 km SSE of the field site (Macara, 2013). The soils are mapped as Argillic-fragic Perch-Gley Pallic Soils (S-Map; Hewitt, 1998), or Aeric Kandiaqualfs (USDA; Soil Survey Staff, 2014), and are characterised by the presence of a low permeability fragipan with an upper boundary between 60 and 90 cm depth. A mole-tile drainage system was installed at the site over 30 years ago, and was mapped and characterised in Chapter 4.

From the 4-metre digital elevation model generated in Chapter 3, section 3.3.1, slope and Topographic Wetness Index (TWI) maps were derived using the Slope tool and Raster Calculator in the ArcGIS Spatial Analyst toolbar. The TWI is a secondary terrain attribute describing the tendency of a cell to accumulate water (Gruber & Peckham, 2009), and is used to quantify the topographic contribution to the moisture state of a given area. The TWI is defined as:

$$TWI = \ln\left[\frac{A}{\tan\beta}\right] \qquad \text{Equation 6-1}$$

where A is the specific catchment area (the local upslope area draining through a certain point per unit contour length) and tanß is the local slope gradient. The D8 flow modelling algorithm (based on 8 deterministic flow directions) (O'Callaghan & Mark, 1984) was used to compute the accumulated flow, which described the potential catchment area of a certain point in the landscape (A). The Slope Tool in ArcMap was used to calculate the local slope angle, β. Four TWI classes and three slope classes were generated (Figure 6-2a and b).

Plate 6-1. Standing to the north of the primary hollow, looking (a) to the south-east, to the basin outlet at the Waianiwa Stream (behind the large shed), and (b) to the south-west, to the head of the basin. The posts with solar panels are soil moisture monitoring sites. The tile drain runs up the hollow from the Waianiwa Stream in plate (a) and terminates about 15 m upstream (i.e., to the west) of the fence in plate (b).

6.3.2 The water balance

Hydrological inputs and outputs of a simple water balance followed the equation:

$$P_v = ET + \Delta\theta_V + R + DD \qquad \text{Equation 6-2}$$

where, P_v is the total precipitation volume (mm) received over time Δt across the catchment, ET is the total evapotranspiration (mm) lost from the surface, $\Delta\theta_V$ is the change in soil volumetric moisture content (mm), R is runoff, which is made up of TF (tile flow, mm) and OF (overland flow, mm), and DD is deep drainage (mm) to groundwater. Subsurface lateral flow (SS) was assumed to be negligible, as it was assumed that the tile drain captured all subsurface drainage other than DD. The assumption of negligible SS was supported by the results of Chapter 7, which indicated that lateral flow above the fragipan was insignificant at this field site. The water balance was calculated for both seasonal and event-based time scales and also assessed as daily time series plots.

The monitoring period was from 1st March 2019 to 28th February 2021. The P, ET, $\Delta\theta_V$ and TF were also captured for the three months of the summer prior to the monitoring period and included in time series plots. However, data from this period were not included in event-based analyses because of data gaps. A weather station was installed at the mouth of the drainage basin in October 2018 (Plate 6-2a). Figure 6-2 shows the field site and experimental setup used to monitor the water balance, the components of which are described in detail below.

6.3.3 Monitoring network components

Precipitation (P) was monitored using a TB4 tipping bucket rain gauge (HyQuest Solutions) at 1-hour intervals (Plate 6-2b), and three manual rain gauges were installed along the length of the field site to validate P measurements. Hourly evapotranspiration was calculated from monitored weather station variables (Plate 6-2c) using the ASCE Standardised Reference Evapotranspiration Equation (Allen et al., 2005) and output at 1-hour intervals.

A network of soil moisture sensors was installed to monitor soil moisture (θ_V). The soil moisture sensors were distributed across landform elements determined from terrain slope and TWI (Table 6-1), which were shown by Lin et al. (2006) to provide a useful interpretation of observed soil moisture patterns. At the highest point of the basin to the west, sites IN1 and IN2 were located on

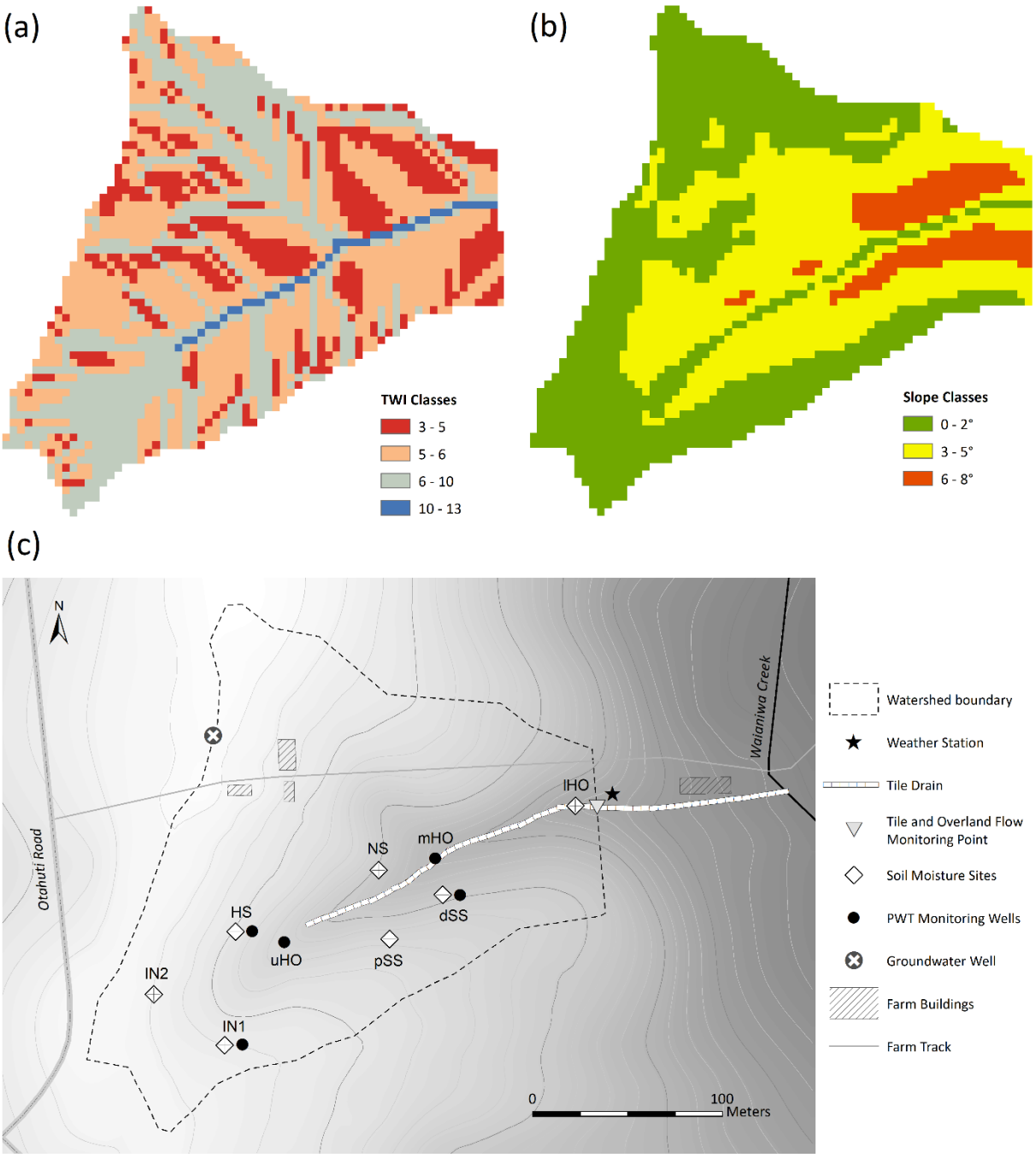

Figure 6-2. Maps of topographic wetness index (a) and slope (b) classes derived from a 4 metre digital elevation model, as well as a diagram of the study site (c) showing the experimental setup. Monitoring sites were located in the groundwater well, as well as at the interfluves (IN1 and IN2), head slope (HS), planar side slope (pSS), divergent side slope (dSS) nose slope (NS), upper hollow (uHO), mid-hollow (mHO) and lower hollow (lHO). Contour lines are shown at 0.5 m (light) and 2 m (dark) intervals.

the broad catchment interfluves (IN) and represent the flattest (0 – 2°) and second highest TWI (6 – 10) classes. Site HS was on the northern side of the head slope (HS) of the primary hollow and site pSS was on a north-facing planar side slope (pSS) to the south. Sites pSS and HS represented the intermediate slope (3 – 5°) and TWI (5 – 6) classes. Site dSS was a slightly divergent side slope

Table 6-1. Summary of topographic characteristics and instrument setup at each of the monitored sites, namely (from the top of the basin to the lowest point of the basin); interfluve 1 (IN1); interfluve 2 (IN2); upper Hollow (uHO); head slope (HS); planar side slope (pSS); divergent side slope (dSS); nose slope (NS); mid-hollow (mHO) and lower hollow (lHO). Ticks identify those sites monitored for soil moisture (θ_V) and perched water table (PWT) height.

Site	IN1	IN2	uHO	HS	pSS	dSS	NS	mHO	lHO
TWI	7.16	6.73	10.56	5.23	5.43	4.74	3.74	11.70	12.39
Slope	2.0˚	2.5˚	2.2˚	3.7˚	4.0˚	6.0˚	5.4˚	2.2˚	2.3˚
Landform	Interfluve	Interfluve	Hollow	Head slope	Planar side slope	Divergent side slope	Nose slope	Hollow	Hollow
θ_V Monitoring	✓	✓	×	✓	✓	✓	✓	×	✓
PWT Monitoring	✓	×	✓	✓	×	✓	×	✓	×

(dSS) with north-west aspect on the true right of the basin drainageway, whereas site NS was on a nose slope (NS) between the two hollows. Sites dSS and NS were located on the steepest slope class (6 – 8°) and lowest TWI class (3 – 5), respectively. Lastly, three sites were located in the floor of the basin and primary hollow. The upper hollow site (uHO) was approximately 15 m upslope of the end of the tile drain. The mid-hollow site (mHO) was situated adjacent to the tile drain and just above the convergence of the two hollows and the lower hollow site (lHO) was located at the mouth of the catchment, adjacent to the tile flow monitoring site.

Soil water dynamics (volumetric water content, θ_v) were monitored at hourly intervals by CS655 Water Content Reflectometers (Campbell Scientific) installed at sites IN1, IN2, HS, pSS, dSS, NS and lHO (Plate 6-2f). The sensors were installed horizontally at depths of 15, 30, 45, 60 and 75/85cm (dependent on the depth of the fragipan), which generally represented the mid-Ah, A/B, mid-Bw (depth of mole channels), lower-Bw, and Bx horizons, respectively (Appendix A.2). Because only the 15 and 45 cm depths were monitored in the lower hollow (due to limited sensor availablilty), missing data at the 30 cm, and 60/80 cm depths were assigned the 15 cm and 45 cm values, respectively. With the exception of the lHO, two sensors were installed per depth, one proximal (within 30 cm) to a mole channel and one distal to (spaced a maximum possible distance from) the mole channels (i.e., 70 – 130 cm). The lHO site had one sensor per depth. The sensors were calibrated according to their depth of placement using soil extracted from the topsoil (0 – 30 cm), subsoil (30 – 60 cm), and fragipan (60 – 90 cm), and following the method outlined in the CS655 user manual (Appendix E).

Time-varying soil moisture deficit (SMD in mm) was calculated for sensor *i* as,

$$SMD_{i,t} = d_i \cdot \left(\theta_{FC_{e,i}} - \theta_{i,t}\right)$$ Equation 6-3

where d_i is the depth increment (mm) assigned to the sensor , $\theta_{FC_{e,i}}$ is the water content measured by a given sensor (i) at effective field capacity (FC_e), and $\theta_{i,t}$ is the time-varying volumetric water content ($cm^3\ cm^{-3}$). Effective field capacity was defined operationally for each sensor as the θ_V at which TF, and hence rapid drainage ceases. Effective field capacity was temporally variable, most dramatically in the A horizon, and was estimated by linear interpolation between field capacities estimated from the immediately preceding and succeeding P events that generated a perched water table at or above the moles. At each site, a single value for θ_v and SMD was calculated by taking the mean across the mole-proximal and mole-distal sensor for each depth and taking the sum of all depths to 100 cm. To quantify the soil moisture storage component of the water balance, these values were then used to calculate area-weighted catchment averages for θ_v and SMD, using the area of TWI classes.

Both overland and tile drain flow components were measured by flow meters. A plywood flow channel was designed to capture overland flow at the outlet of the monitored portion of the basin (Plate 6-2d). Barriers were placed to divert all surface flow through the channel. Overland flow was monitored by a permanently submerged Sontek Argonaut SW Doppler flow meter fitted in the channel base, which measured real-time water height and allowed calculation of flow volume from a stage-discharge curve. The stage-discharge curve was calibrated for flows up to a stage height of 50 mm using simple volumetric gauging; however, due to the flashy and unpredictable nature of overland flow, it was unable to capture events with stage heights greater than 50 mm. Flows with stage heights over 50 mm were calculated using the Manning Equation (Manning et al., 1890), meaning there is larger uncertainty in the rates and volumes associated with larger overland flow events. Data were output at 15 minute intervals, but measurements automatically increased to 1 minute resolution when flow was detected to capture the nature of the flow (i.e., short/long, protracted/flashy).

Tile drain flow was measured using a Krohne Optiflux 2050 electromagnetic flow meter, which was fitted into the tile drain at the mouth of the drainage basin (Plate 6-2e). A measurement error of c. 0.5 % was estimated for flow rates above c. 0.2 mm h^{-1} (2.4 l s^{-1}) using information provided by the manufacturer. However, measurement error increased for flow rates below 0.2 mm h^{-1}, so the maximum likely measurement error was estimated from the range in recorded flow values. The mole channel network was assumed to share the same topography as the soil surface given its

consistent installation depth of c. 45 cm below the surface. Mole channels oriented parallel to the hillslope gradient were identified at all surveyed sites; therefore flow through the mole network is assumed to always follow the direction of steepest slope toward the tile drain and not in directions that cross the catchment boundaries. Data were output at 15 minute intervals.

Deep drainage was the only unmonitored component of the water balance. Assuming that all other outflow pathways have been captured by the monitoring network (i.e., ET, $\Delta\theta$, and R [TF and OF]), all other water leaving the catchment in time Δt must be leaving the area as DD, was shown by:

$$DD = P - ET - \Delta\theta - R \qquad \text{Equation 6-4}$$

6.3.4 Groundwater Table (GWT) monitoring

The deep GWT was monitored using a CS450 pressure transducer installed into a pre-existing 13 m-deep well at the north-western boundary of the drainage basin (Plate 6-3).

6.3.5 Perched water table

The position of the PWT was monitored hourly in five shallow monitoring wells fitted with CS450 pressure transducers. These were located adjacent to soil moisture monitoring stations at five sites including the interfluve at IN1; the basin side slopes at HS and dSS; and the basin floor at mHO and lHO (Table 6-1; Figure 6-2c). Monitoring wells were constructed out of DN 40 PVC-U pipe (Plate 6-4). These were screened along their length to 12.5 cm below the surface and surrounded by a fine mesh liner. Where a fragipan was present, the wells were installed to the depth of its surface (Chapter 3; Table 3-2). Site mHO was drilled to a depth of 1.35 m, intercepting the loess colluvium-gravel boundary at approximately 0.9 m. The PWT depth was presented as relative to the soil surface (m), and such that positive values of PWT were above the surface, while negative values of PWT were below the surface (e.g., a PWT of -0.45 m would be at the depth of the mole network, a PWT of 0 m would be saturating the entire soil profile, and a PWT of +0.1 m would be above the surface).


(a)


(b)

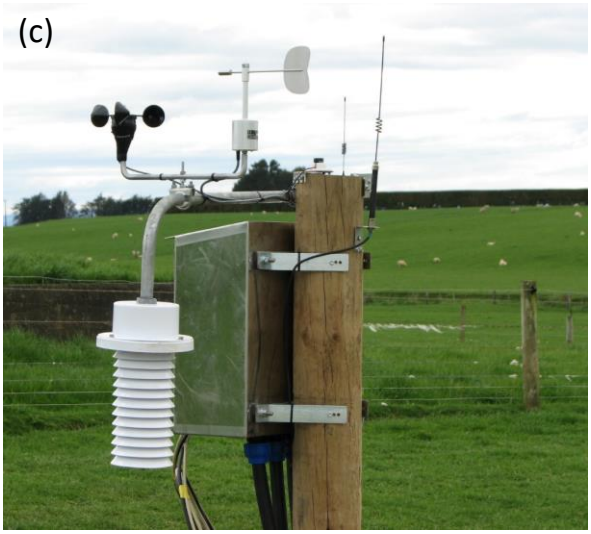
(c)


(d)


(e)


(f)

Plate 6-2. (previous page) All instrumentation for monitoring of the water balance was installed by Nigel Beale and Kirstin Deuss (a) between August 2018 and May 2019. A TB4 Tipping Bucket Rain Gauge (b) was installed 0.5 m off the ground and with a minimum 2 m clearance from the fence. The remaining weather station components (c) were installed on a deer post extending 2m above the ground and included a #41 three-cup anemometer (Maximum Weather Instruments; wind speed), a W200P Potentiometer Windvane (Vector Instruments; wind direction), a CS215 probe (Campbell Scientific) housed in a radiation shield (temperature and relative humidity), and a Li-Cor Li200S pyranometer mounted on top of the post (solar radiation). A Sontek Argonaut SW Doppler flow meter fitted in the base of a plywood flow channel (d) was used to monitor overland flow. Tile drain flow was monitored using a Krohne Optiflux 2050 electromagnetic flow meter (e), which was fitted into a section of the tile drain located almost directly beneath the plywood overland flow channel. Soil moisture was monitored using CS655 Water Content Reflectometers (Campbell Scientific) at five depths (f) and two profiles per each of seven sites located across the different landform elements (second profile in the image is the pit wall opposite the visibly monitored profile). Soil moisture sites were powered by solar panels (f), while 240 V alternating current mains was transformed to 24 V DC, providing continuous and stable power supply to the remaining components.

6.3.6 Data analysis

6.3.6.1 P Event Definition

P events were defined in terms of their statistical independence by deriving a minimum inter-event time (MIT). The MIT represents a minimum time-period of no rain, which separates independent P events. The Coefficient of Variation (CoV) method (Restrepo-Posada & Eagleson, 1982) was used to determine an MIT from the hourly P time series and the CoV statistic was calculated using the 'IETD' package (Duque, 2020) in R 3.6.0 (R Core Team, 2019). The optimal MIT was determined as 5 hours, with a P volume threshold set to >0.2 mm to exclude most insignificant P events.

Statistics for each event were calculated, including total event precipitation volume (P_v mm), total event duration (P_d, hr), average and maximum event precipitation intensity (P_i, mm hr^{-1}). Other data summarised for each P event included the maximum event perched water table height (PWT, m) at each of the monitored sites, the antecedent soil moisture deficit (ASMD, mm) of the soil to 100 cm, and the difference between ASMD and P_v (ASMD-P [mm]). The ASMD was defined as the soil moisture deficit (SMD) at the onset of precipitation for a given event so that negative values of ASMD-P_v imply P_v satisfied the ASMD, whereas positive values indicate a SMD remained after the rainfall event.

Plate 6-3. Groundwater level was monitored in a deep well constructed from concrete rings (a), and accessed via an inspection chamber (b). The well was fitted with a CS450 pressure transducer, fed down a PVC pipe (b) and powered using solar panels (c).

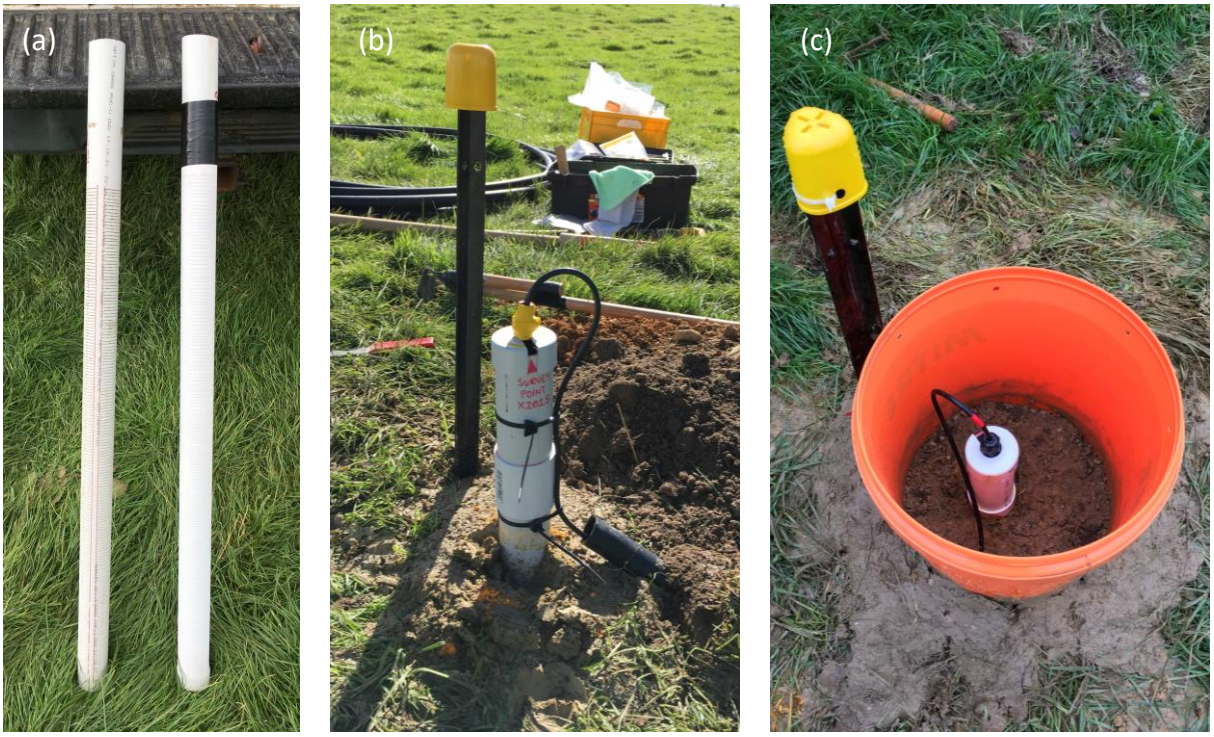

Plate 6-4. Monitoring well installation, showing (a) the full length screen and mesh liner, (b) bentonite seal and georeferenced survey point for referencing water level to the soil surface (taking into account the height of the pipe), and (c) the protective casing, sans lid.

6.3.6.2 TF and OF Event Definition

TF and OF events were visually delineated and assigned to their triggering P event. The start of an event was defined as the timestamp during which a distinct rise in discharge was observed in response to a P event, either from zero flow or some previous event baseflow. The end of the event was defined as when the discharge rate returned to pre-event flow rate. Total discharge (V_t, calculated in mm, using the topographically-defined catchment area of 39,500 m^2), flow duration (R_d, hr), and average (Q_{avg}) and maximum flow rates (Q_{max}, mm h^{-1}) were calculated for each type of flow (TF and OF) and for each event. Hydrograph response time (HRT; hr) was defined as the time between the start of a P event and the start of a runoff event. The runoff ratio (R ratio) was V_t divided by P_v.

Saturation-excess OF was defined operationally as occurring during those OF-generating events that recorded a maximum PWT height of < 10 cm from the soil surface at any of the four monitored sites including, from the top of the slope IN1, then HS and dSS with lHO in the hollow. The site at uHO was not included in the definition, as it exhibited an unusual response that indicated it may have intersected a mole channel during installation.

6.3.6.3 Controls on R

Precipitation events were grouped based on the resulting R type, with the three groups being no runoff (NR), tile flow (TF) and tile and overland flow (TF+OF). Overall relationships between R type and P event and soil moisture metrics were assessed by assigning runoff type to events plotted in P_v- or P_i- ASMD space.

Relationships between R volume and the P event metrics were assessed. All relationships were analysed visually to determine the presence or absence of thresholds in R responses. Where threshold behaviour was observed, the relationship was assessed using piecewise linear regression. The R package *chngpt* (Fong et al., 2017) was used to identify the break point between the two different relationships, and the relationship between the values on either side of the threshold was modelled using simple linear regression. Where the *chngpt*-generated thresholds did not fit the data well the thresholds were determined visually. Two different types of equations were used to fit relationships, including a linear and quadratic function. The relationships are described in terms of the coefficient of determination (R^2), which is rated as strong ($R^2 > 0.7$), moderate ($0.5 < R^2 < 0.7$), weak ($0.3 < R^2 < 0.5$) and very weak ($R^2 < 0.3$), according to Moore and Kirkland (2007).

6.3.6.4 Groundwater recharge analysis and DD rate calculation

Groundwater recharge was analysed by aligning and visually comparing the daily time series for cumulative P (mm), cumulative ET (mm), θ_V (mm SMD), cumulative P-ET (mm), cumulative DD (mm), and GWT depth (m below the surface). Moreover, this information was assessed in the context of the seasonal water balance summary, specifically the behaviour of θ_V.

6.3.6.5 Tile flow and perched water table relationships

To identify the parts of the catchment that were most likely to be contributing to tile flow during events of a given magnitude, the relationship between total tile flow volume (V_t; mm) and normalised maximum perched water table depth (PWT_{max}; m; with positive values of PWT above the surface and negative values of PWT below the surface) was examined as a function of the tile flow runoff ratio (R ratio) for each monitored site (i.e., IN1, uHO, mHO, HS and dSS). Tile flow events were grouped into five R ratio groups (Table 6-2).

For each site, the linear relationship between V_t and normalised PWT_{max} was then assessed for each R ratio group using the coefficient of determination (R^2) which is rated as strong ($R^2 > 0.7$), moderate ($0.5 < R^2 < 0.7$), weak ($0.3 < R^2 < 0.5$) and very weak ($R^2 < 0.3$), according to Moore and Kirkland (2007). It was assumed that the stronger the relationship between TF volume and maximum PWT depth for specific monitoring well sites, the greater the TF generation from those landscape elements in the catchment. Sites with an R^2 of ≥ 0.5 were considered to be major contributing areas to tile flow.

Table 6-2. The grouping rules for assigning events into runoff ratio (R ratio) categories.

Group	Rule
0 – 0.1	R ratios ≤ 0.1
0.1 – 0.2	R ratios > 0.1 and ≤ 0.2
0.2 – 0.3	R ratios > 0.2 and ≤ 0.3
0.3 – 0.4	R ratios > 0.3 and ≤ 0.4
0.4+	R ratios > 0.4

6.4 Results

6.4.1 Meteorological conditions and long-term trend comparison

All P statistics over the monitoring period (1st March 2019 to 28th February 2021) corresponded closely to long-term measurements. Total P was slightly higher in Year 1 (1282 mm) than in Year 2 (1141 mm), and was 3 % above, and 8 % below the long-term annual average (1,244 mm), respectively. Precipitation measurements agreed with those from manual calibration rain gauges. The average hourly above-zero P intensity was low (0.9 ± 1.1 mm h^{-1}) and highly positively skewed (Figure 6-3), with minimal seasonal variation (0.8 – 1.0 mm h^{-1}), and with a maximum intensity of 10.2 mm h^{-1}.

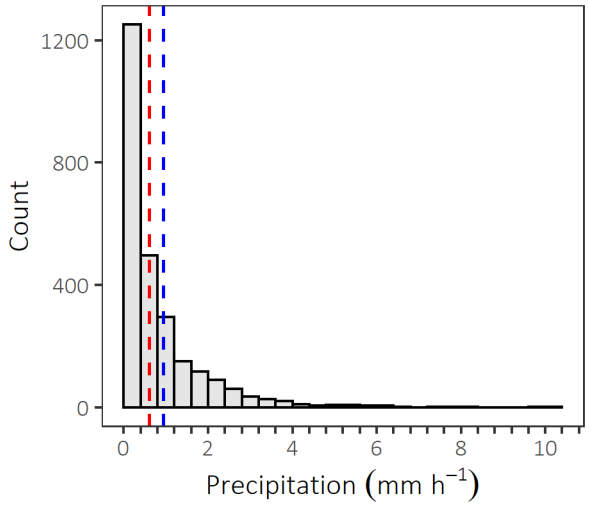

Figure 6-3. Histogram of hourly precipitation volume (mm h^{-1}) between 1st March 2019 and 28th February 2021. Dashed red line shows the median, dashed blue line the mean.

6.4.2 Water balance

Annually, over half of P (55 %) was removed as ET, with runoff (R) accounting for less than one quarter of P input (TF 14 % and OF 4 %). DD, calculated as the only unknown component of the water balance, was the most significant outflow pathway (26 % of P) after ET. Overall, P fell evenly distributed across all four seasons (Figure 6-4a) of the monitoring period, with an average daily mean of 3.3 ± 6.2 mm day^{-1}. Daily ET ranged between c. 3.5 mm day^{-1} at the summer solstice (mid-December), and c. 0.5 mm day^{-1} at the winter solstice (mid-June; Figure 6-4b). The portion of P lost as ET varied (Table 6-3), but was largest in the first summer (132%P) and smallest in the first winter (19 %P). ET was much lower (262 mm) in the second summer relative to the first (313 mm) and third (304 mm) summers.

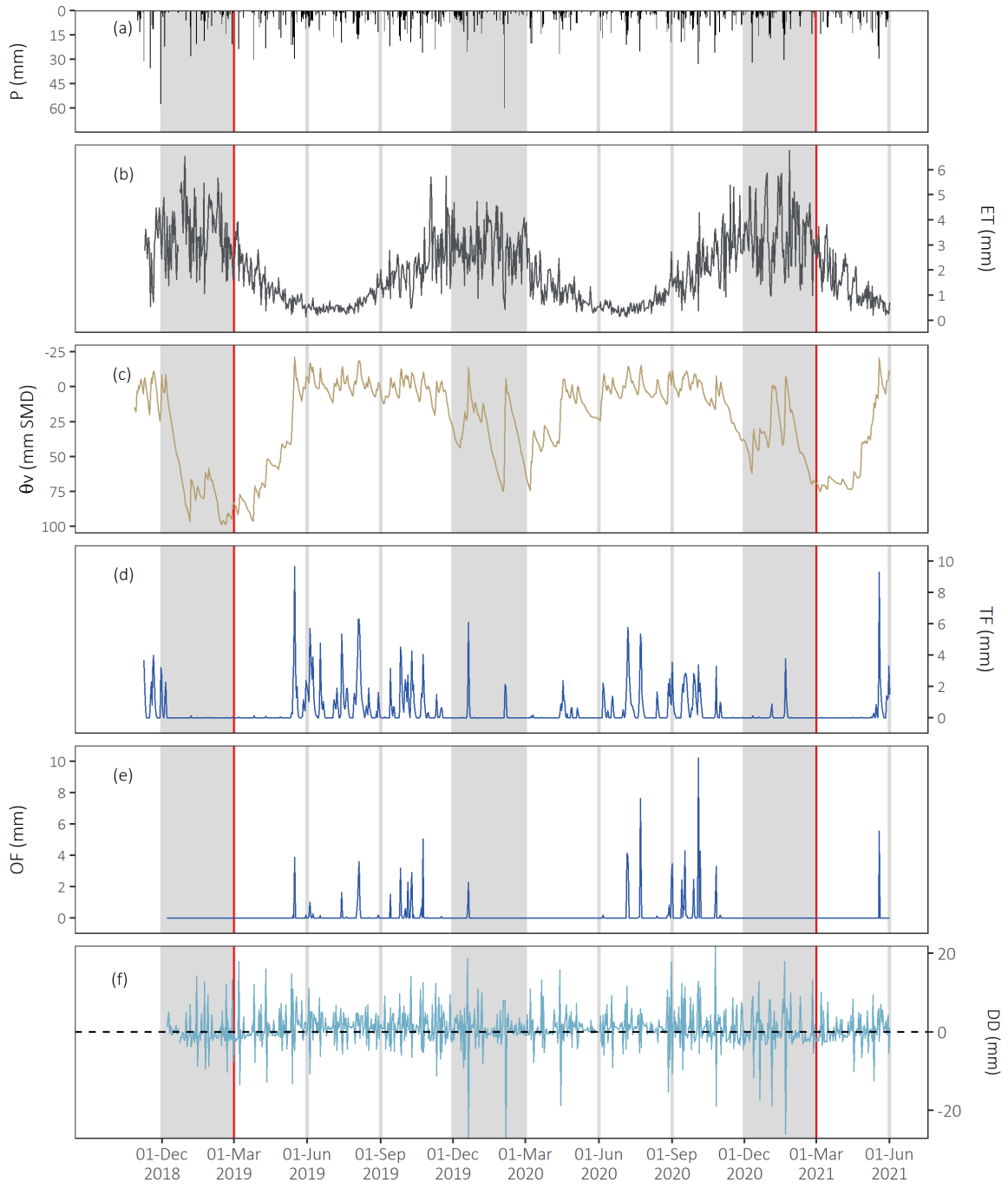

Figure 6-4. Time series of the water balance components, showing daily (a) precipitation [P, mm], (b) evapotranspiration [ET, mm], (c) catchment-averaged volumetric soil moisture content [θ_v, expressed as mm antecedent soil moisture deficit (ASMD) between 0 and 100 cm], (d) tile drain flow [TF, mm], (e) overland flow [OF, mm], and (f) estimated deep drainage [+DD, mm]. The red lines represent the start and end of the monitoring period; 1st March 2019 to 28th February 2021. The shaded periods represent summer; while autumn, winter and spring are distinguished by the vertical light-grey lines.

The soil tended to be in moisture deficit (SMD > 0 mm) during summer and autumn, with the deficit generally increasing over summer and decreasing over autumn (Figure 6-4c). During winter and spring, the soil was often in moisture excess (SMD < 0 mm). To summarise, soil moisture may

be described as exhibiting two approximately seasonally-dependent states; 'wet', and 'dry'. The wet state dominated during the full winter and most of spring for both years (Figure 6-4c). Soil moisture behaviour during the dry state could be further separated into 'drying out' (summer), or 'wetting up' (autumn) phases, which differed predominantly in their average daily ET rates (ca 3.5 mm day^{-1} versus ca 1.5 mm day^{-1}, respectively). The dichotomy is consistent with the ratio of daily ET outputs to daily P inputs, on average, being above 1 in summer and below 1 in autumn.

Once the SMD was refilled during the wetting up phase, TF began occurring frequently (Figure 6-4d). Conversely, the occurrence of TF decreased once the soil entered its drying phase, with large flows only occurring if P events were sufficient to satisfy the SMD. Total seasonal TF was low (≤ 13 mm) in all summers and was only slightly higher in autumn seasons (≤ 31 mm; Table 6-3). In contrast, winter and spring produced total seasonal TF volumes (162 and 122 mm, respectively) that were an order of magnitude higher than summer flows.

In summer and autumn, OF was extremely rare (Figure 6-4e, Table 6-3). Winter and spring, however, cumulatively produced large OF in both years (32 and 60 mm respectively), which generally occurred when SMD was approximately satisfied (i.e., soil at or above FC; Figure 6-4e).

Estimated DD was sometimes negative (Figure 6-4f, Table 6-3), and these negative values were included in the cumulated DD. Negative DD was not taken to mean that the water was moving up into the profile from below, but rather as indicative of measurement errors of the other water balance variables (discussed in section 6.5). Here, DD was considered as active (positive) and inactive (zero or negative). DD was an active outflow pathway during all seasons, with annual DD losses between 264 and 362 mm (Table 6-3). During summer of years one and three, the total DD was negligible (i.e., < 8 mm), compared with the second summer (2019 – 2020) which was much larger (i.e., 56 mm). DD was similar in autumn for both years (i.e., 61 and 63 mm, respectively), with a much larger increase in winter and spring (i.e., 245 and 203 mm, respectively). Calculations of seasonal DD, shown in Table 6-3, indicated that losses to groundwater were the most significant transport pathway for input P during winter (interannual winter range 37 - 44 %P), and were generally second only to ET during the remaining seasons. Large variation in summer P and ET resulted in a wide interannual range of summer DD losses (0 – 20 %P) across the three years. In the dry state, the water balance indicated that DD flux was essentially nil in summers with normal (i.e., consistent with long-term) ET and P inputs. In wetting up (autumn), and in summers with lower than normal ET, DD pathways were active.

Table 6-3. Seasonal summation of the water balance components for each monitored year, including inputs of precipitation (P), and outputs of evapotranspiration (ET), change in soil moisture ($\Delta\theta_V$), runoff (R) as tile flow (TF) and overland flow (OF), and estimated deep drainage (DD). *The summer of 2018 – 2019 water balance is also shown, but it was not included in the event-based water balance summary statistics as there was no information for the other three seasons. Note: All units in millimetres (mm) and percentage of precipitation (%P).

Monitoring Year	Year	Season	P	ET		$\Delta\theta_V$		TF		OF		DD	
			mm	mm	%P	mm	%P	mm	%P	mm	%P	mm	%P
*	2018 – 2019	Summer	**237**	313	(132)	-89	(-38)	5	(2)	0	(0)	8	(3)
Year 1	2019	Autumn	**317**	132	(42)	89	(28)	31	(10)	4	(1)	61	(19)
	2019	Winter	**308**	58	(19)	-3	(-1)	105	(34)	13	(4)	135	(44)
	2019	Spring	**360**	202	(56)	-28	(-8)	57	(16)	19	(5)	110	(31)
	2019 – 2020	Summer	**297**	262	(88)	-37	(-12)	13	(4)	3	(1)	56	(19)
Year 2	2020	Autumn	**230**	114	(50)	43	(19)	10	(5)	0	(0)	63	(27)
	2020	Winter	**284**	60	(21)	34	(12)	61	(21)	25	(9)	104	(37)
	2020	Spring	**344**	212	(62)	-53	(-15)	51	(15)	35	(10)	99	(29)
	2020 – 2021	Summer	**283**	304	(107)	-27	(-10)	8	(3)	0	(0)	-2	(-1)

6.4.3 DD contribution to groundwater recharge

Cumulative DD increased via a series of plateaux with no or very low gradient, and intervening steeper inclines (ramps) through the monitoring period (Figure 6-5e). Plateaux corresponded mostly with summer and autumn seasons when ET exceeded P (Figure 6-5a, b and c) and the soil was drier than field capacity (Figure 6-5d). At these times the GWT receded (Figure 6-5f), presumably as groundwater discharge exceeded very low, or no, recharge. For example, in late spring 2020 to autumn 2021, the soil was predominantly in moisture deficit (i.e., SMD > 0 mm; Figure 6-5d), which was a function of the cumulative P-ET not increasing (Figure 6-5c). As a result, the cumulative DD slope plateaued (Figure 6-5e), indicating that there was no DD occurring during these seasons and correspondingly, the GWT receded (Figure 6-5f).

Cumulative DD ramps aligned with the remaining seasons when soil moisture was at or above field capacity and there was excess of P over ET. At these times the GWT rose, with this switch between fall and rise clearly indicated in Figure 6-5f at time point 1, and less conspicuously at time point 6. The amplitude of GWT variation was about 2 m. At shorter timescales, and during events when P exceeded ET, soil wetting to FC or above resulted in spikes in calculated DD (not visible in Figure 6-5e due to the data being presented as a 3-day rolling average to reduce noise) that aligned with low amplitude, high frequency variation in the GWT. Events such as these caused

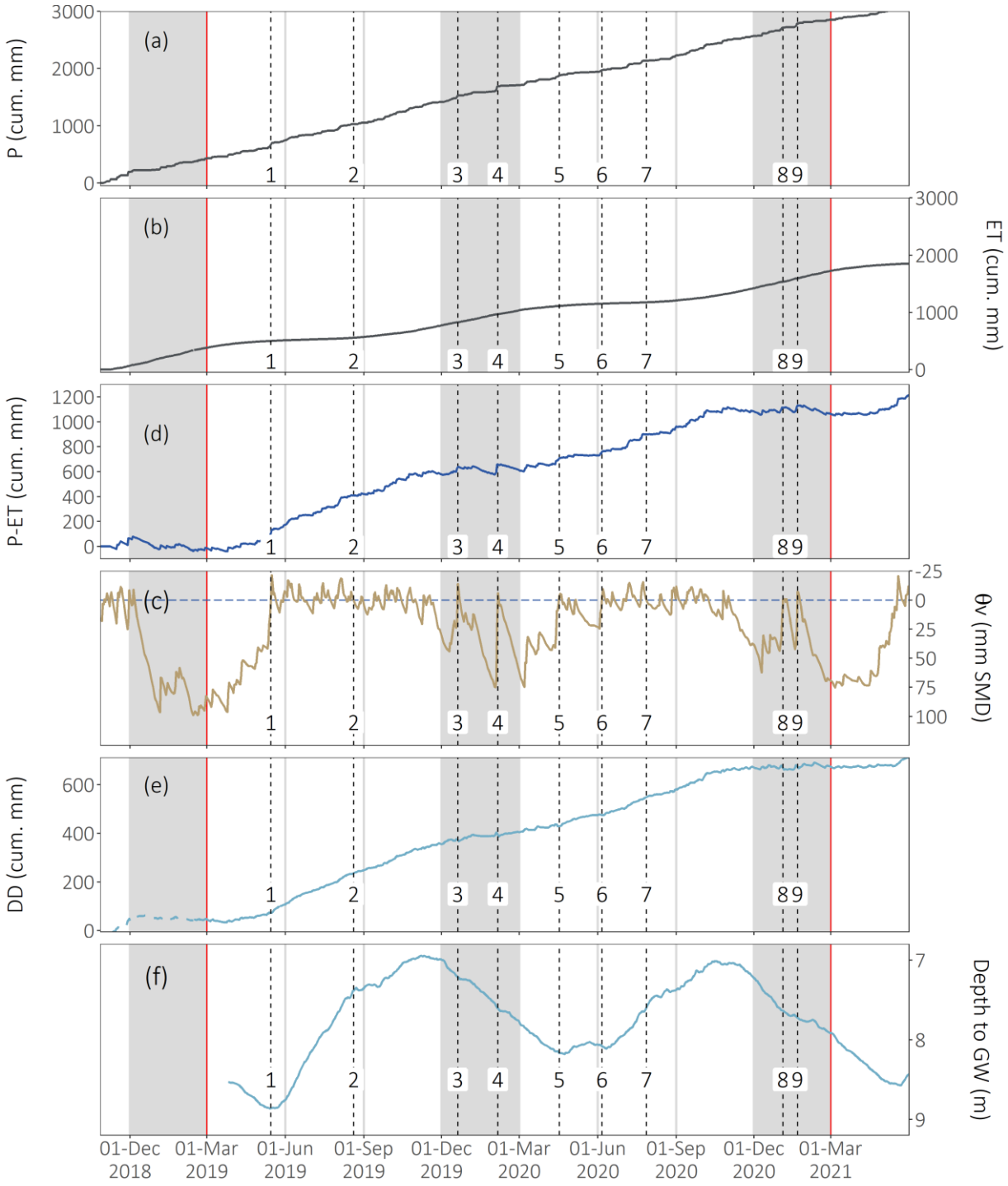

Figure 6-5. Daily time series of (a) cumulative precipitation (P), (b) cumulative evapotranspiration (ET) in mm, (c) cumulative P-ET (mm), (d) catchment-averaged volumetric soil moisture content [θ_v, expressed as mm soil moisture deficit (SMD) between 0 and 100 cm], (e) deep drainage (DD), displayed as the 3-day rolling average to reduced noise, and (f) 7-day rolling average depth to groundwater (GW) in metres. The dashed part of the DD line in plot d does not have OF included in the DD calculation, as it was not yet installed. However, any OF events that were missed were restricted to November 2018, and removal of OF data from the whole time series does not alter the overall trend. The dashed horizontal line in plot c represents a SMD of 0 mm. The red lines represent the start and end of the monitoring period; 1st March 2019 to 28th February 2021. The shaded periods represent summer; autumn, winter and spring are distinguished by the vertical light-grey lines. The numerically labelled, vertical dashed lines identify synchronised responses between the five variables, and are referred to in the text.

pauses in recession of the GWT on its falling limbs (summer – autumn; e.g. Figure 6-5f, time points 3, 4, 5, 8 and 9). Furthermore, prolonged periods of soil moisture deficit that occurred during the rising limb of the GWT caused pauses in the rise of the GWT (e.g. Figure 6-5f, time points 2 and 7). These results provide evidence that the GWT was responsive to DD, but not flashy.

Of note, is that the GWT in the second autumn (2020) did not fall as much as the first and third autumns, and was about 0.5 m higher at time point 5 (i.e., 8 m) than other GWT minima. Figure 6-5e shows that the cumulative DD slope was slightly positive during autumn 2020, unlike the first and third autumn, where it plateaued. It appears, therefore, that the numerous large P events during the summer and autumn of 2020 (i.e., as shown at time points 3, 4 and 5) generated sufficient DD to reduce the magnitude of GWT fall.

DD rates were calculated for each event by dividing the water balance-calculated total DD (P – ET – TF – OF – $\Delta\theta_V$) by the event duration ($P_{d,}$ hr). To minimise the error introduced by TF and OF components, events used for the calculation were limited to those that:

1) generated a minimum PWT of 10 cm head at any given site (i.e. SMD < 0 mm),

2) had a maximum PWT height that did not rise to the depth of the mole network at any site, and

3) did not trigger any form of TF.

Of the 77 events that met the criteria, most occurred during winter and spring (Figure 6-6). Higher DD volumes in the second summer (2019 – 2020; Table 6-3) coincided with more P events. The median DD rate over the monitoring period (0.40 mm h^{-1}) was commensurate with the saturated hydraulic conductivity (K_{sat}) measured for the buried loess sheets in Chapter 3 (0.20 – 0.60 mm h^{-1}).

6.4.4 Runoff frequency, triggering and flow metrics

Of the total of 322 precipitation (P) events, the median event had a duration of 7 hours, volume of 3.5 mm precipitation, precipitation intensity of 0.6 mm h^{-1} and inter-event time (i.e., antecedent dry hours) of 27 hours (Figure 6-7). Characteristics of precipitation, referred to below as P metrics, demonstrated control on the frequency and triggering of runoff (R) response: specifically, i.e., no

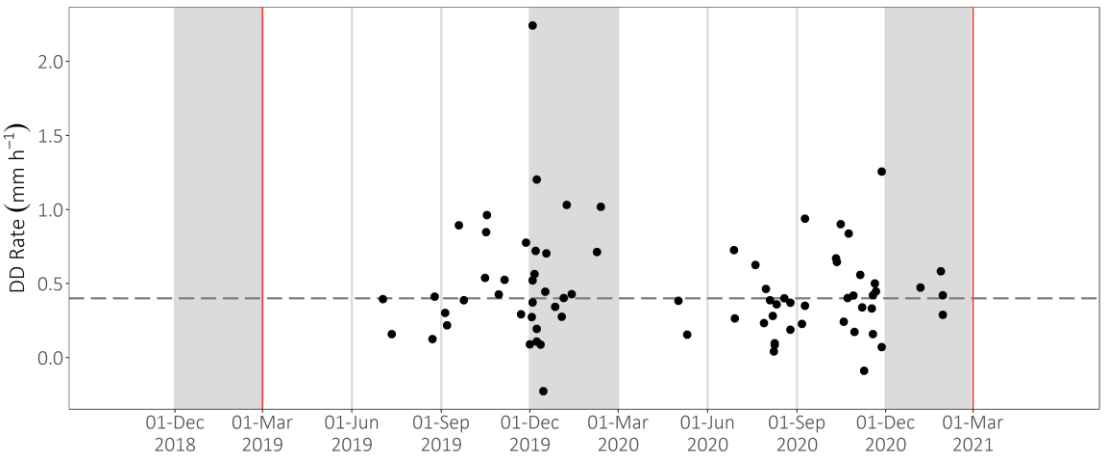

Figure 6-6. Plot of deep drainage (DD) rates (mm h^{-1}) calculated for events that did not trigger tile flow (TF) and which produced some degree of perched water table (PWT), but not at a height that exceeded the mole network. The median is represented by the horizontal dashed line. The red lines represent the start and end of the monitoring period; 1st March 2019 to 28th February 2021. The shaded periods represent summer; while autumn, winter and spring are distinguished by the vertical light-grey lines.

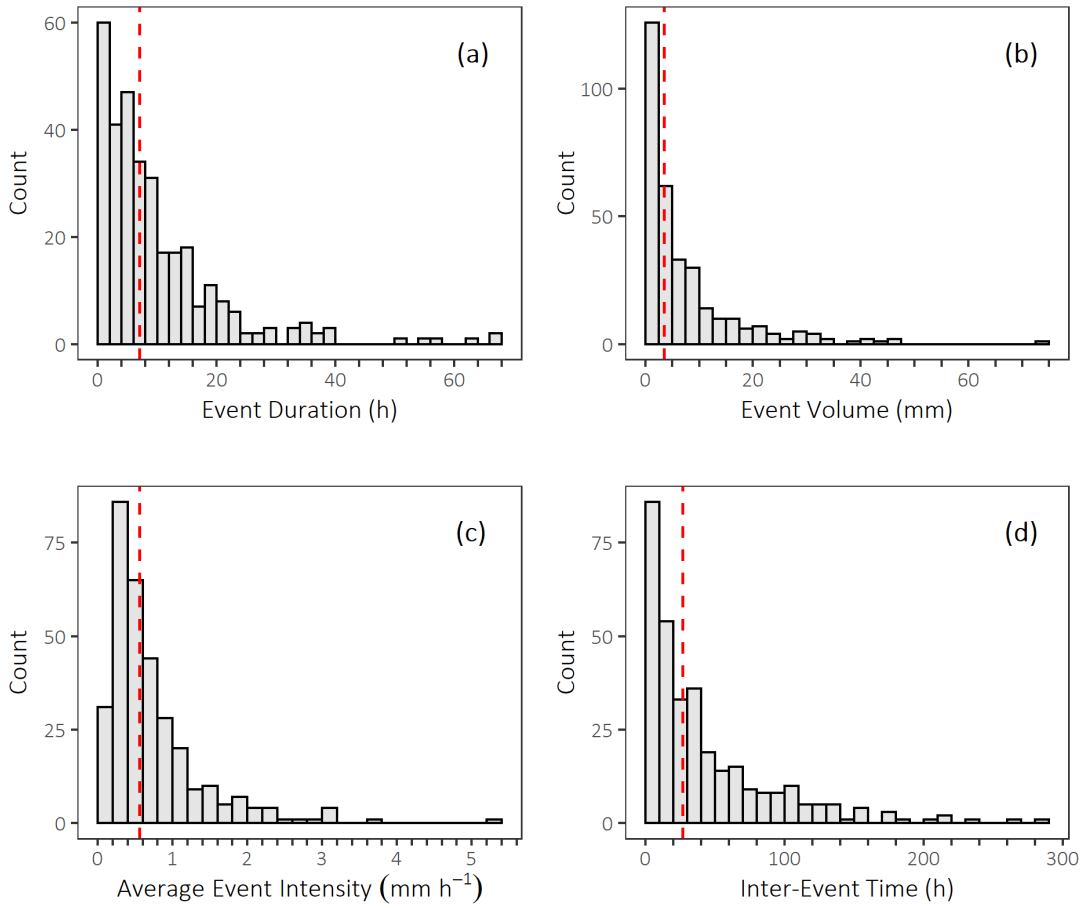

Figure 6-7. Histograms of precipitation event (a) duration [hours; h], (b) volume [mm], (c) average intensity (mm h^{-1}), (c) inter-event time (i.e., antecedent dry hours). Dashed red lines represent median values for the monitoring period: 1st March 2019 and 28th February 2021.

runoff [NR], tile flow runoff [TF] or both tile and overland flow runoff [TF+OF] (Table 6-4a-c). Fewer than half of the P events (46 %) produced no runoff (NR). These NR precipitation events dominantly occurred (n = 60) in the summer when the median event duration (P_d) was short (4 hrs), precipitation volume (P_v) small (2 mm), with average (0.4 mm h^{-1}) and maximum (0.8 mm h^{-1}) event intensity (P_i) also small, and ASMD large (36.4 mm). In other seasons, NR events had similar characteristics. Generalising, NR precipitation events occurred when precipitation duration, intensity and volume were small and ASMD was large.

Of the remaining 54 % of events that did trigger R, most (40 %) produced TF only (Table 6-4b), with the remainder (14 %) generating both TF+OF (Table 6-4c). TF events occurred at similar frequencies across autumn, winter and spring (n = 32 to 39), with slightly fewer events in summer (n = 24). Precipitation events that produced no R in summer had similar P metrics to those events that yielded R in winter, when the antecedent soil condition was wetter (negative ASMD). In the other seasons, TF was associated with precipitation events whose duration, depth and intensity were generally at least two times higher than those associated with NR. It appears that in summer, P metrics dictate TF (i.e., the AMSD was similar for NR and TF events, but the P metrics were much larger), whereas in other seasons both P metrics and ASMD were important.

Almost all TF+OF events occurred in winter and spring (n = 42; Table 6-4c), with only rare events in summer and autumn (n = 3). With the exception of average P_i (0.7 – 1.3 mm h^{-1}), all P metrics were much larger, across all seasons, for TF+OF events compared to TF and NR events. For example, in spring the median P_d was long (22 hrs), P_v large (18.8 mm), with average P_i of 0.7 mm h^{-1} and maximum P_i of 3.6 mm h^{-1}. Winter TF+OF events had similar P metrics to those of spring, with ASMD close to zero in both seasons (0.9 in spring, -1.6 in winter). These results indicate that in winter, events with large P metrics generally were necessary to trigger TF+OF relative to just TF, while ASMD remained similar for both classes of runoff. Conversely, in summer and autumn both the ASMD and P metrics were important, having to be smaller and larger, respectively, to trigger TF+OF.

Both tile and overland flow showed large inter-seasonal variation (Table 6-5). In winter, when most TF events occurred (n = 60), the flow duration was long (i.e., 32 hrs), their volume and flow rate large, runoff ratio was high and HRT short. Spring yielded a similar number of TF events to winter but TF metrics were lower, and similar to those observed in autumn, with HRT the

Table 6-4. Seasonal precipitation (P) event metrics for events with a) no runoff (NR), b) events that triggered tile flow (TF), and c) events that triggered tile and overland flow (TF+OF). The median (lower quartile – upper quartile) P duration (P_d), total P volume (P_v), average and maximum P intensity (P_i) and antecedent soil moisture deficit (0-100 cm; ASMD) are calculated from *n = 322* individual P events occurring between 1st March 2019 and 28th February 2021.

	n	P_d (h)	P_v (mm)	Average P_i (mm h^{-1})	Average Maximum P_i (mm h^{-1})	ASMD (mm)
a) NR						
Summer	*60*	4 (2 – 8)	2.0 (0.9 – 3.0)	0.4 (0.3 – 0.7)	0.8 (0.6 – 1.4)	36.4 (24.4 – 45.5)
Autumn	*32*	6 (2 – 8)	1.6 (0.8 – 3.1)	0.4 (0.3 – 0.6)	1.0 (0.5 – 1.2)	48.7 (40.8 – 67.6)
Winter	*22*	6 (4 – 9)	1.8 (1.1 – 3.0)	0.4 (0.2 – 0.4)	0.8 (0.6 – 1.0)	6.2 (4.3 – 8.4)
Spring	*33*	5 (2 – 9)	1.6 (0.8 – 3.6)	0.5 (0.3 – 0.8)	1.0 (0.6 – 1.6)	12.0 (6.8 – 24.3)
b) TF Only						
Summer	*24*	12 (6 – 9)	9.6 (7.3 – 16.2)	1.1 (0.8 – 1.5)	3.7 (3.0 – 4.8)	38 (20.1 – 44.8)
Autumn	*32*	9 (6 – 15)	7.8 (4.4 – 16.2)	0.9 (0.6 – 1.5)	2.8 (2.3 – 3.7)	12.1 (4.0 – 54.1)
Winter	*39*	8 (4 – 14)	2.4 (1.6 – 5.0)	0.4 (0.3 – 0.6)	1.2 (0.8 – 1.8)	-1.2 (-3.3 – 1.3)
Spring	*34*	6 (2 – 12)	4.0 (2.2 – 7.8)	0.7 (0.5 – 1.1)	1.9 (1.2 – 2.7)	3.0 (-0.8 – 8.8)
c) TF + OF						
Summer	*1*	51	43.4	0.9	6.6	26.5
Autumn	*3*	24 (17 – 30)	21.0 (17.5 – 33.5)	1.3 (0.9 – 1.7)	8.2 (5.7 – 9.1)	2.4 (1.7 – 11.5)
Winter	*21*	21 (19 – 30)	17.0 (11.4 – 23.0)	0.7 (0.6 – 1.1)	3.0 (2.6 – 3.4)	-1.6 (-8.32 – 3.2)
Spring	*21*	22 (14 – 30)	18.8 (11.6 – 26.2)	0.7 (0.5 – 1.1)	3.6 (2.6 – 6.2)	0.9 (-4.0 – 4.2)

Table 6-5. Runoff (R) characteristics of tile flow (TF) and overland flow (OF), triggered by precipitation (P) events occurring between 1st March 2019 and 28th February 2021. The data were highly positively skewed, so only the median (minimum – maximum) values are shown for flow duration [R_d, h], total flow volume [V_t, mm], average flow rate [Q_{avg}, mm h^{-1}] and maximum flow rate [Q_{max}, mm h^{-1}], hydrograph response time [HRT, mm] and R ratio [V_t/P_v].

	n	R_d (h)	V_t (mm)	Q_{avg} (mm h^{-1})	Q_{max} (mm h^{-1})	HRT (h)	R ratio (V_t/P_v)
TF							
Autumn	*35*	11 (1 – 102)	0.3 (0.003 – 15.4)	0.02 (0.001 – 0.25)	0.04 (0.002 – 0.60)	3 (0 – 17)	0.05 (3E-4 – 0.4)
Winter	*60*	32 (1 – 140)	1.3 (0.005 – 12.5)	0.05 (0.005 – 0.26)	0.06 (0.005 – 0.36)	1 (0 – 34)	0.3 (8E-4 – 0.5)
Spring	*55*	10 (1 – 131)	0.3 (0.002 – 11.5)	0.02 (0.002 – 0.12)	0.03 (0.002 – 0.24)	1 (0 – 20)	0.07 (3E-4 – 0.4)
Summer	*25*	3 (1 – 81)	0.018 (0.001 – 8.4)	0.01 (0.001 – 0.12)	0.01 (0.001 – 0.40)	3 (0 – 12)	0.002 (1E-4 – 0.2)
OF							
Autumn	*3*	3 (3 – 14)	0.2 (0.2 – 3.9)	0.07 (0.07 – 0.28)	0.12 (0.11 – 1.15)	18 (6 – 19)	0.01 (0.01 – 0.08)
Winter	*21*	6 (2 – 37)	0.4 (0.049 – 9.4)	0.06 (0.02 – 0.54)	0.11 (0.03 – 1.26)	5 (0 – 14)	0.03 (4E-3 – 0.3)
Spring	*21*	12 (1 – 56)	1.6 (0.019 – 10.4)	0.09 (0.02 – 0.54)	0.36 (0.02 – 2.03)	5 (1 – 20)	0.1 (2E-3 – 0.3)
Summer	*1*	19	2.7	0.14	0.65	5	0.6

exception (autumn HRT > spring HRT). In summer, the TF duration was short, the volume and flow rate small, the runoff ratio small, and the HRT long.

Overland flow occurred much less often than TF (46 vs 175 events), and events were largely confined to winter and spring (Table 6-5). Few events occurred in autumn and summer, which was in contrast to TF. The frequency of OF events was identical in spring and winter but spring events were around twice as large with respect to all OF metrics while HRT remained similar. The only significant difference between the P metrics (Table 6-4) of spring and winter was that maximum P_i was generally larger in spring (3.6 mm h^{-1}) than in winter (3.0 mm h^{-1}).

Triggering of runoff, either TF or TF+OF, was best characterised with respect to precipitation event metrics and ASMD (Figure 6-8). Precipitation events that generated no runoff (NR) generally had small P volumes (P_v < 7 mm), small P intensities (P_i < 2.5 mm h^{-1}), and coincided with antecedent conditions of soil moisture deficit (ASMD > 0 mm; Field I, Figure 6-8a and b). Precipitation events that generated TF with medium runoff ratios (0.01 – 0.50) generally had equally small P volumes (P_v < 7 mm) and small P intensities (P_i < 2.5 mm h^{-1}), but the ASMD was close to zero (i.e., such that it was consequently satisfied by the P_v; Field II, Figure 6-8a and b). Precipitation events that generated TF with small runoff ratios (< 0.01) generally had large P volumes (P_v > 7 mm) and large P intensities (P_i > 2.5 mm h^{-1}), but the P volume was insufficient to satisfy ASMD (Fields III, Figure 6-8a and b).

However, if the P volume did satisfy the ASMD, these same large P volumes (P_v > 7 mm) and large P intensities (P_i > 2.5 mm h^{-1}) generated both TF and OF (TF+OF). In these instances, TF+OF of large runoff ratios (≥ 0.50; Field V, Figure 6-8a) occurred when antecedent soil moisture conditions were above FC (ASMD < 0 mm), whereas runoff ratios were medium (0.01 – 0.50; Field IV, Figure 6-8a and b) if antecedent conditions corresponded to positive soil moisture deficit (ASMD > 0 mm).

Once triggered, TF and OF volume showed seasonally variable dependency on precipitation event metrics, unsatisfied soil moisture deficit (ASMD-P), and PWT depth at one or more sites in the basin. The nature of the relationships (linear, nonlinear (quadratic), threshold, non-threshold) and their strength (R^2) was determined by least-squares regression (Table 6-6). Of the precipitation event metrics, tile flow showed the strongest dependence on ASMD-P. Relationships were strong and linear for all seasons and, with the exception of summer, involved thresholds implying a

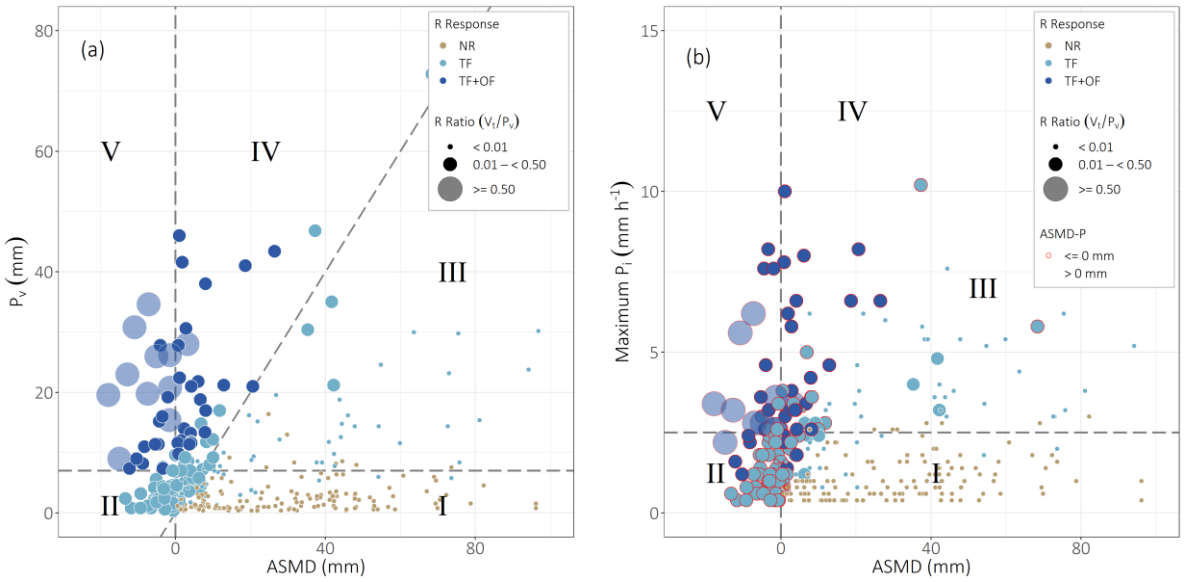

Figure 6-8. Plot of catchment-integrated antecedent soil moisture deficit (ASMD, mm) and (a) total precipitation volume (P_v, mm) and (b) maximum precipitation intensity (P_i, mm h^{-1}) for all monitored events. The colour of each event identifies the type of runoff generated, including no runoff (NR, brown), tile flow (TF, light blue) and tile flow and overland flow (TF+OF, dark blue). The size of each event point represents the total event R ratio (TF+OF; V_t/P_vgrouped as small (< 0.01), medium (0.01 - ≤ 0.50) and large (>= 0.50). In plot (b), the red border highlights events where ASMP-P was ≤ 0 mm and so delineates III from IV. The horizontal line represents P_v of 7 mm in plot (a) and Pi of 2.5 mm h^{-1} in plot (b); the vertical line ASMD of 0 mm, and the sloped line is 1:1. The labelled panels (I – V) are referred to in the text.

satisfied soil moisture deficit (ASMD-P ≤ 0 mm) was necessary. Moderate to strong linear, non-threshold, relationships between TF and P_d or P_v were also observed for winter, spring and summer. The relationships' strength dropped to weak or very weak in autumn.

Relationships between TF and PWT at most sites and seasons were moderate to strong, and quadratic in nature, emphasising the non-linear response of mole and tile flow to water table height above them. The interfluve and upper hollow showed threshold behaviour where the threshold corresponded to the depth at which the PWT intersected the mole network, while the mid-hollow (adjacent to the tile drain) showed a threshold depth that was closer to the depth of the tile drain. The side slopes (dSS and pSS) did not show threshold behaviour.

Only winter and spring were assessed for controls on OF volume, as summer and autumn did not produce enough events. Activation of OF in winter and spring appeared to be controlled by threshold PWT heights at IN1 (0.20 & 0.30 m, respectively), uHO (0.20 & 0.48 m, respectively), HS (0.30 & 0.60 m, respectively) and mHO (0.25 & 0.50 m, respectively), and OF was not recorded when the PWT was below these thresholds (Table 6-6). In winter, a threshold PWT height (0.18

Table 6-6. Linear regression analysis of event runoff (R) volumes (tile flow [TF] and overland flow [OF]; mm) with selected event predictor variables, including maximum precipitation intensity (P_i; mm h^{-1}), precipitation duration (P_d, h), total precipitation volume (P_v, mm), integrated antecedent soil moisture deficit and P_v (ASMD-P; mm), and the maximum event perched water table (PWT; m) height recorded at the interfluve (IN1), the upper hollow (uHO), the head slope (HS), the divergent side slope (dSS), and the mid-hollow (mHO). Relationships with threshold behaviour are those with a threshold value supplied, and the slope is the threshold-exceeded slope. Italicised thresholds were identified using the R-package *chngpt*, all others were identified manually. No data (nd) means that there were not enough events to carry out regression analysis. The subscripts denote the type of fitted relationship: [a] y = mx + c; [b] √y = mx + c; [c] *below threshold* y = mx - c; [d] *above threshold* √y = mx + c; [e] *above threshold* y = mx + c. Strong R^2 values (> 0.70) are in bold.

	Autumn			Winter			Spring			Summer		
Event Variable	Threshold	Slope	R^2	Threshold	Slope	R^2	Threshold	Slope	R^2	Threshold	Slope	R^2
TF												
Maximum Pi	-	0.59[a]	0.32	-	1.2[a]	0.34	-	0.68[a]	0.28	-	0.36[a]	0.33
P_d	-	0.09[a]	0.17	-	0.27[a]	0.64	-	0.17[a]	0.65	-	0.08[a]	0.59
P_v	-	0.12[a]	0.31	-	0.36[a]	**0.84**	-	0.23[a]	**0.73**	-	0.09[a]	0.60
ASMD-P	*-4.09 mm*	-0.37[c]	**0.93**	*-1.76 mm*	-0.29[c]	**0.73**	*-3.11 mm*	-0.28[c]	**0.74**	*0.83 mm*	-0.48[c]	**0.73**
IN1 maximum PWT	0.50 m	6.6[d]	**0.76**	0.50 m	6.1[d]	**0.76**	0.50 m	7.1[d]	**0.72**	*0.57 m*	4.8[d]	**0.90**
uHO maximum PWT	0.53 m	3.4[d]	**0.78**	0.53 m	3.6[d]	**0.77**	0.53 m	3.5[d]	0.64	0.53 m	3.1[d]	**0.90**
HS maximum PWT	-	4.3[b]	0.67	-	4.2[b]	**0.74**	-	6.6[b]	**0.76**	-	5.5[b]	0.47
dSS maximum PWT	-	3.6[b]	**0.81**	-	3.8[b]	**0.77**	-	5.2[b]	0.53	-	4.5[b]	**0.81**
mHO maximum PWT	0.60 m	3.6[d]	0.60	0.60 m	3.5[d]	0.43	0.60 m	5.8[d]	0.29	0.60 m	4.0[d]	0.48
OF												
Maximum Pi	nd	nd	nd	-	0.46[a]	0.21	-	0.5[a]	0.34	nd	nd	nd
P_d	nd	nd	nd	-	0.09[a]	0.29	-	0.07[a]	0.26	nd	nd	nd
P_v	nd	nd	nd	*16.4 mm*	0.41[e]	0.58	*9.8 mm*	0.22[e]	**0.71**	nd	nd	nd
ASMD-P	nd	nd	nd	*-17.03 mm*	-0.28[c]	0.66	*-12.14 mm*	-0.31[c]	**0.78**	nd	nd	nd
IN1 maximum PWT	nd	nd	nd	0.2 m	7.88[d]	0.13	0.30 m	1.54[d]	0.01	nd	nd	nd
uHO maximum PWT	nd	nd	nd	0.2 m	1.47[d]	0.03	0.48 m	2.56[d]	0.35	nd	nd	nd
HS maximum PWT	nd	nd	nd	0.3 m	8.98[d]	**0.75**	0.6 m	9.43[d]	0.18	nd	nd	nd
dSS maximum PWT	nd	nd	nd	0.18 m	14.68[d]	0.61	-	3.28[d]	0.35	nd	nd	nd
mHO maximum PWT	nd	nd	nd	0.25 m	2.71[d]	0.03	0.5 m	3.84[d]	0.08	nd	nd	nd

m) was identified for OF at dSS, but no threshold was identified in spring. These results indicate that the PWT may exert some control on the triggering of OF, with the requirement for a higher PWT in winter than in spring. Despite PWT thresholds being involved in the initiation of OF, only at HS and dSS was there any relationship between PWT height and OF volume (R^2 = 0.75 and 0.61, respectively; Table 6-6) and only in winter, which might indicate that this area is a source of saturation-excess OF. However, there was no evidence that the PWT height plays a major control on OF volume at other locations in the catchment. The P_v showed moderate or stronger relationships with OF volume, with R^2 = 0.71 in spring and 0.58 in winter. Both were linear relationships above thresholds of 9.8 mm and 16.4 mm, respectively. There was also a linear (but negative) moderate to strong relationship between ASMD-P and OF. Similar to TF, these relationships were dependent on thresholds of moisture excess being crossed, -17 mm in winter versus -12 mm in spring.

6.4.4.1 Tile flow and perched water table relationships

The parts of the catchment contributing to TF generation (i.e., R^2 of ≥ 0.5; grey cells in Table 6-7) expanded with increasing runoff ratio. For all but the smallest and largest runoff ratio classes, PWT_{max} at the interfluve and upper hollow had the strongest relationships with TF volume. For the smallest runoff ratio events only the upper hollow appeared to be actively contributing to TF, whereas during the highest runoff ratio events the head slope and divergent side slope complemented the upper hollow and interfluve in generating TF.

Saturation-excess conditions (i.e., any given site having a perched water table [PWT] that reaches 10 cm from the surface) occurred during approximately 50 % of winter OF events, and did not occur during any of the OF events in spring when OF metrics were the largest (data not shown).

Table 6-7. Table of Coefficient of Determination (R^2) values obtained from linear regression analysis of event runoff (R) volumes for tile flow (TF) against maximum event perched water table (PWT) height. Relationships were analysed at the interfluve (IN1), the upper hollow (uHO), the head slope (HS), the divergent side slope (dSS), and the mid-hollow (mHO). The data has been grouped by R ratio (V_t/P_v*100; %). The strength of the R^2 has been highlighted for easier interpretation (<0.5 not highlighted; 0.5 – 0.69 highlighted; >0.7 highlighted and bold).

	Monitoring Site				
R Ratio (%)	IN1	uHO	HS	dSS	mHO
0 - 10	0.19	0.56	0.001	0.07	0.22
10 – 20	**0.74**	**0.8**	0.26	0.24	0.22
20 – 30	0.57	0.61	0.24	0.26	0.14
30 – 40	0.57	0.67	0.44	0.22	0.12
40 – 50 +	0.53	0.51	**0.72**	0.64	0.14

6.5 Discussion

6.5.1 Runoff exports

Runoff (as tile flow and overland flow) was an important component of the water balance, with strong seasonal variation apparent. Most TF occurred in winter and most OF in spring, which was consistent with a study 18 km east of the field site on the same soils, where runoff generally occurred when the soil water content exceeded field capacity (Monaghan et al., 2016). However, our estimates of the annual proportion of P lost to TF (14 %) and OF (3.5 %) were noticeably smaller than their estimates of 20 – 22 % and 5 – 11 %, respectively. Monaghan et al. (2002) found that, on a range of similar soils (including Fragic Perch-gley Pallic, Pallic Firm Brown, Mottled Firm Brown and Typic Firm Brown Soils), TF accounted for ca. 7 – 28 % of annual P, with variation attributable to fragipan characteristics. At the same study site, and on the Fragic Perch-gley Pallic and Pallic Firm Brown Soils, Smith and Monaghan (2003) estimated OF to be ca 4.5 % of annual P.

An important distinction between the aforementioned studies and the present study is that the former were all at the plot scale, and testing freshly installed mole and tile systems, while the present study was at the catchment scale and the mole and tile network was > 30 years old. This difference in the age of the drainage network and measurement scale could also partially explain why the recovery of P as TF was greater in the plot studies, because freshly installed systems are likely to have a functioning artificial fracture network (see Chapter 5) that is more efficient at delivering precipitation from the soil surface to the tile drain. A more efficient fracture network would, however, suggest a greater efficiency of the drainage network to attenuate OF, with smaller recoveries of OF, which is contrary to what was observed. Higher recoveries of annual P as OF in the plot studies relative to the present study may be because at the scale of an entire drainage basin there is likely to be more opportunity for re-infiltration of surface water before the catchment outlet collection point (Gomi et al., 2008; Joel et al., 2002; Kirkby, 2002). This would indicate that plot scale studies may overestimate the OF component by not capturing attenuation processes active at the catchment scale.

6.5.2 Deep drainage exports

Deep drainage was shown to make up a considerable component of the water balance, with 264 – 362 mm (26 % of P) lost annually. These catchment-scale estimates are supported by the profile-scale water balance simulations by Horne and Scotter (2016), who calculated cumulative annual DD volumes of 150 – 450 mm year^{-1} for a similar mole and tile-drained loess soil, equivalent to 15

– 45 % of annual P (Houlbrooke, Horne, Hedley, Hanly, Scotter, et al., 2004). Further soil profile-scale simulations by Vogeler et al. (2021), estimated DD losses of 161 to 202 mm year^{-1} across three undrained fragipan soils under a northern Southland climate, with a rainfall of 855 mm per year (i.e., 19 – 24 % of annual P). Our estimates are slightly higher than those from environmental tracer studies in undrained areas of the Loess Plateau in China, where DD is generally less than 80 mm year^{-1}, equivalent to 10 – 20 % annual precipitation (Huang et al., 2020; Huang et al., 2017; Huang et al., 2019; Lin & Wei, 2006). It is likely that this difference is at least in part a result of the relative difference in loess thickness, as the deposits in China are 40 – 60 m deep. However, significantly different deep drainage estimates were derived from an undrained plot study in the Palouse region of northwestern USA, which ascribed just 2 % of annual precipitation to percolation through the deep loess (McDaniel et al., 2008). Our results; therefore, may have more applicability in New Zealand loess landscapes than in loess landscapes on other parts of the globe.

A degree of error in the estimation of DD was indicated by the negative DD values observed at the daily time scale. Negative DD occurs when one or more of the water balance outputs (ET, TF, OF, $\Delta\theta_V$) is greater than the inputs (P). Relatively infrequent, but large negative values appeared to be associated with precipitation events across the year, but small and consistent negative values occurred predominantly in the summers and autumn (dry soil moisture state) of 2018 – 2019 and 2020 – 2021, suggesting that P, ET or θ_V were likely to be the most frequent source or error. Calculation of ET required assumptions that may have had error associated with them. It is possible that this was the source of the small and consistent negative DD in summer and autumn; however, the estimates of ET were consistent with mean annual Penman-calculated ET monitored 22 km south-east of the field site, indicating that, cumulatively, the ET estimates were reasonable. We attribute the bulk of the large negative DD values to delays in the response of soil moisture to precipitation. Because of the calculation of the water balance at a daily time step, it is possible that a precipitation event occurring in the final hour of one day is first registered by the soil moisture sensors in the first hour of the following day. This would result in a miscalculation of DD at the daily time step; however, such error self-corrects when cumulating over seasonal and annual time periods, so the estimates of DD exports provided in this study can be considered reasonable.

6.5.3 Deep drainage rate and mechanisms

The importance of DD exports to groundwater recharge was demonstrated by analysis of the groundwater table, which appeared to respond quickly to the DD status – rising in response to

active DD and falling in the absence of DD. Estimates of DD rates (ca. 9.6 mm d^{-1}) were consistent with the findings of Vogeler et al. (2019), who demonstrated that a fragipan K_{sat} value of > 12 mm d^{-1} was the best value for predicting temporal soil moisture behaviour using the Agricultural Production Systems sIMulator (APSIM) for the loess-derived Otokia silt loam. However, soil core measurements of the Otokia fragipan K_{sat} appear to be highly variable in the literature, with much smaller values (0.1 mm d^{-1}) measured by Watt (1976) and much larger values (20 – 22 mm d^{-1}) measured by Joe and Watt (1984). It is recognised that soil core measurements of K_{sat} have a high degree of uncertainty (Pollacco et al., 2017; Vogeler et al., 2019), which was also demonstrated in the present study by the large range in fragipan K_{sat} measured from soil cores (4.8 – 260 mm d^{-1}; Chapter 5). Estimates of fragipan K_{sat} may be complicated by the fragipan structure, which commonly comprises prismatic units of large (5 – 50 cm) width (Schaetzl & Thompson, 2015). Scotter et al. (1979) measured extremely slow K_{sat} values of ca. 0.01 – 0.08 mm d^{-1} within the fragipan prisms of the Tokomaru silt loam; however, the low rates were not consistent with the observed soil moisture profiles. They suggested that there was a strong possibility that gleyed interprism areas may have higher permeabilities and form pathways for deep percolation. The integrated measure of DD provided in this study may, therefore, be more appropriate than soil core measures for quantifying DD fluxes at catchment scales, capturing the accumulation of water movement that occurs both between and within fragipan prisms.

It is likely that, despite almost the complete erosion of the intact loess mantle in the hollow, DD rates do not vary significantly across the basin (i.e., dissected parts of the landscape contribute equally to DD relative to parts of the landscape with a deep loess mantle). This conclusion is based on the results of Chapter 3 and Chapter 5. Chapter 3 demonstrated that K_{sat} generally declined with increasing age of the loess deposits, and that the K_{sat} of the underlying clayey and highly weathered Quaternary gravels appeared to be at least as limiting as the more slowly permeable loess sheets. Furthermore, in Chapter 5, it was shown that landscape element had no influence on subsurface K_{sat}. Additionally, the rapid, but not flashy, response of the GWT to DD indicated that piston flow, not preferential flow, was the most likely mechanism for the downward movement of water through the loess, which was consistent with findings in the Loess Plateau of China that used environmental tracers to investigate groundwater recharge mechanisms (Huang et al., 2020; Huang et al., 2017; Huang et al., 2019). It is the pressure fluctuations, attributable to increased gravitational potential by the generation of perched water tables, that are likely to have activated the piston flow pathways, and results from Chapter 7 suggest that these perched water tables are

rapidly removed in the hollow by the tile drain. These findings together suggest that 'focussed infiltration' in the hollow, as proposed by Gates et al. (2011), Huang et al. (2019) and Lin and Wei (2006) is unlikely to be the primary recharge mechanism in this Southland loess landscape; however further, more detailed research is required to confirm this hypothesis.

6.5.4 R Controls

Thresholds in multiple hydrological metrics appeared to be important for triggering R responses. The observed thresholds provide insight into the soil properties (natural and anthropogenic) that control water movement in this landscape.

Soil moisture, itself regulated by the P-ET balance, appeared to govern the runoff response to precipitation characteristics. An ASMD of approximately 7 mm separated the majority of medium to large R events (R ratio ≥ 0.01) from small R events (R ratio < 0.01). This ASMD roughly defined the approximate boundary between two soil moisture states: wet (SMD < 7 mm) and dry (SMD > 7 mm), which was consistent with the duality of moisture states that has previously been described for undrained catchments (De Lannoy et al., 2006; Farrick & Branfireun, 2014; Grayson et al., 1997; Martini et al., 2015; Robinson et al., 2012; Tromp-van Meerveld & McDonnell, 2006a). Furthermore, and similar to the conclusions by Grayson et al. (1997), lateral movement of excess soil water (i.e., TF and OF) was predominantly restricted to the wet state.

In the wet state, TF was always activated in response to precipitation, with the volume of event TF almost entirely goverened by the volume of event precipitation, and not ASMD. Conversely, in the dry state, the volume of event TF was regulated by both Pv and ASMD, with thresholds in ASMD-P detected. Similar behaviour was observed in the streamflow response to precipitation of an undrained forest catchment of volcanic origin by Farrick and Branfireun (2014), who concluded that at sufficiently low ASMD, less precipitation was being diverted into storage and more was being translated into runoff. We additionally detected thresholds for PWT height, which indicated that tile flow only activated once water began moving into the mole channels upslope of the tile drain. Similar ASMD-P and PWT thresholds were observed in a non-drained, till-mantled catchment by Detty and McGuire (2010a), who suggested the PWT threshold might represent activation of rapid lateral flow as the PWT rises into highly transmissive near-surface soils. The low macroporosity of the soil at our site at all depths makes it almost certain that the majority of rapid lateral flow is occurring via the mole network and not laterally through the soil matrix.

In the wet state, or when P inputs satisfied the ASMD, a P_i in excess of 2.5 shifted runoff from TF only to TF+OF. This low P_i threshold points towards equally low soil infiltration rates, which is consistent with results from Chapter 5, that showed the median surface K_{sat} to be 3.5 mm h^{-1}. Evidence of a low soil surface infiltration rate was also provided by the very large increases in OF metrics in spring, relative to winter, which occurred in response to small increases in P_i (i.e., median maximum P_i of 3.0 mm h^{-1} in winter versus 3.6 mm h^{-1} in spring). Furthermore, in the dry state, a P_i of ca 2.5 mm h^{-1} initiated TF events, suggesting that natural, surface-vented preferential flow pathways were active and transporting water directly from the surface to the drain. For these pathways to activate in the absence of saturation, there must be surface ponding so that water at zero or low matric potential is available to flow into large pores (Hillel, 1982). The concurrent P_v threshold of ≥ ca. 7 mm precipitation observed for dry state TF events, was likely sufficient to wet the surface and reduce sorptivity close to zero, such that ponding could develop in response to above-threshold P_i. The majority of TF events that appeared to occur as a result of natural, surface-vented preferential flow paths had extremely low R ratios, despite the common assumption that preferential flow from the surface to the mole channel fracture network is a key functional component of these drainage systems (Goss et al., 1983; Leeds-Harrison et al., 1982; Robinson et al., 1987; Youngs, 1985). Thus the catchment area contributing to TF under these conditions was probably small, and was consistent with the results in Chapter 5, which found no evidence of a functional fracture network. In plot studies of freshly installed mole and tile systems, surface-sourced preferential flow is often assumed to be the primary flow pathway involved in the activation of tile flow (Monaghan & Smith, 2003; Monaghan & Smith, 2004; Monaghan et al., 2007; Oliver et al., 2005; Ross & Donnison, 2003). The results presented here again suggest that an assumption of substantial preferential flow between the surface and the mole network is not appropriate for mature mole drainage networks.

6.5.5 Infiltration- versus saturation-excess overland flow

We saw evidence that saturation-excess conditions were rare, and did not occur during any of the OF events in spring when OF metrics were the largest. Thresholds corresponding to deep perched water tables, and the strong relationship between above-threshold P_v and OF volume provide further evidence that infiltration-excess OF was the predominant mechanism of surface runoff in spring. Contrastingly, in winter, only half of OF events demonstrated saturation-excess at a minimum of one monitored site. From these results, we can infer that infiltration-excess OF was the most common form of surface runoff. This is logical, as the functional purpose of

subsurface drainage systems is to increase the rate of excess water removal and increase the potential water storage capacity, thereby reducing the likelihood of saturation excess (Armstrong, 1986b; Robinson et al., 1987). That saturation-excess is rare also supports our findings in Chapter 4 of a dense, well-connected and functional mole network. These findings are important for hydrological and nutrient-loss modelling of these soil landscapes. Under the current low-intensity climatic conditions, OF accounts for only a small proportion of the annual water balance. However, climate models for Southland forecast increases in both average annual precipitation and precipitation intensity, specifically over winter and spring (Zammit et al., 2018). Given these seasons already account for almost all of annual OF, even slight increases in precipitation metrics could result in the runoff pathway becoming a much more important component of the water balance, and factor governing surface water quality.

Despite the apparent importance of infiltration-excess OF, OF volume was poorly related to maximum P_i. This is inconsistent with other studies that demonstrated increasing OF discharge in response to increasing P_i (Bou Lahdou et al., 2019; Wei et al., 2014). The absence of a relationship may be due to the disparity between the frequency of P measurement and the scale of the response of the OF. OF was monitored at 1-minute resolution and reactions in flow behaviour were apparent at the sub-5 minute resolution. Precipitation, on the other hand, was measured at hourly intervals, possibly obscuring any emergent relationship. We are therefore restricted to an approximate understanding of the threshold trigger for OF (i.e. ca 2.5 – 3.5 mm h^{-1}).

6.5.6 Tile flow source area

Our results, which estimated the effective runoff contributing areas using R ratios (Detty & McGuire, 2010b), provide some insight into important source areas for tile flow. For smaller TF events (R ratio = 0.1 – 0.2), TF was predominantly sourced from the interfluves and upper hollow but as the catchment wet up, the source area expanded out until most of the catchment was contributing to TF. For R ratios below 0.1, none of the sites produced strong relationships between PWT and TF volume, which is presumably because most events of this magnitude occurred in the dry state events when tile flow was produced via surface-sourced, natural preferential flow mechanisms. It is, therefore, unclear which parts of the catchment produce more TF than others when the catchment is in the dry state and natural preferential flow is the dominant mechanism. The relationship at the steeper or divergent slopes (dSS and HS) was only strong for events with the largest R ratios (> 0.4), suggesting that these areas only contribute during the largest events

once the catchment is near saturation. Furthermore, the mean R ratio for tile flow across the monitoring period was 0.14 ± 0.14, which was the runoff ratio class that had a strong relationship between TF volume and PWT on the interfluve and upper hollow. The steep side slope classes only became hydrologically connected once the R ratio was over 0.4, which occurred infrequently. Crucially, there was no evidence that the area of the hollow fitted with the tile drain (i.e., mHO) was an important contributing area to TF. In undrained catchments, such areas of high convergence are thought to remain saturated throughout the wet state and act as the origin of both surface and subsurface runoff (Grayson et al., 1997; Tromp-van Meerveld & McDonnell, 2006a). The results presented here are consistent with the idea developed by Williams et al. (2019) who suggested that TF was activated by saturated upslope areas, and that flow occurred in the tile before saturation of the depression where the tile was located.

6.6 Conclusions

The current study used a water balance approach, combined with event–scale analysis of precipitation, soil moisture and runoff characteristics, to show that deep drainage, tile flow and overland flow are important and seasonally variable components of the water balance, controlled by thresholds of volumetric soil moisture content, precipitation volume and intensity, perched water tables.

Runoff occurred predominantly in winter and spring, with tile flow greatest in winter and overland flow greatest in spring. Deep drainage was shown to constitute an important temporally variable flow pathway, particularly in the winter when it was the largest water balance component. It was activated by excess soil moisture that triggered piston flow in the presence of perched water tables, with an estimated groundwater recharge rate of c. 0.40 mm h^{-1}. Deep drainage flux was likely to occur uniformly across the landscape. Soil moisture governed the runoff response to precipitation characteristics. Intrinsic and extrinsic runoff thresholds interacted to regulate tile flow response. Precipitation volume and/or instensity thresholds discriminated event runoff response depending on antecedent soil moisture state (dry or wet). Furthermore, as a result of low surface infiltration capacity, infiltration-excess overland flow was the most common form of surface runoff. Spatially, tile flow was predominantly sourced from the interfluves and upper hollow. With wetting up of the catchment, the source area expanded; however, events of the magnitude required to activate the side slopes occurred infrequently. The area of the hollow fitted with the tile drain was not identified as a key tile flow- or deep drainage-contributing area.

The results of this study demonstrate that the common assumption of negligible deep drainage may be inappropriate when modelling flow pathways in slowly permeable loess, with or without artificial drainage. They also point towards a hydrologically sensitive landscape which demonstrates a highly non-linear response to variations in precipitation intensity, such that a shift in the distribution of precipitation intensity with climate change could make dramatic changes in the components of the water balance (i.e. more OF). Finally, the results identify winter and spring as key seasons and the interfluves and upper hollow as key areas of the landscape that could be targeted for mitigating surface water contamination from mole and tile-drained loess landscapes.

Chapter 7

Spatiotemporal dynamics of hydrological connectivity in a small mole and tile trained basin with fragipans

7.1 Abstract

Hydrological connectivity is an important concept used to explain the mechanisms underpinning water movement from one part of the landscape to another. The dynamics of hydrological connectivity are regulated by spatial and temporal soil moisture patterns. Few studies have investigated the spatiotemporal dynamics of hydrological connectivity in agronomically-important, artificially drained loess soils, yet freshwater bodies in these landscapes are under increasing pressure from agricultural runoff. The aim of this chapter was to understand the spatiotemporal dynamics of hydrological connectivity in mole and tile-drained, slowly permeable, loess-derived soils in Southland, New Zealand. It was achieved by empirical analyses of the behaviour of soil volumetric water content and perched water tables (PWT) at different landscape elements and their relationship with tile flow behaviour. The role of interflow was also examined by estimating the downslope travel distance (DTD) of excess water above the fragipan. Spatial soil moisture patterns appeared to be influenced by perched water tables and the drainage network, while topographic wetness index (TWI) was, on its own, a poor predictor of spatial soil moisture variability. The lower hollow was one of the driest parts of the catchment in winter and spring, indicating that the tile drain was regulating spatial soil moisture variability. The transition from dry state to wet state soil moisture conditions lasted approximately two weeks and appeared to begin at the lower catchment hollow. With increasing catchment wetness, tile flow regulation (i.e., hydrological connectivity) expanded from the excess moisture at the lower hollow, to the PWTs at the mid- to upper hollow, and eventually up to the interfluve PWTs. Hydrological connection was mediated by the mole channel network, and its interception by PWTs. Only rainfall periods with exceptionally large precipitation volumes and intensities were able to trigger PWTs on the slopes, and these PWTs only demonstrated control on tile flow once all other parts of the catchment were saturated. There was no evidence that natural interflow, either as matrix or natural, surface-sourced, preferential flow, was a significant mechanism for hydrological connectivity. Flat, upslope areas prone to the development of PWTs should be focussed on when considering water quality mitigation strategies in mole-tile drain loess landscapes with slowly permeable subsoils, especially in winter.

7.2 Introduction

Hydrological connectivity is a concept that describes the water-mediated transfer of energy and matter within and between elements of the hydrologic cycle (Pringle, 2003). Studies of hillslope- and catchment hydrology utilise the concept of hydrological connectivity to explain the mechanisms underpinning water movement from one part of the landscape to another (Detty & McGuire, 2010b; Farrick & Branfireun, 2014; Macrae et al., 2019; McGuire & McDonnell, 2010; Oswald et al., 2011; Wilson et al., 2017). Water movement in the form of surface and subsurface runoff can connect contaminant source areas in agricultural landscapes with surface water bodies and is known to be a major source of freshwater contamination by nutrients, sediments, pathogens and agricultural chemicals (Carpenter et al., 1998; Deasy et al., 2009; Dodds & Smith, 2016; Gilpin et al., 2020; Havens et al., 2020; Snelder et al., 2020). Of particular concern, is the contribution to water quality degradation by landscapes modified with mole and tile drainage systems. These drainage systems are commonly installed in soils with low-permeability fragipans to expedite the removal of excess moisture. Loess soils often contain fragipans, and once drained, these soils form some of the world's most productive agricultural landscapes (Catt, 2001), including large areas of Southland, New Zealand, where they support nationally-significant pasture-based systems (Moran et al., 2017). Similar to many parts of the world where slowly permeable loess has been artificially drained, Southland's freshwater resources are under pressure from contamination by agricultural runoff, and these is a need to better understand the mechanisms by which these landscapes become hydrologically connected to freshwater systems.

Mole and tile drainage systems can rapidly relocate water, with or without entrained contaminants, from distal parts of the catchment to surface water receiving bodies (Houlbrooke, Horne, Hedley, Hanly, Scotter, et al., 2004; Monaghan et al., 2002; Schottler et al., 2014). Despite the fact that these subsurface drainage systems significantly alter water flow pathways in naturally low-permeability soils (Armstrong, 1986b; Armstrong & Garwood, 1991; Blann et al., 2009; Goss et al., 1983; Schilling et al., 2012; Smith & Monaghan, 2003), few studies have investigated the spatiotemporal dynamics of hydrological connectivity in these modified catchments. When considering water quality mitigation strategies or land use change for mole and tile-drained landscapes, an understanding of the spatiotemporal dynamics of hydrological connectivity is paramount, as these systems are likely to modify the source area of, and controls on, catchment discharge.

The dynamics of hydrological connectivity are regulated by spatial and temporal soil moisture patterns, which control water balance partitioning of precipitation into runoff, deep drainage, storage and evapotranspiration; and pathways of water flux (e.g., lateral and vertical fluxes, preferential flow, matrix flow) and solute transport (Grayson et al., 1997). An accurate representation of soil moisture distribution is, consequently, one of the most important factors in hydrological and environmental modelling. Topography (slope, aspect, curvature and location on the slope), vegetation, antecedent conditions and soil properties are all known to influence spatial and temporal soil moisture patterns in undrained catchments (Guo et al., 2020; Hawley et al., 1983; Lin et al., 2006). In undrained catchments under pasture, soil moisture may show control by surface topography and soil depth (Grayson et al., 1997; Hawley et al., 1983; Lin et al., 2006; Western et al., 1999), and highly topographically convergent areas such as hollows accumulate water and are often found to be the wettest part of the landscape, especially in the winter and spring (Boersma et al., 1972; Martini et al., 2015).

Spatial patterns of soil moisture are commonly estimated using information about surface topographic variation as a substitute for soil moisture data (Hawley et al., 1983). One of the most frequently used metrics for estimating relative soil wetness within a landscape is the topographic wetness index (TWI), which describes the tendency of an area to accumulate water as a function of its local upslope contributing area and slope (Barling et al., 1994; Beven & Kirkby, 1979; Chaplot & Walter, 2003; McKenzie & Ryan, 1999; Sørensen et al., 2006; Western et al., 1999; Zhu et al., 2014). Good TWI-soil moisture relationships have often been shown to exist in humid climates, where high rainfall keeps the soil in a wet condition (Barling et al., 1994). Whether the TWI is an appropriate measure of soil moisture patterns in mole and tile-drained landscapes in humid climates is not well understood. Tile drains have been shown to significantly modify the spatial patterns of soil moisture, and convert the hollows in which they are installed from the wettest to the driest part of the landscape (Williams et al., 2019). Mole channels have the potential to alter the spatial and temporal soil moisture dynamics; however, there is little or no literature that addresses this.

Subsurface hydrological connectivity is often inferred from continuity in the spatial patterns of perched water tables (PWTs) or soil moisture content (Detty & McGuire, 2010b; McDaniel et al., 2008; McGuire & McDonnell, 2010; Oswald et al., 2011). These studies generally interpret spatially-connected PWTs between hillslopes and drainage channels to mean that soil water from the slopes is moving laterally downslope to form a component of the runoff that leaves the basin

via the drainage channel as 'interflow' (Meles Bitew et al., 2020). Interflow (also known as 'throughflow', 'subsurface lateral flow', 'subsurface stormflow' and 'subsurface runoff') is considered to be an important flow pathway in landscapes where vertical hydraulic conductivity is restricted by an impeding layer, such as a fragipan (Meles Bitew et al., 2020; Weiler et al., 2005). Interflow occurs through both the soil matrix and, more rapidly, through macropores or other natural preferential flow pathways, where it bypasses large parts of the soil matrix and is transferred to sink areas (Farrick & Branfireun, 2014; Grangeon et al., 2021). Because of its rapid transfer, short residence times and limited opportunity for assimilation or filtration, preferential flow has attracted a lot of attention for its role in catchment hydrology and water quality (Clothier et al., 2008; Garrido & Helmhart, 2012; Gurdak et al., 2008; Kelly & Pomes, 1998; McLeod et al., 2008; Monaghan & Smith, 2004; Noguchi et al., 1999; Sidle et al., 2001; Stone & Wilson, 2006; Weiler, 2017; Zhang et al., 2018).

Studies of undrained loess landscapes in the Palouse region of north-western USA and the fragipan-containing till deposits of the Allegheny Plateau in eastern USA have shown that interflow may account for a considerable component of the water balance, especially in winter (McDaniel et al., 2008; Miller et al., 1971). However, there is a lack of understanding of the importance of interflow, both rapid and slow, in artificially-drained slowly permeable loess. The fragipan-containing loess soils of Southland are considered to be at medium to high risk of preferential flow in their undrained, natural state (Figure 7-1) but few studies are available to confirm these estimates, especially at the catchment scale. A lysimeter study by McLeod et al. (2003) indicated that preferential flow was a significant pathway for the rapid transfer of microbes through undrained Pallic soils with fragipans. Greenwood (1999) additionally demonstrated that a surface-applied bromide tracer could be found at greater depths in an undrained Pallic soil after 30 minutes when the antecedent soil conditions were dry relative to when they were wet. This was attributed to preferential flow via deep, surface-vented cracks, which formed as a result of soil shrinkage during desiccation. In the tile drained, but un-moled, thin loess and glacial till landscapes of the US-Midwest, Vidon et al. (2012) found that macropore flow contributed up to 50 % of total catchment scale tile flow. Given its generally greater density and effective drainage area, the mole network has the potential to have much greater influence on hydrological connectivity than tile drains alone, as they have the potential to link all areas of a basin. Further investigations are, therefore, required to determine the spatiotemporal dynamics and mechanisms of interflow in artificially drained landscapes.

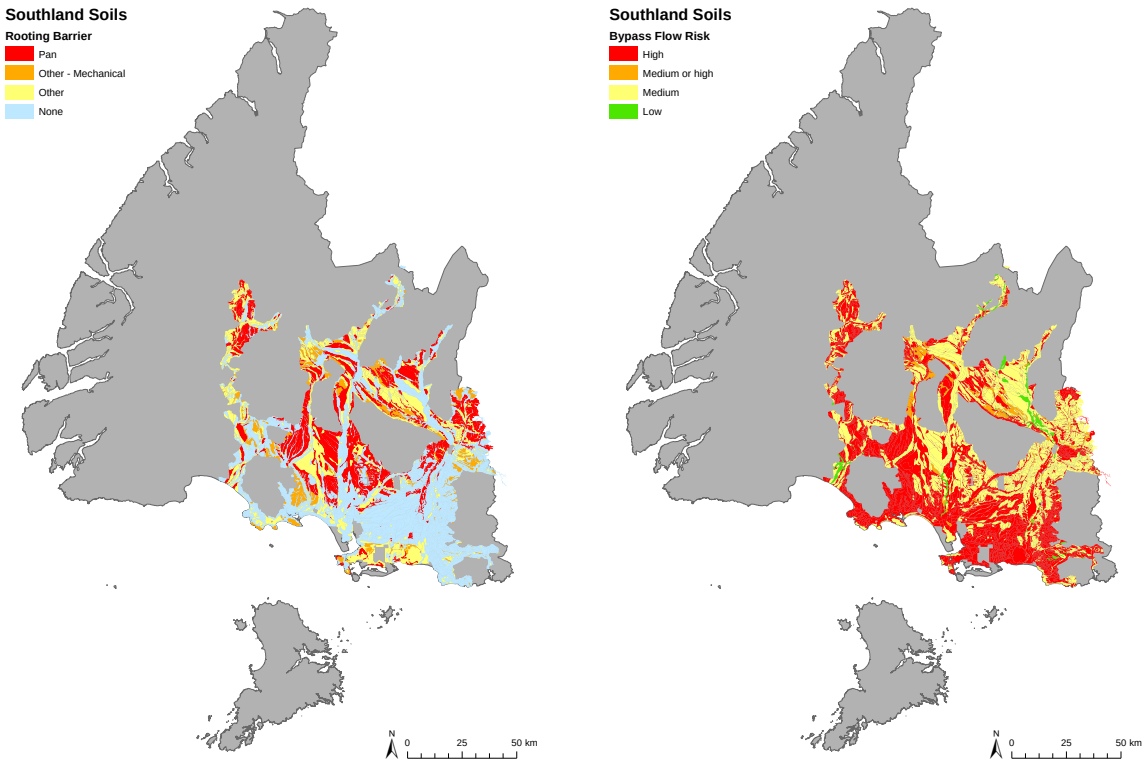

Figure 7-1. Rooting barrier type (left) and preferential flow risk (right) for the mapped soils of Southland, New Zealand. Source: S-Map Soils Database, Manaaki Whenua - Landcare Research (2022).

Ultimately, the mole and tile network has the potential to act as a highly-connected, expansive, artificial preferential flow network. It is essential to understand the role of these systems in catchment hydrological connectivity, as accurate representations of hydrological connectivity are essential for developing and improving the performance of catchment-scale groundwater-surface water models (Hansen et al., 2013). Excess soil moisture is presumably a crucial element for the activation of mole and tile flow, as water will not flow out of the soil into a large cavity or drain unless the pressure of soil water is greater than atmospheric (Hillel, 1982, p. 261). Therefore, it is likely that a PWT that submerges the drainage network is a primary requirement for hydrological connectivity in these landscapes. Alternatively, flow in the drainage network may be generated by surface-sourced preferential flow to the artificial drainage channels through natural and artificial cracks in the soil. While a few studies on hydrological connectivity exist for landscapes drained by a single tile drain (Vidon et al., 2012; Williams et al., 2019), there is a distinct lack of information

available for landscapes modified by mole drainage. In a tile drained (but un-moled) landscape formed in the Wisconsinan glacial till of north-eastern Indiana, Williams et al. (2019) found that the formation and drainage of PWTs on depression hillslopes were likely the main mechanism of subsurface connectivity and source of tile flow.

Despite general consensus that interflow is an important hydrological pathway, there is debate in the literature around the mechanisms of interflow, specifically with regard to the implicit assumption that 'spatially' connected PWTs are always 'hydrologically' connected (i.e., responsible for runoff generation), and especially in cases where the impeding layer is 'leaky'. Klaus and Jackson (2018) calculated the potential distance that a water parcel could travel downslope within a saturated wedge before percolating into the underlying impeding layer (the downslope travel distance; DTD). They found that in 14 of 17 published studies on hydrological connectivity in undrained landscapes, the slope lengths were significantly longer than the DTDs, and, that only soil water in the lowest part of the hillslope was likely to reach the stream channel as interflow. Similar results were shown by Jackson et al. (2014) and Meles Bitew et al. (2020). Wilson et al. (2017) suggest that a spatially-connected PWT may imply that lateral hydraulic conductivity is, in fact, insufficient to disperse the water rapidly downslope, and therefore indicates dis-connectivity. The relationship between PWTs and lateral interflow is rarely studied in mole drained catchments, so there is little information available about the contribution of lateral interflow to hydrological connectivity in these landscapes. Presumably this component of hydrological connectivity would be virtually eliminated, as most drainage should be diverted into the artificial drainage network; however, this assumption requires experimental evidence.

The aim of this research was to understand the spatiotemporal dynamics of hydrological connectivity in mole and tile-drained, slowly permeable, loess-derived soils. The specific research questions and objectives were as follows:

1) Is the topographic wetness indices useful for understanding relative wetness in a mole and tile-drained landscape?

    - Qualitatively analyse the behaviour of volumetric soil moisture and perched water tables across different landscape elements.

2) What is the influence of the PWT and the mole network on catchment-wide hydrological connectivity and how does hydrological connectivity vary spatially and with time?

    - Qualitatively analyse tile flow responses to PWT and volumetric soil moisture content with time.

3) What is the role of lateral throughflow in hydrological connectivity?

    - Estimate the downslope travel distance (DTD) of excess water above the fragipan.

7.3 Methods

7.3.1 Study site

The study area was previously described in Chapter 3, section 3.3.1. In brief, the study site is a 3.95 ha zero-order, un-channelled basin in Southland, New Zealand (Figure 7-2). The basin drains into the Waianiwa Stream, which is a tributary of the Oreti River, the mainstem of the Oreti Catchment. A mole and tile network was installed at the site over 30 years ago and the mole network is still highly-connected and in good condition (Chapter 4). The soils are mapped as Argillic-fragic Perch-Gley Pallic Soils (S-Map; Hewitt, 1998), or Aeric Kandiaqualfs (USDA; Soil Survey Staff, 2014), and are characterised by the presence of a low permeability fragipan with an upper boundary between 60 and 90 cm depth. Sampling from previous work (Chapter 5), showed that macroporosity is low in both the topsoil (< 7 %) and subsoil (< 9 %), and that the saturated hydraulic conductivity of the soil profile above the mole network is between ca 10 and 30 mm h^{-1}, while below the mole network it is 2 – 9 mm h^{-1}. A map of topographic wetness index (Figure 7-2) was generated in Chapter 6 to describe the tendency of different parts of landscape to accumulate water, and is used in this chapter to compare the TWI-defined spatial variability in moisture content with actual observed patterns.

7.3.2 Precpitation, soil moisture and tile flow monitoring

Precipitation was monitored hourly and tile drain flow was monitored at 15-min intervals. These components are described in detail in Chapter 6, section 6.3.3. Hourly volumetric soil moisture content (θ_v) was monitored at the interfluves (IN1 and IN2), head slope (HS), planar side slope (pSS), divergent side slope (dSS), nose slope (NS) and lower hollow (lHO), as described in Chapter 6, section 6.3.3). Five depths were monitored at two profiles per site; however, because the lHO only had sensors at 15 and 45 cm, only these two depths were considered for analysis in this chapter. Profile-integrated θ_v (mm) and soil moisture deficit (SMD; mm; Equation 6-3, Chapter 6) were calculated to 100 cm for each site by taking the mean across the two profiles for each depth and summing the two depths. The perched water table (PWT) was monitored hourly in five shallow monitoring wells, as described in Chapter 6, section 6.3.5. These were located adjacent to soil moisture monitoring stations at IN1, HS, dSS, the mid-hollow (mHO) and lHO. Due to sensor malfunction, no PWT data was available for site dSS from May 2021 onward.

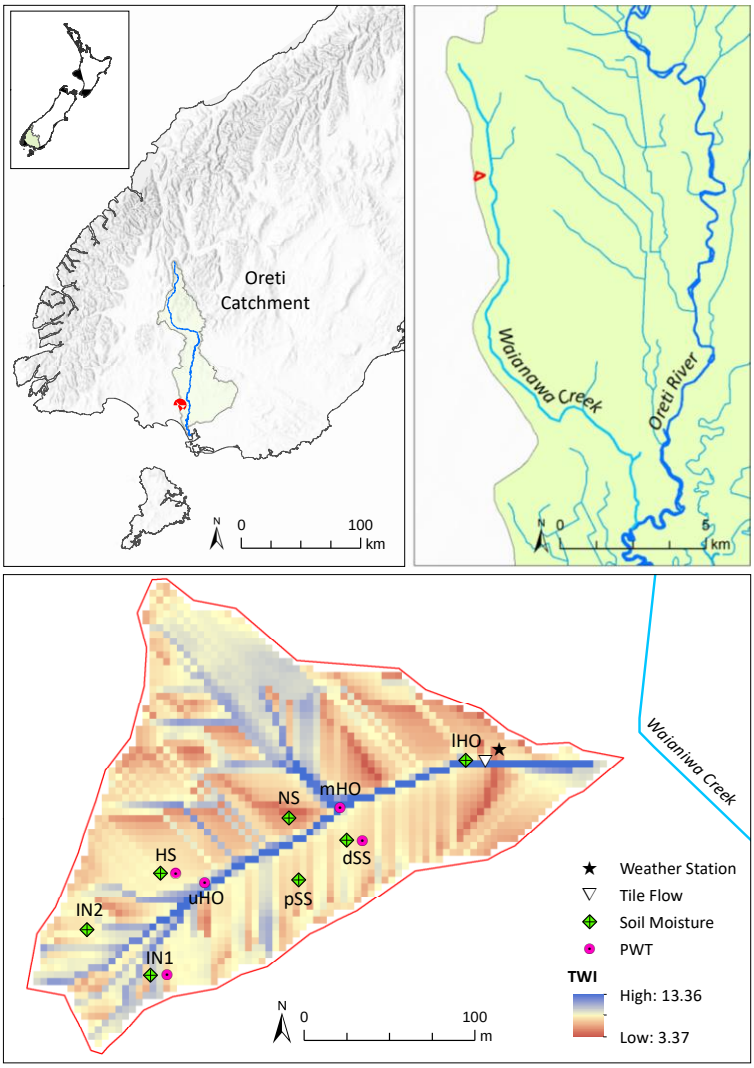

Figure 7-2. Study site location within the Oreti Catchment, Southland, New Zealand (top) and topographic wetness index (TWI) and instrumentation map of the monitored drainage basin (bottom). Monitoring sites were located on the interfluves (IN1 and IN2), head slope (HS), planar side slope (pSS), divergent side slope (dSS) and nose slope (NS). Three sites were located in the hollow running up the main axis of the basin from the Waianiwa Stream to the east: the upper hollow (uHO), mid-hollow (mHO) and the lower hollow (lHO).

7.3.3 Calculation of downslope travel distance (DTD)

The potential distance that a water parcel can travel laterally downslope via saturated matrix flow (i.e., interflow), before percolating into the underlying impeding layer is termed the downslope travel distance (DTD; Jackson et al., 2014; Klaus & Jackson, 2018). Estimating the DTD is important for understanding the role of interflow in catchment hydrological connectivity (Figure 7-3). In this mole and tile-drained study catchment, it is assumed that saturated lateral flow through the highly connected and dense artificial macropore network (i.e., the mole channels) dominates any interflow pathways in the soil layer above the mole network (i.e., 0 – 45 cm).

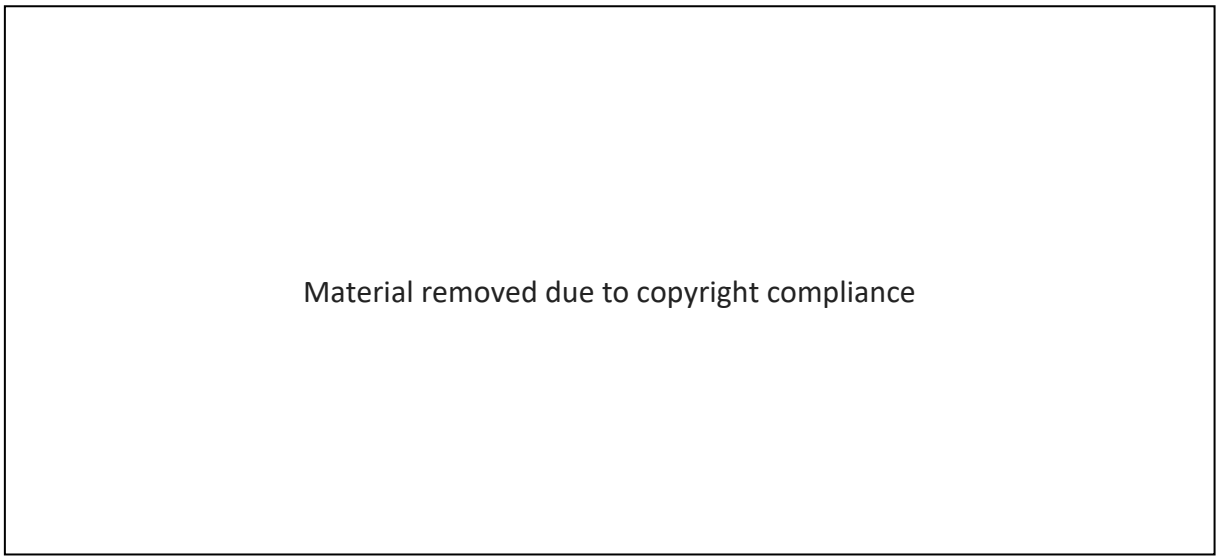

Figure 7-3. Soil characteristics (described in text) used to calculate downslope travel distance (DTD) for saturated lateral flow with percolation (deep drainage) in a hillslope above an impeding layer not connected to an underlaying groundwater body. Modified from Jackson et al. (2014) and Klaus and Jackson (2018).

However, there could still be an important contribution of throughflow occurring below the mole network and above the fragipan. Therefore, two values of DTD were estimated:

(1) DTD for the saturated lens occurring between the fragipan surface and the mole channel network,

(2) DTD of a fully saturated profile, assuming no influence of the drainage network.

The latter provides an indication of the natural throughflow contribution to hydrological connectivity prior to installation of the drainage network and assumes that K_{sat} has not been modified by the presence of drainage. This assumption was supported by the results of Chapter 5, which found no influence due to mole channel proximity on soil hydraulic and physical properties.

The DTD is estimated as the product of the normal thickness of the saturated lens above the impeding horizon (i.e., the fragipan) and the ratios of the soil conductivity and hydraulic gradients, following:

$$\text{DTD (m)} = \frac{K_{upper}}{K_{lower}} \cdot \frac{l_h}{l_n} \cdot N \qquad \text{Equation 7-1}$$

where, K_{upper} is the hydraulic conductivity of the upper soil (mm h^{-1}), K_{lower} is the hydraulic conductivity of the lower (i.e., impeding [fragipan]) soil (mm h^{-1}), l_h is the slope parallel hydraulic

gradient, l_n is the normal hydraulic gradient, and N is the normal thickness (m) of the perched saturated zone. The hydraulic gradient (l_h/l_n) is calculated as:

$$\frac{l_h}{l_n} = \frac{\sin\theta}{[(N + C_n)/C_n]} \qquad \text{Equation 7-2}$$

where, θ is the hillslope angle (˚) and C_n is the normal thickness (m) of the lower, impeding horizon.

The DTD was estimated for seven sites: IN1, IN2, HS, pSS, dSS, NS and lHO. The hillslope angle (θ) at each site was interpolated from the elevation point cloud used to generate the DEM, described in Chapter 3, section 3.3.1. The normal thickness of the lower, impeding horizon (C_n) was calculated as the total normal thickness of loess between the surface of the fragipan and the surface of the underlying gravels (i.e., including all of the intervening loess sheets) measured from auger stratigraphy analysis in Chapter 3 (Table 3-2). An important assumption of the DTD calculation is that the lower impeding layer (i.e., C_n) is saturated, and drains to a layer with zero hydraulic head. It is unlikely that the full loess column that forms the impeding layer is saturated when perching occurs above the fragipan, as the soil does not exhibit morphological indicators of such long periods of saturation. By assuming that the entire loess is saturated, C_n is a maximum, the vertical hydraulic gradient is a minimum and the calculated downslope distance is, therefore, a maximum (i.e., longest possible) DTD. Collection of saturated hydraulic conductivity (K_{sat}) data was described in Chapter 3, section 3.3.4. K_{lower} was the mean K_{sat} calculated from cores taken from within the fragipan at each site.

To estimate (1) DTD for the saturated lens occurring between the fragipan surface and the mole channel network, K_{upper} was taken as the mean saturated hydraulic conductivity (K_{sat}) of the soil measured from soil cores at depths of 45 and 60 cm below the surface. Site NS was excluded from this estimate of DTD, as the mole network here had been installed within the impeding layer and appeared to have partially collapsed (see Chapter 4, section 4.4.2). The normal thickness of the perched saturated zone (N) was the normal depth between the mole network (i.e., 45 cm) and the local surface of the fragipan.

To estimate (2) DTD of a fully saturated, "undrained" profile, K_{upper} was calculated as the mean saturated hydraulic conductivity (K_{sat}) of the soil as measured from soil cores at depths of 15, 30, 45 and 60 cm below the surface. At NS, K_{upper} was calculated from only the 15 and 30 cm, as the deeper cores were in the shallow fragipan. The normal thickness of the perched saturated zone (N)

was estimated as the normal depth between the soil surface and the local surface of the fragipan, such that $N = D_n$ and $D_n = D \cos \theta$.

7.3.4 Data analysis

Distribution statistics were calculated for the soil moisture content (θ_v) at each site and for each of summer, autumn, winter and spring. Spearman's correlation coefficient was used to test the strength of the monotonic relationship between TWI and soil moisture content for each season. The non-parametric Kruskal-Wallis test with Dunn's multiple comparison post-hoc test with a 99% confidence level ($p < 0.01$; using the Bonferroni correction) were used to test for statistically significant differences in median seasonal soil moisture content between each of the sites.

Qualitative analysis of the relationship between precipitation, tile flow and the perched water table (PWT) at each site aimed to provide insight into the spatial and temporal controls on catchment hydrological connectivity. Data was assessed for the entire monitoring period, but also more closely over a 17 day period for each of summer (2nd – 19th February 2019), autumn (9th – 26th May 2019), winter (11th – 28th July 2019) and spring (8th – 25th September 2019). These dates were chosen as they showed typical responses to precipitation in their respective season. The term precipitation 'event' is avoided here, as it is used throughout this thesis in a specific context, the definition of which is provided in Chapter 6. In the seasonal analysis of soil moisture and tile flow dynamics, the term 'period of rainfall' is used to indicate the precipitation under discussion.

7.4 Results

7.4.1 Soil moisture dynamics

Volumetric soil moisture (θ_v; mm) was either not correlated or weakly correlated with topographic wetness index (TWI; Figure 7-4a), for each of the four seasons (i.e., summer rho = 0.07; autumn rho = -0.04, winter rho = 0; spring rho = 0.25). The NS and dSS both had the lowest index values for topographic wetness, yet in summer and autumn these two sites had contrasting soil moisture contents, with NS being the wettest, and dSS being the driest parts of the catchment. Conversely, the lHO had the highest TWI, but in winter and spring was one of the driest parts of the landscape.

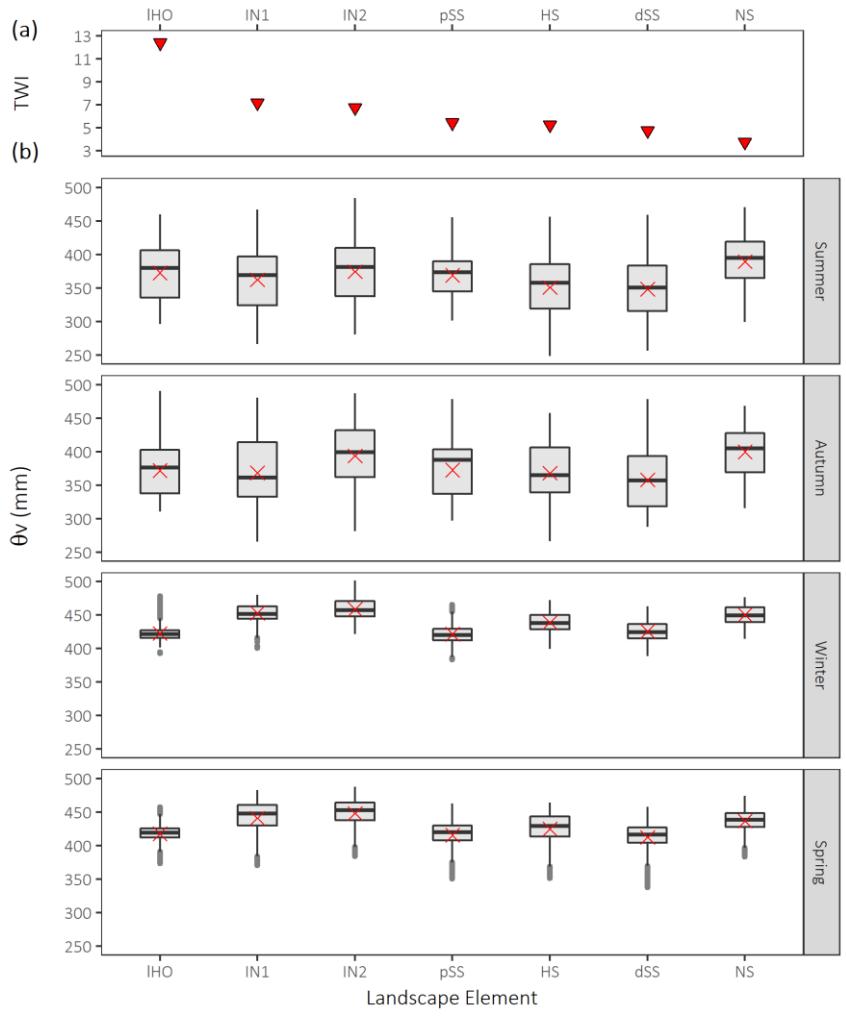

Figure 7-4. Plots of (a) the topographic wetness index (TWI) and (b) the associated seasonal distributions of soil moisture content (θ_v; mm) at each of the landscape elements, including the lower hollow (lHO); interfluves (IN1 and IN2), planar side slope (pSS); head slope (HS); divergent side slope (dSS) and nose slope (NS). Boxplot features include the median (black line), mean (red cross) and outliers (black points).

Distributions of soil moisture content were similar within seasons across sites (Figure 7-4b). The range in θ_v was larger at all sites in summer and autumn relative to winter and spring (Figure 7-4b and Table 7-1). When the catchment was treated as a whole mean θ_v varied seasonally by ca 70 mm, while the intra-seasonal variation was consistent (i.e., summer = 367 ± 14 mm; autumn = 376 ± 15 mm; winter = 439 ±16 mm; 428 ± 14 mm). In summer and autumn, the sites with the highest median θ_v were NS and IN2, which were significantly different from each other and all other sites ($p < 0.01$; Kruskal-Wallis and Dunn's Pairwise tests; Figure 7-5). The site with the lowest median θ_v was dSS, which was significantly drier than all other sites in summer, autumn and winter. In winter and spring, the sites with the highest median θ_v were IN2, IN1, NS and HS, which were significantly different from each other and all other sites. In winter, pSS and lHO, although not significantly different from each other, were significantly drier than all other sites.

Soil moisture at 15 cm (i.e., the topsoil) was generally highest at the upslope sites across the monitored time period (November 2018 to December 2021), and lowest in the hollow and side

Table 7-1. Seasonal descriptive statistics for soil moisture content (mm) at each of the monitored sites.

	lHO	IN1	IN2	pSS	HS	dSS	NS
Summer							
Mean	372.8	362.6	374.8	369.3	351.3	348.9	389.9
Std. Error	0.50	0.60	0.58	0.36	0.57	0.54	0.46
Std. Deviation	40.3	48.2	46.9	29.3	46.1	43.4	37.0
Median	380.4	369.3	381.5	373.9	358.2	351.0	395.2
IQR	71.0	72.5	72.6	44.8	66.4	68.1	54.1
Autumn							
Mean	371.8	368.2	393.8	372.7	368.0	358.0	399.8
Std. Error	0.42	0.66	0.61	0.50	0.55	0.52	0.45
Std. Deviation	34.5	53.8	49.7	40.9	45.0	42.5	37.0
Median	376.5	361.5	399.1	387.6	364.5	357.0	404.9
IQR	64.8	81.5	70.0	66.5	67.5	74.9	58.6
Winter							
Mean	422.6	453.1	458.8	421.5	439.2	425.9	450.5
Std. Error	0.14	0.17	0.19	0.16	0.17	0.20	0.16
Std. Deviation	11.1	14.1	15.3	13.4	14.1	16.3	13.2
Median	421.4	452.0	457.4	420.6	438.0	424.4	449.3
IQR	11.8	19.0	22.7	17.2	21.0	22.1	21.7
Spring							
Mean	418.0	440.9	448.1	415.6	425.1	412.6	436.8
Std. Error	0.18	0.32	0.30	0.26	0.31	0.28	0.22
Std. Deviation	14.3	26.0	24.1	21.2	25.0	22.8	17.9
Median	419.1	447.6	452.5	419.7	429.0	416.7	438.7
IQR	14.0	30.5	26.6	22.2	30.1	23.0	20.9

Summer:	NS > IN2* > lHO* > pSS > IN1 > HS > dSS
Autumn:	NS > IN2 > pSS¥ > lHO*¥ > HS* > IN1* > dSS
Winter:	IN2 > IN1 > NS > HS > dSS > lHO* > pSS*
Spring:	IN2 > IN1 > NS > HS > pSS* > lHO* > dSS

Figure 7-5. The order of median soil moisture (θ_v) decrease by site for summer, autumn, winter and spring. All sites were statistically different from each other ($p < 0.01$; Kruskal-Wallis and Dunn's Pairwise tests), unless as indicated by the * and ¥ symbols.

slopes (Figure 7-6). At 45 cm (i.e., the subsoil), soil moisture was generally highest at the nose slope, interfluve and hollow, and lowest on the side slopes. With the exception of the topsoil in the summer of 2019 – 2020, the variability in soil moisture across the catchment appeared to be consistent, despite large fluctuations at each site across the seasons. The transition from the dry state (soil moisture deficit [SMD] > ca 7 mm) to the wet state (SMD < ca 7 mm) occurred in autumn, and lasted approximately two weeks in 2019, one week in 2020, and three weeks in 2021 (Figure 7-7).

The temporal response of the perched water table to precipitation varied across the catchment (Figure 7-8). At the interfluves and upper hollow, PWTs were persistent from late autumn until late spring, and were generally maintained at ca 0.5 metres below the surface (mbs), which is the approximate depth of the base of the mole channel network. During this period, and in response to precipitation, the PWT at these sites spiked, often to within 0.2 m of the soil surface, before rapidly receding back to 0.5 mbs once precipitation ceased. At the upper hollow, the peaks in PWT often exceeded the soil surface (this behaviour is described in more detail in section 7.4.2.1). The mid-hollow displayed similar PWT behaviour to the interfluves and upper hollow, with a persistent PWT over winter and spring; however, it was generally maintained at a depth of ca 0.8 mbs, which is the approximate depth of the base of the tile drain. It often rose to within 0.2 m of the soil surface, and occasionally saturated the whole profile. The behaviour at the head slope and divergent side slope was quite different to what was seen at IN1, uHO and mHO, with generally fewer and smaller peaks, and the PWT was not maintained at the mole network over winter, but dissipated relatively quickly. Spikes in PWT at all parts of the landscape tended to align with spikes in soil moisture content and tile flow rate, demonstrating an important relationship between PWT formation, soil moisture and tile drain flow.

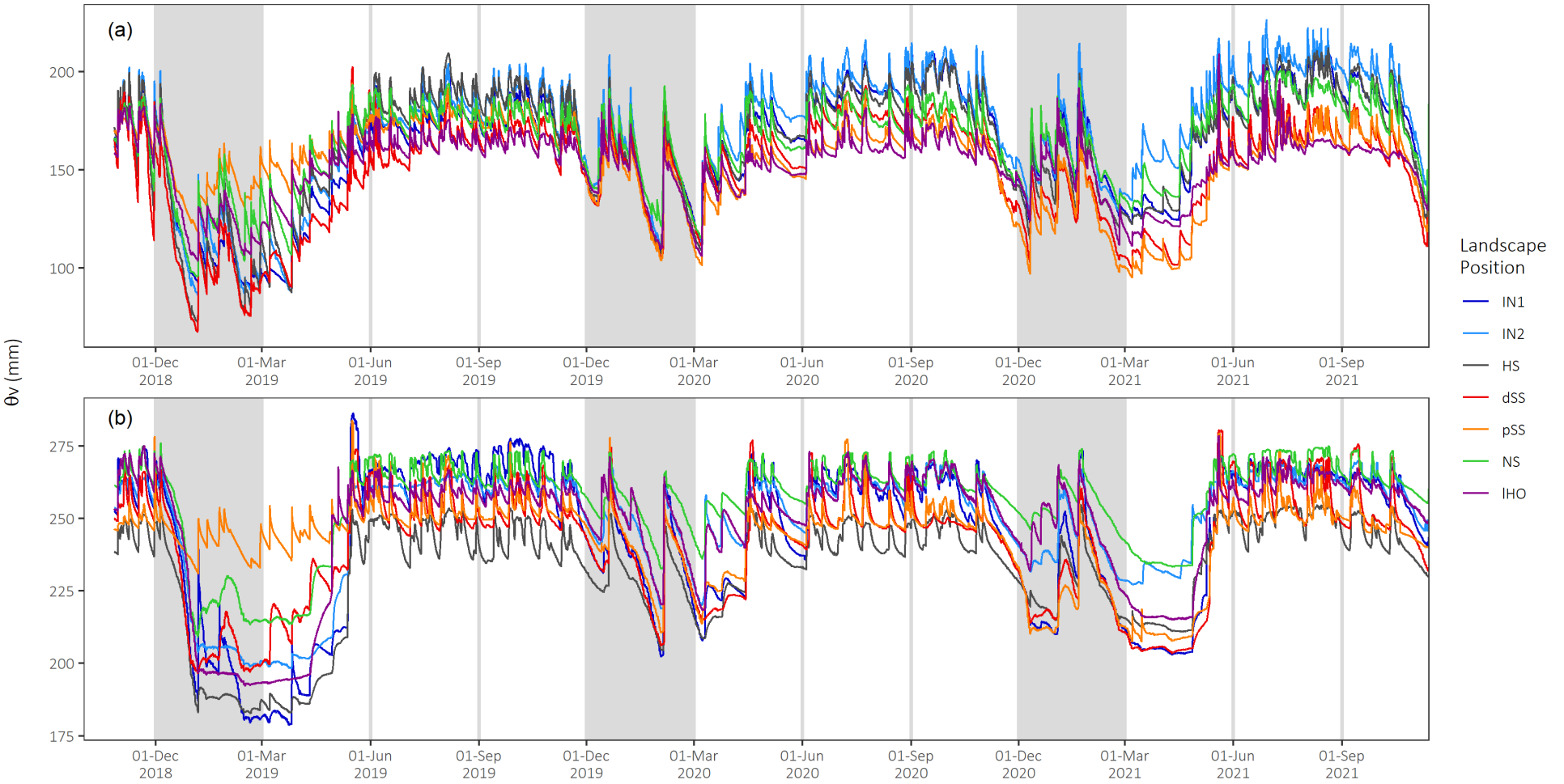

Figure 7-6. Time series of volumetric soil moisture content (θ_v; mm) at (a) 15 cm and (b) 45 cm, measured at each of the different landscape elements, including the interfluves (IN1; dark blue and IN2; light blue), the head slope (HS; grey), the divergent side slope (dSS; red), the planar side slope (pSS; orange), the nose slope (NS; green) and the lower hollow (lHO; magenta). Shaded time periods represent summer; autumn, winter and spring are distinguished by vertical light-grey lines.

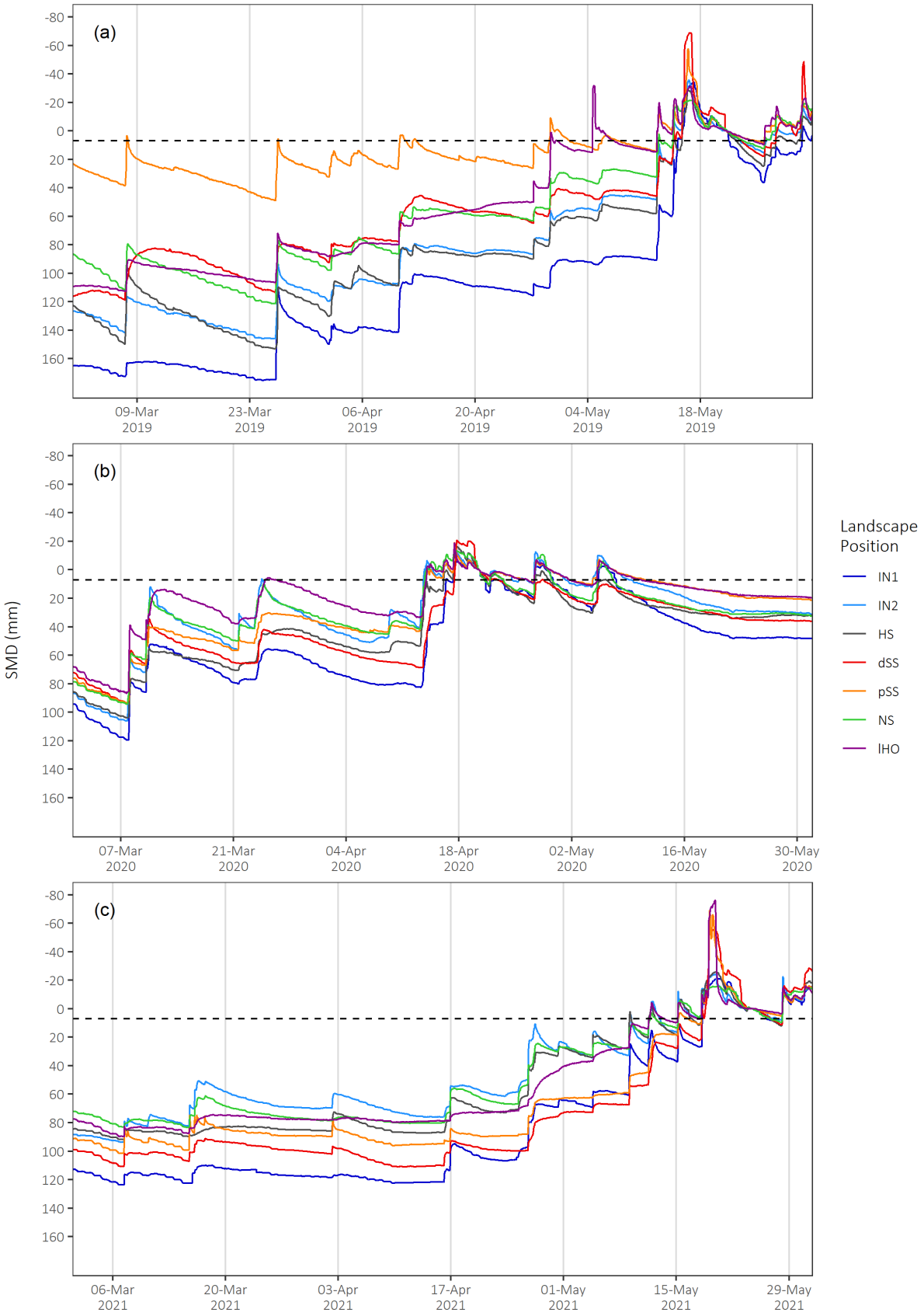

Figure 7-7. The autumn soil moisture transition from wet state to dry state in (a) 2019, (b) 2020 and (c) 2021. The dashed line at a soil moisture deficit (SMD) of 7 mm represents the approximate boundary between the two states (Chapter 6). Monitored landscape positions include the interfluves (IN1; dark blue and IN2; light blue), the head slope (HS; grey), the divergent side slope (dSS; red), the planar side slope (pSS; orange), the nose slope (NS; green) and the lower hollow (lHO; magenta). Plot grid lines represent two week intervals.

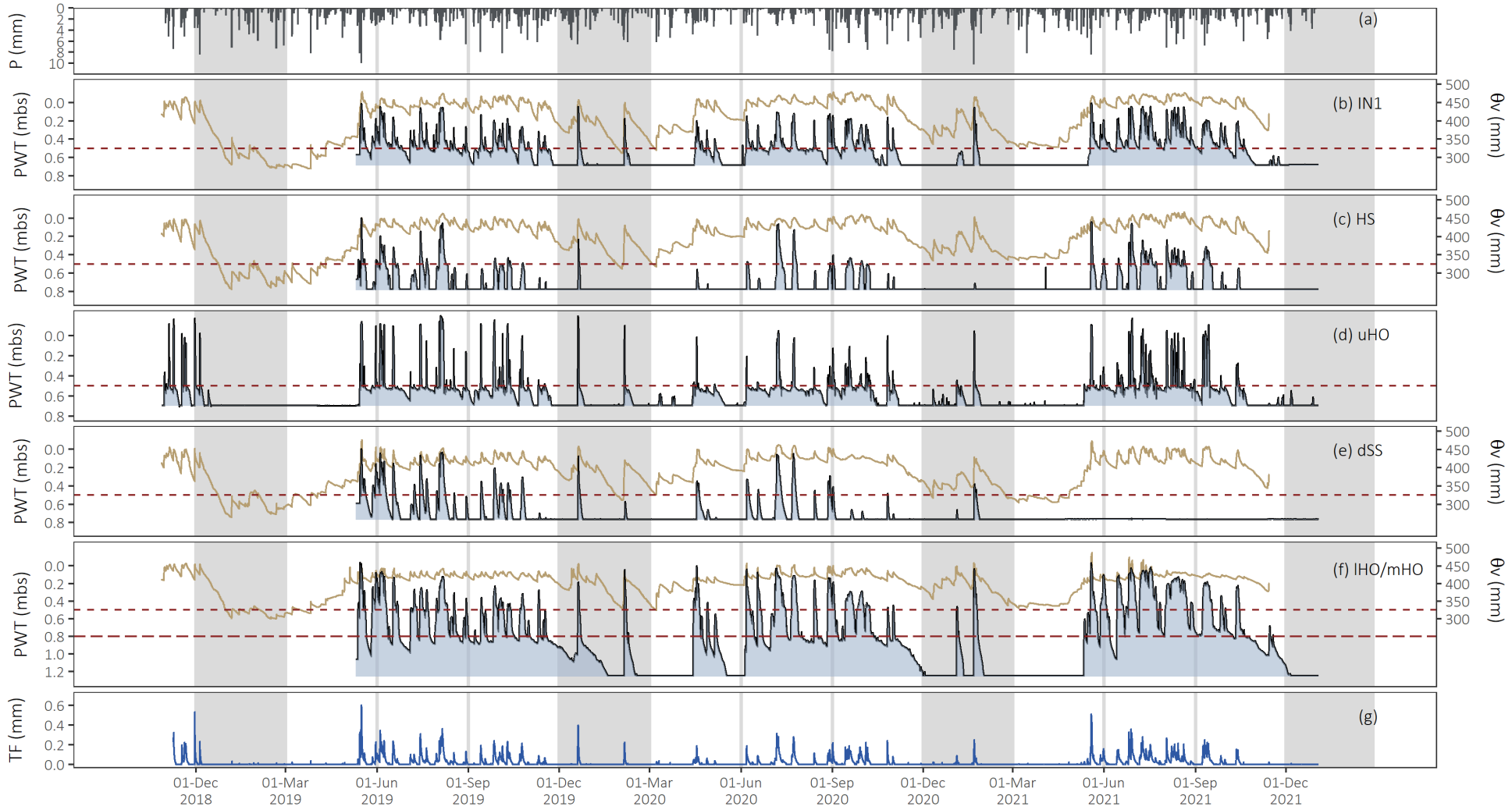

Figure 7-8. Hourly time series plots of (a) precipitation (P; mm) and the response by (b) – (f) profile-integrated volumetric soil moisture content (θ_v; mm; solid brown line) and perched water table height (PWT; mbs; shaded blue area) at the interfluve (IN1), head slope (HS), upper hollow (uHO [PWT only]), divergent side slope (dSS), mid- and lower hollow (mHO [PWT only] and lHO [SMD only]), as well as (g) tile flow rate (TF; mm h^{-1}). The base of the shaded area shows the depth that each monitoring well is installed to. Horizontal short-dashed lines at 0.5 mbs represent the depth of the mole network. The horizontal heavy dashed line at 0.8 mbs represents the depth of the tile drain at mHO. Shaded time periods represent summer; autumn, winter and spring are distinguished by vertical light-grey lines. Note that no PWT data was available at site dSS following autumn 2021.

7.4.2 Spatiotemporal analysis of tile flow-regulating processes

7.4.2.1 Summer

A total of 101 mm precipitation fell between the 2nd and 19th February 2020 (summer), which generated 4.4 mm of tile flow (i.e., runoff ratio = 0.04), but no overland flow (data not shown; Figure 7-9a). On the 4th February, precipitation of intensities up to 6 mm h^{-1} activated tile flow and generated two prominent peaks in TF rate. This precipitation event was the largest event by rainfall volume recorded over the two year monitoring period described in Chapter 6, with a total of 72.8 mm precipitation over 67 hours. All parts of the landscape had large antecedent soil moisture deficits (SMD; i.e., 70 - 120 mm), and the previous episode of saturation had occurred approximately one month prior.

In response to the precipitation on 4th February, tile flow started before the development of PWTs across the landscape and before the SMD was satisfied, but the flow rate was small and did not exceed 0.06 mm h^{-1} (i.e., ca 0.05 mm h^{-1}; peak 1). This tile flow sans moisture-excess must have been triggered by rapid flow between the soil surface and the tile drain (i.e., preferential flow). A second small peak in tile flow (i.e., ca 0.05 mm h^{-1}; peak 2) also occurred while PWTs did not exist. This peak coincided with soil moisture at the lower hollow rising above field capacity (i.e. precipitation exceeded the SMD) suggesting excess moisture in the lower catchment was responsible for this second pulse of tile flow. The low tile flow rate is consistent with a small source area. The lag between tile flow and the development of a PWT varied with landscape element (i.e., ca 15 hours at IN1; 13 hours at uHO; 30 hours at dSS and 15 hours at mHO). Once the SMD was approximately zero, PWTs rose rapidly into the topsoil (i.e., ≤ 0.2 mbs) at the interfluve, upper and mid hollow, but not at the head slope or divergent side slope. Despite the large volume of precipitation, no PWT was generated at the head slope during the 17 day summer period. Tile flow rate peaks (i.e., 0.25 mm h^{-1}; peak 3) aligned with peaks in PWT at uHO and mHO. At the divergent side slope the PWT formed later and slower, and never exceeded the depth of the mole network, and its peak was not aligned with a peak in tile flow rate. Tile flow persisted during periods when the PWTs at uHO and dSS were below the mole network. However, tile flow ceased at the same time that the PWT at the interfluve and mid-hollow receded below the mole network, and also at the same time as the moisture content in the lower hollow dropped back to zero mm SMD; this despite the PWT remaining above the tile drain at the mid-hollow. This suggests there may have been an area of flow attenuation somewhere low in the system, before the catchment outlet.

The behaviour of the PWT at uHO was noteworthy, as the rapid rise in PWT exceeded the soil surface by 0.1 m (i.e., - 0.1 mbs) and produced a peak that aligned precisely with the first peak in tile flow. A PWT height in excess of the soil surface could indicate either saturation-excess overland flow or positive pressure in the monitoring well. A head of 0.1 m above the surface would suggest a substantial volume of overland flow; however, no overland flow was recorded during the period. Furthermore, field observations confirmed that a PWT head of 0.1 m above the soil surface did not necessarily coincide with the presence of overland flow at uHO. We therefore hypothesise that the monitoring well at uHO may have intercepted a mole channel, and that positive pressure in the monitoring well would result once the upslope mole channels were active and connecting the landscape elements to produce a hydraulic head between the surface of the upslope PWTs and the uHO monitoring well. This behaviour was observed across all seasons at this upper hollow site (Figure 7-9a-d; subplots iv).

In summary, antecedent soil moisture deficits were large at all parts of the landscape. Tile flow initially occurred when the catchment was in soil moisture deficit, indicative of natural, surface-vented preferential flow. With increasing precipitation, moisture excess in the hollow began contributing to and regulating tile flow, beginning at the lower hollow and moving towards the upper hollow. Excess upslope soil moisture appeared to be attenuated before reaching the catchment outlet.

7.4.2.2 Autumn

A total of 109 mm precipitation fell between the 9th and 26th of May 2019 (autumn), which generated 23.3 mm of tile flow (i.e., runoff ratio = 0.21), and 4.1 mm of overland flow (data not shown; Figure 7-9b). The antecedent SMD varied with landscape element, and showed a general trend of increasing wetness with more downslope position. Six months had passed since the most recent saturation episode prior to this 17-day autumn period, and during that six month period the soil was predominantly under a large SMD (i.e., between +75 and +100 mm; see Figure 6-4, Chapter 6).

During this time, four main periods of precipitation occurred, each activating tile flow. The first period of rainfall on 12th – 13th May produced 25 mm of precipitation over 32 hours with a maximum intensity of 3.2 mm h^{-1}, and triggered a single, small tile flow peak (i.e., ca 0.06 mm h^{-1}; peak 1). Only the mid-hollow developed perching in response to this precipitation; however, tile flow rate peaked

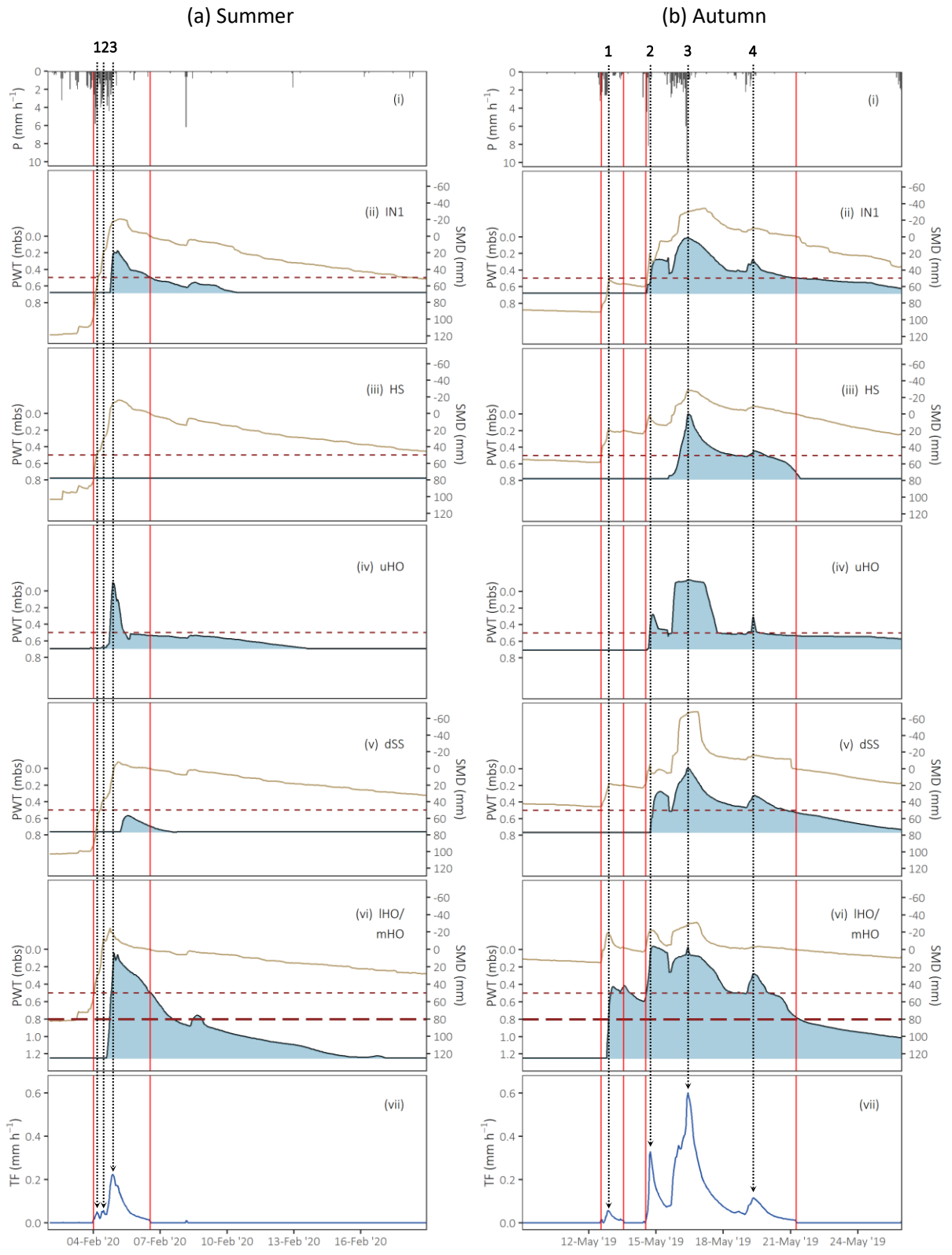

Figure 7-9. Seventeen day period over (a) summer (2nd – 19th February 2019), (b) autumn (9th – 26th May 2019), (c) winter (11th – 28th July 2019) and (d) spring (8th – 25th September 2019). Each plot shows (i) precipitation (P; mm h^{-1}), and the response by landscape element (ii – vi) of soil moisture deficit (SMD; mm; solid brown line) and perched water table height (PWT; mbs; shaded blue area), as well as (vii) tile flow rate (TF; mm h^{-1}). The PWT and SMD were monitored at the interfluve (IN1), head slope (HS), upper hollow (uHO [PWT only]), divergent side slope (dSS), mid- and lower hollow (mHO [PWT only] and lHO [SMD only]). Vertical red lines provide reference for TF start/end times against SMD and PWT at each landscape element. Horizontal dashed lines at 0.5 and 0.8 mbs represent the depth of the mole network and tile drain (where present), respectively. Numbered, downward-pointing arrows that cross the subplots (a-g) of each figure align P, SMD and PWT with TF peaks.

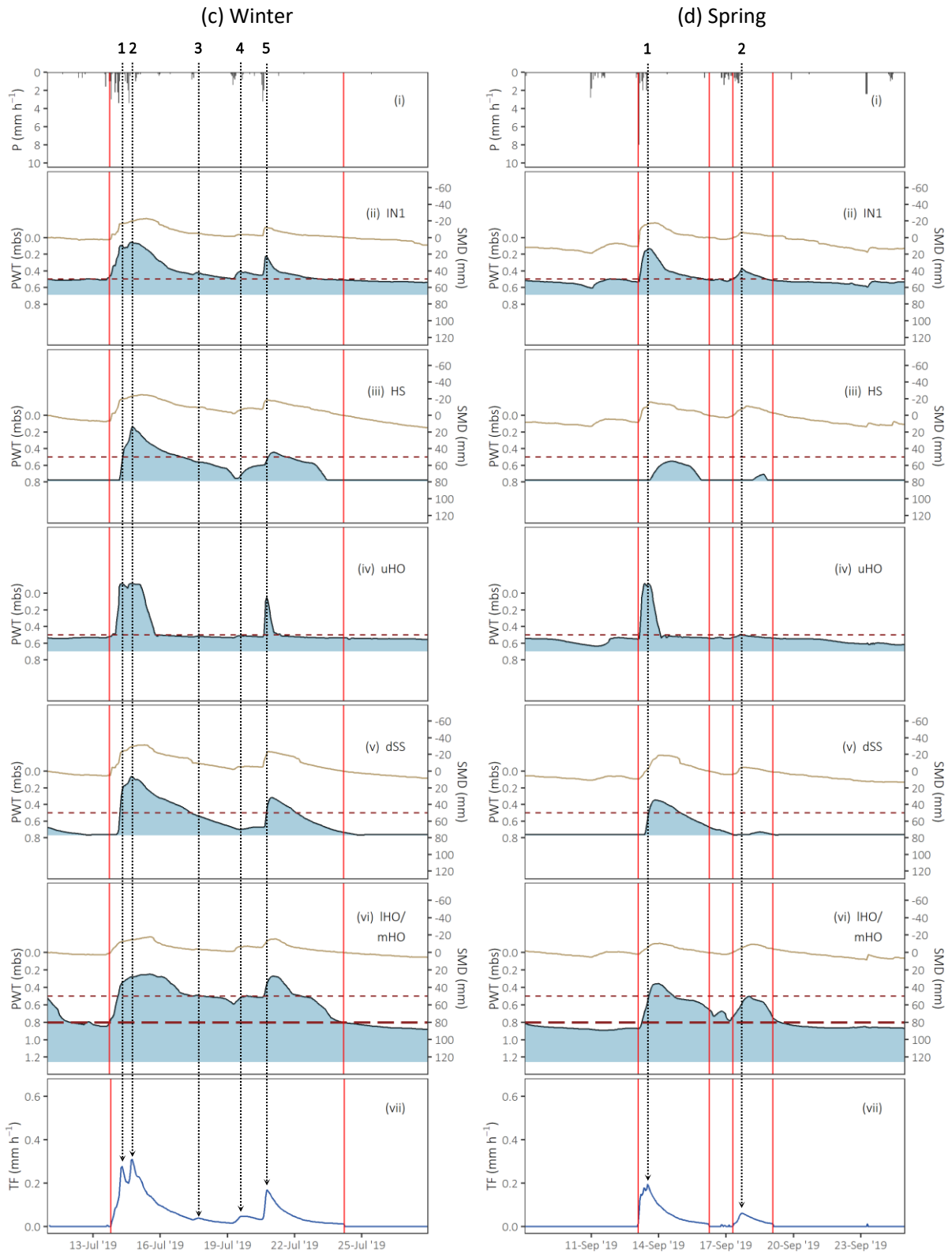

Figure 7-9. continued.

before the PWT peak. The peak in tile flow rate did, however, align with the soil moisture content exceeding field capacity (i.e., SMD = -20 mm) at the lower hollow, similar to observations in summer (Figure 7-9a; subplot vi; peak 2). Unlike in summer, the antecedent SMD at the lower hollow was small (i.e., ca +10 mm compared to ca +80 mm in summer), demonstrating a potential for rapid saturation at this part of the landscape. Tile flow ceased once the excess moisture in the lower hollow was removed (i.e., ca ≥0 mm SMD), and despite the PWT in the mid-hollow being ca 0.4 m above the tile drain at mHO. This behaviour at mHO was also observed during summer (Figure 7-9a; subplot vi), and was speculated to relate to flow attenuation.

The second period of rainfall between the 14th and 15th May produced 21 mm precipitation over 10 hours with a maximum intensity of 8.2 mm h^{-1}, and triggered a single large tile flow peak (i.e., ca 0.35 mm h^{-1}; peak 2), as well as 0.2 mm of overland flow (data not shown). Perched water tables formed rapidly in response to this precipitation; at IN1, uHO and dSS the PWTs rose above the mole network to the base of the topsoil (ca 0.3 mbs), and at mHO the PWT rose to the soil surface. The tile flow peak aligned most closely with PWT peaks at the mid- and upper hollow, but no synchronous PWT peaks occurred at IN1 or dSS, suggesting that landscape soil moisture controls on tile flow had extended up the hollow since the first period of rainfall, but had not extended to the slopes or interfluves.

The PWT behaviour at IN1, dSS and mHO was unusual during this second autumn period of rainfall, as it persisted at a fairly uniform height (i.e., ca 0.25 mbs at IN1 and dSS, and the soil surface at mHO), despite the rapid drop in tile flow rate. This behaviour suggests that the mole network was not functioning to remove excess water from these parts of the landscape, despite being submerged beneath a PWT. Furthermore, once the PWT did begin to recede at these sites, the recession was rapid, and indicative of a lock being released. It was unclear what caused this behaviour, but it did indicate that the PWTs at these parts of the landscape were not primary regulators of tile flow rate during this second autumn period of rainfall.

Perched water tables (at all sites except uHO) and tile flow were present at the onset of the third period of rainfall, which occurred between the 15th and 17th of May, and produced 46 mm precipitation over 35 hours with a maximum intensity of 10 mm h^{-1}. In response to this precipitation, PWTs rose to the soil surface at all sites across the landscape and 4 mm of overland flow was generated (data not shown). The very large tile flow peak (i.e., ca 0.6 mm h^{-1}; peak 3) was one of only three events between November 2018 and January 2022 to exceed 0.4 mm h^{-1} and it

aligned with peaks in PWT at all of the monitored sites. The alignment indicates that flow was being contributed by all parts of the landscape during this period of large rainfall; however, the relative magnitude of the PWT peaks at dSS and HS, suggest that these parts of the landscape were the major drivers of tile flow rate once the catchment was fully saturated.

The tile drain was flowing at the onset of the fourth period of autumn rainfall (18th – 19th May), and perched water tables at least as high at the mole network were present at all landscape positions. This event produced 7.6 mm of precipitation over 15 hours with a maximum intensity of 2.2 mm h^{-1}, and triggered a small peak in tile flow (i.e., ca 0.1 mm h^{-1}; peak 4). The PWT rose above the mole network at all sites in response to this period of rainfall, and the peak tile flow rate aligned with PWT peaks at all landscape elements, suggesting that tile flow was being sourced from all parts of the basin at this point. Tile flow continued after the PWT at HS, uHO and mHO receded to below the mole network. The deactivation of tile flow was aligned closely with the moment that the PWT dropped below the mole network at IN1 and dSS, as well as the moment the PWT dropped below the tile drain at mHO, indicating control by these parts of the landscape on late-stage flows. This was different to the behaviour following the first period of autumn rainfall (as well as the end of the period of summer rainfall; Figure 7-9a, subplot vi), when tile flow ceased despite the presence of a PWT above the tile drain at mHO, and suggested that the attenuation processes observed in the dry state were inactive in the wet state.

The recession curve of the head slope hydrograph following the third and fourth periods of autumn rainfall was noteworthy (Figure 7-9b, subplot iii). Following a peak height at the soil surface, the PWT followed a negative exponential recession that appeared to have its asymptote at approximately the depth of the mole network. However, once the PWT dropped below the mole network, the rate of recession increased dramatically, rapidly dissipating the PWT. This switch to increased recession rate was closely aligned with the time period in which the PWT at IN1 dropped to below the mole network. Similar behaviour was observed at the mid-hollow, where PWT recession appeared to pause for extended periods at around the height of the mole network following rainfall periods three and four, before falling rapidly to the tile drain depth and then slowing again. This behaviour was observed every time PWTs were generated at these sites (Figure 7-8, subplots c & f).

In summary, antecedent soil moisture deficit was spatially variable, but generally higher with more downslope position. Tile flow was initially activated by excess moisture in the lower hollow,

and upslope excess moisture was attenuated before reaching the catchment outlet. With increasing precipitation inputs, excess moisture at the mid-, and then upper hollow began contributing to, and regulating, tile flow, but upslope excess moisture continued to be attenuated before reaching the catchment outlet. Upon complete saturation of the catchment, all areas of the landscape were contributing to tile flow, with the side slopes the major drivers of flow rate.

7.4.2.3 Winter

A total of 45.4 mm precipitation fell between the 11th and 28th July 2019 (winter), which generated 18.2 mm of tile flow (i.e., runoff ratio = 0.40), and 1.8 mm of overland flow (data not shown; Figure 7-97c). Several small rainfall periods of intensities no greater than 4 mm h^{-1} activated tile flow and generated several peaks in flow rate (i.e., peaks 1 – 5). The SMD remained close to zero at all parts of the landscape throughout the 17-day winter period, but rapidly moved into moisture-excess (SMD ≤ 0 mm) with precipitation inputs.

Across the full 17-day winter period, PWTs were always present at IN1, uHO and mHO and persisted between periods of precipitation. At IN1 and uHO, the PWTs were constrained by the mole network between periods of precipitation (i.e., persisting at ca 0.5 mbs), while at mHO, the PWT was constrained by the tile drain (i.e., persisting at ca 0.8 mbs). No PWTs were present at the HS or dSS at the onset of the first winter precipitation. In response to the first period of rainfall, tile flow activated once the PWT rose above the mole network at IN1 and above the tile drain at mHO, suggesting control from the upper and lower parts of the catchment on early winter flows. The first period of rainfall generated two peaks in tile flow, the first of which (i.e., 0.28 mm h^{-1}; peak 1) aligned with PWT peaks at the uHO and IN1 and the second of which (i.e., 0.3 mm h^{-1}; peak 2) aligned with PWT peaks close to the soil surface at all sites except the mid-hollow. This pattern suggests a transition with increasing wetness whereby the contributing area extended to almost all parts of the catchment, with the apparent exception of the mid-hollow. Following this initial period of rainfall, perched water tables receded at all sites, but remained above the mole network at IN1, and tile flow rate also dropped, but did not cease. Two very small rainfall periods then triggered small peaks in PWT at IN1 (but not at any other part of the landscape), and these peaks appeared to increase interfluve contributions to tile flow, as they aligned with two peaks in flow rate (i.e., 0.04 mm h^{-1}; peak 3 & 0.05 mm h^{-1}; peak 4). The final, slightly larger period of rainfall generated a larger peak in tile flow (i.e., 0.20 mm h^{-1}; peak 5) that aligned with PWT peaks at IN1 and uHO. The PWT at other parts of the landscape (i.e., HS, dSS and mHO) also rose above the

mole network in response to this period of rainfall but their peaks occurred several hours after the peak tile flow rate (e.g., 6 hours at HS and dSS). Tile flow ceased when the PWT dropped below the mole network at IN1 and, unlike summer and autumn, at the same time the PWT dropped below the tile drain at mHO. This indicated that the suspected upslope flow attenuation was no longer active.

In summary, the antecedent soil moisture deficit was close to zero at all parts of the landscape, and PWTs were present on the interfluves and in the hollow. Excess moisture in the upper hollow and interfluves was no longer attenuated and early tile flow/ small flow rates were primarily regulated by soil moisture excess on the interfluves. Excess moisture on the slopes continued to be attenuated until the whole basin became saturated, at which point the area contributing to tile flow extended to all parts of the catchment. The PWT at the mid-hollow, however, did not significantly regulate flow rate at any stage during the wet state.

7.4.2.4 Spring

A total of 52 mm precipitation fell between the 8th and 25th September 2019 (spring), which generated 6.7 mm of tile flow (i.e., runoff ratio = 0.13), and 1.5 mm of overland flow (data not shown; Figure 7-9d). Three small rainfall periods occurred during this period, two of which activated tile flow. The hydrological response to rainfall was very similar to that observed in winter.

A period of small rainfall on the 11th of September triggered rises in PWT height at IN1 and uHO but the PWT did not exceed the height of the mole network and no tile flow was initiated. The second period of rainfall (13th September) produced two consecutive hours of precipitation intensities of 5 – 8 mm h^{-1}. This immediately triggered PWT responses at IN1, uHO and mHO. Tile flow activated once the PWT intercepted the mole network at IN1 and uHO and the tile flow peak (i.e., ca 0.2 mm h^{-1}; peak 1) aligned with PWT peaks at these sites. Delayed PWTs formed at HS and dSS; however, similar to in winter, their peaks occurred several hours after peak tile flow rate. Tile flow ceased once the PWT fell below the mole network on the interfluve. The third period of rainfall on 17 September was smaller in intensity and produced a similar response.

In summary, the hydrological response mimicked that of winter. When the basin was not completely saturated, the excess moisture on the slopes appeared to be attenuated before reaching the catchment outlet. Excess moisture in the upper hollow and interfluves was not attenuated, and tile flow was primarily regulated by soil moisture excess on the interfluves.

7.4.3 Downslope travel distance calculations

At all of the landscape elements, the estimates of perched interflow downslope travel distances (DTD, m) were very small (i.e., less than 2 m) for both considered scenarios; (1) the saturated lens occurring between the fragipan surface and the mole channel network (Table 7-2a), and (2) a fully saturated profile, assuming no influence of the drainage network (Table 7-2b).

The DTD was always greater for scenario (2) than scenario (1). For both scenarios, the DTD was shortest at IN1 and HS and longest at pSS. For scenario (1), DTD ranged from just 0.02 m to 0.72 m, while for scenario (2), the DTD ranged from 0.09 m to 1.90 m.

Table 7-2. Perched interflow downslope travel distances (DTD, m) for the interfluve 1 (IN1); interfluve 2 (IN2); head slope (HS); planar side slope (pSS); divergent side slope (dSS) and nose slope (NS). DTD was calculated from the mean saturated hydraulic conductivity of the fragipan (K_{lower}), and the soil above the fragipan (K_{upper}), as well as the hillslope angle (°), the normal thickness of the saturated zone (N, m) and the normal thickness of the lower, impeding horizon (Cn, m).

Profile depth scenario		IN1	IN2	HS	pSS	dSS	NS
	θ (°)	2.0	2.5	3.7	4.0	6.0	5.4
	C_n (m)	2.69	3.67	1.90	1.93	0.53	0.43
	K_{lower}	3.24	2.26	5.64	0.50	0.56	0.42
(a) Below Mole Network							
	N (m)	0.15	0.15	0.20	0.20	0.35	-
	K_{upper}	14.5	20.3	11.1	28.4	9.23	-
	DTD (m)	**0.02**	**0.06**	**0.02**	**0.72**	**0.36**	**-**
(b) Full profile							
	N (m)	0.60	0.60	0.65	0.65	0.80	0.40
	K_{upper}	17.9	26	19.6	28.1	10.5	12.9
	DTD (m)	**0.09**	**0.26**	**0.11**	**1.90**	**0.62**	**0.59**

7.5 Discussion

7.5.1 Spatiotemporal variation in soil moisture

Spatial soil moisture patterns were seasonally variable. Perched water tables and the drainage network both appeared to contribute towards these spatial distributions. The variation in profile-averaged soil moisture across the catchment was similar for all seasons (i.e., ± 15 mm), which contrasted with findings from other studies that showed negative correlations between spatial variability and the mean soil moisture (Brocca et al., 2007; Hupet & Vanclooster, 2002; Tromp-van Meerveld & McDonnell, 2006a; Zhu et al., 2014). This suggests that in present study, either the wet state is more variable, or the dry state is less variable relative to the former studies. There is no obvious explanation for the similarity in spatial soil moisture variability between seasons. It is possible that, in the dry state, the tile drain acts to reduce variability by reducing moisture extremes in the highly topographically convergent hollow (relative to in an undrained basin); while in the wet state, it may be the case that the mole channel network acts to increase spatial soil moisture variability relative to an undrained basin, as a result of spatially variable behaviour.

Previous work at this field site showed that the catchment exhibited two, flow path-regulating states for soil moisture: wet (summer and autumn) and dry (winter and spring; Chapter 6). This study showed that when the catchment was in the dry state, the shallowest soils (i.e., the nose slope; fragipan surface at 40 cm) were the wettest part of the catchment, while the deepest soils (i.e., divergent side slope; fragipan surface 80 cm) were the driest part of the catchment. The remaining sites had soils with similar depths (60 – 70 cm), but showed a relatively large range in mean soil moisture, indicating that other, additional factors were regulating moisture distribution. These results contrasted with those of Tromp-van Meerveld and McDonnell (2006a), who demonstrated that soil moisture on shallower soils was lower than deep soils in the dry state, attributed to a smaller total volume of water that could be removed earlier by evapotranspiration than the larger volumes of deeper soils. It is possible that high dry state moisture in the shallow nose slope was reflecting a dominating influence by the fragipan, which presents a barrier to root penetration (Schoeneberger et al., 2012), such that losses via root uptake and transpiration are likely to be restricted. The nose slope fragipan had its surface at 40 cm, so the subsoil moisture sensor was 5 cm below the fragipan surface, and soil profile descriptions from Chapter 3 (Appendix A.2) clearly demonstrated low counts of fine roots in the fragipan across the catchment. In winter and spring, soil moisture increased at all parts of the catchment, and the interfluves became the wettest part of

the catchment, followed by the shallow soils at the nose slope. It is well established that conditions where the groundwater is near the surface maintain higher soil moisture content as a result of capillary rise from the water table (Chen & Hu, 2004; McMillan & Srinivasan, 2015; Soylu et al., 2011). The capillary fringe above perched water tables (PWT) at the interfluve from late autumn to late spring may therefore have dominated the effect of soil depth on soil moisture, explaining why the interfluve became wetter than the nose slope. Despite being a highly divergent part of the landscape, the nose slope was also one of the wettest parts of the catchment in the wet state, which may be explained by the fact that mole channels located at the nose slope were severely degraded (Chapter 4), and therefore unlikely to be rapidly removing excess water. Excess water at all other sites was being drained by highly connected and functional mole network.

The topographic wetness index (TWI) was, on its own, a poor predictor of spatial soil moisture variability at any time across the year, and the weakest TWI- θ_v relationships were observed in winter (rho = 0). This contrasted to results by (Chaplot & Walter, 2003), who found soil wetness to be significantly correlated to TWI in an undrained catchment with poorly-permeable (< 5 mm d^{-1}) sub-horizons, with the strongest correlations in the wet seasons. Western et al. (1999) also found TWI to be a strong univariate predictor of soil moisture distribution in the wet state for hillslope soils formed in siltstone bedrock (Western & Grayson, 1998). Similarly, in podzols formed in till, Nyberg (1996) showed that the large variability in catchment soil moisture was well described by TWI. However, studies on sandy loam soils formed in granodiorite bedrock under a humid climate (Tromp-van Meerveld & McDonnell, 2006a), and on soils formed in a combination of basalt and sandstone under a Mediterranean climate (Robinson et al., 2012) did not identify topographic variables, including TWI, as useful predictors for soil moisture in either the dry or wet moisture state. One of the characteristics of the wet state in an undrained basin, as described by Grayson et al. (1997), is that drainage lines, and other areas of high topographic convergence remain at persistently larger soil moisture contents than other parts of the catchment. At our study site, the lower hollow had the highest TWI, yet, along with the planar side slope, was the driest part of the catchment in winter, and second driest part of the landscape, behind the divergent side slope, in spring. These results are suggestive of an influence due to the mole and tile network on soil moisture spatial variability in the wet state especially, expressed most significantly in the tile-drained hollow where the drain appears to reduce soil moisture. Williams et al. (2019) also showed that the bottom of landscape depressions, previously the wettest area, after tile drain installation became the driest area.

7.5.2 Mole and tile network regulation of PWTs

Tile flow rate demonstrated clear, but variable responses to PWTs in all seasons, with relationships a function of landscape position and PWT magnitude above the mole network. Water perched for substantial periods of time, especially in upslope flat (i.e., the interfluves) and topographically convergent (i.e., the drainage hollow) areas from late autumn to late spring. This behaviour indicates a low subsoil permeability, which was previously demonstrated by estimates of DD rates (0.4 mm h^{-1}) in Chapter 6. It also indicates that the soil core measurements of fragipan saturated hydraulic conductivity (K_{sat}; 3 mm h^{-1}, Chapter 5) are over-estimates, as such high permeability should be too high to result in substantial periodic saturation under most climatic conditions in New Zealand (Vogeler et al., 2019). Where the PWTs persisted, their magnitude appeared to be constrained by the mole network or, where present, the tile drain, such that exceedances of the drainage network were rapidly returned to their antecedent position once precipitation inputs ceased. This was similar to observations of a mole drained heavy clay soil by Goss et al. (1983), in which the antecedent PWT had its surface at ca 0.5 mbs, just below the mole network. Our results here support our previous suggestions of a functional drainage network (Chapter 4, Chapter 5 & Chapter 6), despite its age of 30+ years.

7.5.3 Spatiotemporal dynamics of hydrologic connectivity

Here we describe the mechanisms behind the transition from the dry to the wet soil moisture state (Figure 7-10). Tile flow was uncommon in the dry state, unless precipitation volumes were sufficient to satisfy the large soil moisture deficit. There was evidence of water flow that bypassed the soil matrix, but no evidence that this type of flow was a significant mechanism for hydrological connectivity in the dry state, as it corresponded to very small tile flow contributions and runoff ratios that were suggestive of a small contributing area. This contrasted with results on similar soils by McLeod et al. (2003) and Greenwood (1999), which indicated that, at the scale of a lysimeter or soil profile, these soils should be at considerable risk of preferential flow. The disparity may come down to the variability in processes occurring over different spatial scales, that can result in the over- or underestimation of certain flow pathway contributions when upscaling from small scales to the level of a catchment (Gomi et al., 2008; Joel et al., 2002; Kirkby, 2002). The results, however, additionally contrasted with those from several larger-scale studies (i.e., 6 – 8 ha) of soils formed in thin loess over glacial till of the Leary Weber Ditch Watershed in the US-Midwest. These studies employed water chemistry analyses to estimate preferential flow contributions to a 30+ year

old tile drain (Cuadra & Vidon, 2011; Stone & Wilson, 2006; Vidon et al., 2012). They identified preferential flow contributions of more than 50 % for large events and around 20 % for small precipitation events. However, these studies do not provide information on soil properties, so it is difficult to explain why preferential flow appeared to be a much more significant pathway in their soils. It is commonly assumed that natural, surface-sourced preferential flow plays a major role in the hydrology of mole and tile-drained soils, specifically through the influence of the mole channel 'fracture network', which is a legacy of the installation process (Horne, 1985; Monaghan & Smith, 2004). Our conclusion of insignificant surface-sourced preferential flow is consistent with the findings in Chapter 5, which did not identify evidence of an active fracture network. Furthermore, topsoil macroporosity (a measure of the pores capable of conducting free water) was shown to be very low in our study catchment, which suggests a reduced potential for natural preferential flow. One process of preferential flow pathway generation, often considered relevant to the Pukemutu (Manaaki Whenua Landcare Research, 2022) soil family in our study is drying-induced soil cracking (Beyer et al., 2016; Drewry et al., 2000; Greenwood, 1999; Houlbrooke et al., 2009; Killick, 2018; McLeod et al., 2008). It was noted that two of the three tile flow events that exceeded flow rates of 0.4 mm h^{-1} between November 2018 and January 2022 were the first significant events of the wet season (May 2019 and May 2021) and followed long dry spells. This suggests that periods of prolonged (i.e., 1 – 6 months) and large soil moisture deficit may have increased the soil macroporosity, possibly through crack formation; however, the effect appeared to be transient and did not persist into the next events. This suggests that surface-connected preferential flow pathways, formed through either artificial fracture networks or drying-induced soil cracking, were not a significant hydrological feature of this landscape. This transient nature signals a natural capacity of the soil to heal cracks, and may partially explain the apparent absence of a mechanically-induced mole fracture network, as described in Chapter 5. Tile flow rates of < 0.4 mm h^{-1} for the remaining events were probably reflective of the integrated K_{sat} of the soil matrix.

The transition from dry state (Figure 7-10a) to wet state (Figure 7-10b) soil moisture conditions appeared to begin at the lower catchment hollow. With increased wetting, excess soil moisture accumulated at the lower hollow, which appeared to be the source area for early flow in the dry state and regulated flow activation/deactivation. Larger events in the dry state generated perched water tables, which formed first along the hollow and on the interfluve (areas of high TWI; Figure 7-10c). Initially, these PWTs did not appear to be hydrologically connected to the tile drain, which may have been a result of spatially variable soil moisture that created areas of water attenuation

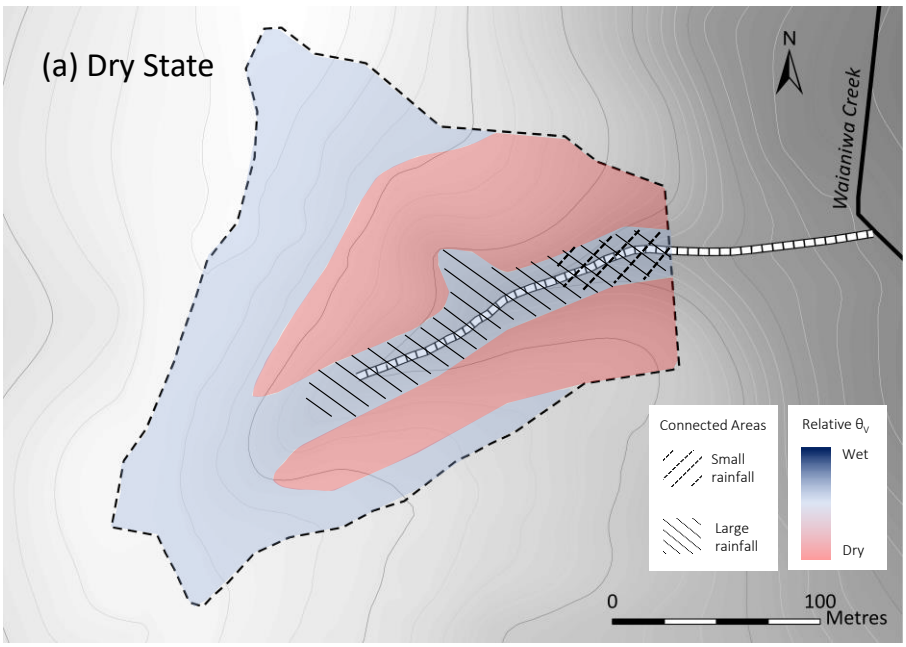
(a) Dry State
N
Waianiwa Creek
Connected Areas
Small rainfall
Large rainfall
Relative θ_v
Wet
Dry
0
100
Metres

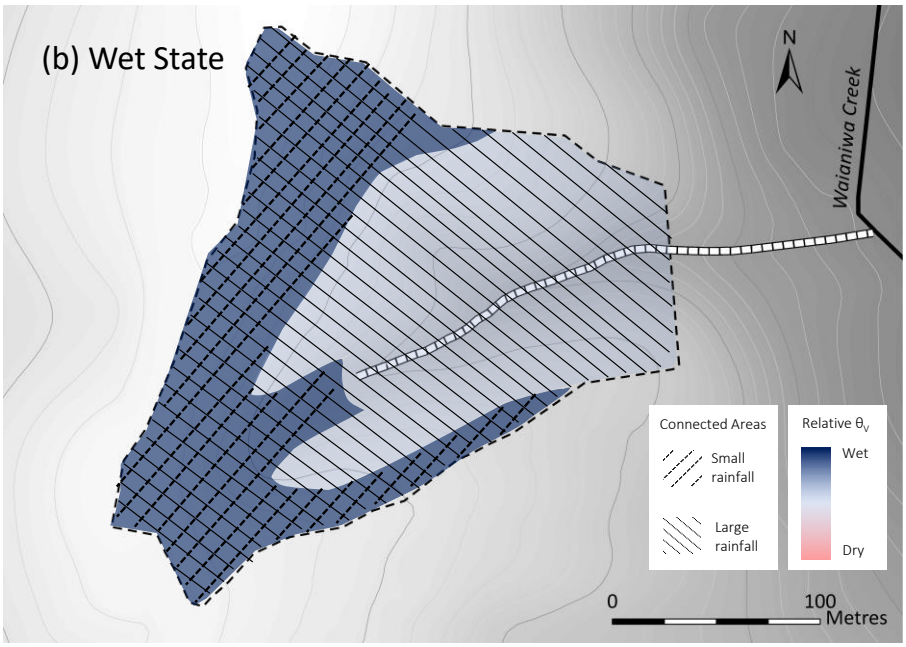
(b) Wet State
N
Waianiwa Creek
Connected Areas
Small rainfall
Large rainfall
Relative θ_v
Wet
Dry
0
100
Metres

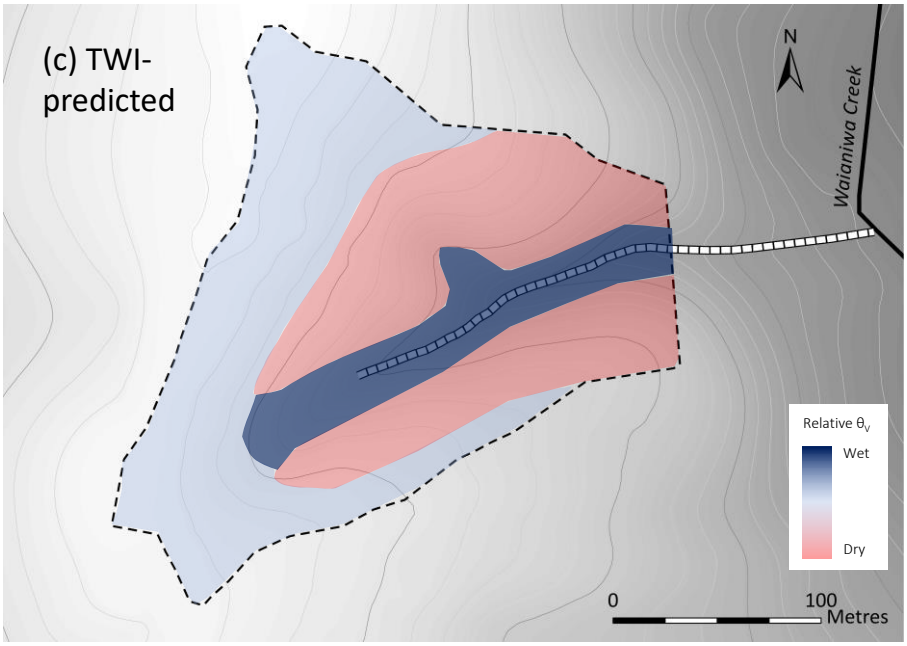
(c) TWI-predicted
N
Waianiwa Creek
Relative θ_v
Wet
Dry
0
100
Metres

Figure 7-10. (Previous page). Conceptualisation of spatial antecedent volumetric soil moisture content (θ_V) and hydrological connectivity in the mole and tile-drained loess basin with fragipans. In the dry state (a), the interfluves and hollow have high relative antecedent θ_V and the slopes have low relative θ_V. Hydrological connectivity is limited to the lower catchment hollow for rainfall with small metrics, and increases up the hollow as rainfall metrics increase. Despite relatively high θ_V, the interfluves are not hydrologically connected in the dry state. In the wet state (b), the interfluves and upper hollow have high relative θ_V, and the mid to lower hollow and slopes have low relative θ_V. Small rainfall metrics trigger hydrological connectivity between the interfluves and the tile drain, while under large rainfall metrics, the entire basin becomes hydrologically connected. The topographic wetness index (TWI)-predicted soil moisture pattern (c) shows the highest relative θ_V in the hollow and the lowest θ_V on the slopes.

(i.e., water was absorbed in transit within the mole channel in the presence of uneven wetting). Such behaviour was noted in an investigation into the impact of mole drainage on soil water on the very similar Tokomaru silt loam (Aeric Fragiaqualf; Soil Survey Staff, 2014) by Horne (1985, p. 31). Absorptive losses to the soil matrix were observed in dry soils, resulting in retarded water movement and delayed flow responses. With increasing catchment wetness, tile flow regulation expanded from the excess moisture at the lower hollow, to the PWTs at the mid- to upper hollow, and eventually up to the interfluve PWTs. This pattern of soil moisture dynamics is consistent with the description of soil moisture transition between the wet and dry states by Grayson et al. (1997), who explained that decreasing evapotranspiration leads to increasing soil moisture at areas of high local convergence, and the rapid wetting up of drainage lines as a result of the downslope movement of excess water. It is also consistent with the common simulations of variable source area hydrology (VSA), which assume that the drainage channel and riparian area immediately surrounding the channel responds most quickly to precipitation, saturating first to contribute towards initial channel flow before expanding upslope (Baker et al., 1995, pp. 115-120). Like what was observed by Tromp-van Meerveld and McDonnell (2006a), the transition period lasted on average two weeks.

Once the hydrological connection between the lower hollow and interfluve had been established, the catchment had completed the (rapid) transition into the wet state, and the interfluve PWT and mole network became the primary regulator of tile flow. Catchment hydrological response to precipitation became consistent among the periods of rainfall. Areas where PWTs were maintained at the depth of the drainage channels were primed to respond promptly to precipitation. A PWT intercepting the mole network on the interfluves activated tile flow, which, for small to medium sized rainfall responses, was regulated by the PWT height at the interfluve and upper hollow (indicated by the alignment of tile flow and PWT hydrograph peaks). Our results contrast

with those from a mole-drained heavy clay soil, in which tile flow peaks always occurred in advance to PWT peaks (Goss et al., 1983); however, the authors attributed the behaviour to significant preferential flow through the artificial fissure network which, as already discussed, was not an important route for water movement in our study catchment. Hydrological connectivity between the interfluve and upper hollow was clearly demonstrated in the response of the monitoring well at the upper hollow, which presumably intercepted a mole channel and was placed under positive pressure whenever the upslope PWT intercepted the mole network. Only rainfall periods with exceptionally large precipitation volumes and intensities were able to trigger PWTs on the slopes, and these PWTs only demonstrated control on tile flow once all other parts of the catchment were at saturation. Such precipitation events where shown in Chapter 6 to generate tile flow runoff ratios of greater than 40 % (Chapter 6, section 6.4.4.1), which occurred during only 4 % of all events monitored between 1st March 2019 to 28th February 2021. Similar results were reported by Tromp-van Meerveld and McDonnell (2006b), who showed that hillslopes became hydrologically connected to the stream for only ca 5 % of rainstorms, which occurred on average 4.3 times per year. Once these PWTs exceeded a height threshold of 0.2 – 0.3 metres below the surface, their height fluctuations were clearly reflected in the tile flow rate. Soil moisture at the mid-hollow, while likely contributing toward tile flow water, did not appear to play a significant role in tile flow behaviour. Late stage flows were controlled by the PWT and mole network at the interfluve. Once the PWT dropped below the mole network there, they became hydrologically disconnected from the tile drain, despite the persistence of PWTs below the mole network. Recession of the PWT in the hollow to below the tile drain coincided with the ceasing of tile flow also, but given the absence of control on tile flow from this area, the coincidence may have been a function of the termination of water supply from the interfluves (i.e., not causation).

As most precipitation events in this landscape are of modest size and rarely generate flow-regulating PWTs on the slopes (Chapter 6), it was fluctuations in PWT at upslope areas, particularly the interfluves, that dominated control of tile flow for the majority of the year. It is these areas, therefore, that should be of focus when considering water quality mitigation strategies in mole-tile drain loess landscapes with slowly permeable subsoils. The mechanisms underpinning the behaviour of the PWT on the slopes requires further research, as it is not clear why these sites drain so rapidly relative to the interfluves; however, it is possible that the high density of closely-spaced, downslope mole channels contributed to the removal of the PWTs from these sites. At some sites the mole network appeared to actually inhibit the rate of water removal, which was

probably related to an increase in water supply from upslope areas via the mole channels. In the hollow, once this mole-sourced delivery ceased, the tile drain was able to rapidly remove the excess moisture.

7.5.4 The role of interflow

Estimations of downslope travel distance (DTD) indicated that lateral throughflow (interflow) rarely, if ever, plays a large role in hydrological connectivity in these landscapes. The results suggest that the extensive and dense mole channel network virtually eliminates any potential matrix throughflow, diverting excess water into the mole and tile network, where it leaves the catchment as tile flow. Calculations, with and without the mole and tile network, suggested that a single water particle at the surface would travel a maximum of 2 metres before percolating into the fragipan and becoming vertical deep drainage. It is important to note that the estimates provided are likely to be over-estimates of DTD, due to the calculation assumption of a saturated loess column. By assuming that the entire loess was saturated, the lowest possible vertical hydraulic gradient was used, and the calculated downslope distance was the maximum possible distance. In support of these numbers, virtually no tile flow was observed in the wet state unless PWTs were above the mole network. This contrasts with what was found by McDaniel et al. (2008) in the Palouse region of north-western USA, who attributed flow in the tile drain at the base of a hydrologically isolated, un-moled 35m × 18 m hillslope plot to subsurface lateral flow, which was a large component of the overall catchment water balance (89 % in winter) in their loessial soils with fragipans. In undrained till deposits of the Allegheny Plateau, lysimeter studies indicated up to 30 % of annual precipitation was estimated to be lost via interflow pathways above the fragipan surface (Miller et al., 1971). Also in the Palouse region, Reuter et al. (1998) attributed downslope transport of an applied bromide tracer to rapid preferential flow, and suggested that this flow occurred in both the Bw horizon, above the fragipan, and also in the Ap horizon, above an E horizon of low macroporosity and permeability. Lateral flow via the topsoil was also inferred from a study of heavy clay soils by (Goss et al., 1983) and suggested to significantly influence peak tile flow rates. It was unlikely, however, that the topsoil was a preferred zone of lateral flow in fully saturated soils at our site, as the topsoil macroporosity of our soils was lower than that of the upper subsoil, and the mean K_{sat} did not vary significantly between the topsoil and subsoil (Chapter 5, Table 5-5).

It is also unlikely that the basin hollow was a zone of lateral flow attenuation via deep drainage to groundwater. A PWT was maintained from late autumn to late spring just below the tile drain.

No fragipan was detected from excavations of the hollow (Appendix A.1 and A.2), and the lithological discontinuity between the loess mantle and the clayey gravels was just 0.1 m beneath the tile drain. As such, the persistence of the PWT pointed towards a low K_{sat} of the underlying gravels – rejecting the idea that this area formed a sink for subsurface lateral flow.

An alternative, or coincidental, reason for absence of significant throughflow in our watershed could be a more permeable fragipan relative to those of loess regions in the USA, where throughflow does appear to be significant. Soil core estimates of fragipan K_{sat} at our site were ca 3 mm h^{-1}, with variation from 0.2 to 10.8 mm h^{-1} (Chapter 5), whereas fragipan K_{sat} in the Palouse region of northern Idaho has been measured as 0.04 – 0.09 mm h^{-1} (Reuter et al., 1998), and in the Allegheny Plateau as < 0.25 mm h^{-1} (Miller et al., 1971). Monaghan et al. (2002) found larger cumulative volumes of tile drain flow were associated with plots with a more distinct (less permeable) fragipan, in a range of soils similar to those at our field site (including Fragic Perch-gley Pallic, Pallic Firm Brown, Mottled Firm Brown and Typic Firm Brown Soils). However, a detailed water balance analysis of deep drainage rates in Chapter 6 produced an integrated estimate of 0.4 mm h-1, so it appears that, at the scale of the catchment, the contrast in Ksat between our site and those in the USA may not be as extreme as core measurements would indicate.

Our results suggest that assumptions of significant lateral flow in mole and tile-drained landscapes with slowly permeable subsoils must be made with caution. They also demonstrate a need for further research into the mechanisms behind flow pathway regulation in different landscapes.

7.6 Conclusions

Spatial soil moisture patterns were seasonally variable. Perched water tables and the artificial drainage network contributed to the changing patterns of soil moisture. Topographic wetness index (TWI) was, on its own, a poor predictor of spatial soil moisture variability at any time across the year, especially in winter. The lower hollow had the highest TWI, yet, along with the planar side slope, was one of the driest parts of the catchment in winter and spring, indicating that the tile drain is acting to regulate spatial soil moisture patterns. Perched water tables (PWTs) were maintained in upslope flat (i.e., the interfluve) and topographically convergent (i.e., the drainage hollow) areas from late autumn to late spring, but appeared to be constrained in their magnitude by the mole network or, where present, the tile drain, such that exceedances of the drainage network were rapidly returned to their antecedent position once precipitation inputs ceased. On some areas of the slopes, and potentially in the tile drained parts of the hollow, the mole network appeared to delay the removal of excess water, possibly by acting as a delivery system for upslope water. The transition from dry state to wet state soil moisture conditions lasted approximately two weeks and appeared to begin at the lower catchment hollow. Initial upslope PWTs were not hydrologically connected to the tile drain in the dry state, which may have been a result of spatially variable soil moisture that created areas of water attenuation. With increasing catchment wetness, tile flow regulation expanded from the excess moisture at the lower hollow, to the PWTs at the mid- to upper hollow, and eventually up to the interfluve PWTs. Once the hydrological connection between the lower hollow and interfluve had been established, the catchment had completed the transition into the wet state, and the interfluve PWT and mole network became the primary regulator of tile flow. Only rainfall periods with exceptionally large precipitation volumes and intensities were able to trigger PWTs on the slopes, and these PWTs only demonstrated control on tile flow once all other parts of the catchment were at saturation. For the remainder of the wet state, catchment hydrological response to precipitation was consistent. There was no evidence that natural preferential flow was a significant mechanism for hydrological connectivity. Interflow was not identified as a significant pathway for catchment hydrological connectivity. Flat, upslope areas prone to the development of PWTs should be focussed on when considering water quality mitigation strategies in mole-tile drain loess landscapes with slowly permeable subsoils, especially in winter.

Chapter 8

Conclusions and future research

8.1 Overview

Contamination of surface and groundwater is a serious environmental concern in the artificially drained agricultural landscapes of Southland. An improved understanding of the controls on spatial and temporal variability in soil properties and catchment hydrological behaviour is required to mitigate freshwater contamination. To develop such knowledge requires an interdisciplinary, integrated approach that incorporates pedology, soil physics and hydrology to bridge scales and provide insight into the fundamental process that regulate water movement in the landscape.

The aim of this PhD research was:

- To fill a gap in our understanding of the intrinsic and extrinsic controls on the variability of soil hydraulic properties and soil hydrological behaviour in low permeability loess landscapes in which mole-tile drainage has been installed.

To achieve this aim, five overarching thesis objectives were addressed separately in five research chapters. These chapters were all focused on the same small, mole and tile-drained basin formed in a loess-mantled downland, a landscape typical of the Central Plains in Southland, New Zealand.

8.1.1 Thesis Objective 1

> Characterise the spatial distribution of soils within a dissected loess landscape and determine (a) whether multisequal soils are an important component of these landscapes and (b) if their recognition as distinctive taxa would improve characterisation of soils in a way that would facilitate better soil and environmental management.

Landscapes mantled in thick loess sheets and with small relief often contain soils formed entirely in the uppermost loess sheet, and have relatively low spatial variability. The complexity of the soil pattern increases where loess sheets are thinner, or relief is greater, as hillslopes crosscut buried loess sheets and their associated paleosols, and form multisequal, polygenetic soils. Such inheritance of paleopedological features from buried loess sheets may produce soils that are

sufficiently morphologically, physically, chemically and mineralogically distinct to warrant definition as separate soil taxa. At present, no soil maps explicitly recognise associations of unisequal and multisequal soils resulting from differential erosion and exhumation of buried loess sheets on hillslopes. The aim of Chapter 3 was to conceptualise the loess stratigraphy and characterise the distribution of soil properties on a loess-mantled downland in Southland where the relief is often greater than the combined thickness of the loess mantle. The following research questions were addressed by a morphological investigation using auger boring and soil pit methods as well as quantitative analysis of soil accessory properties:

1) Are multisequal soils an important component of the soil-landscape?

2) Would the recognition of multisequal soils as distinctive taxa improve characterisation of soils in a way that would provide information necessary to facilitate better soil and environmental management?

The drainage basin hillslopes cut across four buried loess sheets. Soils on the interfluves were formed entirely in the uppermost loess sheet, while hillslope soils were compound soils involving at least two loess sheets and their associated soils. Principal component analysis (PCA) on soil samples collected from five depths showed that vertical differentiation of soils by topdown pedogenesis was the dominant driver of heterogeneity in soil physical, hydraulic and chemical attributes. Other factors, likely related to the legacy of pedogenesis in buried loess sheets and burial-related consolidation, were important for understanding subsoil variability. The *k*-means algorithm produced clusters that corresponded closely with morphological soil horizons. Clusters corresponded with the first order vertical sequence of horizons characteristic of Pallic Soils (A; A/B; Bw; Bx). Increasing the number of clusters differentiated the Bx horizon, discriminating those formed in the upper loess sheet from those of paleosol origin or of contrasting lithology.

Main conclusions:

- Multisequal soils are an important component of hillslopes on loess-mantled downlands with thin loess sheets; unisequal soils formed in the uppermost loess sheet dominate the interfluves.

- Catchment side slopes had greater variability of soil attributes relative to the interfluves, suggesting that the multisequal nature of hillslope soils is relevant to understanding soil

spatial variability and that hillslope/multisequal soils are sufficiently different that distinct taxa should be recognised. A more refined understanding of the soil-geomorphology of loess-mantled downlands may lead to better soil-landscape models, more accurate soil maps and better characterisation of soil variability.

- Both qualitative and quantitative methods of horizon designation can be employed to achieve a similar partitioning of soil hydraulic and physical attribute variability.

- Vertical differentiation of soils by topdown pedogenesis was the dominant driver of heterogeneity, while other factors, likely related to the legacy of pedogenesis in buried loess sheets and burial-related consolidation, were important for understanding subsoil variability.

8.1.2 Thesis Objective 2

> Characterise a mole and tile drainage network (i.e., drain depth, orientation, location, integrity, connectedness, density) that is likely to be representative of similar artificial drainage systems across slowly permeable loess soils in Southland.

Information regarding the design characteristics, specific density metrics and longevity of mole channel and tile drainage systems is necessary for managing the problematic secondary effects of mole and tile drainage; however, such information is scarce. Subsurface drainage may cover 75 % of agricultural land in Southland, so their influence on regional hydrology and water quality is likely to be significant. The aim of Chapter 4 was to test whether or not ground-penetrating radar (GPR) could be used to identify and map a typical mole and tile network, and provide information on the physical characteristics of the network and individual mole channels. The following research questions were addressed using GPR survey techniques:

1) Can GPR be used to identify and map mole channels and a tile drain in a loess-derived soil?

2) What are the characteristics of a mole drainage system constructed from repeat episodes of moling?

3) How persistent are mole channels in Southlands loess-derived Pallic Soils?

High frequency GPR coupled with a GNSS antenna successfully located mole channels and a tile drain, showing high lateral precision, accuracy, and utility for mapping. High resolution surveys of six plots showed that the mole network was complex in terms of its design and had a high density of mole channels (1.6 m m^{-2}) which appeared to have been developed over several generations of mole ploughing. The 30 + year old mole channels showed a high degree of connectivity and structural integrity.

Main conclusions:

- GPR is highly effective at mapping mole channels and tile drains in loess soils; however, the method applied here is unlikely to be efficient at catchment or regional scales.

- The density of mole channels can be extremely high in landscapes where re-moling is practised, and their networks highly connected.

- Multi-generational mole channels in loess-derived soils result in inter-connected multidirectional channels with a high drainage density (1.6 m m^{-2} observed)

- The network can retain connectivity and good condition for 30 years or more, provided it is installed in the subsoil horizon above the fragipan.

- Visual observations and short range variability of soil properties provide no evidence for persistence of a soil fracture network induced at the time moles were installed; however, root growth and worm burrowing into the mole channels suggest that they are hydraulically connected to the surrounding soil through natural macropores.

- These results have significance for understanding catchment-scale hydrodynamics and water quality, especially considering that the life span of these artificial drainage networks has been shown to be considerably longer than previous (7 – 10 years) estimates for this soil type.

8.1.3 Thesis Objective 3

> Quantify the direct and indirect influence of mole drainage channels on soil hydraulic properties, as well as the influence on the overall soil moisture regime classification.

Secondary artificial fracture networks, induced during mole channel installation, are considered to be a key functional element of mole and tile drainage systems, but it is unclear how these legacy installation effects, or the current mole network, influence the soil properties and moisture regime when the mole channels are mature (30 + years). The aim of Chapter 5 was to understand the direct and indirect influence of mature mole channels on soil properties and behaviour, and to assess the moisture regime of loess soils under long-term mole channel drainage. The following research questions and objectives were addressed:

1) Does the landscape retain a fracture network (induced when moles were installed) that still influences soil hydraulic properties?

    - Objective: Quantify differences in surface saturated hydraulic conductivity (K_{sat}), as well as key subsoil hydraulic and physical properties, between 'mole-proximal' and 'mole-distal' locations at a range of depths.

2) Is K_{sat} a dynamic property that is dependent on antecedent soil moisture state (wet state versus dry state)?

    - Objective: Quantify the effect of antecedent soil moisture content on soil surface K_{sat}.

3) Are morphologically determined permeability and drainage classifications (as used in S-Map) consistent with observed soil hydrological behaviour?

    - Objective: Classify the permeability and drainage class for a mole and tile-drained soil using spatial, temporal and point-scale measurements of soil hydraulic properties.

Measurements of surface and subsurface soil hydraulic and physical properties found no effect of mole channel proximity. Surface K_{sat} appeared to be controlled by the antecedent soil moisture content, but only on the interfluves where K_{sat} was significantly greater in wet state antecedent

conditions than dry state antecedent conditions. The permeability profile classification was consistent with that provided by the New Zealand Soil Classification, however the assessment of drainage class varied with respect to the method used.

Main conclusions:

- Mole channel longevity does not imply equivalent longevity of the mole fracture network: the well-connected mature (30 + year) mole network in this study showed no evidence of a functional, mechanically-induced fracture network, near or distant from the mole, despite the mole channels themselves being in remarkably good condition (Chapter 4). This has implications for hydrological and water quality modelling as preferential flow via the fracture network is commonly considered to be the major route for rapid water and contaminant transfer in mole and tile-drained soils.

- The persistence of perched water tables and the associated capillary rise appears to result in a more well-connected pore network that increases surface K_{sat} relative to dry antecedent soil conditions. Therefore, depending on the depth of the drainage network and soil properties, mole and tile drainage may indirectly influence soil K_{sat}, by influencing the dynamics of the PWT.

- Soil morphology-based interpretations of drainage class may not be consistent with functional descriptions of soil drainage (i.e., months above field capacity) for mole and tile-drained soils.

8.1.4 Thesis Objective 4

> Construct a water balance and examine the temporal variability in runoff pathways, quantify runoff generation controls and thresholds and characterise and quantify groundwater recharge at event-based time scales.

The understanding of flow processes in mole and tile-drained soils remains elusive, particularly with regard to runoff mechanisms and their temporal and spatial, as well as intrinsic and extrinsic controls. Moreover, deep drainage is often considered negligible, despite there being too few empirical studies to support this assumption. The aim of Chapter 6 was to quantify the

spatiotemporal variability and controls of runoff and deep drainage. It was achieved by monitoring catchment meteorology, soil water dynamics and runoff fluxes over a two year period, as well as event–scale analysis of precipitation, soil moisture and runoff characteristics. The following research questions and objectives were addressed:

1) What is the rate of DD and how does it depend on other components of the water balance?

    - Using a water balance approach, estimate deep drainage by difference.

2) What are the triggers of runoff and the controls on runoff volume?

    - Relate event-scale precipitation, soil moisture and runoff (tile and overland flow) flow characteristics.

3) What are the key source areas of tile flow?

    - Relate event-scale tile flow characteristics to the perched water table (PWT) across different landscape elements.

The groundwater table was responsive to estimated DD contributions, but not flashy. Deep drainage rate was estimated at 0.4 mm h^{-1}, which was consistent with modelled estimates by Vogeler et al. (2019). Thresholds in multiple hydrological metrics appeared to be important for triggering runoff responses. Two soil moisture states, 'wet' and 'dry', dominated hydrological response to precipitation, and were consistent with the duality of moisture states described for undrained catchments (Grayson et al., 1997; Tromp-van Meerveld & McDonnell, 2006a). Event tile flow volume was most strongly correlated with maximum PWT height at the interfluve and upper hollow, and only showed strong correlations with PWT on the slopes when runoff ratios were at their largest, i.e., during precipitation events with exceptional precipitation metrics.

Main conclusions:

- Deep drainage was an important, temporally variable flow pathway, demonstrating that the common assumption of negligible deep drainage may be inappropriate when modelling flow pathways in slowly permeable loess, with or without artificial drainage.

- Deep drainage appeared to occur via piston flow through the fragipan and underlying loess, and in response to excess soil moisture in the overlying soil horizons.

- Natural, surface-vented preferential flow pathways were active in the dry state, but the volume of water moved via this pathway was hydrologically insignificant. In the wet state, activation of artificial preferential flow pathways (i.e., mole-mediated flow) required exceedance of PWT height thresholds and indicated that tile flow required submergence of the mole network.

- Intrinsic and extrinsic runoff thresholds interacted to regulate tile flow response. Precipitation volume and/or intensity thresholds could discriminate event runoff responses depending on antecedent soil moisture state (dry or wet). Low precipitation intensity thresholds indicated equally low soil surface infiltration rates.

- Infiltration-excess overland flow was the most common form of surface runoff, probably as a result of low surface infiltration capacity, and saturation-excess overland flow was rare. Possible relationships between precipitation intensity and overland flow rate were obscured by the disparity between the frequency of P measurement (hourly) and the scale of the response of the overland flow (sub 5-minute).

- Tile flow from small events was predominantly sourced from the interfluves and upper hollow. The slopes only contributed to tile flow when events were large enough to wet up, and saturate, the whole catchment. Runoff source area appeared, therefore, to be linked to precipitation event size.

- Southland's artificially drained, slowly permeable loess soils are hydrologically sensitive landscapes demonstrating large shifts in their (non-linear) responses to small variations in precipitation intensity. Shifts in the distribution of precipitation intensity with climate could significantly change the magnitudes and relative contributions of the components of the water balance (i.e. more OF).

- Winter and spring are key seasons and the interfluves and upper hollow are key areas for generating runoff and these times and places should be targeted for mitigating surface water contamination from mole and tile-drained loess landscapes.

8.1.5 Thesis Objective 5

> Qualitatively analyse the soil moisture, perched water table and runoff dynamics in order to identify mechanisms of hydrological connectivity in artificially drained landscapes.

Few studies have investigated the spatiotemporal dynamics of hydrological connectivity in agronomically-important, artificially drained loess soils, yet freshwater bodies in these landscapes are under increasing pressure from agricultural runoff. The aim of Chapter 7 was to understand the spatiotemporal dynamics of hydrological connectivity in mole and tile-drained, slowly permeable, loess-derived soils in Southland, New Zealand. The following research questions and objectives were addressed:

1) Is the topographic wetness index useful for understanding relative wetness in a mole and tile-drained landscape?

    - Qualitatively analyse the behaviour of volumetric soil moisture and perched water tables across different landscape elements.

2) What are the mechanisms underpinning hydrological connectivity and how do they vary spatially and with time?

    - Qualitatively analyse tile flow responses to PWT and volumetric soil moisture content with time.

3) What is the role of interflow in hydrological connectivity?

    - Estimate the downslope travel distance (DTD) of excess water above the fragipan.

Qualitative analyses of spatial soil moisture patterns suggested they were influenced by perched water tables and the drainage network. Volumetric soil moisture was either not correlated or weakly correlated with topographic wetness index (TWI), for each of the four seasons. The transition from dry state to wet state soil moisture conditions lasted approximately two weeks. With increasing antecedent wetness, hydrological connectivity expanded up the hollow and eventually up to the interfluve. Only rainfall periods with exceptionally large precipitation volumes and intensities were able to connect the slopes in both wet and dry states. Calculated downslope

travel distances (DTD) of excess water above the fragipan were less than 2 m at all landscape elements.

Main conclusions:

- TWI on its own is not an appropriate predictor of soil moisture spatial patterns in mole and tile-drained, low permeability loess soils. It was likely that the tile drain was regulating soil moisture in the hollow, as, despite being the most topographically convergent part of the landscape, it was also the driest.

- The transition from dry state to wet state soil moisture conditions lasted approximately two weeks and appeared to begin at the lower catchment hollow. Initial upslope PWTs were not hydrologically connected to the tile drain in the dry state. With increasing catchment wetness, tile flow regulation expanded from the excess moisture at the lower hollow, to the PWTs at the mid- to upper hollow, and eventually up to the interfluve PWTs. Once the hydrological connection between the lower hollow and interfluve had been established, the catchment had completed the transition into the wet state, and the interfluve PWT and mole network became the primary regulator of tile flow. Only rainfall periods with exceptionally large precipitation volumes and intensities were able to trigger PWTs on the slopes, and these PWTs only demonstrated a control on tile flow once all other parts of the catchment were at saturation.

- There was no evidence that interflow, either as matrix or natural preferential flow, was a significant mechanism for hydrological connectivity.

8.2 General conclusions

This research highlights the need to ensure that significant sources of soil variation are accurately represented in current soil classification and mapping. In loess landscapes, such a source of variation appears to be associated with the loess and soil stratigraphy, paleopedology, geomorphic history and current morphometry. In order to understand the soil hydrological (and chemical) dynamics of both drained and undrained loess, it is necessary to recognise that a one meter profile of loess material in one part of the landscape may be significantly functionally different to that found in another part of the landscape when loess sheets are thin and topography is sloping.

Results of the mole and tile mapping exercise, as well as the demonstrated influence of these systems on soil moisture patterns and runoff dynamics, reveal why it is important to have a detailed understanding of the extent and condition of the drainage network, especially with regard to mole channels, and especially in areas under pressure from agricultural freshwater contamination. There may also be an argument for regulating the installation of mole channels, as a simple requirement to notify the local regional council of their presence would provide an extremely useful database of the areal extent and potential density of mole channels across the region – information that would be invaluable for hydrology and contaminant modelling.

The soil hydrological dynamics of artificially drained, loess landscapes with fragipans is poorly understood, yet decision-making around land and water management is often based on assumptions about their hydrological behaviour. This thesis demonstrated that several common assumptions about flow pathways (i.e., mole channel fracture networks, negligible deep drainage, significant natural interflow and insignificant overland flow) may be inappropriate and, consequently, their use in decision-making may lead to unsatisfactory agronomic, economic and environmental outcomes.

8.3 Recommendations for future research

- This study demonstrated that mole networks have the potential to be dense, well-connected, and functional even after 30+ years (Chapter 4); however, the results were limited to a single, small catchment. Future research could focus on both characterising and comparing existing artificial drainage systems in different soil-landscape combinations, as well as investigating methods for regional-scale quantification and characterisation of these networks. Geophysical technologies offer potential in this area when mounted to unmanned aerial vehicles, e.g., GPR, visible-colour, multispectral, and thermal infrared imagery.

- Deep drainage was shown to be an important component of the water balance (Chapter 6); however, only inferences were able to be made about the flow pathways and source areas of groundwater recharge (Chapter 6; Chapter 7). Future studies should investigate the mechanisms by which water moves through the loess mantle and the attenuation capacity of the vadose zone.

- Source areas of overland flow, an important flow pathway in winter and spring, were not investigated in this study, and should be addressed in future research. Our understanding of

the mechanisms of overland flow, including infiltration-excess, saturation-excess and return flow, could be further refined using tracer experiments and soil water electrical conductivity measurements.

- The results from this research suggest that 'steady state' hydraulic conductivity may be a function of antecedent soil moisture state (Chapter 5); however, the findings were limited to a small number of sites on a single soil type. Given the key importance of surface infiltration to partitioning of hydrological pathways, this finding deserves more detailed quantification across a range of soils, particularly on sloping lands. Further investigations into the influence of persistent perched water tables on pore connectivity would improve our understanding of K_{sat} variability in soils.

- The accuracy of estimates of spatiotemporal controls on runoff (Chapter 6) could be improved in future research by installing tensiometers at each soil moisture monitoring site and at all five depths, to enable the site-specific definition of 'soil moisture deficit' to be obtained (i.e., capture the explicit volumetric moisture content at which the soil at a given depth and site experiences moisture excess).

- TWI was not a very useful index for characterising catchment moisture distribution yet it was used as a means for weighting point measurements to provide catchment averages, demonstrating a limitation of this study (Chapter 6; Chapter 7). Additionally, spatial soil moisture response was limited in this study to seven point scale measurements and five depths. Differential proximal soil sensing techniques such as electromagnetic induction, gamma-ray spectrometry and ground penetrating radar in combination with data-averaging techniques (e.e., kriging) could be used at different times across the year to investigate high-spatial resolution moisture response to evapotranspiration over broader spatial scales, or at different times across a precipitation event (e.g., before, during, and after). Such investigations would give a better representation of zones of different soil water behaviour, which might lead to a more appropriate means of estimating catchment scale wetness.

- The soil investigated in this study showed indications of compaction (Chapter 3; Chapter 5; Chapter 6), which was possibly involved in regulating catchment hydrological response (Chapter 6). Further work is required to specifically investigate the role of compaction, and potential compaction thresholds, on soil and landscape hydrological response to

precipitation at the catchment scale. This has significant potential to modify soil moisture patterns, surface and subsurface hydrological connectivity and water balance partitioning. Potential strategies for reducing further compaction and ameliorating existing compaction should also be investigated.

- The information revealed in this study about the hydrological dynamics of an artificially drained catchment formed in loess can now be used to develop our understanding of contaminant losses from these landscapes, their source areas, and their relationship with the temporal dynamics of stream and groundwater chemistry. Future research should include quantification of contaminant losses (including nitrogen, phosphorus, sediment, *E. coli* and *Campylobacter*) in tile and overland flow, and their temporal variation. Furthermore, low topsoil macroporosity and high year-round soil moisture were characteristics identified of the study catchment (Chapter 5; Chapter 6; Chapter 7), and suggest that the redox dynamics of these artificially drained landscapes should be investigated, especially in terms of their spatial and temporal potential for denitrification (i.e., their contribution to nitrate leaching and nitrous oxide emissions).

References

"Invercargill - Southernmost city in the world". (1900, 16. June). *Southland Times*. https://paperspast.natlib.govt.nz/newspapers/ST19000616.2.31.2

Allen, R. G., Walter, I. A., Elliott, R., Howell, T. A., Itenfisu, D., & Jensen, M. E. (2005). The ASCE standardized reference evapotranspiration equation. In. Idaho: Task Committee on Standardization of Reference Evapotranspiration.

Alloway, B. V., Almond, P. C., Moreno, P. I., Sagredo, E., Kaplan, M. R., Kubik, P. W., & Tonkin, P. J. (2018). Mid-latitude trans-Pacific reconstructions and comparisons of coupled glacial/interglacial climate cycles based on soil stratigraphy of cover-beds. *Quaternary Science Reviews*, *189*, 57-75. https://doi.org/10.1016/j.quascirev.2018.04.005

Allred, B. J., Daniels, J. J., & Ehsani, M. R. (2008). *Handbook of Agricultural Geophysics*. CRC Press.

Allred, B. J., Fausey, N. R., Peters, L., Chen, C., Daniels, J. J., & Youn, H. (2004). Detection of Buried Agricultural Drainage Pipe with Geophysical Methods. *Applied Engineering in Agriculture*, *20*(3), 307-318. https://doi.org/10.13031/2013.16067

Allred, B. J., Martinez, L., Fessehazion, M. K., Rouse, G., Williamson, T. N., Wishart, D., Koganti, T., Freeland, R., Eash, N., Batschelet, A., & Featheringill, R. (2020). Overall results and key findings on the use of UAV visible-color, multispectral, and thermal infrared imagery to map agricultural drainage pipes. *Agricultural Water Management*, *232*, 106036. https://doi.org/10.1016/j.agwat.2020.106036

Allred, B. J., & Redman, J. D. (2010). Location of Agricultural Drainage Pipes and Assessment of Agricultural Drainage Pipe Conditions Using Ground Penetrating Radar. *Journal of Environmental & Engineering Geophysics*, *15*(3), 119-134. https://doi.org/10.2113/jeeg15.3.119

Allred, B. J., Wishart, D., Martinez, L., Schomberg, H., Mirsky, S., Meyers, G., Elliott, J., & Charyton, C. (2018). Delineation of Agricultural Drainage Pipe Patterns Using Ground Penetrating Radar Integrated with a Real-Time Kinematic Global Navigation Satellite System. *Agriculture*, *8*(11), 167. https://doi.org/10.3390/agriculture8110167

Allroggen, N., Booth, A. D., Baker, S. E., Ellwood, S. A., & Tronicke, J. (2019). High‐resolution imaging and monitoring of animal tunnels using 3D ground‐penetrating radar. *Near Surface Geophysics*, *17*(3 - GPR in Civil and Environmental Engineering: Recent Methodological Advances), 291-298. https://doi.org/10.1002/nsg.12039

Almond, P. C., & Tonkin, P. J. (1999). Pedogenesis by upbuilding in an extreme leaching and weathering environment, and slow loess accretion, south Westland, New Zealand. *Geoderma*, *92*(1-2), 1-36. https://doi.org/10.1016/s0016-7061(99)00016-6

Arduini, I., Baldanzi, M., & Pampana, S. (2019). Reduced Growth and Nitrogen Uptake During Waterlogging at Tillering Permanently Affect Yield Components in Late Sown Oats. *Front Plant Sci*, *10*, 1087. https://doi.org/10.3389/fpls.2019.01087

Armstrong, A. C. (1986a). Drainage of clay lands for grassland production: Problems, effects, benefits In A. L. M. Van Wijk & J. Wesseling (Eds.), *Agricultural Water Management*. CRC Press.

Armstrong, A. C. (1986b). Mole drainage of a Hallsworth Series soil. *Soil Use and Management*, *2*, 54-58.

Armstrong, A. C., & Garwood, E. A. (1991). Hydrological consequences of artificial drainage of grassland. *Hydrological Processes*, *5*(2), 157-174. https://doi.org/10.1002/hyp.3360050204

Baker, M., de Dios Benavides-Solorio, J., & Talavera-Zuniga, E. (1995). Relationship between precipitation and streamflow on El Carrizal watershed, Tapalpa, Jalisco. In C. Acquirre-Bravo, L. Eskew, C. E. Gonzalez-Vicente, & A. B. Villa-Sala (Eds.), *Partnerships for sustainable forest ecosystem managment: Fifth Mexico/U.S. Biennial Symposium; 1994 October 17-20; Guadalajara, Jalisco, Mexico.* . USDA Forest Service, Rocky Mountain Forest and Range Experiment Station.

Barkle, G., Stenger, R., Moorhead, B., & Clague, J. (2021). The importance of the hydrological pathways in exporting nitrogen from grazed artificially drained land. *Journal of Hydrology*, *597*, 126218. https://doi.org/10.1016/j.jhydrol.2021.126218

Barling, R. D., Moore, I. D., & Grayson, R. B. (1994). A quasi-dynamic wetness index for characterizing the spatial distribution of zones of surface saturation and soil water content. *Water Resources Research*, *30*(4), 1029-1044. https://doi.org/10.1029/93WR03346

Bartholomew, N., Brunton, C., Mitchell, P., Williamson, J., & Gilpin, B. (2014). A waterborne outbreak of campylobacteriosis in the South Island of New Zealand due to a failure to implement a multi-barrier approach. *J Water Health*, *12*(3), 555-563. https://doi.org/10.2166/wh.2014.155

Beven, K. J. (2012). *Rainfall-Runoff Modelling : The Primer*. John Wiley & Sons, Incorporated. http://ebookcentral.proquest.com/lib/lincoln-ebooks/detail.action?docID=822562

Beven, K. J., & Kirkby, M. J. (1979). A physically based, variable contributing area model of basin hydrology / Un modèle à base physique de zone d'appel variable de l'hydrologie du bassin versant. *Hydrological Sciences Bulletin*, *24*(1), 43-69. https://doi.org/10.1080/02626667909491834

Beyer, M., Rissmann, C., Rodway, E., Marapara, T. R., & Hodgetts, J. (2016). *Physiographics of Southland Part 1: Delineation of key drivers of regional hydrochemistry and water quality Technical Chapter 2: Discrimination of Recharge Mechanisms and Vulnerability to Bypass Flow*. Southland Regional Council (Environment Southland).

Blakemore, L. C., Searle, P. L., & Daly, B. K. (1987). Methods for Chemical Analysis of Soils. New Zealand Soil Bureau Scientific Report 80. 103 p.

Blann, K. L., Anderson, J. L., Sands, G. R., & Vondracek, B. (2009). Effects of Agricultural Drainage on Aquatic Ecosystems: A Review. *Critical Reviews in Environmental Science and Technology*, *39*(11), 909-1001. https://doi.org/10.1080/10643380801977966

Bodner, G., Scholl, P., & Kaul, H. P. (2013). Field quantification of wetting–drying cycles to predict temporal changes of soil pore size distribution. *Soil and Tillage Research*, *133*, 1-9. https://doi.org/10.1016/j.still.2013.05.006

Boersma, L., Simonson, G. H., & Watts, D. G. (1972). Soil Morphology and Water Table Relations: I. Annual Water Table Fluctuations. *Soil Science Society of America Journal*, *36*(4), 644-648. https://doi.org/10.2136/sssaj1972.03615995003600040040x

Borella, J., Quigley, M., Sohbati, R., Almond, P., Gravley, D. M., & Murray, A. (2016). Chronology and processes of late Quaternary hillslope sedimentation in the eastern South Island, New Zealand. *Journal of Quaternary Science*, *31*(7), 691-712. https://doi.org/10.1002/jqs.2905

Bou Lahdou, G., Bowling, L., Frankenberger, J., & Kladivko, E. (2019). Hydrologic controls of controlled and free draining subsurface drainage systems. *Agricultural Water Management*, *213*, 605-615. https://doi.org/10.1016/j.agwat.2018.10.038

Bowler, D. G. (1976). The drainage problem and research needs. Proceedings of Soil and plant Water Symposium, Palmerston North, 10 – 12 April 1973,

Bowler, D. G. (1980). *The drainage of wet soils*. Hodder & Stoughton Ltd.

Brocca, L., Morbidelli, R., Melone, F., & Moramarco, T. (2007). Soil moisture spatial variability in experimental areas of central Italy. *Journal of Hydrology*, *333*(2), 356-373. https://doi.org/https://doi.org/10.1016/j.jhydrol.2006.09.004

Bruce, J. (1983). Effect of climate on morphological features of soils from loess in the southern part of South Island, New Zealand. *Soil Research*, *21*(4), 359-371. https://doi.org/10.1071/SR9830359

Bruce, J. G. (1972). Loess soils in the South Island. In J. P. C. Watt (Ed.), *Loess and problems of land use on the downlands of the South Island, New Zealand. Publication No. 4* (pp. 1–28). Otago Catchment Board

Bruce, J. G. (1973a). Loessial deposits in southern South Island, with a definition of Stewarts Claim Formation. *New Zealand Journal of Geology and Geophysics*, *16*(3), 533-548. https://doi.org/10.1080/00288306.1973.10431376

Bruce, J. G. (1973b). A time-stratigraphic sequence of loess deposits on near-coastal surfaces in the Balclutha district. *New Zealand Journal of Geology and Geophysics*, *16*(3), 549-556. https://doi.org/10.1080/00288306.1973.10431377

Bruce, J. G. (1996). Morphological characteristics and interpretation of some polygenetic soils in loess in southern South Island, New Zealand. *Quaternary International*, *34-36*, 205-211. https://doi.org/10.1016/1040-6182(95)00086-0

Bruce, J. G., Ives, D. W., & Leamy, M. L. (1973). *Maps and sections showing the distribution and stratigraphy of South Island loess deposits, New Zealand* [map]. N.Z. Soil Bureau.

Cahill, J. P. (1995). Evolution of the Winton Basin, Southland. *New Zealand Journal of Geology and Geophysics*, *38*(2), 245-258. https://doi.org/10.1080/00288306.1995.9514652

Campbell Scientific Inc. (2018). *Instruction Manual: CS650 and CS655 Water Content Reflectometers*.

Carpenter, S. R., Caraco, N. F., Correll, D. L., Howarth, R. W., Sharpley, A. N., & Smith, V. H. (1998). Nonpoint Pollution of Surface Waters with Phosphorus and Nitrogen. *Ecological Applications*, *8*(3), 559-568. https://doi.org/10.1890/1051-0761(1998)008[0559:Nposww]2.0.Co;2

Carrick, S., Buchan, G., Almond, P., & Smith, N. (2011). Atypical early-time infiltration into a structured soil near field capacity: The dynamic interplay between sorptivity, hydrophobicity, and air encapsulation. *Geoderma*, *160*(3), 579-589. https://doi.org/10.1016/j.geoderma.2010.11.006

Catt, J. A. (2001). The agricultural importance of loess. *Earth-Science Reviews*, *54*(1), 213-229. https://doi.org/10.1016/S0012-8252(01)00049-6

Chaney, K., & Swift, R. S. (1984). The influence of organic matter on aggregate stability in some British soils. *Journal of Soil Science*, *35*(2), 223-230. https://doi.org/10.1111/j.1365-2389.1984.tb00278.x

Chaplot, V., & Walter, C. (2003). Subsurface topography to enhance the prediction of the spatial distribution of soil wetness. *Hydrological Processes*, *17*(13), 2567-2580. https://doi.org/10.1002/hyp.1273

Chen, X., & Hu, Q. (2004). Groundwater influences on soil moisture and surface evaporation. *Journal of Hydrology*, *297*(1), 285-300. https://doi.org/https://doi.org/10.1016/j.jhydrol.2004.04.019

Churchman, G. J., & Bruce, J. G. (1987). Relationships between loess deposition and mineral weathering in some soils in Southland, New Zealand. International Symposium on Loess, New Zealand.

Claydon, J. J. (1989). Determination of particle size in fine grained soils – pipette method. Division of Land and Soil Sciences Technical Record (LH5), DSIR Division of Land & Soil Sciences.

Clothier, B. E., Green, S. R., & Deurer, M. (2008). Preferential flow and transport in soil: progress and prognosis. *European Journal of Soil Science*, *59*(1), 2-13. https://doi.org/10.1111/j.1365-2389.2007.00991.x

Critchfield, H. J. (1954). The Growth of Pastoralism in Southland, New Zealand. *Economic Geography*, *30*(4), 283-300. https://doi.org/10.2307/142116

Cuadra, P. E., & Vidon, P. (2011). Storm nitrogen dynamics in tile-drain flow in the US Midwest [journal article]. *Biogeochemistry*, *104*(1), 293-308. https://doi.org/10.1007/s10533-010-9502-x

Davies-Colley, R. J. (2013). River water quality in New Zealand: an introduction and overview. In J. R. Dymond (Ed.), *Ecosystem services in New Zealand: conditions and trends* (pp. 432-447). Manaaki Whenua Press, Landcare Research.

Day, R. L., Calmon, M., Stiteler, J. M., Jabro, J., & Cunningham, R. L. (1998). Water balance and flow patterns in a fragipan using in situ soil block. *Soil Science*, *163*(7), 517-528. https://doi.org/10.1097/00010694-199807000-00001

De Lannoy, G. J. M., Verhoest, N. E. C., Houser, P. R., Gish, T. J., & Van Meirvenne, M. (2006). Spatial and temporal characteristics of soil moisture in an intensively monitored agricultural field (OPE3). *Journal of Hydrology*, *331*(3-4), 719-730. https://doi.org/10.1016/j.jhydrol.2006.06.016

Deasy, C., Brazier, R. E., Heathwaite, A. L., & Hodgkinson, R. (2009). Pathways of runoff and sediment transfer in small agricultural catchments. *Hydrological Processes*, *23*(9), 1349-1358. https://doi.org/https://doi.org/10.1002/hyp.7257

Detty, J. M., & McGuire, K. J. (2010a). Threshold changes in storm runoff generation at a till-mantled headwater catchment. *Water Resources Research*, *46*(7). https://doi.org/10.1029/2009WR008102

Detty, J. M., & McGuire, K. J. (2010b). Topographic controls on shallow groundwater dynamics: implications of hydrologic connectivity between hillslopes and riparian zones in a till mantled catchment. *Hydrological Processes*, *24*(16), 2222-2236. https://doi.org/10.1002/hyp.7656

Dodds, W. K., & Smith, V. H. (2016). Nitrogen, phosphorus, and eutrophication in streams. *Inland Waters*, *6*(2), 155-164. https://doi.org/10.5268/IW-6.2.909

Drewry, J. J., Cameron, K. C., & Buchan, G. D. (2008). Pasture yield and soil physical property responses to soil compaction from treading and grazinga review. *Soil Research*, *46*(3), 237-256. https://doi.org/https://doi.org/10.1071/SR07125

Drewry, J. J., Lowe, J. A. H., & Paton, R. J. (1999). Effect of sheep stocking intensity on soil physical properties and dry matter production on a Pallic Soil in Southland. *New Zealand Journal of Agricultural Research*, *42*(4), 493-499. https://doi.org/10.1080/00288233.1999.9513399

Drewry, J. J., Lowe, J. A. H., & Paton, R. J. (2000). Effect of subsoiling on soil physical properties and pasture production on a Pallic Soil in Southland, New Zealand. *New Zealand Journal of Agricultural Research*, *43*(2), 269-277. https://doi.org/10.1080/00288233.2000.9513427

Drewry, J. J., & Paton, R. J. (2000). Effects of cattle treading and natural amelioration on soil physical properties and pasture under dairy farming in Southland, New Zealand. *New Zealand Journal of Agricultural Research*, *43*(3), 377-386. https://doi.org/10.1080/00288233.2000.9513438

Duque, L. F. (2020). *IETD: Inter-Event Time Definition*. In (Version 1.0.0) https://CRAN.R-project.org/package=IETD

Edemsky, D., Popov, A., Prokopovich, I., & Garbatsevich, V. (2021). Airborne Ground Penetrating Radar, Field Test. *Remote Sensing*, *13*(4), 667. https://doi.org/10.3390/rs13040667

Ekanayake, J., Carrick, S., & Penny, V. (2019). *MWLR Infiltrometer Manual (Contract Report LC3616)*. Manaaki Whenua Landcare Research.

Ellis, T., Hodgetts, J., & McMecking, J. (2018). *Stream bank erosion in Murihiku/Southland and why we should think differently about sediment (Report No 2018-06)*. Environment Southland.

Environment Southland. *Southland Physiographics Zone - Gleyed Zone (Technical Information)*.

Environment Southland. (2014). Land Use Change – Agriculture. The changing face of farming in Southland. In. Invercargill, NZ: Environment Southland (Southland Regional Council).

Environment Southland. (2018). *Environmental Data Archive: Air Temperature (Degrees Celsius) at Winton Essex Street. Subset used: 24 Sep 2006 - 1 Dec 2018*.

Esri. (2021). *Coincident Points (Environment setting)*. Retrieved 10/01 from https://desktop.arcgis.com/en/arcmap/latest/tools/environments/coincident-points.htm

Evans, C. V., & Franzmeier, D. P. (1988). Color index values to represent wetness and aeration in some Indiana soils. *Geoderma*, *41*(3-4), 353-368. https://doi.org/10.1016/0016-7061(88)90070-5

Ewans, R. (2016). *Environment Southland Wetland Inventory Project: Monitoring wetland extent on non-public conservation land in the Southland region - Interim report for 2016.*

Farrick, K. K., & Branfireun, B. A. (2014). Soil water storage, rainfall and runoff relationships in a tropical dry forest catchment. *Water Resources Research*, *50*(12), 9236-9250. https://doi.org/10.1002/2014WR016045

Fausey, N. R., & Schwab, G. O. (1969). Soil Moisture Content, Tilth, and Soybean (Glycine max.) Response with Surface and Subsurface Drainage1. *Agronomy Journal*, *61*(4), 554-557. https://doi.org/10.2134/agronj1969.00021962006100040021x

Fayer, M. J., & Hillel, D. (1986). Air Encapsulation: I. Measurement in a Field Soil. *Soil Science Society of America Journal*, *50*(3), 568-572. https://doi.org/https://doi.org/10.2136/sssaj1986.03615995005000030005x

Feick, S., Siebert, S., & Döll, P. (2005). *A Digital Global Map of Artificially Drained Agricultural Areas*. Institute of Physical Geography, Frankfurt University. https://doi.org/10.13140/2.1.3971.3923

Fernández-Gálvez, J., Pollacco, J. A. P., Lassabatere, L., Angulo-Jaramillo, R., & Carrick, S. (2019). A general Beerkan Estimation of Soil Transfer parameters method predicting hydraulic parameters of any unimodal water retention and hydraulic conductivity curves: Application to the Kosugi soil hydraulic model without using particle size distribution data. *Advances in Water Resources*, *129*, 118-130. https://doi.org/10.1016/j.advwatres.2019.05.005

Fernández-Gálvez, J., Pollacco, J. A. P., Lilburne, L., McNeill, S., Carrick, S., Lassabatere, L., & Angulo-Jaramillo, R. (2021). Deriving physical and unique bimodal soil Kosugi hydraulic parameters from inverse modelling. *Advances in Water Resources*, *153*, 103933. https://doi.org/10.1016/j.advwatres.2021.103933

Fong, Y., Huang, Y., Gilbert, P. B., & Permar, S. R. (2017). chngpt: threshold regression model estimation and inference. *BMC Bioinformatics*, *18*(1), 454. https://doi.org/10.1186/s12859-017-1863-x

Franzluebbers, A. J. (2002). Water infiltration and soil structure related to organic matter and its stratification with depth. *Soil and Tillage Research*, *66*(2), 197-205. https://doi.org/10.1016/S0167-1987(02)00027-2

Freeman, M., Robson, M., L., L., McCallum-Clark, M., Cooke, A., & McNae, D. (2016). *Using OVERSEER in regulation - technical resources and guidance for the appropriate and consistent use of OVERSEER by regional councils, August 2016. Report prepared by Freeman Environmental Ltd for the OVERSEER Guidance Project Board*.

Garrido, F., & Helmhart, M. (2012). Lead and soil properties distributions in a roadside soil: Effect of preferential flow paths. *Geoderma*, *170*, 305-313. https://doi.org/https://doi.org/10.1016/j.geoderma.2011.10.017

Gates, J. B., Scanlon, B. R., Mu, X., & Zhang, L. (2011). Impacts of soil conservation on groundwater recharge in the semi-arid Loess Plateau, China. *Hydrogeology Journal*, *19*(4), 865-875. https://doi.org/10.1007/s10040-011-0716-3

Gilpin, B. J., Walker, T., Paine, S., Sherwood, J., Mackereth, G., Wood, T., Hambling, T., Hewison, C., Brounts, A., Wilson, M., Scholes, P., Robson, B., Lin, S., Cornelius, A., Rivas, L., Hayman, D. T. S., French, N. P., Zhang, J., Wilkinson, D. A., . . . Jones, N. (2020). A large scale waterborne Campylobacteriosis outbreak, Havelock North, New Zealand. *Journal of Infection*, *81*(3), 390-395. https://doi.org/https://doi.org/10.1016/j.jinf.2020.06.065

Godwin, R. J., Spoor, G., & Leeds-Harrison, P. (1981). An experimental investigation into the force mechanics and resulting soil disturbance of mole ploughs. *Journal of Agricultural Engineering Research*, *26*(6), 477-497. https://doi.org/https://doi.org/10.1016/0021-8634(81)90081-0

Gomi, T., Sidle, R. C., Miyata, S., Kosugi, K. i., & Onda, Y. (2008). Dynamic runoff connectivity of overland flow on steep forested hillslopes: Scale effects and runoff transfer. *Water Resources Research*, *44*(8). https://doi.org/10.1029/2007WR005894

Goss, M. J., Harris, G. L., & Howse, K. R. (1983). Functioning of mole drains in a clay soil. *Agricultural Water Management*, *6*(1), 27-30. https://doi.org/10.1016/0378-3774(83)90023-9

Gradwell, M. W., & Birrell, K. S. (1979). Methods for Physical Analysis of Soils. New Zealand Soil Bureau Scientific Report 10C.

Gramlich, A., Stoll, S., Stamm, C., Walter, T., & Prasuhn, V. (2018). Effects of artificial land drainage on hydrology, nutrient and pesticide fluxes from agricultural fields – A review. *Agriculture, Ecosystems & Environment*, *266*, 84-99. https://doi.org/10.1016/j.agee.2018.04.005

Grangeon, T., Ceriani, V., Evrard, O., Grison, A., Vandromme, R., Gaillot, A., Cerdan, O., & Salvador-Blanes, S. (2021). Quantifying hydro-sedimentary transfers in a lowland tile-drained agricultural catchment. *CATENA*, *198*, 105033. https://doi.org/https://doi.org/10.1016/j.catena.2020.105033

Grant, D. (2008). *Southland region - Geology and landforms, Te Ara - the Encyclopedia of New Zealand*. Retrieved 17 February 2022 from http://www.TeAra.govt.nz/en/southland-region/page-2

Grayson, R. B., Western, A. W., Chiew, F. H. S., & Blöschl, G. (1997). Preferred states in spatial soil moisture patterns: Local and nonlocal controls. *Water Resources Research*, *33*(12), 2897-2908. https://doi.org/10.1029/97WR02174

Greenwood, P. B. (1999). *Irrigation of Farm Dairy Effluent in Southland. SoilWork Ltd Report SW-MR-0196.*

Griffiths, E., Webb, T. H., Watt, J. P. C., & Singleton, P. L. (1999). Development of soil morphological descriptors to improve field estimation of hydraulic conductivity. *Soil Research*, *37*(5), 971-982. https://doi.org/10.1071/SR98066

Gruber, S., & Peckham, S. (2009). Chapter 7 Land-Surface Parameters and Objects in Hydrology. In T. Hengl & H. I. Reuter (Eds.), *Developments in Soil Science* (Vol. 33, pp. 171-194). Elsevier. https://doi.org/https://doi.org/10.1016/S0166-2481(08)00007-X

Guo, X., Fu, Q., Hang, Y., Lu, H., Gao, F., & Si, J. (2020). Spatial Variability of Soil Moisture in Relation to Land Use Types and Topographic Features on Hillslopes in the Black Soil (Mollisols) Area of Northeast China. *Sustainability*, *12*(9). https://doi.org/10.3390/su12093552

Gupta, R. P., & Swartzendruber, D. (1964). Entrapped Air Content and Hydraulic Conductivity of Quartz Sand During Prolonged Liquid Flow. *Soil Science Society of America Journal*, *28*(1), 9-12. https://doi.org/https://doi.org/10.2136/sssaj1964.03615995002800010016x

Gurdak, J. J., Walvoord, M. A., & McMahon, P. B. (2008). Susceptibility to Enhanced Chemical Migration from Depression-Focused Preferential Flow, High Plains Aquifer. *Vadose Zone Journal*, *7*(4), 1218-1230. https://doi.org/10.2136/vzj2007.0145

Hallard, M., & Armstrong, A. C. (1992). Observations of water movement to and within mole drainage channels. *Journal of Agricultural Engineering Research*, *52*, 309-315. https://doi.org/10.1016/0021-8634(92)80069-5

Hansen, A. L., Refsgaard, J. C., Baun Christensen, B. S., & Jensen, K. H. (2013). Importance of including small-scale tile drain discharge in the calibration of a coupled groundwater-surface water catchment model [Article]. *Water Resources Research*, *49*(1), 585-603. https://doi.org/10.1029/2011WR011783

Hardie, M., Cotching, W., Doyle, R., Holz, Lisson, & Mattern. (2010). *Effect of antecedent soil moisture on preferential flow in a texture-contrast soil* (Vol. 398). https://doi.org/10.1016/j.jhydrol.2010.12.008

Havens, S. M., Hedman, C. J., Hemming, J. D. C., Mieritz, M. G., Shafer, M. M., & Schauer, J. J. (2020). Occurrence of estrogens, androgens and progestogens and estrogenic activity in surface water runoff from beef and dairy manure amended crop fields. *Science of The Total Environment*, *710*, 136247. https://doi.org/https://doi.org/10.1016/j.scitotenv.2019.136247

Hawley, M. E., Jackson, T. J., & McCuen, R. H. (1983). Surface soil moisture variation on small agricultural watersheds. *Journal of Hydrology*, *62*(1), 179-200. https://doi.org/10.1016/0022-1694(83)90102-6

Hewitt, A. E. (1998). *New Zealand Soil Classification*. Manaaki Whenua Press, Landcare Research.

Hewitt, A. E., Balks, M. R., & Lowe, D. J. (2021). *The Soils of Aotearoa New Zealand*. Springer Nature Switzerland AG.

Hewitt, A. E., & Shepherd, T. G. (1997). Structural vulnerability of New Zealand soils. *Soil Research*, *35*(3), 461-474. https://doi.org/10.1071/S96074

Hill, K., Hodgkinson, R., Harris, D., & Newell Price, P. (2018). Field drainage guide. Principles, installations and maintenance. In: Agriculture and Horticulture Development Board.

Hillel, D. (1982). *Introduction to soil physics*. Academic Press, Inc. https://doi.org/10.1016/C2009-0-03052-9

Hooghoudt, S. B. (1937). Bijdragen tot de kennis van eenige natuurkundige grootheden van den grond, 6. *Versl. Landb. Ond.* (43), 461-676.

Horne, D. J. (1985). *Some consequences of mole draining a yellow-grey earth under pasture : a thesis presented in partial fulfilment of the requirements for the degree of Doctor of Philosophy in Soil Science at Massey University* [Doctoral, Massey University].

Horne, D. J., & Scotter, D. R. (2016). The available water holding capacity of soils under pasture. *Agricultural Water Management*, *177*, 165-171.

Houlbrooke, D., Drewry, J. J., Hu, W., Laurenson, S., & Carrick, S. (2021). *Soil structure: its importance to resilient pastures in New Zealand (review)* Resilient Pastures Symposium 2021

Houlbrooke, D. J., Drewry, J. J., Monaghan, R. M., Paton, R. J., Smith, L. C., & Littlejohn, R. P. (2009). Grazing strategies to protect soil physical properties and maximise pasture yield on a Southland dairy farm. *New Zealand Journal of Agricultural Research*, *52*(3), 323-336. https://doi.org/10.1080/00288230909510517

Houlbrooke, D. J., Horne, D. J., Hedley, M. J., Hanly, J. A., Scotter, D. R., & Snow, V. O. (2004). Minimising surface water pollution resulting from farm‐dairy effluent application to mole‐pipe drained soils. I. An evaluation of the deferred irrigation system for sustainable land treatment in the Manawatu. *New Zealand Journal of Agricultural Research*, *47*(4), 405-415. https://doi.org/10.1080/00288233.2004.9513609

Houlbrooke, D. J., Horne, D. J., Hedley, M. J., Hanly, J. A., & Snow, V. O. (2004). A review of literature on the land treatment of farm‐dairy effluent in New Zealand and its impact on water quality. *New Zealand Journal of Agricultural Research*, *47*(4), 499-511. https://doi.org/10.1080/00288233.2004.9513617

Hu, W., Drewry, J., Beare, M., Eger, A., & Müller, K. (2021). Compaction induced soil structural degradation affects productivity and environmental outcomes: A review and New Zealand case study. *Geoderma*, *395*, 115035. https://doi.org/10.1016/j.geoderma.2021.115035

Huang, T., Ma, B., Pang, Z., Li, Z., & Long, Y. (2020). How does precipitation recharge groundwater in loess aquifers? Evidence from multiple environmental tracers. *Journal of Hydrology*, *583*, 124532. https://doi.org/10.1016/j.jhydrol.2019.124532

Huang, T., Pang, Z., Liu, J., Ma, J., & Gates, J. (2017). Groundwater recharge mechanism in an integrated tableland of the Loess Plateau, northern China: insights from environmental tracers. *Hydrogeology Journal*, *25*(7), 2049-2065. https://doi.org/10.1007/s10040-017-1599-8

Huang, Y., Evaristo, J., & Li, Z. (2019). Multiple tracers reveal different groundwater recharge mechanisms in deep loess deposits. *Geoderma*, *353*, 204-212. https://doi.org/10.1016/j.geoderma.2019.06.041

Hughes, B., Wilson, K., Rissman, C., & Rodway, E. (2019). *Physiographics of Southland: Development and application of a classification system for managing land use effects on water quality in Southland (Technical Report 2016/11). Version 2 - Final*. Southland Regional Council (Environment Southland).

Hughes, M. W., Almond, P. C., & Roering, J. J. (2009). *Increased sediment transport via bioturbation at the last glacial-interglacial transition* (Vol. 37). https://doi.org/10.1130/G30159A.1

Hughes, M. W., Almond, P. C., Roering, J. J., & Tonkin, P. J. (2010). Late Quaternary loess landscape evolution on an active tectonic margin, Charwell Basin, South Island, New Zealand. *Geomorphology*, *122*(3), 294-308. https://doi.org/10.1016/j.geomorph.2009.09.034

Hupet, F., & Vanclooster, M. (2002). Intraseasonal dynamics of soil moisture variability within a small agricultural maize cropped field. *Journal of Hydrology*, *261*(1), 86-101. https://doi.org/10.1016/S0022-1694(02)00016-1

International Commission on Irrigation and Drainage. (2017). *World drained areas*. International Commission on Irrigation and Drainage. http://www.icid.org/world - drained - area.pdf

Jackson, C. R., Bitew, M., & Du, E. (2014). When interflow also percolates: downslope travel distances and hillslope process zones. *Hydrological Processes*, *28*(7), 3195-3200. https://doi.org/10.1002/hyp.10158

Jacobs, P. M., & Mason, J. A. (2007). Late Quaternary climate change, loess sedimentation, and soil profile development in the central Great Plains: A pedosedimentary model. *Geological Society of America Bulletin*, *119*(3-4), 462-475. https://doi.org/10.1130/b25868.1

Jha, M. K., & Koga, K. (1995). Mole drainage: Prospective drainage solution to Bangkok clay soils. *Agricultural Water Management*, *28*(3), 253-270. https://doi.org/10.1016/0378-3774(95)01162-C

Joe, E. N., & Watt, J. P. C. (1984). Soil water characterisation of 11 soils in central and coastal Otago, New Zealand. *N.Z. Soil Bureau SWAMP Data sheets*, pp 1-11.

Joel, A., Messing, I., Seguel, O., & Casanova, M. (2002). Measurement of surface water runoff from plots of two different sizes. *Hydrological Processes*, *16*(7), 1467-1478. https://doi.org/10.1002/hyp.356

Johnson, D. L. (1990). Biomantle Evolution and the Redistribution of Earth Materials and Artifacts. *Soil Science*, *149*(2), 84-102. https://doi.org/10.1097/00010694-199002000-00004

Johnson, D. L., Domier, J. E. J., & Johnson, D. N. (2005). Animating the biodynamics of soil thickness using process vector analysis: a dynamic denudation approach to soil formation. *Geomorphology*, *67*(1), 23-46. https://doi.org/10.1016/j.geomorph.2004.08.014

Johnson, D. L., Keller, E. A., & Rockwell, T. K. (1990). Dynamic Pedogenesis: New Views on Some Key Soil Concepts, and a Model for Interpreting Quaternary Soils. *Quaternary Research*, *33*(3), 306-319. https://doi.org/10.1016/0033-5894(90)90058-S

Jol, H. M. (2008). *Ground Penetrating Radar Theory and Applications*. Elsevier Science. https://books.google.co.nz/books?id=y__uIi-5RvgC

Kaiser, H. F. (1960). The Application of Electronic Computers to Factor Analysis. *Educational and Psychological Measurement*, *20*(1), 141-151. https://doi.org/10.1177/001316446002000116

Karásek, P., & Nováková, E. (2020). Agricultural Tile Drainage Detection within the Year Using Ground Penetrating Radar [journal article]. *Journal of Ecological Engineering*, *21*(4), 203-211. https://doi.org/10.12911/22998993/119976

Kellaway, R. G. (1970). *The changing agricultural geography of Southland 1878-1940* University of Canterbury].

Kelly, B. P., & Pomes, M. L. (1998). Preferential Flow and Transport of Nitrate and Bromide in Clay pan Soil. *Groundwater*, *36*(3), 484-494. https://doi.org/https://doi.org/10.1111/j.1745-6584.1998.tb02820.x

Kemp, R. A., & McIntosh, P. D. (1989). Genesis of a texturally banded soil in Southland, New Zealand. *Geoderma*, *45*(1), 65-81. https://doi.org/10.1016/0016-7061(89)90056-6

Killick, M. (2018). *lnvestigation of cracking soils: Heddon Bush, January 2018.* https://www.es.govt.nz/repository/libraries/id:26gi9ayo517q9stt81sd/hierarchy/environment/consents/notified-consents/2019/Woldwide%20Four%20Ltd%20and%20Woldwide%20Five%20Ltd/Investigation%20of%20Cracking%20Soils%20-%20WW4%20and%20WW5.pdf

King, K. W., Fausey, N. R., & Williams, M. R. (2014). Effect of subsurface drainage on streamflow in an agricultural headwater watershed. *Journal of Hydrology*, *519*, 438-445. https://doi.org/10.1016/j.jhydrol.2014.07.035

King, K. W., Williams, M. R., Macrae, M. L., Fausey, N. R., Frankenberger, J., Smith, D. R., Kleinman, P. J., & Brown, L. C. (2015). Phosphorus transport in agricultural subsurface drainage: a review. *J Environ Qual*, *44*(2), 467-485. https://doi.org/10.2134/jeq2014.04.0163

Kirkby, M. (2002). Modelling the interactions between soil surface properties and water erosion. *CATENA*, *46*(2), 89-102. https://doi.org/10.1016/S0341-8162(01)00160-6

Klaiber, L. B., Kramer, S. R., & Young, E. O. (2020). Impacts of Tile Drainage on Phosphorus Losses from Edge-of-Field Plots in the Lake Champlain Basin of New York. *Water*, *12*(2), 328.

Klaus, J., & Jackson, C. R. (2018). Interflow Is Not Binary: A Continuous Shallow Perched Layer Does Not Imply Continuous Connectivity. *Water Resources Research*, *54*(9), 5921-5932. https://doi.org/https://doi.org/10.1029/2018WR022920

Knadel, M., Thomsen, A., Schelde, K., & Greve, M. H. (2015). Soil organic carbon and particle sizes mapping using vis–NIR, EC and temperature mobile sensor platform. *Computers and Electronics in Agriculture*, *114*, 134-144. https://doi.org/10.1016/j.compag.2015.03.013

Koch, S., Bauwe, A., & Lennartz, B. (2013). Application of the SWAT Model for a Tile-Drained Lowland Catchment in North-Eastern Germany on Subbasin Scale. *Water Resources Management*, *27*(3), 791-805. https://doi.org/10.1007/s11269-012-0215-x

Koganti, T., Ghane, E., Martinez, L. R., Iversen, B. V., & Allred, B. J. (2021). Mapping of Agricultural Subsurface Drainage Systems Using Unmanned Aerial Vehicle Imagery and Ground Penetrating Radar. *Sensors*, *21*(8), 2800.

Kokulan, V., Macrae, M. L., Ali, G. A., & Lobb, D. A. (2019). Hydroclimatic controls on runoff activation in an artificially drained, near-level vertisolic clay landscape in a Prairie climate. *Hydrological Processes*, *33*(4), 602-615. https://doi.org/10.1002/hyp.13347

Kuang, B., Mahmood, H. S., Quraishi, M. Z., Hoogmoed, W. B., Mouazen, A. M., & van Henten, E. J. (2012). Chapter four - Sensing Soil Properties in the Laboratory, In Situ, and On-Line: A Review. In D. L. Sparks (Ed.), *Advances in Agronomy* (Vol. 114, pp. 155-223). Academic Press. https://doi.org/https://doi.org/10.1016/B978-0-12-394275-3.00003-1

Lai, X., Zhu, Q., Castellano, M. J., & Liao, K. (2022). Soil rock fragments: Unquantified players in terrestrial carbon and nitrogen cycles. *Geoderma*, *406*, 115530. https://doi.org/10.1016/j.geoderma.2021.115530

Langer, S., Cichota, R., Thomas, S., Wallace, D., Van der Klei, G., George, M., Johns, T., Almond, P., Maley, S., Arnold, N., Hu, W., Srinivasan, M. S., Rajanayaka, C., Dodson, M., Hayman, R., & Ghimire, C. (2020). Understanding water losses from irrigated pastures on loess-derived hillslopes. *Journal of New Zealand Grasslands*, *82*, 103-110. https://doi.org/10.33584/jnzg.2020.82.438

Lassabatere, L., Angulo-Jaramillo, R., & Winiarski, T. (2013). BEST method: Characterization of soil unsaturated hydraulic properties. In I. R. Berdugo, Caicedo, B., Hoyos, L., Murillo, C., & Esteban, C. J. (Ed.), *Advances in Unsaturated Soils* (Vol. 1, pp. 545-550). Taylor & Francis Group. https://doi.org/10.1201/b14393-78

Leamy, M. L., Milne, J. D. G., Pullar, W. A., & Bruce, J. G. (1973). Paleopedology and soil stratigraphy in the New Zealand Quaternary succession. *New Zealand Journal of Geology and Geophysics*, *16*(3), 723-744. https://doi.org/10.1080/00288306.1973.10431393

Leco. (2003). Total/organic carbon and nitrogen in soils. LECO Corporation, St. Joseph, MO, Organic Application Note 203-821-165.

Leeds-Harrison, P., Spoor, G., & Godwin, R. J. (1982). Water flow to mole drains. *Journal of Agricultural Engineering Research*, *27*(2), 81-91. https://doi.org/10.1016/0021-8634(82)90095-6

Leng, M., Yu, Y., Wang, S., & Zhang, Z. (2020). Simulating the Hydrological Processes of a Meso-Scale Watershed on the Loess Plateau, China. *Water*, *12*(3). https://doi.org/10.3390/w12030878

Lilburne, L. R., Hewitt, A. E., Webb, T. H., & Carrick, S. (2004). *S-map – a new soil database for New Zealand* Australian New Zealand Soils Conference, University of Sydney, Australia.

Lin, H. (2003). Hydropedology: Bridging Disciplines, Scales, and Data. *Vadose Zone Journal*, *2*(1), 1-11. https://doi.org/https://doi.org/10.2136/vzj2003.1000

Lin, H. S., Kogelmann, W., Walker, C., & Bruns, M. A. (2006). Soil moisture patterns in a forested catchment: A hydropedological perspective. *Geoderma*, *131*(3), 345-368. https://doi.org/10.1016/j.geoderma.2005.03.013

Lin, H. S., McInnes, K. J., Wilding, L. P., & Hallmark, C. T. (1998). Macroporosity and initial moisture effects on infiltration rates in vertisols and vertic intergrades. *Soil Science*, *163*(1), 2-8. https://doi.org/10.1097/00010694-199801000-00002

Lin, R., & Wei, K. (2006). Tritium profiles of pore water in the Chinese loess unsaturated zone: Implications for estimation of groundwater recharge. *Journal of Hydrology*, *328*(1-2), 192-199. https://doi.org/10.1016/j.jhydrol.2005.12.010

Linden, D. R., & Dixon, R. M. (1976). Soil Air Pressure Effects on Route and Rate of Infiltration. *Soil Science Society of America Journal*, *40*(6), 963-965. https://doi.org/10.2136/sssaj1976.03615995004000060042x

Linna, P., Halla, A., & Narra, N. (2022). Ground-Penetrating Radar-Mounted Drones in Agriculture. In T. Lipping, P. Linna, & N. Narra (Eds.), *New Developments and Environmental Applications of Drones*. Springer. https://doi.org/10.1007/978-3-030-77860-6_8

Lowe, D., Tonkin, P. J., Palmer, A., & Palmer, J. (2008). Dusty horizons (A Continent on the Move, 1st edition.). In (pp. 270-273).

Lynch, J., Marschner, P., & Rengel, Z. (2012). Chapter 13 - Effect of Internal and External Factors on Root Growth and Development. In P. Marschner (Ed.), *Marschner's Mineral Nutrition of Higher Plants (Third Edition)* (pp. 331-346). Academic Press. https://doi.org/https://doi.org/10.1016/B978-0-12-384905-2.00013-3

Macara, G. R. (2013). *The Climate and Weather of Southland* (NIWA Sience and Technology Series, Issue.

Macrae, M. L., Ali, G. A., King, K. W., Plach, J. M., Pluer, W. T., Williams, M., Morison, M. Q., & Tang, W. (2019). Evaluating Hydrologic Response in Tile-Drained Landscapes: Implications for Phosphorus Transport. *J Environ Qual*, *48*(5), 1347-1355. https://doi.org/https://doi.org/10.2134/jeq2019.02.0060

Magesan, G. N., White, R. E., & Scotter, D. R. (1995). The influence of flow rate on the concentration of indigenous and applied solutes in mole-pipe drain effluent. *Journal of Hydrology*, *172*(1), 23-30. https://doi.org/10.1016/0022-1694(95)02751-A

Magesan, G. N., White, R. E., & Scotter, D. R. (1996). Nitrate leaching from a drained, sheep-grazed pasture. I. Experimental results and environmental implications. *Soil Research*, *34*(1), 55-67. https://doi.org/10.1071/SR9960055

Magesan, G. N., White, R. E., Scotter, D. R., & Bolan, N. S. (1994). Estimating leaching losses from sub-surface drained soils. *Soil Use and Management*, *10*(2), 87-93. https://doi.org/10.1111/j.1475-2743.1994.tb00464.x

Manaaki Whenua - Landcare Research. (2022). S-Map Online. The digital soil map for New Zealand. Version: 4.1.107. https://smap.landcareresearch.co.nz/

Manaaki Whenua Landcare Research. (2000). *FSL - Permeability Profile* https://lris.scinfo.org.nz/layer/48105-fsl-permeability-profile/

Manaaki Whenua Landcare Research. (2018). *Smap Soil Drainage February 2018* https://lris.scinfo.org.nz/layer/93657-smap-soil-drainage-february-2018/

Manaaki Whenua Landcare Research. (2022). *Pukemutu_6a.1* (Soil Report, Issue. https://smap.landcareresearch.co.nz/

Manderson, A. (2018). *Mapping the extent of artificial drainage in New Zealand. Contract Report LC3325*. Manaaki Whenua – Landcare Research.

Manning, R., Griffith, P., Pigot, T. F., & Vernon-Harcourt, L. F. (1890). *On the flow of water in open channels and pipes*.

Martini, E., Wollschläger, U., Kögler, S., Behrens, T., Dietrich, P., Reinstorf, F., Schmidt, K., Weiler, M., Werban, U., & Zacharias, S. (2015). *Spatial and Temporal Dynamics of Hillslope-Scale Soil Moisture Patterns: Characteristic States and Transition Mechanisms*. https://doi.org/10.2136/vzj2014.10.0150

McCraw, J. D. (1975). *Quaternary airfall deposits of New Zealand* (Vol. 13). Bulletin of Royal Society of New Zealand.

McDaniel, P. A., & Falen, A. L. (1994). Temporal and Spatial Patterns of Episaturation in a Fragixeralf Landscape. *Soil Science Society of America Journal*, *58*(5), 1451-1457. https://doi.org/https://doi.org/10.2136/sssaj1994.03615995005800050025x

McDaniel, P. A., Regan, M. P., Brooks, E., Boll, J., Barndt, S., Falen, A., Young, S. K., & Hammel, J. E. (2008). Linking fragipans, perched water tables, and catchment-scale hydrological processes. *CATENA*, *73*(2), 166-173. https://doi.org/10.1016/j.catena.2007.05.011

McDonnell, J. J., Sivapalan, M., Vaché, K., Dunn, S., Grant, G., Haggerty, R., Hinz, C., Hooper, R., Kirchner, J., Roderick, M. L., Selker, J., & Weiler, M. (2007). Moving beyond heterogeneity and process complexity: A new vision for watershed hydrology. *Water Resources Research*, *43*(7). https://doi.org/https://doi.org/10.1029/2006WR005467

McGlone, M. S., & Bathgate, J. L. (1983). Vegetation and climate history of the Longwood Range, South Island, New Zealand, 12 000 B. P. to the present. *New Zealand Journal of Botany*, *21*(3), 293-315. https://doi.org/10.1080/0028825X.1983.10428560

McGuire, K. J., & McDonnell, J. J. (2010). Hydrological connectivity of hillslopes and streams: Characteristic time scales and nonlinearities. *Water Resources Research*, *46*(10). https://doi.org/https://doi.org/10.1029/2010WR009341

McIntosh, P. D. (1994). *Guide to the Soils of the Kaihiku-Hokonui Land Region* (Vol. 4). Manaaki Whenua Landcare Research.

McKenzie, N. J., & Ryan, P. J. (1999). Spatial prediction of soil properties using environmental correlation. *Geoderma*, *89*(1-2), 67-94. https://doi.org/10.1016/s0016-7061(98)00137-2

McLeod, M., Aislabie, J., Ryburn, J., & McGill, A. (2008). Regionalizing potential for microbial bypass flow through New Zealand soils. *J Environ Qual*, *37*(5), 1959-1967. https://doi.org/10.2134/jeq2007.0572

McLeod, M., Aislabie, J., Ryburn, J., McGill, A., & Taylor, M. (2003). Microbial and chemical tracer movement through two Southland soils, New Zealand. *Soil Research*, *41*(6). https://doi.org/10.1071/sr02149

McMillan, H. K., & Srinivasan, M. S. (2015). Characteristics and controls of variability in soil moisture and groundwater in a headwater catchment. *Hydrology and Earth System Sciences*, *19*(4), 1767-1786. https://doi.org/10.5194/hess-19-1767-2015

McPhillips, M. (1979). *Drainage of Farmland*. Ministry of Agriculture and Fisheries.

Meles Bitew, M., Jackson, C. R., Goodrich, D. C., Younger, S. E., Griffiths, N. A., Vaché, K. B., & Rau, B. (2020). Dynamic domain kinematic modelling for predicting interflow over leaky impeding layers. *Hydrological Processes*, *34*(13), 2895-2910. https://doi.org/https://doi.org/10.1002/hyp.13778

Messing, I., & Wesström, I. (2006). Efficiency of old tile drain systems in soils with high clay content: differences in the trench backfill zone versus the zone midway between trenches. *Irrigation and Drainage*, *55*(5), 523-531. https://doi.org/10.1002/ird.277

Metson, A. J., Blakemore, L. C., & Rhoades, D. A. (1979). Methods for the determination of soil organic carbon: a review, and application to New Zealand soils. NZ Journal of Science 22:205 -228.

MfE, & StatsNZ. (2015a). *Estimated contemporary and pre-human wetland area, by region (2008 estimate)*. https://data.mfe.govt.nz/table/52593-estimated-contemporary-and-pre-human-wetland-area-by-region-2008-estimate/

MfE & StatsNZ. (2015b). *Prediction of wetlands before humans arrived. Environmental Reporting Dataset*. https://data.mfe.govt.nz/layer/52677-prediction-of-wetlands-before-humans-arrived/

MfE & StatsNZ. (2016). *Current wetland extent, 2013. Environmental Reporting Dataset* Ministry for the Environment and Statistics New Zealand. https://data.mfe.govt.nz/layer/52676-current-wetland-extent-2013/

Miller, F. P., Holowaychuk, N., & Wilding, L. P. (1971). Canfield Silt Loam, a Fragiudalf: I. Macromorphological, Physical, and Chemical Properties. *Soil Science Society of America Journal*, *35*(2), 319-324. https://doi.org/https://doi.org/10.2136/sssaj1971.03615995003500020040x

Milne, G., Beckley, V. A., Gethin Jones, G. H., Martin, W. S., Griffith, G., & Raymond, L. W. (1936). *Amani memoirs: A provisional soil map of East Africa (Kenya, Uganda, Tanganyika, and Zanzibar). With explanatory memoir*.

Milne, J. D. G., Clayden, B., Singleton, P., & Wilson, A. (1995). *Soil description handbook*. Manaaki Whenua Press. https://doi.org/10.7931/DL1JG6

Ministry for the Environment. (2020a). *LUCAS NZ Land Use Map 1990 2008 2012 2016 v008* https://data.mfe.govt.nz/layer/52375-lucas-nz-land-use-map-1990-2008-2012-2016-v008/

Ministry for the Environment. (2020b). National Policy Statement for Freshwater Management 2020. ME1518

Ministry for the Environment & Ministry for Primary Industries. (2021). *Managing intensive winter grazing: A discussion document on proposed changes to intensive winter grazing regulations*. Ministry for the Environment and Ministry for Primary Industries.

Ministry of Health. (2012). *Communicable Disease Control Manual*.

Monaghan, R. M. (2014). *The influence of land use, soil properties and seasonal factors on contaminant accumulation and loss from farming systems to water* (RE500/2014/106). E. Southland.

Monaghan, R. M., Paton, R. J., & Drewry, J. J. (2002). Nitrogen and phosphorus losses in mole and tile drainage from a cattle ‐ grazed pasture in eastern Southland. *New Zealand Journal of Agricultural Research*, *45*(3), 197-205. https://doi.org/10.1080/00288233.2002.9513510

Monaghan, R. M., Paton, R. J., Smith, L. C., Drewry, J. J., & Littlejohn, R. P. (2005). The impacts of nitrogen fertilisation and increased stocking rate on pasture yield, soil physical condition and nutrient losses in drainage from a cattle ‐ grazed pasture. *New Zealand Journal of Agricultural Research*, *48*(2), 227-240. https://doi.org/10.1080/00288233.2005.9513652

Monaghan, R. M., & Smith, C. (2003, 14-21 August 2002). *Effluent movement through mole-tile drainage systems in a grazed, effluent-irrigated, New Zealand dairy pasture* 17th World Congress of Soil Science, Bangkok, Thailand.

Monaghan, R. M., & Smith, L. C. (2004). Minimising surface water pollution resulting from farm ‐ dairy effluent application to mole ‐ pipe drained soils. II. The contribution of preferential flow of effluent to whole ‐ farm pollutant losses in subsurface drainage from a West Otago dairy farm. *New Zealand Journal of Agricultural Research*, *47*(4), 417-428. https://doi.org/10.1080/00288233.2004.9513610

Monaghan, R. M., Smith, L. C., & Muirhead, R. W. (2016). Pathways of contaminant transfers to water from an artificially-drained soil under intensive grazing by dairy cows. *Agriculture, Ecosystems & Environment*, *220*, 76-88. https://doi.org/10.1016/j.agee.2015.12.024

Monaghan, R. M., Wilcock, R. J., Smith, L. C., Tikkisetty, B., Thorrold, B. S., & Costall, D. (2007). Linkages between land management activities and water quality in an intensively farmed catchment in southern New Zealand. *Agriculture, Ecosystems & Environment*, *118*(1), 211-222. https://doi.org/https://doi.org/10.1016/j.agee.2006.05.016

Moore, D. S., & Kirkland, S. (2007). *The basic practice of statistics* (Vol. 2). WH Freeman New York.

Moran, E., Pearson, L., Couldrey, M., & Eyre, K. (2017). *The Southland Economic Project: Agriculture and Forestry. Technical Report. Publication no. 2017-02.*

Moriarty, E. M., McEwan, N., Mackenzie, M., Karki, N., Sinton, L. W., & Wood, D. R. (2011). Incidence and prevalence of microbial indicators and pathogens in ovine faeces in New Zealand. *New Zealand Journal of Agricultural Research*, *54*(2), 71-81. https://doi.org/10.1080/00288233.2011.556129

Morrison, R. B. (1978). Quaternary soil stratigraphy - concepts, methods and problems. *Quaternary soils*, 77-108.

National Committee on Soil and Terrain. (2009). *Australian Soil and Land Survey Field Handbook* (3 ed.). CSIRO Publishing. https://doi.org/10.1071/9780643097117

Negri, S., Raimondo, E., D'Amico, M. E., Stanchi, S., Basile, A., & Bonifacio, E. (2021). Loess-derived polygenetic soils of North-Western Italy: A deep characterization of particle size, shape and color to draw insights about the past. *CATENA*, *196*. https://doi.org/10.1016/j.catena.2020.104892

New Zealand Petroleum & Minerals. (2020). *South Island Regional Airborne-Geophysical Survey Project (RASP) 2015 - 2020* (MR5400. https://data.nzpam.govt.nz/GOLD/system/mainframe.asp

NIWA. (2018). *NZ Water Model - Hydrology*. Retrieved 09/02/2022 from https://niwa.co.nz/freshwater-and-estuaries/research-projects/nz-water-model-hydrology-nzwam-hydro

NIWA. (2021). *CliFlo: NIWA's National Climate Database on the Web*. http://cliflo.niwa.co.nz/

Noguchi, S., Tsuboyama, Y., Sidle, R. C., & Hosoda, I. (1999). Morphological Characteristics of Macropores and the Distribution of Preferential Flow Pathways in a Forested Slope Segment. *Soil Science Society of America Journal*, *63*(5), 1413-1423. https://doi.org/10.2136/sssaj1999.6351413x

Norton, N., Wilson, K., Rodway, E., Hodson, R., Roberts, K., Ward, N., O'Connell-Milne, S., DeSilva, N., & Greer, M. (2019). *Current Environmental State and the "Gap" to Draft Freshwater Objectives for Southland: Technical Report*.

Nyberg, L. (1996). Spatial variability of soil water content in the covered catchment at Gårdsjön, Sweden. *Hydrological Processes*, *10*(1), 89-103. https://doi.org/https://doi.org/10.1002/(SICI)1099-1085(199601)10:1<89::AID-HYP303>3.0.CO;2-W

O'Callaghan, J. F., & Mark, D. M. (1984). The extraction of drainage networks from digital elevation data [Article]. *Computer Vision, Graphics, & Image Processing*, *28*(3), 323-344. https://doi.org/10.1016/S0734-189X(84)80011-0

O'Geen, A. T., McDaniel, P. A., & Boll, J. (2002). Chloride Distributions as Indicators of Vadose Zone Stratigraphy in Palouse Loess Deposits. *Vadose Zone Journal*, *1*(1), 150-157. https://doi.org/https://doi.org/10.2136/vzj2002.1500

Oliver, D. M., Heathwaite, L., Haygarth, P. M., & Clegg, C. D. (2005). Transfer of Escherichia coli to Water from Drained and Undrained Grassland after Grazing. *J Environ Qual*, *34*(3), 918-925. https://doi.org/10.2134/jeq2004.0327

Olson, C. G. (1997). Systematic soil-geomorphic investigations - contributions to R.V. Ruhe to pedologic interpretation. *Advances in Geoecology*, *29*(29).

Oswald, C. J., Richardson, M. C., & Branfireun, B. A. (2011). Water storage dynamics and runoff response of a boreal Shield headwater catchment. *Hydrological Processes*, *25*(19), 3042-3060. https://doi.org/https://doi.org/10.1002/hyp.8036

Overseer Support. (2020). *OVERSEER: How soil information impacts the model*. Retrieved 12/02/2022 from https://support.overseer.org.nz/hc/en-us/articles/900001020463-How-soil-information-impacts-the-model

Øygarden, L., Kværner, J., & Jenssen, P. D. (1997). Soil erosion via preferential flow to drainage systems in clay soils. *Geoderma*, *76*(1), 65-86. https://doi.org/10.1016/S0016-7061(96)00099-7

Palmer, A., Horne, D. J., Kelly, T., Holmes, C., Shadbolt, N., Kemp, P., Harrington, K., Thatcher, A., & Quinn, A. (2006). The Massey University Organic-Conventional Dairy Production Trial: Soil and fertility management. 1st IFOAM International Conference on Animals in Organic Production,

Parkinson, R. J., & Reid, I. (1986). Effect of local ground slope on the performance of tile drains in a clay soil. *Journal of Agricultural Engineering Research*, *34*(2), 123-132. https://doi.org/10.1016/S0021-8634(86)80005-1

Parlange, M. B., Steenhuios, T. S., Timlin, D. J., Stagnitti, F., & Bryant, R. B. (1989). Subsurface Flow above a Fragipan Horizon. *Soil Science*, *148*(2), 77-86. https://doi.org/10.1097/00010694-198908000-00001

Parliamentary Commissioner for the Environment. (2018). *Overseer and regulatory oversight: Models, uncertainty and cleaning up our waterways*. https://www.pce.parliament.nz/publications/overseer-and-regulatory-oversight-models-uncertainty-and-cleaning-up-our-waterways

Pearson, L. (2015). *Artificial subsurface drainage in Southland (Technical Report No. 2015-07)*. Environment Southland. Environment Southland: https://www.es.govt.nz/repository/libraries/id:26gi9ayo517q9stt81sd/hierarchy/environment/water/southland-science-programme/land-use-inputs/documents/Report%20-%20Artificial%20subsurface%20drainage%20in%20Southland.pdf

Pearson, L., & Couldrey, M. (2016). *Methodology for GIS-based Land Use Maps for Southland (Publication No 2016-10)*. Environment Southland (Southland Regional Council).

Pires, L. F., Bacchi, O. O. S., & Reichardt, K. (2005). Gamma ray computed tomography to evaluate wetting/drying soil structure changes. *Nuclear Instruments and Methods in Physics Research Section B: Beam Interactions with Materials and Atoms*, *229*(3), 443-456. https://doi.org/https://doi.org/10.1016/j.nimb.2004.12.118

Pollacco, J. A. P., Webb, T. H., McNeill, S., Hu, W., Carrick, S., Hewitt, A. E., & Lilburne, L. R. (2017). Saturated hydraulic conductivity model computed from bimodal water retention curves for a range of New Zealand soils. *Hydrology and Earth System Sciences*, *21*(6), 2725-2737. https://doi.org/10.5194/hess-21-2725-2017

Poulsen, D. (2013). *The hydrogeological significance of loess in Canterbury* (R13/60). https://api.ecan.govt.nz/TrimPublicAPI/documents/download/1853775

Presley, D. R., Hartley, P. E., & Ransom, M. D. (2010). Mineralogy and morphological properties of buried polygenetic paleosols formed in late quaternary sediments on upland landscapes of the central plains, USA. *Geoderma*, *154*(3-4), 508-517. https://doi.org/10.1016/j.geoderma.2009.03.015

Pringle, C. (2003). What is hydrologic connectivity and why is it ecologically important? *Hydrological Processes*, *17*(13), 2685-2689. https://doi.org/https://doi.org/10.1002/hyp.5145

Pye, K. (1984). Loess. *Progress in Physical Geography: Earth and Environment*, *8*(2), 176-217. https://doi.org/10.1177/030913338400800202

Pye, K. (1995). The nature, origin and accumulation of loess. *Quaternary Science Reviews*, *14*(7), 653-667. https://doi.org/10.1016/0277-3791(95)00047-X

Qi, H., & Qi, Z. (2017). Simulating phosphorus loss to subsurface tile drainage flow: a review. *Environmental Reviews*, *25*(2), 150-162. https://doi.org/10.1139/er-2016-0024

Qiao, S. Y. (2014). *Modeling Water Flow and Phosphorus Fate and Transport in a Tile-Drained Clay Loam Soil Using HYDRUS (2D/3D)* McGill University]. Quebec, Canada.

Quinn, J. M., Williamson, R. B., Smith, R. K., & Vickers, M. L. (2010). Effects of riparian grazing and channelisation on streams in Southland, New Zealand. 2. Benthic invertebrates. *New Zealand Journal of Marine and Freshwater Research*, *26*(2), 259-273. https://doi.org/10.1080/00288330.1992.9516520

R Core Team. (2019). *R: A Language and Environment for Statistical Computing*. In (Version 3.6.0) R Foundation for Statistical Computing. https://www.R-project.org/

Raeside, J. D. (1964). Loess Deposits of the South Island, New Zealand, and Soils Formed on them. *New Zealand Journal of Geology and Geophysics*, *7*(4), 811-838. https://doi.org/10.1080/00288306.1964.10428132

Rahman, M. M., Lin, Z., Jia, X., Steele, D. D., & DeSutter, T. M. (2014). Impact of subsurface drainage on streamflows in the Red River of the North basin. *Journal of Hydrology*, *511*, 474-483. https://doi.org/https://doi.org/10.1016/j.jhydrol.2014.01.070

Ray, L. L. (1963). Silt-Clay Ratios of Weathering Profiles of Peorian Loess along the Ohio Valley. *The Journal of Geology*, *71*(1), 38-47.

Rekker, J. H. (1998). *Central Southland Plains Groundwater Study; Results from Field Surveys & Assessment*. Southland Regional Council.

Restrepo-Posada, P. J., & Eagleson, P. S. (1982). Identification of independent rainstorms. *Journal of Hydrology*, *55*(1), 303-319. https://doi.org/https://doi.org/10.1016/0022-1694(82)90136-6

Reuter, R. J., McDaniel, P. A., Hammel, J. E., & Falen, A. L. (1998). Solute Transport in Seasonal Perched Water Tables in Loess-Derived Soilscapes. *Soil Science Society of America Journal*, *62*(4), 977-983. https://doi.org/https://doi.org/10.2136/sssaj1998.03615995006200040019x

Reynolds, W. D., & Zebchuk, W. D. (1996). Hydraulic Conductivity in a Clay Soil: Two Measurement Techniques and Spatial Characterization. *Soil Science Society of America Journal*, *60*(6), 1679-1685. https://doi.org/10.2136/sssaj1996.03615995006000060011x

Rissmann, C., Rodway, E., Beyer, M., Hodgetts, J., Snelder, T., Pearson, L., Killick, M., Marapara, T. R., Akbaripasand, A., Hodson, R., Dare, J., Millar, R., Ellis, T., Lawton, M., Ward, N., Ba., H., Kb., W., McMecking, J., Horton, T., . . . Kees, L. (2016). *Physiographics of Southland Part 1: Delineation of key drivers of regional hydrochemistry and water quality (Technical Report 2016/3). Version 2 - Preliminary*. Southland Regional Council (Environment Southland).

Ritzema, H. P. (1994). *Drainage principles and applications* (2 ed., Vol. 16). International Institute for Land Reclamation and Improvement.

Robertson, H., Ausseil, A.-G., Rance, B., Betts, H., & Pomeroy, E. (2018). Loss of wetlands since 1990 in Southland, New Zealand. *New Zealand Journal of Ecology*. https://doi.org/10.20417/nzjecol.43.3

Robinson, D., Abdu, H., Lebron, I., & Jones, S. (2012). *Imaging of hill-slope soil moisture wetting patterns in a semi-arid oak savanna catchment using time-lapse electromagnetic induction* (Vol. s 416–417). https://doi.org/10.1016/j.jhydrol.2011.11.034

Robinson, M., Mulqueen, J., & Burke, W. (1987). On flows from a clay soil—Seasonal changes and the effect of mole drainage. *Journal of Hydrology*, *91*(3), 339-350. https://doi.org/10.1016/0022-1694(87)90210-1

Roering, J. J., Almond, P., Tonkin, P., & McKean, J. (2004). Constraining climatic controls on hillslope dynamics using a coupled model for the transport of soil and tracers: Application to loess-mantled hillslopes, South Island, New Zealand. *Journal of Geophysical Research: Earth Surface*, *109*(F1). https://doi.org/10.1029/2003JF000034

Ross, C., & Donnison, A. (2003). Campylobacter and farm dairy effluent irrigation. *New Zealand Journal of Agricultural Research*, *46*(3), 255-262. https://doi.org/10.1080/00288233.2003.9513551

Royer, T. V., David, M. B., & Gentry, L. E. (2006). Timing of Riverine Export of Nitrate and Phosphorus from Agricultural Watersheds in Illinois: Implications for Reducing Nutrient Loading to the Mississippi River. *Environmental Science & Technology*, *40*(13), 4126-4131. https://doi.org/10.1021/es052573n

Ruhe, R. V. (1956). Geomorphic surfaces and the nature of soils. *Soil Science*, *82*(6), 441-456.

Ruhe, R. V., & Olson, C. G. (1980). Soil Welding. *Soil Science*, *130*(3), 132-139.

Rycroft, D. W. (1972). A literature review on the background to mole drainage

FDEU Technical Bulletin, *72/10*.

Saey, T., Van Meirvenne, M., De Pue, J., Van De Vijver, E., & Delefortrie, S. (2014). Reconstructing mole tunnels using frequency-domain ground penetrating radar. *Applied Soil Ecology*, *80*, 77-83. https://doi.org/10.1016/j.apsoil.2014.03.019

Saffarpour, S., Western, A. W., Adams, R., & McDonnell, J. J. (2016). Multiple runoff processes and multiple thresholds control agricultural runoff generation. *Hydrol. Earth Syst. Sci.*, *20*(11), 4525-4545. https://doi.org/10.5194/hess-20-4525-2016

Santra, P., Sahoo, R. N., Das, B. S., Samal, R. N., Pattanaik, A. K., & Gupta, V. K. (2009). Estimation of soil hydraulic properties using proximal spectral reflectance in visible, near-infrared, and shortwave-infrared (VIS–NIR–SWIR) region. *Geoderma*, *152*(3), 338-349. https://doi.org/10.1016/j.geoderma.2009.07.001

Saunders, W. M. H. (1965). Phosphate retention in New Zealand soils and its relationship to free sesquioxides, organic matter and other soil properties. New Zealand Journal of Agricultural Research 8:30 – 57.

Schaetzl, R. J., & Thompson, M. L. (2015). Soil genesis and profile differentiation. In *Soils: Genesis and Geomorphology* (2 ed.). Cambridge University Press.

Schilling, K. E., Jindal, P., Basu, N. B., & Helmers, M. J. (2012). Impact of artificial subsurface drainage on groundwater travel times and baseflow discharge in an agricultural watershed, Iowa (USA). *Hydrological Processes*, *26*(20), 3092-3100. https://doi.org/https://doi.org/10.1002/hyp.8337

Schmidt, J., Almond, C., Basher, L. R., Carrick, S., Hewitt, A. E., Lynn, I. H., & Webb, T. H. (2005). Modelling loess landscapes for the South Island, New Zealand, based on expert knowledge. *New Zealand Journal of Geology and Geophysics*, *48*(1), 117-133. https://doi.org/10.1080/00288306.2005.9515103

Schmidt, J., Almond, P. C., Basher, L., Carrick, S., Hewitt, A. E., Lynn, I. H., & Webb, T. H. (2005). Modelling loess landscapes for the South Island, New Zealand, based on expert knowledge. *New Zealand Journal of Geology and Geophysics*, *48*(1), 117-133.

Schoeneberger, P. J., Wysocki, D. A., Benham, E. C., & Soil Survey Staff. (2012). Field book for describing and sampling soils, Version 3.0. . In. Lincoln, NE: Natural Resources Conservation Service, National Soil Survey Center.

Schottler, S. P., Ulrich, J., Belmont, P., Moore, R., Lauer, J. W., Engstrom, D. R., & Almendinger, J. E. (2014). Twentieth century agricultural drainage creates more erosive rivers. *Hydrological Processes*, *28*(4), 1951-1961. https://doi.org/10.1002/hyp.9738

Scott, C., Geohring, L., & Walter, M. (1998). Water quality impacts of tile drains in shallow, sloping, structured soils as affected by manure application. *Applied Engineering in Agriculture*, *14*. https://doi.org/10.13031/2013.19428

Scott, R. S. (1963). The effect of mole drainage and winter pugging on grassland production. NZ Grassland Association Proceedings, New Plymouth.

Scotter, D. R., Clothier, B. E., & Corker, R. B. (1979). Soil water in a fragiaqualf. *Australian Journal of Soil Research*, *17*(3), 443. https://doi.org/10.1071/sr9790443

Scotter, D. R., & Kanchanasut, P. (1981). Anion Movement in a Soil under Pasture. *Australian Journal of Soil Research*, *19*, 299-307.

Sharpley, A. N., Bergström, L., Aronsson, H., Bechmann, M., Bolster, C. H., Börling, K., Djodjic, F., Jarvie, H. P., Schoumans, O. F., Stamm, C., Tonderski, K. S., Ulén, B., Uusitalo, R., & Withers, P. J. A. (2015). Future agriculture with minimized phosphorus losses to waters: Research needs and direction. *AMBIO*, *44*(2), 163-179. https://doi.org/10.1007/s13280-014-0612-x

Shipitalo, M. J., Nuutinen, V., & Butt, K. R. (2004). Interaction of earthworm burrows and cracks in a clayey, subsurface-drained, soil. *Applied Soil Ecology*, *26*(3), 209-217. https://doi.org/10.1016/j.apsoil.2004.01.004

Sidle, R. C., Noguchi, S., Tsuboyama, Y., & Laursen, K. (2001). A conceptual model of preferential flow systems in forested hillslopes: evidence of self-organization. *Hydrological Processes*, *15*(10), 1675-1692. https://doi.org/10.1002/hyp.233

Sidle, R. C., Tsuboyama, Y., Noguchi, S., Hosoda, I., Fujieda, M., & Shimizu, T. (2000). Stormflow generation in steep forested headwaters: a linked hydrogeomorphic paradigm. *Hydrological Processes*, *14*(3), 369-385. https://doi.org/10.1002/(sici)1099-1085(20000228)14:3<369::Aid-hyp943>3.0.Co;2-p

Singh, S. K., Pahlow, M., Goeller, B., & Matheson, F. (2021). Data- and model-driven determination of flow pathways in the Piako catchment, New Zealand. *Journal of Hydro-environment Research*, *37*, 82-94. https://doi.org/https://doi.org/10.1016/j.jher.2021.06.004

Smedema, L. K., Vlotman, W. F., & Rycroft, D. (2004). *Modern Land Drainage: Planning, Design and Management of Agricultural Drainage Systems*. Taylor & Francis Group.

Smedema, L. K., Vlotman, W. F., & Rycroft, D. (2014). *Modern Land Drainage: Planning, Design and Management of Agricultural Drainage Systems*. CRC Press. https://books.google.co.nz/books?id=b0lZDwAAQBAJ

Smith, L. C., & Monaghan, R. M. (2003). Nitrogen and phosphorus losses in overland flow from a cattle‐grazed pasture in Southland. *New Zealand Journal of Agricultural Research*, *46*(3), 225-237. https://doi.org/10.1080/00288233.2003.9513549

Snelder, T. H., Whitehead, A. L., Fraser, C., Larned, S. T., & Schallenberg, M. (2020). Nitrogen loads to New Zealand aquatic receiving environments: comparison with regulatory criteria. *New Zealand Journal of Marine and Freshwater Research*, *54*(3), 527-550. https://doi.org/10.1080/00288330.2020.1758168

Snow, V. O., Houlbrooke, D. J., & Huth, N. I. (2010). Predicting soil water, tile drainage, and runoff in a mole‐tile drained soil. *New Zealand Journal of Agricultural Research*, *50*(1), 13-24. https://doi.org/10.1080/00288230709510278

Soil Science Division Staff. (2017). *Soil Survey Manual*. Government Printing Office.

Soil Survey Staff. (2014). *Keys to Soil Taxonomy* (12 ed.). USDA-Natural Resources Conservation Service.

Sokolov, A. A., & Chapman, T. G. (1974). *Methods for water balance computations: an international guide for research and practice. A contribution to the International Hydrological Decade* (Vol. 17). The UNESCO Press. https://unesdoc.unesco.org/notice?id=p::usmarcdef_0000011523

Sørensen, R., Zinko, U., & Seibert, J. (2006). On the calculation of the topographic wetness index: evaluation of different methods based on field observations. *Hydrol. Earth Syst. Sci.*, *10*(1), 101-112. https://doi.org/10.5194/hess-10-101-2006

Soylu, M. E., Istanbulluoglu, E., Lenters, J. D., & Wang, T. (2011). Quantifying the impact of groundwater depth on evapotranspiration in a semi-arid grassland region. *Hydrol. Earth Syst. Sci.*, *15*(3), 787-806. https://doi.org/10.5194/hess-15-787-2011

Spoor, G., & Ford, R. A. (1987). Mechanics of mole drainage channel deterioration. *Journal of Soil Science*, *38*(2), 369-382. https://doi.org/10.1111/j.1365-2389.1987.tb02151.x

Spoor, G., Leeds-Harrison, P. B., & Godwin, R. J. (1982). Potential role of soil density and clay mineralogy in assessing the suitability of soils for mole drainage. *Journal of Soil Science*, *33*(3), 427-441. https://doi.org/10.1111/j.1365-2389.1982.tb01778.x

Statistics New Zealand. (2020). *Total Area of Farms (Table reference AGR001AA)*. http://infoshare.stats.govt.nz

Stevens, R. M., & Prior, L. D. (1994). The Effect of Transient Waterlogging on the Growth, Leaf Gas Exchange, and Mineral Composition of Potted Sultana Grapevines. *American Journal of Enology and Viticulture*, *45*(3), 285-290. https://www.ajevonline.org/content/ajev/45/3/285.full.pdf

Stone, W. W., & Wilson, J. T. (2006). Preferential flow estimates to an agricultural tile drain with implications for glyphosate transport. *J Environ Qual*, *35*(5), 1825-1835. https://doi.org/10.2134/jeq2006.0068

Taylor, N., & Pohlen, I. J. (1962). *Soil survey method : A New Zealand handbook for the field study of soils* (Soil Bureau bulletin ; 25 ed.). New Zealand Dept. of Scientific and Industrial Research.

Thorley, M., & Ettema, M. (2007). *Review of water allocation limits for the South Canterbury downlands. Report No. U07/09. Environment Canterbury Technical Report.*

Thornley, S., & Bos, A. W. (1985). Effects of livestock wastes and agricultural drainage on water quality: An Ontario case study. *Journal of Soil and Water Conservation*, *40*(1), 173. http://www.jswconline.org/content/40/1/173.abstract

Tromp-van Meerveld, H. J., & McDonnell, J. J. (2006a). On the interrelations between topography, soil depth, soil moisture, transpiration rates and species distribution at the hillslope scale. *Advances in Water Resources*, *29*(2), 293-310. https://doi.org/10.1016/j.advwatres.2005.02.016

Tromp-van Meerveld, H. J., & McDonnell, J. J. (2006b). Threshold relations in subsurface stormflow: 1. A 147-storm analysis of the Panola hillslope. *Water Resources Research*, *42*(2). https://doi.org/https://doi.org/10.1029/2004WR003778

Tuohy, P. (2013). *Land Drainage: A farmers practical guide to draining grassland in Ireland*. Agriculture and Food Development Authority.

Turnbull, I. M., & Allibone, A. H. (2003). *Geology of the Murihiku area: scale 1:250,000*. Institute of Geological and Nuclear Sciences.

Tyson, K. C., Garwood, E. A., Armstrong, A. C., & Scholefield, D. (1992). Effects of field drainage on the growth of herbage and the liveweight gain of grazing beef cattle. *Grass and forage science.*, *47*(3), 290-301. https://doi.org/10.1111/j.1365-2494.1992.tb02273.x

USDA NASS. (2017). 2017 Census of Agriculture. United States Summary and State Data (AC-17-A-51). In *Geographic Area Series* (Vol. 1, Part 51). United States Department of Agriculture, National Agricultural Statistics Service.

VanderZaag, A. C., Campbell, K. J., Jamieson, R. C., Sinclair, A. C., & Hynes, L. G. (2010). Survival of Escherichia coli in agricultural soil and presence in tile drainage and shallow groundwater. *Canadian Journal of Soil Science*, *90*(3), 495-505. https://doi.org/10.4141/cjss09113

Vidon, P., Hubbard, H., Cuadra, P. E., & Hennessy, M. (2012). Storm Flow Generation in Artificially Drained Landscapes of the US Midwest: Matrix Flow, Macropore Flow, or Overland Flow. *WATER journal*, *4*. https://doi.org/10.14294/water.2012.8

Vogeler, I., Carrick, S., Cichota, R., & Lilburne, L. (2019). Estimation of soil subsurface hydraulic conductivity based on inverse modelling and soil morphology. *Journal of Hydrology*, *574*, 373-382. https://doi.org/10.1016/j.jhydrol.2019.04.002

Vogeler, I., Carrick, S., Lilburne, L., Cichota, R., Pollacco, J. A. P., & Fernández-Gálvez, J. (2021). How important is the description of soil unsaturated hydraulic conductivity values for simulating soil saturation level, drainage and pasture yield? *Journal of Hydrology*, *598*, 126257. https://doi.org/https://doi.org/10.1016/j.jhydrol.2021.126257

Walker, P. H., & Green, P. (1976). Soil trends in two valley fill sequences. *Australian Journal of Soil Research*, *14*(3), 291-303. https://doi.org/10.1071/SR9760291

Watt, J. P. C. (1976). Relationships between soil moisture depletion, potential evaporatranspiration, and available moisture for a sequence of loess soils in Otago and Southland. *Proceedings of Soil and plant Water Symposium. New Zealand Soil Bureau Publication 789*, pp 21–33.

Webb, T. H., & Burgham, S. J. (1997). Soil-landscape relationships of downlands soils formed from loess, eastern South Island, New Zealand. *Soil Research*, *35*(4), 827-842. https://doi.org/10.1071/S96077

Webb, T. H., & Lilburne, L. R. (2011). *Criteria for defining the soil family and soil sibling: the fourth and fifth categories of the New Zealand Soil Classification*. Manaaki Whenua - Landcare Research.

Wei, W., Jia, F., Yang, L., Chen, L., Zhang, H., & Yu, Y. (2014). Effects of surficial condition and rainfall intensity on runoff in a loess hilly area, China. *Journal of Hydrology*, *513*, 115-126. https://doi.org/https://doi.org/10.1016/j.jhydrol.2014.03.022

Weiler, M. (2017). Macropores and preferential flow—a love-hate relationship. *Hydrological Processes*, *31*(1), 15-19. https://doi.org/https://doi.org/10.1002/hyp.11074

Weiler, M., McDonnell, J. J., Tromp-van Meerveld, I., & Uchida, T. (2005). Subsurface Stormflow. In *Encyclopedia of Hydrological Sciences*. https://doi.org/https://doi.org/10.1002/0470848944.hsa119

Western, A. W., & Grayson, R. B. (1998). The Tarrawarra Data Set: Soil moisture patterns, soil characteristics, and hydrological flux measurements. *Water Resources Research*, *34*(10), 2765-2768. https://doi.org/https://doi.org/10.1029/98WR01833

Western, A. W., Grayson, R. B., Blöschl, G., Willgoose, G. R., & McMahon, T. A. (1999). Observed spatial organization of soil moisture and its relation to terrain indices. *Water Resources Research*, *35*(3), 797-810. https://doi.org/10.1029/1998wr900065

Wheeler, D. M. (2018). *Hydrology. OVERSEER® Technical Manual Technical Manual for the description of the OVERSEER® Nutrient Budgets engine*. OVERSEER Limited.

Wheeler, D. M., Ledgard, S. F., De Klein, C. A. M., Monaghan, R. M., Carey, P. L., McDowell, R. W., & Johns, K. L. (2003). OVERSEER® nutrient budgets - moving towards on-farm resource accounting. *Proceedings of the New Zealand Grassland Association*, 191-194. https://doi.org/10.33584/jnzg.2003.65.2484

Williams, M. R., Livingston, S. J., Heathman, G. C., & McAfee, S. J. (2019). Thresholds for run-off generation in a drained closed depression. *Hydrological Processes*, *33*(18), 2408-2421. https://doi.org/10.1002/hyp.13477

Williamson, R. B., Smith, R. K., & Quinn, J. M. (2010). Effects of riparian grazing and channelisation on streams in Southland, New Zealand. 1. Channel form and stability. *New Zealand Journal of Marine and Freshwater Research*, *26*(2), 241-258. https://doi.org/10.1080/00288330.1992.9516519

Wilson, G. V., Nieber, J. L., Fox, G. A., Dabney, S. M., Ursic, M., & Rigby, J. R. (2017). Hydrologic connectivity and threshold behavior of hillslopes with fragipans and soil pipe networks. *Hydrological Processes*, *31*(13), 2477-2496. https://doi.org/https://doi.org/10.1002/hyp.11212

Wood, B. L., Marwick, J., Leed, H., Couper, R. A., McQueen, D. R., & Harris, J. W. (1956). The geology of the Gore subdivision, Gore sheet district (S170). Wellington: Department of Scientific and Industrial Research. *New Zealand Geological Survey bulletin 53*, 127 p.

Wu, K., Rodriguez, G. A., Zajc, M., Jacquemin, E., Clément, M., De Coster, A., & Lambot, S. (2019). A new drone-borne GPR for soil moisture mapping. *Remote Sensing of Environment*, *235*, 111456. https://doi.org/10.1016/j.rse.2019.111456

Youngs, E. G. (1985). An analysis of the effect of the vertical fissuring in mole-drained soils on drain performances. *Agricultural Water Management*, *9*(4), 301-311. https://doi.org/https://doi.org/10.1016/0378-3774(85)90040-X

Zammit, C., Pearce, P., Mullan, B., Sood, A., Collins, D., Stephens, S., Woolley, J. M., Bell, R., & Wadhwa, S. (2018). *Southland climate change impact assessment. Prepared for Environment Southland, Invercargill City Council, Southland District Council and Gore District Council by National Institute of Water & Atmospheric Research Ltd (NIWA).*

Zhang, Y., Zhang, Z., Ma, Z., Chen, J., Akbar, J., Zhang, S., Che, C., Zhang, M., Cerdà, A., & Lupwayi, N. (2018). A review of preferential water flow in soil science. *Canadian Journal of Soil Science*, *98*(4), 604-618. https://doi.org/10.1139/cjss-2018-0046

Zhao, D., Arshad, M., Li, N., & Triantafilis, J. (2021). Predicting soil physical and chemical properties using vis-NIR in Australian cotton areas. *CATENA*, *196*. https://doi.org/10.1016/j.catena.2020.104938

Zhao, D., Zhao, X., Khongnawang, T., Arshad, M., & Triantafilis, J. (2018). A Vis-NIR Spectral Library to Predict Clay in Australian Cotton Growing Soil. *Soil Science Society of America Journal*, *82*(6), 1347-1357. https://doi.org/10.2136/sssaj2018.03.0100

Zhou, W., & Lin, X. (1995). Effects of waterlogging at different growth stages on physiological characteristics and seed yield of winter rape (Brassica napus L.). *Field Crops Research*, *44*(2), 103-110. https://doi.org/https://doi.org/10.1016/0378-4290(95)00075-5

Zhou, X., Lin, H. S., & White, E. A. (2008). Surface soil hydraulic properties in four soil series under different land uses and their temporal changes. *CATENA*, *73*(2), 180-188. https://doi.org/10.1016/j.catena.2007.09.009

Zhu, H. D., Shi, Z. H., Fang, N. F., Wu, G. L., Guo, Z. L., & Zhang, Y. (2014). Soil moisture response to environmental factors following precipitation events in a small catchment. *CATENA*, *120*, 73-80. https://doi.org/https://doi.org/10.1016/j.catena.2014.04.003

Zumr, D., Dostál, T., & Devátý, J. (2015). Identification of prevailing storm runoff generation mechanisms in an intensively cultivated catchment. *Journal of Hydrology and Hydromechanics*, *63*(3), 246-254. https://doi.org/doi:10.1515/johh-2015-0022

List of Appendices

Appendix A
Soil Descriptions

A.1 Loess stratigraphy descriptions

Table A-1. Loess stratigraphy descriptions for the underpass (UP) and each of the auger drillings (1-19).

Auger ID	Horizon Designation	Depth (cm)	Matrix Colour	Mottle Colour, Abundance & Size	Veins Colour, Abundance & Size	Segregations Colour, Abundance & Size	Texture	Consistence	Loess Sheet Descriptor (field)	Notes	Loess Sheet
UP	Ah	0 - 19	10YR 5/3	-	-	-	zl	-	-	Clear, wavy boundary. Wk, fi-co sbg blky	L1/L2
UP	A/Bw(g)	19 - 42	2.5Y 6/4	-	-	Com med dist 5YR 2.5/1 Mn nodules	cl	-	-	Clear, wavy bndry. V co blky- mod med sbg blky	L1/L2
UP	Bw(g)	42 - 78	2.5Y 6/3	-	-	Many thick black 2.5YR 2.5/1 Mn hypocoats. Many 10YR 6/8 redox concs. Few 2.5YR 2.5/1 med nodules	cl	-	-	Clear, irreg bndry. Str med blky.	L1/L2
UP	Bx(f)	78 - 141	10YR 6/4 (80%) 2.5Y 6/4 (20%)	-	-	Com fine 2.5YR 2.5/1 Mn hypocoats	cl	-	-	Clear, smo bndry. Mod v.-co prism. Abund fine roots btwn prisms	L3/L4/L5
UP	2Btg	141 - 170	10YR 6/8 - 5/8	-	10YR 8/1 (20%)	-	c	-	-	very gravelly (>35%); clasts compl weathered; wkly wthrd quarz clasts; com thin clay skins; mod med blky structure; coa gravel (USDA); few fine roots	-
UP	2Btg2	170 - 247+	7.5YR 5/8	-	-	-	gravelly scl	-	-	mod med blky; fi-med grvl clasts; mod-str wthered; few fi roots	-
1	Ah	0 - 25	-	-	-	-	-	-	-	-	L1/L2
1	Bw(f)	25 - 80	2.5Y 6/4	-	-	-	zl	-	-	-	L1/L2

Table A-1. Loess stratigraphy descriptions for the underpass (UP) and each of the auger drillings (1-19).

Auger ID	Horizon Designation	Depth (cm)	Matrix Colour	Mottle Colour, Abundance & Size	Veins Colour, Abundance & Size	Segregations Colour, Abundance & Size	Texture	Consistence	Loess Sheet Descriptor (field)	Notes	Loess Sheet
1	Bx	80 - 130	10YR 6/8	-	few 2.5Y 7/3 veins	few thin Mn coatings	zc	brittle	-	-	L1/L2
1	bBw(g)	130 - 147	10YR 5/8	-	com 1cm grey veins	many fine black Mn coatings	zl	brittle	-	-	L3/L4?
1	bBx(g)?	147 - 175	10YR 5/8 (60%)	-	5Y 7/1 grey veins (40%)	very little Mn	cl	brittle	-	-	L3/L4?
1	b2Bw(g)?	175 - 211	10YR 6/6 (85%)	-	5Y 7/1 grey veins (15%)	com med-coa Mn nodules	cl	plastic	-	-	L5
1	2b2Btg	211 - +	10YR 6/8	-	5Y 7/1 (10%)		gravelly cl			few med-compl weathered gravels	-
2	Ah	0 - 27	10YR 4/3	-	-	-	zl	-	"red brown"	-	L1
2	Bw(f)	27 - 43	2.5Y 5/4	com med dist 7.5YR 5/8 mottles	-	-	zc	-	"red brown"	-	L1
2	Bxg	43 - 53?	2.5Y 6/2	com coa dist 7.5YR 5/6 mottles	grey veins	-	zc	-	"red brown"	-	L1
2	Bxtg	53 - 105?	10YR 5/8 (80%) ; changes to 10YR 6/8 with depth	-	5Y 6/2 (20%)	-	zl	-	"red brown"	-	L1
2	bBtg	105 - 121	10YR 6/8	-	?10GY 7 com? (hard to read)	many coa thin black Mn hypocoats	zl	-	"orangey brown"	-	L2
2	bBx	121 - 168?	10YR 5/8	-	-	-	zc	brittle	"orangey brown"	-	L2
2	b2Bt	168 - 182	10YR 5/6	-	few fine grey veins	many fine Mn mottles or coats	zl	crumbly	"tan"	pale tan	L3
2	b2Bx	182 - 237	uniform 10YR 5/6	-	few fine grey veins	-	zl	brittle	"tan"	pale tan	L3
2	b3Bt	237 - 248	10YR 5/8	-	-	com med-coa Mn mottles or hypocoats	zc	-	"yellow"	no veins	L4
2	b3Bx	248 - 319	uniform 10YR 5/8	-	-	-	zl	brittle	"yellow"	no veins	L4
2	b4?Bt(x)	319 - 353	10YR 6/6 (70%) 5Y 6/2 (30%)	-		-	zl	brittle	"orangey brown"	stll b3?; no veins	L5

Table A-1. Loess stratigraphy descriptions for the underpass (UP) and each of the auger drillings (1-19).

Auger ID	Horizon Designation	Depth (cm)	Matrix Colour	Mottle Colour, Abundance & Size	Veins Colour, Abundance & Size	Segregations Colour, Abundance & Size	Texture	Consistence	Loess Sheet Descriptor (field)	Notes	Loess Sheet
2	b4Btg	353 - 377	10YR 6/8 (80%)	-	5Y 7/2 (20%)	com fi-med Mn hypocoats	zc	brittle	"orangey brown"	no veins, except at 353-364 (more clay and more grey veins)	L5
2	b4Btg(2)	377 - 396	10YR 5/8 (90%)	-	5Y 8/1 (10%)		zc	plastic	"orangey brown"	no veins; brighter orange	L5
2	b4Btg	396 - 414	10YR 4/6	-	-	com fine Mn hypocoats (Mn-rich zone)	-	-	"orangey brown"	no veins	L5
3	Ah	0 - 30	10YR 5/3	-	-	-	zl	-	-	-	L1
3	Bw	30 - 54	2.5Y 6/4	-	-	-	zcl	-	-	-	L1
3	Bx(g)	54 - 114	10YR 6/8	-	pale veins	-	zc	-	-	red-brown	L1
3	bBt(g)	114 - 137	10YR 5/8 - 6/8	-	-	Mn rich	zc	-	"orangey brown"	orange brown	L2
3	bBt(g)2	137 - 155	uniform 10YR 5/8	-	-	-	c	-	"orangey brown"	-	L2
3	bBx(g)	155 - 177	10YR 5/6	-	-	-	zc	brittle	"orangey brown"	orange brown; crumbly	L2
3	b2Bt(g)	177 - 191	2.5Y 5/6	-	-	-	-	plastic	"tan"	pale tan	L3
3	b2Bx	191 - 237	10YR 5/6	-	-	at 191 Mn rich	zl	brittle	"tan"	-	L3
3	b3Bt	237 - 263	10YR 6/8	-	-	-	zc	-	"yellow brown"	yellow	L4
3	b3Bx	263 - 284	10YR 5/8	-	-	-	zl	-	"yellow brown"	yellow	L4
3	b4Bt	284 - 330	10YR 4/6	-	-	-	cl	-	"orangey brown"	brown; may incl weathered clasts	L5
4	Ah	0 - 27	10YR 4/3	-	-	-	zl	-	-	-	L1/L2
4	Bw(f)	27 - 49	2.5Y 5/4	com med dist 10YR 5/8 mottles	-	-	zl	-	-	-	L1/L2
4	Bx(g)	49 - 69	10YR 5/8 (90%)	-	5Y 7/1 (10%)	com coa Mn nodules	zl	-	-	-	L3?
4	Bx(g)2	69 - 88	10YR 6/6 (70%)	-	2.5Y7/2 (30%)	-	zl	-	-	less bright	L4

Table A-1. Loess stratigraphy descriptions for the underpass (UP) and each of the auger drillings (1-19).

Auger ID	Horizon Designation	Depth (cm)	Matrix Colour	Mottle Colour, Abundance & Size	Veins Colour, Abundance & Size	Segregations Colour, Abundance & Size	Texture	Consistence	Loess Sheet Descriptor (field)	Notes	Loess Sheet
4	bBtg	88 - 110	10YR 4/6	-	-	com med black Mn hypocoats	zl	-	-	-	L5
4	bBtg2	110 - 131	10YR 6/8 (80%)	-	5Y 7/2 (20%) grey veins appearing	many med black Mn mottles	zc	-	-	-	L5
5	Ah	0 - 29	10YR 5/3	-	-	-	zl	-	-	colluvial material, no primary loess	Rw
5	Bw(f)	29 - 51	2.5Y 6/4	com coa dist 10YR 6/6 mottles	-	-	zl	-	-	-	Rw
5	Bt	51 - 79	10YR 6/8 (60%) 2.5Y 6/4 (40%)	-	-	-	zc	-	-	few str weathered clasts	Rw
6	Ah	0 - 21	-	-	-	-	zl	-	-	-	Rw
6	Bw	21 - 44	2.5Y 6/4	-	-	-	zc	-	-	-	Rw
6	Bt	44 - 70	2.5Y 6/4 (60%) 10YR 5/6 (40%)	-	-	com coa black Mn nodules	zc	-	-	-	Rw
7	Ah	0 - 58	2.5Y 5/3	-	-	-	zl	-	-	between 33-45 noted some gravels	Rw
7	A/Bg	58 - 84	2.5Y 5/3 (70%)	com dist coa 10YR 5/8 mottles	2.5Y 6/2 (30%)	-	-	-	-	-	Rw
7	2Bw(g)	84 - +	10YR 4/6	-	2.5Y 6/2	-	gravelly cl	-	-	-	Rw
8	Ah	0 - 32	2.5Y 5/3	-	-	-	zl	-	-	btwn 24-32 noted some gravels	Rw
8	Bw(f)	32 - 50	2.5Y 6/4	few fine dist 7.5YR 4/6 mottles	-	-	zl	-	-	-	Rw
8	Bw(g)	50 - 102	10YR 4/6	-	2.5Y 6/1	between 67-81 com fi Mn mottles/concretions	zc	soft	-	-	Rw
9	Ah	0 - 33	2.5Y 5/3	-	-	-	zl	-	-	-	Rw
9	Bw(f)	33 - 57	2.5Y 6/3	com dist fine 10YR 4/6 mottles	-	-	zl	-	-	-	Rw
9	Bg	57 - 130	2.5Y 7/1 and bright 10YR 6/8 zone at 103	40% (many) med dist 10YR 4/6 mottles	-	-	zc	softer	-	brighter at 103; grey at 112	Rw

Table A-1. Loess stratigraphy descriptions for the underpass (UP) and each of the auger drillings (1-19).

Auger ID	Horizon Designation	Depth (cm)	Matrix Colour	Mottle Colour, Abundance & Size	Veins Colour, Abundance & Size	Segregations Colour, Abundance & Size	Texture	Consistence	Loess Sheet Descriptor (field)	Notes	Loess Sheet
10	Ah	0 - 19	10YR 4/3	-	-	-	zl	-	-	-	Rw
10	Bw(f)	19 - 47	10YR 5/4 (50%) 2.5YR 6/4 (20%)	30% 7.5YR 4/6 orange mottles* (*mottles=ripped up bits of Bx that's actually bBx?)	-	Fe concretions/nodules	zc	-	-	-	Rw
10	Bx	47 - 65	7.5YR 4/6 (15%) 2.5YR 7/2 (15%)	-	-	many coa-v. coa Mn mottles & concretions (pit shows >70% Mn mottles)	-	brittle	-	-	L5
10	bBt(g)?	65 - 83	10YR 5/8 (80%) 2.5Y 7/2 (20%)	mottled	-	-	c	softer	-	-	L5
11	Ah	0 - 31	2.5Y 5/3	-	-	-	zl	-	-	-	Rw
11	Bw(f)	31 - 74	2.5Y 6/4	com fi dist 7.5YR 4/6 mottles	-	-	zc	soft	-	pale tan	Rw
11	Bg	74 - 126	10YR 4/6 (50%) 5Y 7/1 (50%); turns 7.5YR 5/8 just above contact with gravels	-	-	just above contact w gravels Mn-Fe nodules % hypocoats 4mm thick	zc	soft, v plastic	-	orange grey; at 117 bright red	L5
12	Ah	0 - 26	2.5Y 5/3	-	-	-	zl	-	-	-	Rw
12	Bw(f)	26 - 63	2.5Y 6/4	com med faint 2.5Y 6/6 mottles	-	-	zl	plastic	-	-	Rw
12	Bg	63 - 105	2.5Y 6/2 (60%) 10YR 4/6 (40%)	mottling?	-	-	zc	-	-	-	Rw
12	Bfm	105 - 112	5YR 4/6	-	-	black Mn coats; strongly cemented; iron pan	-	brittle	-	-	
12	bBg	112 - 146	7.5YR 5/6 (50%) 2.5Y 7/2 (50%)	-	-	-	zl	soft	-	-	L5
12	2bBw	146 - =	10YR 5/6	-	-	-	-	-	-	-	-
13	Ah	0 - 35	5Y 5/2	-	-	-	zl	-	-	-	L1/L2

Table A-1. Loess stratigraphy descriptions for the underpass (UP) and each of the auger drillings (1-19).

Auger ID	Horizon Designation	Depth (cm)	Matrix Colour	Mottle Colour, Abundance & Size	Veins Colour, Abundance & Size	Segregations Colour, Abundance & Size	Texture	Consistence	Loess Sheet Descriptor (field)	Notes	Loess Sheet
13	Bw(f)	35 - 55	2.5Y 6/3	com med dist 10YR 6/4 mottles	-	-	zc	-	-	-	L1/L2
13	Bw(g)	55 - 74	10YR 5/6 (60%)	-	2.5Y 6/2 (40%)	-	zc	-	-	crunchy at 66	L3?
13	Bw(g)2	74 - 160	10YR 5/8 (80%) 5Y 7/1 (20%)	-	-	some Mn at 121	cl	soft grading to brittle	-	-	L4?
13	bBt	160 - 211	10YR 5/8 tending to 10YR 6/8	-	-	-	cl	plastic	-	lost a lot of grey	L5
13	2bB?	211 - +	10YR 6/8	-	-	-	zc	-	-	-	-
14	Ah	0 - 30	2.5Y 5/3	-	-	-	zl	-	-	-	L1
14	Bw(f)	30 - 60	2.5Y 6/3	com coa dist 7.5YR 5/6 mottles	-	-	zc	-	-	-	L1
14	Bx	60 - 118	10YR - 7.5YR 5/8 (80%) 2.5Y 7/2 (20%)	-	-	some Mn	zc	semi-deformable	-	reddish	L1
14	bBt(g)	118 - 137	uniform 10YR 5/6	-	-	many dist thin Mn hypocoats	-	brittle	-	orangey	L2
14	bBx	137 - 162	10YR 5/6	-	few 2.5Y 7/1 - 7/2 grey veins	-	c	grades from slightly plastic to v brittle	-	-	L2
14	b2Btg	162 - 174	10YR 6/6	-	com (15%) 5Y 8/1 veins	many thin Mn hypocoats	zl-zc	brittle	-	tan?	L3
14	b2Bx	174 - 211	10YR - 2.5Y 6/6	-	-	-	zl-zc	brittle	-	pale tan	L3
14	b3Bt/Bx	211 - 287	7.5YR 6/8	-	-	many Mn hypocoats at 259	c	grade from slightly plastic to v strong & brittle	-	yellow	L4
14	b4Bt(g)	287 - 329	10YR 6/8 (80%)	-	coarse 5Y8/1 (20%) veins	some Mn in grey veins	zc	semi-deformable	-	-	L5
15	Ah	0 - 30	10YR 4/3	-	-	-	zl	-	-	-	L1
15	Bw(f)	30 - 72	2.5Y 5/4	com coa faint 10YR 5/8 mottles	-	-	zc	plastic	-	-	L1

Table A-1. Loess stratigraphy descriptions for the underpass (UP) and each of the auger drillings (1-19).

Auger ID	Horizon Designation	Depth (cm)	Matrix Colour	Mottle Colour, Abundance & Size	Veins Colour, Abundance & Size	Segregations Colour, Abundance & Size	Texture	Consistence	Loess Sheet Descriptor (field)	Notes	Loess Sheet
15	Bx	72 - 137	2.5Y 7/3 (30%) 7.5YR 5/8 (70%)	-	grey veins appearing toward base	-	c	-	-	more orange & uniform	L1
15	bBtx(g)	137 - 212	7.5YR 5/8 (85%) 2.5Y 6/4 (15%); grading to uniform 2.5Y 6/6	-	-	coarse Mn hypocoats in top 20cm; less Mn in lower 171-212	zc	brittle; more plastic from 174-212	-	pale tan? In lower 174-212	L2
15	b2Bw(x)	212 - 270	7.5YR 6/8 (90%) 2.5Y 7/3 (10%)	-	-	rich in Mn top 30-40cm; bright orange concretions in top 30-40cm	zl	very brittle grading to less brittle	-	browner; tan? Slightly more uniform colour in lower part	L3
15	b3Btx	270 - 338	10YR 6/8	-	few 2.5Y 7/3 grey veins	-	zc	plastic	-	yellower?	L4
15	b4Bw(x)	338 - 353	7.5YR 6/8 (90%) 2.5Y 7/3 (10%)	-	-	some Mn between 323-341	zl	brittle	-	tan? Slightly more uniform colour	L5
15	b4Btx	353 - 399	10YR 6/8	-	com coa dist GLEY1 8/10Y veins	-	zc	plastic	-	yellower? Slightly brighter	L5
15	b4Bt(g)	399 - 427	10YR 6/8	-	com coa dist GLEY1 8/10Y veins	Mn rich	zc	brittle	-	-	L5
16	Ah	0 - 30	2.5Y 5/3	-	-	-	zl	-	"red brown"	-	L1
16	Bw(f)	30 - 70	2.5Y 6/4	com coa dist 10YR 4/6 mottles	-	com coa dist black Mn hypocoats	zc	crumbly	"red brown"	-	L1
16	Bx(g)	70 - 117	10YR 5/6 (70%)	-	2.5Y 7/2 (15%) 5Y 7/1 (15%) veins	many coa dist Mn hypocoats in top 20cm	zc-c	plastic, grades to brittle at very base	"red brown"	orange w grey veins & Mn	L2?
16	bBt(g)	117 - 144	10YR 5/8 (70%)	-	(30%) prominent 2.5Y 7/1 veins	com coa Mn nodules at top grading to none	zc	very plastic grading to slightly brittle at base	"orangey"	-	L2
16	bBx	144 - 165	10YR 6/6 (70%)	-	(30%) less prominent 2.5Y 6/2 veins	com med Mn hypocoats (Mn rich)	zc	brittle grading to plastic	-	yellower; tan?	L3

Table A-1. Loess stratigraphy descriptions for the underpass (UP) and each of the auger drillings (1-19).

Auger ID	Horizon Designation	Depth (cm)	Matrix Colour	Mottle Colour, Abundance & Size	Veins Colour, Abundance & Size	Segregations Colour, Abundance & Size	Texture	Consistence	Loess Sheet Descriptor (field)	Notes	Loess Sheet
16	b2Btg	165 - 190	Uniform 2.5Y 6/4 - 6/6 (85%)	-	(15%) faint med 5Y 6/2 veins	-	zc	very plastic	-	brown; tan?	L3
16	b2Bx	190 - 227	10YR 5/8 - 6/8	-	10% coa grading to fine 5Y 7/1 veins	low Mn grading to higher Mn	zl	brittle	-	much brighter colour	L3/L4?
16	b3Btg	227 - 255	10YR 6/8	-	15% coa 5Y 7/1 veins (large, distinct & v pale)	com coa Mn nodules (very high in Mn; chunky Mn)	zc	slightly plastic	-	orangey	L4
16	2b3Btg	255 - +	10YR 5/8	-	Large white veins	-	lighter zc	-	-	-	L5
17	Ah	0 - 24	2.5Y 5/3	-	-	-	-	-	"red-orange"	-	L1/L2
17	Bw(f)	24 - 50	2.5Y 6/6	com med faint 10YR 5/6 mottles	-	little Mn	zl	-	"red-orange"	yellow-bright brown	L1/L2
17	Bw(g)	50 - 76	2.5Y 6/4	com coa dist 10YR 5/6 mottles	com coa faint 2.5Y 7/2 veins	-	zl-zc	slightly brittle	"red-orange"	pale brown	L2
17	Bx	76 - 105	10YR 6/8	-	(20%) 5Y 6/2 less grey/less distinctthan above	large com dist Mn hypocoats & weakly cemented concretions	heavy zl	brittle	"red-orange"	dark orange	L3?
17	bBt(g)	105 - 137	10YR 7/6 (60%) 2.5Y 7/3 (40%)	-	few, very faint pale-brown-grey veins	-	c	plastic	"yellow"	tan?	L3/L4?
17	bBw	137 - 156	10YR 6/6	-	-	-	zl	plastic but silty	"yellow"	brighter colour	L3/L4?
17	b2Bt(g)	156 - 203	10YR 5/6 (70%)	-	(30%) dist fine 5Y 7/1 veins	-	zc	plastic	"orange1"	orange, with white-grey veins	L4
17	b3?	203 - 244	10YR 6/8 (70%)	-	30% coa 5Y 7/1 veins	5 mm Fe concretions/nodules	c	soft	"orange2"	yellow w large white veins	L5
17	b3?Bw	244 - 258	uniform 10YR 5/6	-	30% coa 5Y 7/1 veins grading to none	-	zl	plastic veins grading to uniform silty	"orange2"	bright yellow-orange	L5
18	Ah	0 - 24	2.5Y 5/3	-	-	-	zl	-	-	-	L1/L2
18	Bw(f)	24 - 47	2.5Y 6/6	few med faint 7.5YR 5/6 mottles	-	com black Mn hypocoats	zl	-	-	-	L1/L2

Table A-1. Loess stratigraphy descriptions for the underpass (UP) and each of the auger drillings (1-19).

Auger ID	Horizon Designation	Depth (cm)	Matrix Colour	Mottle Colour, Abundance & Size	Veins Colour, Abundance & Size	Segregations Colour, Abundance & Size	Texture	Consistence	Loess Sheet Descriptor (field)	Notes	Loess Sheet
18	Bx	47 - 87	bright orange 10YR 6/8 (80%)	-	none grading to (20%) 5Y 6/2 veins	Mn nodules	zc	v plastic	-	-	L4
18	bBx(g)	87 - 133	10YR 6/6	-	5Y 7/1 veins (15%)	many thin large 5Y 8/1 Mn hypocoats	-	brittle and silty	-	tan with white veins	L5
18	2bBtg	133 - 153	10YR 4/6	-	-	5Y 8/1 black Mn coatings	heavy zl	-	-	transition to gravel at base (soil formed in gravel)	-
19	Ah	0 - 36	2.5Y 5/3	-	-	-	zl	-	-	-	L1
19	Bw(f)	36 - 65	2.5Y 6/3	Com. Coa. Fai 10YR 5/6	-	-	Zl-zc	plastic	“orange”		L1
19	Bx	65 - 113	10YR 6/8	-	Com large 5Y 6/2 & 5Y 7/1	Large Mn coatings @ 60-73 & com Mn nodules @ 112	Zc - c	plastic	“tan”		L2
19	bBtg	113 - 139	10YR 6/6 & 2.5Y 6/3	-	Thin and few grading to none	Few Mn nodules at 112- 178	zc	brittle	“yellow”? “orange”?		L3
19	bBw	139 - 165	Uniform 2.5Y 6/4	Few orange mottles at base	-	Few, large, thin Mn coats	c	plastic	“tan”		L3
19	b2Btg	165 - 209	10YR 6/8	-	Lower 20cm very white 5Y 8/1	-	zc	Slightly brittle	“orangey yellow”	Much brighter	L4
19	b2Bx	209 - 249	10YR 6/6 (80%) 5Y 6/2 (20)	-	-	Few fine Mn coats	zc	brittle		paler	L4
19	b3Btg	249 - 301	10YR 6/8	-	5% Very large 5Y 8/1	Few gine Mn coats	Heavy zc grading to zc	Plastic grading to brittle		Brighter & more orange	L5

Figure A-1. Example of an auger boring (auger 2) between the topsoil (top of right-most column) and the gravels (bottom of left-most column), showing the change in colouring with depth.

A.2 Soil profile descriptions and images

Survey Notes

- Profiles described here are from sites IN1, IN2, HS, NS, dSS, pSS
- These were my first attempts at describing soil
- Structure of the Bx is potentially inaccurate (was not assessed at a large scale – lack of experience)
- All colours are moist colours unless otherwise stated

A.2.1 Interfluve 1 (IN1)

Site: Interfluve 1 (IN1)
Profile Code: OTA18-05
Survey: Otahuti
Region: Southland
Location: Otahuti PhD field site, true right interfluve of the southernmost arm of the drainage basin gully. Pit excavated to expose two profiles, one profile proximal to a mole channel (~30cm) and the second profile distal to a mole channel (~0.7m). Only distal profile was described but proximal profile is very similar, unless otherwise stated.
Landform: Downland interfluve; flat to gently undulating (1.9 degree slope angle)
Grid Reference: NZTM 1229095.712 E 4868623.424 N
Date Described: 01/09/2018
Author: Kirstin Deuss
Site Notes: N/A
NZSC: Mottled Fragic Pallic (PXM)
Drainage Class: Imperfect

Ap	0-23	Texture:	Silt loam (clay rich)
		Colour:	10YR 4/3
		Mottles:	5% 5YR 4/6 along root channels
		Concretions:	None
		Structure:	Granular
		Boundary:	Indistinct smooth boundary
		Cohesive/Non-cohesive:	Cohesive
		Strength:	Slightly firm
		Failure:	Very friable
		Penetration resistance:	Low penetration resistance
		Plasticity:	Very plastic
		Stickiness:	Slightly sticky
		Soil water state:	Slightly moist
		Roots:	Abundant micro to extremely fine roots
A/B	23-32	Texture:	*Not described*
		Colour:	*Not described*
		Mottles:	Common medium 5YR 4/6 orange mottles (2-5mm)
		Concretions:	*Not described*
		Structure:	*Not described*
		Boundary:	Distinct wavy boundary
		Cohesive/Non-cohesive:	*Not described*
		Strength:	*Not described*
		Failure:	*Not described*
		Penetration resistance:	*Not described*
		Plasticity:	*Not described*
		Stickiness:	*Not described*
		Soil water state:	*Not described*
		Roots:	Abundant micro to extremely fine roots
Bw(f)	32-70	Texture:	Silty clay
	(32-60, 32-80)	Colour:	2.5Y 5/3
		Mottles:	Common coarse 7.5YR 4/6 orange mottles
		Concretions:	-
		Structure:	Angular blocky?
		Boundary:	Abrupt irregular boundayr
		Cohesive/Non-cohesive:	Cohesive

		Strength:	Slightly firm
		Failure:	Friable
		Penetration resistance:	Moderate penetration resistance
		Plasticity:	Very plastic
		Stickiness:	Slightly sticky
		Soil water state:	Moderately to extremely moist
		Roots:	Many micro fine to extremely fine roots; Few fine to medium worm channels to the base of the horizon
Bx(g)	70-95+	Texture:	Silty clay
		Colour:	20% 2.5Y 5/3 (matrix)
		Mottles:	50% 7.5YR 5/8 orange mottles 30% fine 2.5Y 6/2 grey veins
		Concretions:	10% fine 2.5YR 2.5/1 manganese concretions
		Structure:	Massive?
		Boundary:	-
		Cohesive/Non-cohesive:	Cohesive
		Strength:	Firm
		Failure:	Brittle
		Penetration resistance:	High penetration resistance
		Plasticity:	Very plastic
		Stickiness:	Slightly sticky
		Soil water state:	Moderately to extremely moist
		Roots:	Few micro fine to extremely fine roots; 2% very fine pores

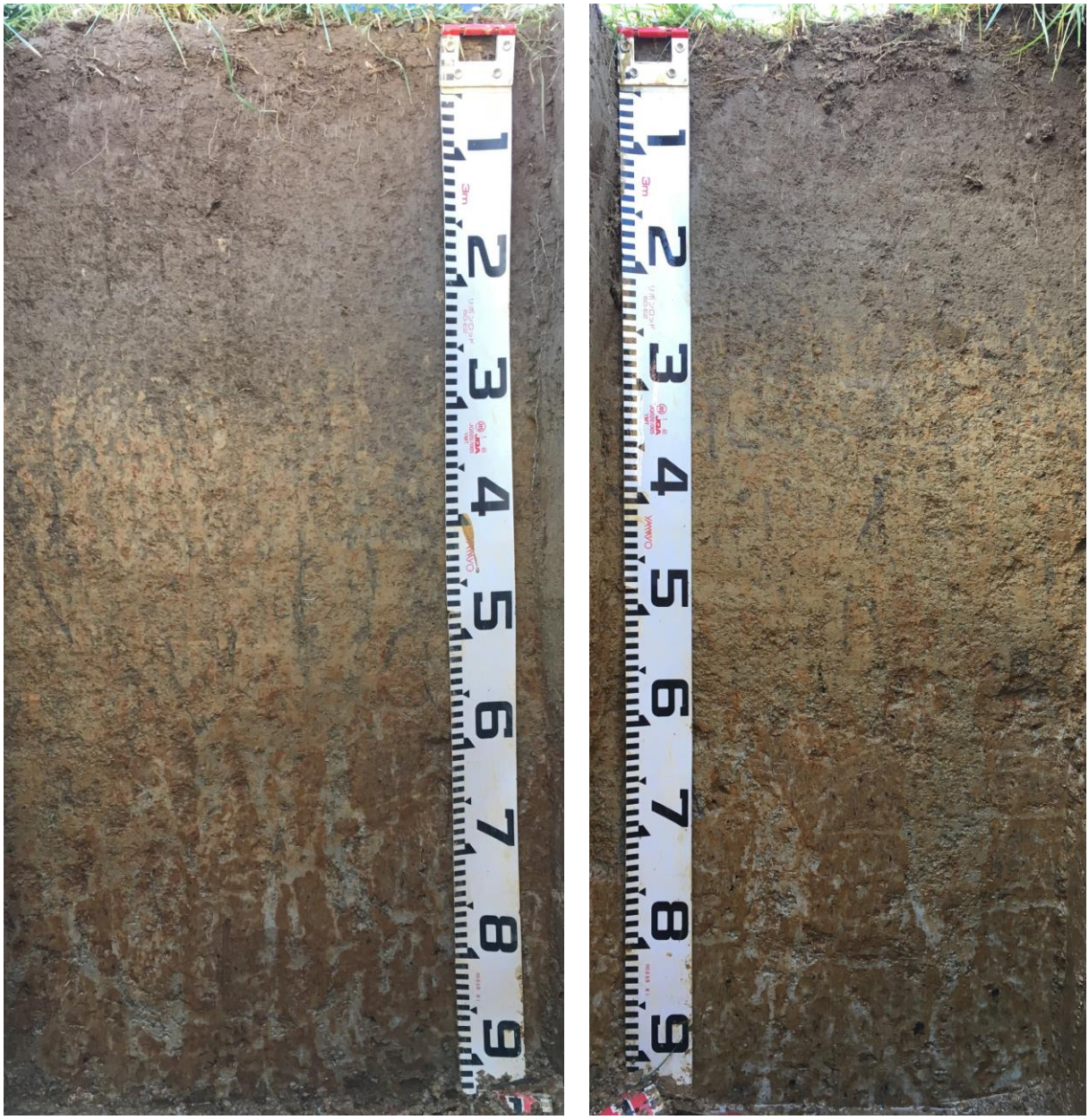

Figure A-2. Soil profile images at site IN1 (interfluve). Left image is proximal to the mole channel, right image is distal to the mole channel.

A.2.2 Interfluve 2 (IN2)

Site: Interfluve 2 (IN2)
Profile Code: OTA18-06
Survey: Otahuti
Region: Southland
Location: Otahuti PhD field site, head slope of the southernmost arm of the drainage basin gully. Pit excavated to expose two profiles, one profile proximal to a mole channel (~25cm) and the second profile distal to a mole channel (~0.7m). Only distal profile was described but proximal profile is very similar, unless otherwise stated.
Landform: Downland head slope; flat to gently undulating (2.3 degree slope angle)
Grid Reference: NZTM 1229058.442 E 4868650.14 N
Date Described: 07/09/2018
Author: Kirstin Deuss
Site Notes: N/A
NZSC: Mottled Firm Brown (BFM)
Drainage Class: Imperfect

Ap	0-26	Texture:	Silt loam (clay rich)
		Colour:	10YR 4/2
		Mottles:	5% 5YR 4/6 along root channels
		Concretions:	-
		Structure:	Granular
		Boundary:	Smooth indistinct boundary
		Cohesive/Non-cohesive:	Cohesive
		Strength:	Slightly firm
		Failure:	Friable
		Penetration resistance:	Low penetration resistance
		Plasticity:	Very plastic
		Stickiness:	Slightly sticky
		Soil water state:	Slightly moist
		Roots:	Abundant micro to extremely fine roots; few very fine roots
A/B	26-34	*Not described*	A/B has 5-10% 1-5mm sized 7.5YR 3/3 Mn nodules
Bw(f)	34-60 (34-43, 34-80)	Texture:	Silt loam (clay rich)
		Colour:	2.5Y 5/4 (matrix)
		Mottles:	Common (15%) coarse (10mm+) 7.5YR 5/8 mottles
		Concretions:	Common (15%) fine and few medium 7.5YR 3/3 FeMn nodules – nodules are concentrated mainly between 25-54cm and are associated with the mottles
		Structure:	Subangular blocky
		Boundary:	Abrupt irregular occluded boundary
		Cohesive/Non-cohesive:	Cohesive
		Strength:	Friable
		Failure:	Slightly firm
		Penetration resistance:	Low penetration resistance
		Plasticity:	Very plastic
		Stickiness:	Moderately sticky
		Soil water state:	Moderately to extremely moist
		Roots:	Abundant micro to extremely fine roots
Bx(g)	70-85+	Texture:	Silt loam (clay rich)
		Colour:	20% 2.5Y 5/4 (matrix)
		Mottles:	50% coarse 10YR 5/8 orange mottles 30% medium 5Y 6/2 grey veins
		Concretions:	Common (20%) fine Mn nodules
		Structure:	Platey? (plates of soil separating when removing cores)
		Boundary:	-
		Cohesive/Non-cohesive:	Cohesive
		Strength:	Very firm
		Failure:	Brittle
		Penetration resistance:	High penetration resistance
		Plasticity:	Very plastic
		Stickiness:	Very sticky
		Soil water state:	Slightly moist
		Roots:	Few extremely to very fine roots

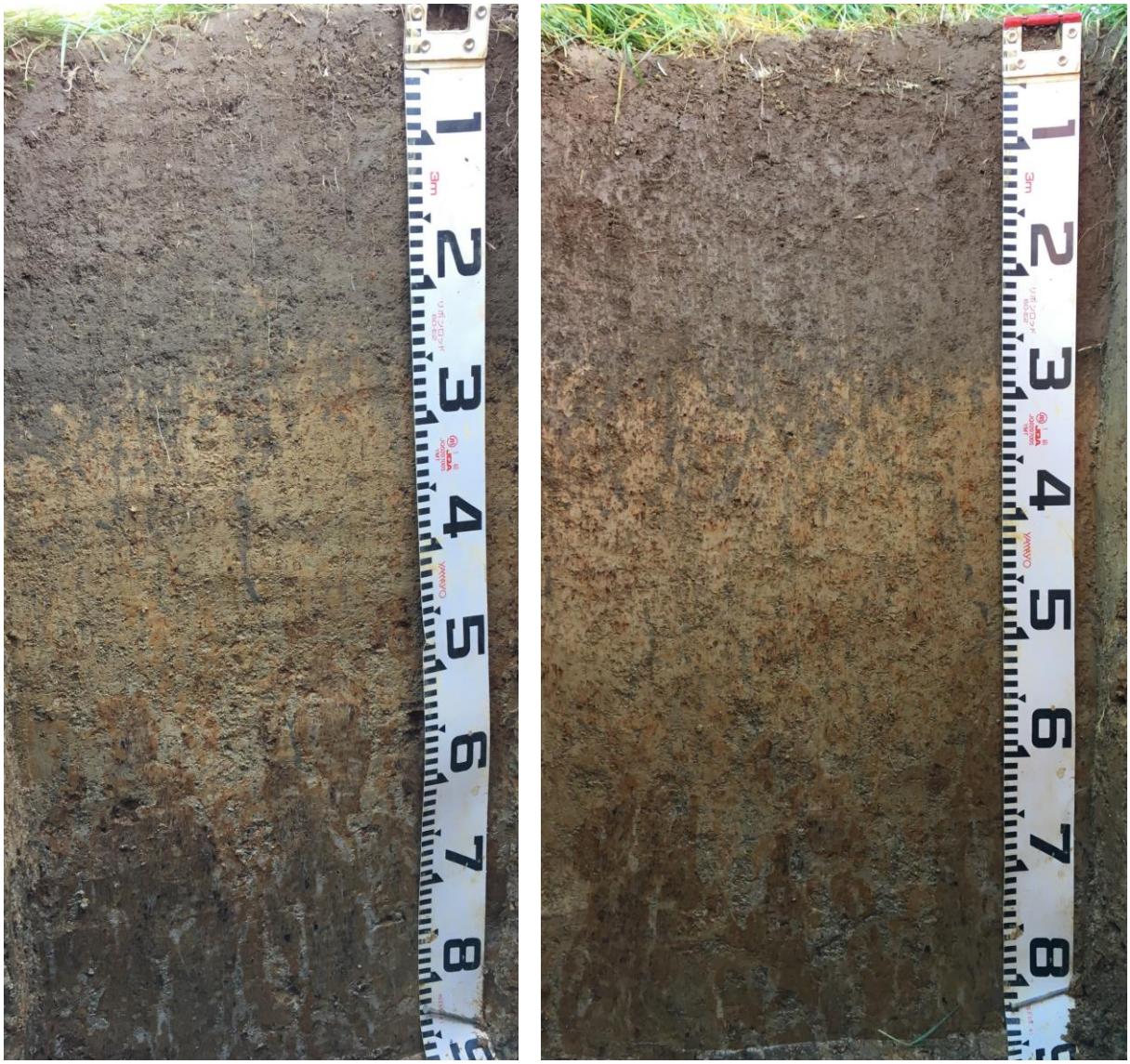

Figure A-3. Soil profile images at site IN2 (interfluve). Left image is proximal to the mole channel, right image is distal to the mole channel.

A.2.3 Head slope (HS)

Site: Head slope (HS)
Profile Code: OTA18-04
Survey: Otahuti
Region: Southland
Location: Otahuti PhD field site, true right head slope – side slope transition of the southernmost arm of the drainage basin gully. Pit excavated to expose two profiles, one profile proximal to a mole channel (~30cm) and the second profile distal to a mole channel (~0.8m). Only proximal profile was described but distal profile is very similar, unless otherwise stated.
Landform: Downland side slope-head slope transition; gently undulating (3.9 degree slope angle)
Grid Reference: NZTM 1229099.642 E 4868683.126 N
Date Described: 28/08/2018
Author: Kirstin Deuss
Site Notes:
NZSC: Mottled Firm Brown (BFM)
Drainage Class: Imperfect

Ap	0-28	Texture:	Silt loam
		Colour:	10YR 4/3
		Mottles:	-
		Concretions:	1% (2-3mm) Mn nodules
		Structure:	Granular
		Boundary:	Smooth abrupt boundary
		Cohesive/Non-cohesive:	Cohesive
		Strength:	Weak
		Failure:	Friable
		Penetration resistance:	Low penetration resistance
		Plasticity:	Very plastic
		Stickiness:	Slighlty sticky
		Soil water state:	Slightly moist
		Roots:	Abundant micro to extremely fine roots; few very fine roots
A/B	28-40	*Not described*	2% (5-10mm) 5YR 4/6 orange mottles; wavy indistinct boundary
Bw(fx)	40-57 (40-50, 40-65)	Texture:	Silty clay
		Colour:	2.5Y 5/4 (matrix)
		Mottles:	50% (40-70mm) Bx occlusions – periphery (10-20mm) of occlusions is dark orange 5YR 4/6, centre of larger occlusions is 30% 7.5YR 5/8 (lighter orange), 30% 2.5Y 5/4(matrix colour), 30% 2.5Y 6/2 (grey), 10% extremely fine 5YR 2.5/1 (black) Mn concretions
		Concretions:	Limited to within occlusions
		Structure:	Subangular blocky
		Boundary:	Convolute occluded diffuse boundary
		Cohesive/Non-cohesive:	Cohesive
		Strength:	Slightly firm
		Failure:	Friable
		Penetration resistance:	Moderate penetration resistance
		Plasticity:	Very plastic
		Stickiness:	Moderately sticky
		Soil water state:	Slightly moist
		Roots:	Common micro to extremely fine roots; Few fine to medium worm channels to the base of the horizon
Bx(g)	57-95+	Texture:	Silty clay
		Colour:	70% 7.5YR 5/8 (orange matrix)
		Mottles:	30% medium 2.5Y 6/2 (grey vertical mottles)
		Concretions:	1% very fine Mn concretions
		Structure:	Platey?
		Boundary:	-
		Cohesive/Non-cohesive:	Cohesive
		Strength:	Very firm
		Failure:	Brittle
		Penetration resistance:	High penetration resistance
		Plasticity:	Very plastic
		Stickiness:	Moderately sticky
		Soil water state:	Slightly moist
		Roots:	Few micro-extremely fine roots

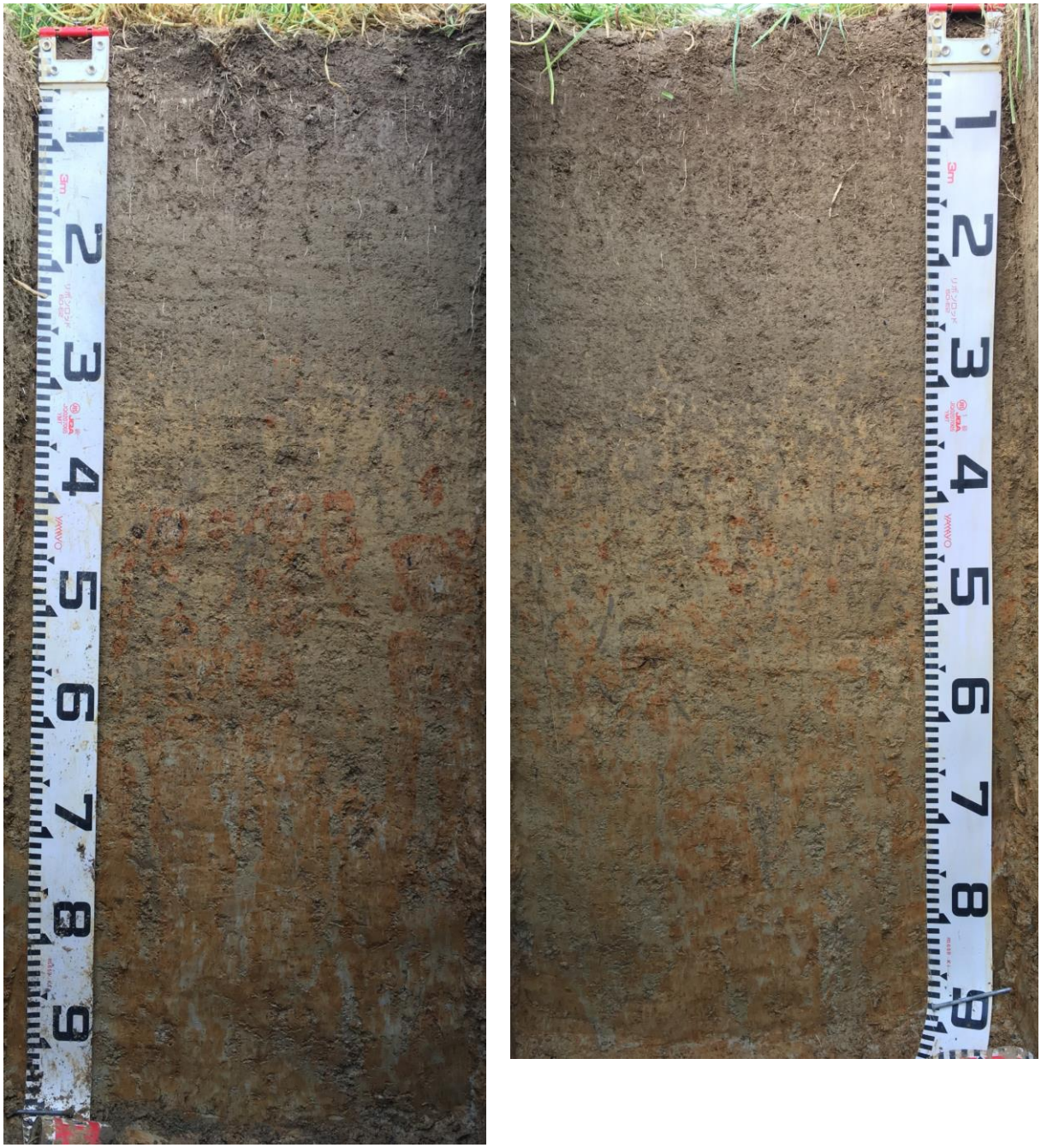

Figure A-4. Soil profile images at site HS (head slope). Left image is proximal to the mole channel, right image is distal to the mole channel.

A.2.4 Nose slope (NS)

Site: Nose slope (NS)
Profile Code: OTA18-03
Survey: Otahuti
Region: Southland
Location: Otahuti PhD field site, nose slope between the two arms of the drainage basin gully. Pit excavated to expose two profiles, one profile proximal to a mole channel (~30cm) and the second profile distal to a mole channel (~1m). Only distal profile was described but proximal profile is very similar, unless otherwise stated.
Landform: Downland nose slope; undulating (5.5 degree slope angle)
Grid Reference: NZTM 1229175.897 E 4868702.72 N
Date Described: 14/08/2018
Author: Kirstin Deuss
Site Notes: *First profile description ever made → lacks details*
NZSC: Mottled Firm Brown (BFM)
Drainage Class: Imperfect

Ap	0-27	Texture:	Silt loam
		Colour:	10YR 4/3
		Mottles:	*Not described*
		Concretions:	*Not described*
		Structure:	Granular
		Boundary:	Abrupt smooth boundary
		Cohesive/Non-cohesive:	*Not described*
		Strength:	*Not described*
		Failure:	*Not described*
		Penetration resistance:	*Not described*
		Plasticity:	*Not described*
		Stickiness:	*Not described*
		Soil water state:	*Not described*
		Roots:	*Not described*
Bw(f)	27-38	Texture:	Silt loam
		Colour:	10YR 5/4 (matrix)
		Mottles:	Few medium 7.5YR 4/6 (orange) mottles
		Concretions:	*Not described*
		Structure:	Subangular blocky
		Boundary:	Abrupt smooth boundary
		Cohesive/Non-cohesive:	*Not described*
		Strength:	*Not described*
		Failure:	*Not described*
		Penetration resistance:	*Not described*
		Plasticity:	*Not described*
		Stickiness:	*Not described*
		Soil water state:	*Not described*
		Roots:	*Not described*
Bx(g)	38-60	Texture:	Silty clay
		Colour:	10% 10YR 5/4
		Mottles:	30% 7.5YR 4/6 (orange) 20% 2.5YR 6/4 (grey) 40% coarse to very coarse 5YR 2.5/1 (black) mottles
		Concretions:	*Not described*
		Structure:	Angular blocky?
		Boundary:	Distinct smooth boundary
		Cohesive/Non-cohesive:	*Not described*
		Strength:	Very firm to hard
		Failure:	Brittle
		Penetration resistance:	*Not described*
		Plasticity:	*Not described*
		Stickiness:	*Not described*
		Soil water state:	Base of Bw(xg) saturated (60cm) – water perching on Bx
		Roots:	*Not described*
Bx	60-75	Texture:	*Not described*
		Colour:	10YR 5/8
		Mottles:	20% 2.5Y 7/2
		Concretions:	*Not described*

		Structure:	*Not described*
		Boundary:	*Not described*
		Cohesive/Non-cohesive:	*Not described*
		Strength:	*Not described*
		Failure:	*Not described*
		Penetration resistance:	*Not described*
		Plasticity:	*Not described*
		Stickiness:	*Not described*
		Soil water state:	*Not described*
		Roots:	*Not described*
2B?	75+		Few very weathered gravels at the very base of the profile

Figure A-5. Soil profile images at site NS (nose slope). Left image is proximal to the mole channel, right image is distal to the mole channel.

A.2.5 Divergent side slope (dSS)

Site: Divergent side slope (dSS)
Profile Code: OTA18-01
Survey: Otahuti
Region: Southland
Location: Otahuti PhD field site, true right slope of the southernmost arm of the drainage basin gully. Pit excavated to expose two profiles, one profile proximal to a mole channel (~30cm) and the second profile distal to a mole channel (~1.5m). Only distal profile was described but proximal profile is very similar, unless otherwise stated.
Landform: Downland side slope; undulating (6 degree slope angle)
Grid Reference: NZTM 1229210.683 E 4868702.72 N
Date Described: 28/08/2018
Author: Kirstin Deuss
Site Notes: Bx(g) initially dry, soon after excavating became wet from perched water
NZSC: Mottled Firm Brown (BFM)
Drainage Class: Imperfect

Ap	0-23	Texture:	Silt loam/silty clay
		Colour:	2.5Y 5/3 (dry), 2.5Y4/3 (moist)
		Mottles:	-
		Concretions:	-
		Structure:	granular structure
		Boundary:	diffuse smooth boundary
		Cohesive/Non-cohesive:	cohesive
		Strength:	slightly firm
		Failure:	friable
		Penetration resistance:	very low penetration resistance
		Plasticity:	very plastic
		Stickiness:	slightly sticky
		Soil water state:	slightly moist
		Roots:	abundant extremely fine roots & few very fine roots
A/B	23-34	*Not described*	
Bw(f)	34-50	Texture:	Silty clay
		Colour:	2.5Y 5/4 (matrix)
		Mottles:	Few (2%) medium 7.5YR 5/8 mottles
		Concretions:	Between 29-41cm common fine-medium Mn nodules (7.5YR 2.5/2)
		Structure:	Subangular blocky
		Boundary:	Smooth abrupt boundary
		Cohesive/Non-cohesive:	Cohesive
		Strength:	Weak
		Failure:	Friable
		Penetration resistance:	Moderate penetration resistance
		Plasticity:	Very plastic
		Stickiness:	Slightly sticky
		Soil water state:	Slightly moist
		Roots:	Abundant extremely fine roots
Bw(g)	50-80	Texture:	Silty clay
		Colour:	2.5Y 5/4 (matrix)
		Mottles:	Few 10% 2.5Y 7/3 (grey) mottles Common 20% 7.5YR 5/8 (orange) mottles
		Concretions:	Common 15% coarse Fn-Mn concretions Note: *In the profile proximal to mole channel only: between 51-59cm Few (2%) coarse Mn nodules (GLEY1 2.5/N) – not present in profile distal to mole.*
		Structure:	Angular blocky
		Boundary:	Sharp smooth boundary (occluded)
		Cohesive/Non-cohesive:	Cohesive
		Strength:	Slightly firm
		Failure:	Friable
		Penetration resistance:	Moderate penetration resistance
		Plasticity:	Very plastic
		Stickiness:	Moderately sticky
		Soil water state:	Very to extremely moist

Bx(g)	80-94	Roots:	Abundant extremely fine roots proliferating at the base of the horizon/surface of the Bx; few worm casts all the way from A/B to the surface of the Bx
		Texture:	Silty clay
		Colour:	50% 10YR 5/6 (matrix)
		Mottles:	20% coarse 2.5Y 7/2 vertical grey veins 30% 7.5YR 5/8 coarse orange mottles
		Concretions:	Few fine to medium Mn concretions
		Structure:	Platey
		Boundary:	-
		Cohesive/Non-cohesive:	Cohesive
		Strength:	Hard to very hard
		Failure:	Brittle
		Penetration resistance:	Very high penetration resistance
		Plasticity:	Very plastic
		Stickiness:	Very sticky
		Soil water state:	Dry
		Roots:	No roots
bBx(g)	94-100+		

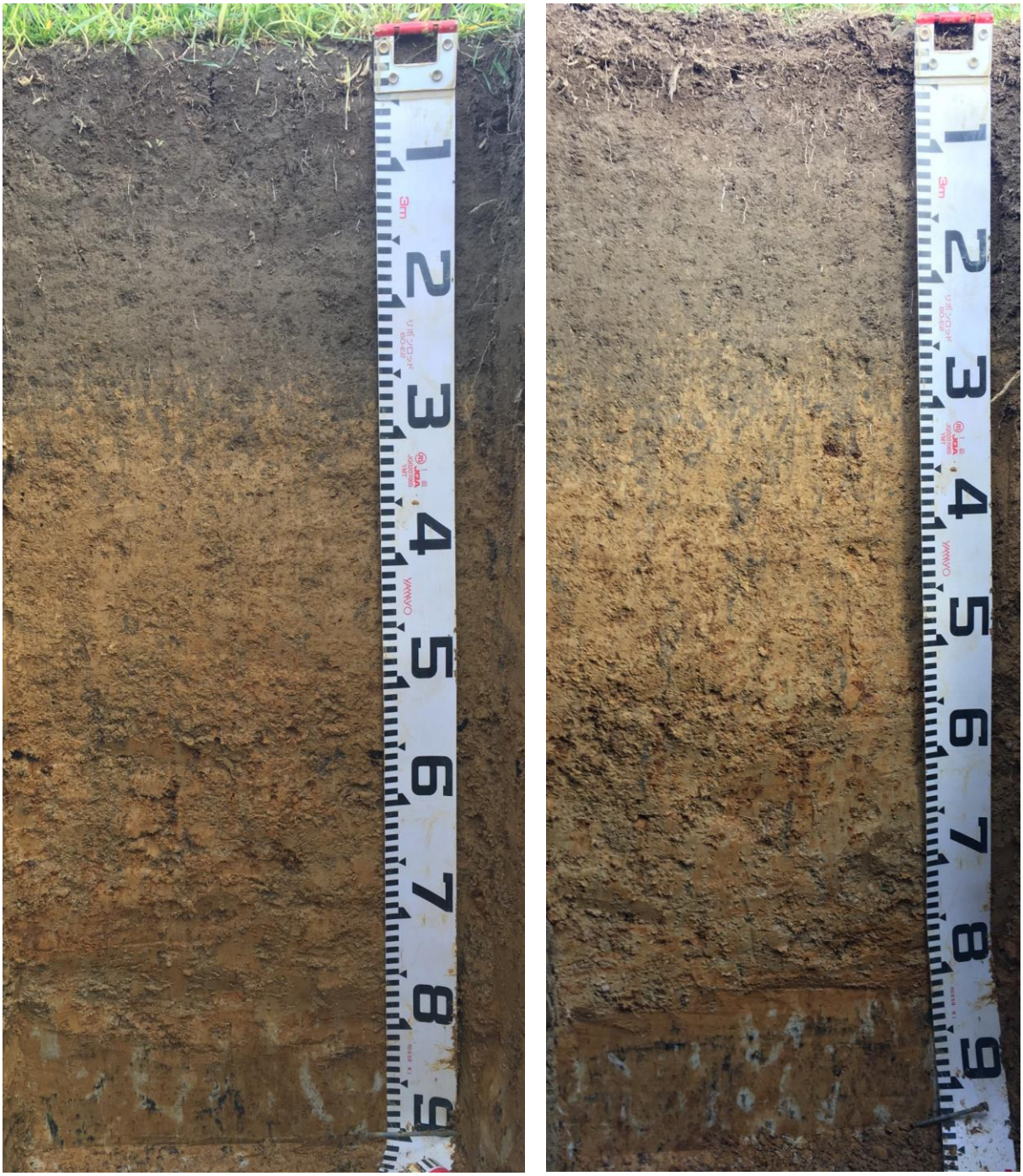

Figure A-6. Soil profile images at site dSS (divergent side slope). Left image is proximal to the mole channel, right image is distal to the mole channel.

A.2.6 Planar side slope (pSS)

Site: Planar side slope (pSS)
Profile Code: OTA18-02
Survey: Otahuti
Region: Southland
Location: Otahuti PhD field site, true right slope of the southernmost arm of the drainage basin gully. Pit excavated to expose two profiles, one profile proximal to a mole channel (~30cm) and the second profile distal to a mole channel (~1m). Only proximal profile was described but distal profile is very similar, unless otherwise stated.
Landform: Downland shoulder slope; undulating (4 degree slope angle)
Grid Reference: NZTM 1229182.682 E 4868679.312 N
Date Described: 20/08/2018
Author: Kirstin Deuss
Site Notes: *Second profile description ever made → lacks details*
NZSC: Mottled Firm Brown (BFM)
Drainage Class: Imperfect

Ap	0-27	Texture:	Silt loam
		Colour:	10YR 4/3
		Mottles:	-
		Concretions:	-
		Structure:	Granular
		Boundary:	Indistinct smooth boundary
		Cohesive/Non-cohesive:	*Not described*
		Strength:	*Not described*
		Failure:	*Not described*
		Penetration resistance:	*Not described*
		Plasticity:	*Not described*
		Stickiness:	*Not described*
		Soil water state:	*Not described*
		Roots:	Many micro to extremely fine roots, few very fine roots
A/B	27-35	*Not described*	*Not described*
Bw(f)	35-63	Texture:	Clay loam
		Colour:	10YR 5/4 (matrix)
		Mottles:	20% 7.5YR 4/6 mottles
		Concretions:	*Not described*
		Structure:	Subangular blocky
		Boundary:	Abrupt wavy boundary (occluded)
		Cohesive/Non-cohesive:	*Not described*
		Strength:	*Not described*
		Failure:	*Not described*
		Penetration resistance:	*Not described*
		Plasticity:	*Not described*
		Stickiness:	*Not described*
		Soil water state:	*Not described*
		Roots:	Many micro to extremely fine roots, worm channels to 60cm
Bw(xg)	63-75	Texture:	Clay loam
		Colour:	5% 10YR 5/4 (matrix)
		Mottles:	40% 2.5Y 6/3 (grey) 50% 10YR 5/6 (orange)
		Concretions:	5% 5YR 2.5/1 fine to medium manganese concretions
		Structure:	*Not described*
		Boundary:	Indistinct wavy boundary
		Cohesive/Non-cohesive:	*Not described*
		Strength:	Hard to very hard soil strength (bottle jack under truck towbar required to extract core and insert moisture sensors at 75cm)
		Failure:	*Not described*
		Penetration resistance:	Very high
		Plasticity:	*Not described*
		Stickiness:	*Not described*
		Soil water state:	*Not described*
		Roots:	Few roots
Bx(g)	75-93+	Texture:	Silty clay
		Colour:	70% 2.5Y 5/2

		Mottles:	10% 2.5Y 6/3 (grey) mottles 15% 10YR 5/6 (orange) mottles
		Concretions:	5% very fine to fine manganese concretions
		Structure:	*Not described*
		Boundary:	*Not described*
		Cohesive/Non-cohesive:	*Not described*
		Strength:	Hard to very hard soil strength
		Failure:	*Not described*
		Penetration resistance:	Very high
		Plasticity:	*Not described*
		Stickiness:	*Not described*
		Soil water state:	Saturated spot at base of profile (macropore?)
		Roots:	*Not described*

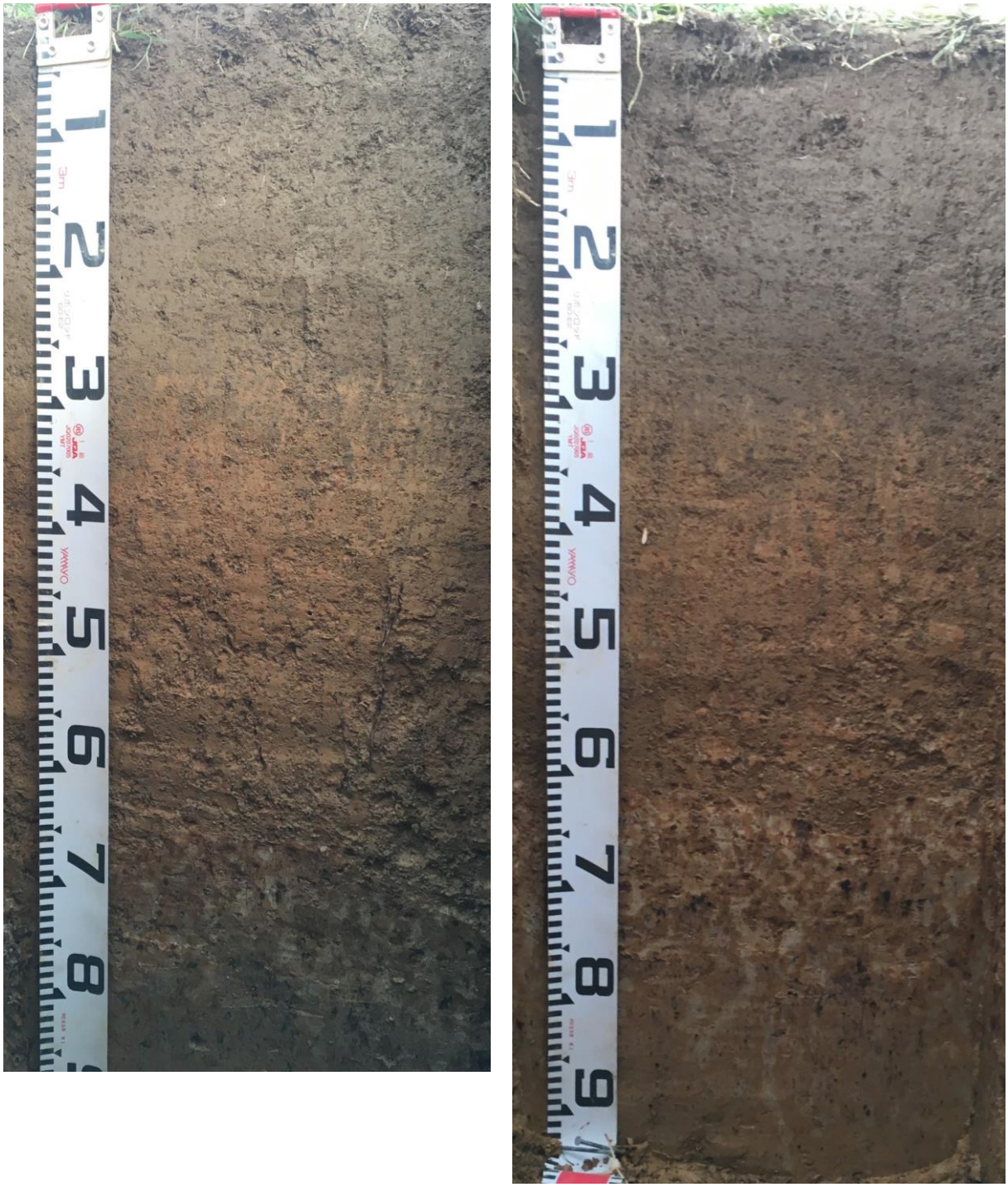

Figure A-7. Soil profile images at site pSS (planar side slope). Left image is proximal to the mole channel, right image is distal to the mole channel.

A.2.7 Lower hollow (lHO)

Site: Lower hollow (lHO)
Profile Code: OTA18-07
Survey: Otahuti
Region: Southland
Location: Otahuti PhD field site, in the gully at the mouth of the drainage basin, adjacent to the tile drain
Landform: Downland gully; flat to gently undulating (2.6 degree slope angle)
Grid Reference: NZTM 1229290.134 E 4868748.785 N
Date Described: 26/10/2018
Author: Peter Almond and Kirstin Deuss
Site Notes: N/A
NZSC: Mottled Orthic Brown (BOM)
Drainage Class: Imperfect

Ah	0-55	Texture:	Clay loam
		Colour:	2.5Y 4/2
		Mottles:	-
		Concretions:	-
		Structure:	Weak subangular blocky grading to moderately developed fine and medium subangular blocky
		Boundary:	Gradual irregular boundary
		Cohesive/Non-cohesive:	*Not described*
		Strength:	Firm
		Failure:	Brittle
		Penetration resistance:	*Not described*
		Plasticity:	*Not described*
		Stickiness:	*Not described*
		Soil water state:	*Not described*
		Roots:	*Not described*
A/Bw(g)	55-70	Texture:	Clay loam
		Colour:	30% 2.5Y 4/2 and 5Y 6/3
		Mottles:	Many distinct coarse 7.5YR 5/8 mottles
		Concretions:	-
		Structure:	Weak very coarse subangular blocky breaking to weak fine subangular blocky
		Boundary:	*Not described*
		Cohesive/Non-cohesive:	*Not described*
		Strength:	Friable
		Failure:	Semi deformable
		Penetration resistance:	*Not described*
		Plasticity:	*Not described*
		Stickiness:	*Not described*
		Soil water state:	*Not described*
		Roots:	*Not described*
Bt(g)	70-90+	Texture:	Clay
		Colour:	40% 5Y 6/3 and 60% 7.5YR 5/8
		Mottles:	-
		Concretions:	-
		Structure:	Weak fine subangular blocky
		Boundary:	*Not described*
		Cohesive/Non-cohesive:	*Not described*
		Strength:	*Not described*
		Failure:	*Not described*
		Penetration resistance:	*Not described*
		Plasticity:	*Not described*
		Stickiness:	*Not described*
		Soil water state:	*Not described*
		Roots:	*Not described*

Figure A-8. Soil profile image at site lHO (lower hollow).

A.2.8 Catchment outlet

Site: Catchment outlet
Profile Code: OTA18-08
Survey: Otahuti
Region: Southland
Location: Otahuti PhD field site, in the gully at the mouth of the drainage basin – at the site of the tile drain flow meter installation.
Landform: Downland gully; flat to gently undulating (0.6 degree slope angle)
Grid Reference: NZTM 1229296.33 E 4868748.343 N
Date Described: 24/10/2018
Author: Peter Almond and Kirstin Deuss
Site Notes: Bg1 and Bg2 gully fill encapsulating at least one episodic erosion and backfill
NZSC: Fill Anthropic (AF)
Drainage Class: Imperfect

A/B Fill (Tile drain backfill – anthropogenic)	0-81	Texture:	Clay loam
		Colour:	10YR 4/3 and 15% 10YR 6/6
		Mottles:	-
		Concretions:	-
		Structure:	Moderately developed fine nutty structure
		Boundary:	Sharp wavy boundary
		Cohesive/Non-cohesive:	*Not described*
		Strength:	*Not described*
		Failure:	*Not described*
		Penetration resistance:	*Not described*
		Plasticity:	*Not described*
		Stickiness:	*Not described*
		Soil water state:	*Not described*
		Roots:	*Not described*
Bg1	81-91	Texture:	Clay loam
		Colour:	2.5Y 7/2
		Mottles:	30% common coarse distinct 7.5YR 5/6 mottles
		Concretions:	Appears to have V-shaped rills (from 91cm extending to 104cm), filled in with 2-5mm re-worked nodules. Boundary at top of rills abrupt and wavy
		Structure:	Weak fine prismatic structure
		Boundary:	Abrupt irregular boundary
		Cohesive/Non-cohesive:	*Not described*
		Strength:	Slightly firm
		Failure:	Brittle
		Penetration resistance:	*Not described*
		Plasticity:	*Not described*
		Stickiness:	*Not described*
		Soil water state:	*Not described*
		Roots:	*Not described*
Bg2	91-112	Texture:	Silty clay
		Colour:	40% 2.5Y 7/2; 40% 2.5Y 7/1
		Mottles:	20% coarse distinct 7.5YR 5/6 mottles
		Concretions:	-
		Structure:	Weak medium prismatic
		Boundary:	Wavy
		Cohesive/Non-cohesive:	*Not described*
		Strength:	Slightly firm
		Failure:	Semi deformable
		Penetration resistance:	*Not described*
		Plasticity:	*Not described*
		Stickiness:	*Not described*
		Soil water state:	*Not described*
		Roots:	*Not described*
2B	112+	*Not described*	Coarse gravel in silty-clayey matrix

Figure A-9. Soil profile images at site of tile flow meter installation (catchment outlet).

Appendix B
Soil Sample Lab Results

B.1 Particle Size Distribution

Environmental Chemistry Laboratory
Manaaki Whenua – Landcare Research
Riddet Rd, Massey University Campus,
Private Bag 11052, Palmerston North 4442

Manaaki Whenua
Landcare Research

IANZ
ACCREDITED LABORATORY

Job number: LJ18039_PSD
Results reported by: John Dando, Senior Technician
Customer: Kirstin Deuss c/o Sam Carrick, Manaaki Whenua – Landcare Research PO Box 69040, Lincoln 7640
Date received: 24th October & 6th November 2018
Date reported: 15th January 2019

Table B-1. Particle Size Distribution.

						Fine–Earth Particle Size Distribution (Method No. 190 (ii))				
Client ID	Pit No.	Site ID	Mole Proximity	Depth (mm)	Lab ID	Coarse Sand 2-0.6 mm	Medium Sand 0.6-0.2 mm	Fine Sand 0.2-0.06 mm	Silt 0.06-0.002 mm	Clay <0.002 mm
1808-50	1	dSS	Distal	110-185	M18/1588	1	1	6	66	26
1808-52	1	dSS	Distal	260-335	M18/1589	0	1	6	64	29
1808-54	1	dSS	Distal	410-485	M18/1590	1	0	4	63	32
1808-56	1	dSS	Distal	560-635	M18/1591	3	2	5	52	38
1808-68	1	dSS	Distal	810-885	M18/1592	0	1	6	47	46
1808-58	1	dSS	Proximal	110-185	M18/1593	1	1	6	64	28
1808-60	1	dSS	Proximal	260-335	M18/1594	0	0	5	65	30
1808-62	1	dSS	Proximal	410-485	M18/1595	1	0	5	59	35
1808-64	1	dSS	Proximal	560-635	M18/1596	5	2	5	47	41
1808-66	1	dSS	Proximal	810-885	M18/1597	1	2	7	45	45
1808-24	2	pSS	Distal	110-185	M18/1598	0	1	5	68	26
1808-28	2	pSS	Distal	260-335	M18/1599	0	0	5	65	30
1808-32	2	pSS	Distal	410-485	M18/1600	0	0	5	61	34
1808-42	2	pSS	Distal	560-635	M18/1601	2	2	8	55	33
1808-34	2	pSS	Distal	635-710	M18/1603	2	1	6	55	36
1808-48	2	pSS	Distal	710-785	M18/1602	1	1	6	62	30
1808-38	2	pSS	Distal	860-935	M18/1604	0	0	4	59	37
1808-22	2	pSS	Proximal	110-185	M18/1605	0	1	5	66	28
1808-26	2	pSS	Proximal	260-335	M18/1606	0	1	5	64	30
1808-30	2	pSS	Proximal	410-485	M18/1607	0	0	4	60	36
1808-44	2	pSS	Proximal	560-635	M18/1608	2	1	5	57	35
1808-36	2	pSS	Proximal	635-710	M18/1610	2	1	5	56	36
1808-46	2	pSS	Proximal	710-785	M18/1609	0	0	5	57	38
1808-40	2	pSS	Proximal	860-935	M18/1611	1	0	4	58	37
1808-08	3	NS	Distal	110-185	M18/1612	3	2	6	62	27
1808-10	3	NS	Distal	260-335	M18/1613	1	1	6	61	31
1808-12	3	NS	Distal	410-485	M18/1614	0	1	8	59	32
1808-14	3	NS	Distal	560-635	M18/1615	1	1	7	47	44
1808-16	3	NS	Distal	710-785	M18/1616	1	2	6	39	52
180814-02	3	NS	Proximal	110-185	M18/1617	1	1	5	65	28
180814-04	3	NS	Proximal	260-335	M18/1618	2	1	5	61	31
1808-06	3	NS	Proximal	410-485	M18/1619	0	1	8	59	32
1808-18	3	NS	Proximal	560-635	M18/1620	1	1	7	48	43
1808-20	3	NS	Proximal	710-785	M18/1621	0	2	7	38	53

Table B-1. *continued*. Particle Size Distribution.

						Fine–Earth Particle Size Distribution (Method No. 190 (ii))				
Client ID	Pit No.	Site ID	Mole Proximity	Depth (mm)	Lab ID	Coarse Sand 2-0.6 mm	Medium Sand 0.6-0.2 mm	Fine Sand 0.2-0.06 mm	Silt 0.06-0.002 mm	Clay <0.002 mm
1808-110	4	HS	Proximal	110-185	M18/1622	0	1	6	67	26
1808-112	4	HS	Proximal	260-335	M18/1623	0	0	5	67	28
1808-114	4	HS	Proximal	410-485	M18/1624	0	0	6	65	29
1808-116	4	HS	Proximal	560-635	M18/1625	0	0	6	63	31
1808-118	4	HS	Proximal	710-785	M18/1626	0	0	5	59	36
1808-120	4	HS	Distal	110-185	M18/1627	0	1	5	68	26
1808-122	4	HS	Distal	260-335	M18/1628	0	1	5	68	26
1808-124	4	HS	Distal	410-485	M18/1629	1	1	6	65	27
1808-126	4	HS	Distal	560-635	M18/1630	0	0	5	66	29
1808-128	4	HS	Distal	710-785	M18/1631	0	0	5	60	35
1808-70	5	IN1	Proximal	110-185	M18/1632	0	1	5	67	27
1808-72	5	IN1	Proximal	260-335	M18/1633	0	0	5	67	28
1808-74	5	IN1	Proximal	410-485	M18/1634	0	0	5	64	31
1808-76	5	IN1	Proximal	560-635	M18/1635	0	0	5	61	34
1808-78	5	IN1	Proximal	810-885	M18/1636	0	0	4	59	37
1808-80	5	IN1	Distal	110-185	M18/1637	0	0	5	68	27
1808-82	5	IN1	Distal	260-335	M18/1638	0	0	5	66	29
1808-84	5	IN1	Distal	410-485	M18/1639	0	0	5	62	33
1808-86	5	IN1	Distal	560-635	M18/1640	0	0	5	59	36
1808-88	5	IN1	Distal	810-885	M18/1641	0	0	4	55	41
1808-100	6	IN2	Proximal	110-185	M18/1642	0	1	6	68	25
1808-102	6	IN2	Proximal	260-335	M18/1643	0	0	5	69	26
1808-104	6	IN2	Proximal	410-485	M18/1644	0	0	7	61	32
1808-106	6	IN2	Proximal	560-635	M18/1645	0	0	7	60	33
1808-108	6	IN2	Proximal	710-785	M18/1646	0	0	5	61	34
1808-90	6	IN2	Distal	110-185	M18/1647	1	1	5	68	25
1808-92	6	IN2	Distal	260-335	M18/1648	0	0	6	69	25
1808-94	6	IN2	Distal	410-485	M18/1649	0	0	6	69	25
1808-96	6	IN2	Distal	560-635	M18/1650	0	0	6	61	33
1808-98	6	IN2	Distal	710-785	M18/1651	0	0	5	61	34
1808-01	7	lHO	NA	110-185	M18/1723	1	1	8	62	28
1808-03	7	lHO	NA	410-485	M18/1724	1	1	9	59	30

B.2 Soil Chemistry

Environmental Chemistry Laboratory
Manaaki Whenua – Landcare Research
Riddet Rd, Massey University Campus,
Private Bag 11052, Palmerston North 4442

Job number: LJ18039_PSD
Results reported by: Ngaire Foster, Lab Manager
Customer: Kirstin Deuss c/o Sam Carrick, Manaaki Whenua – Landcare Research PO Box 69040, Lincoln 7640
Date received: 24th October & 6th November 2018
Date reported: 4th June 2019

Table B-2. Soil Chemistry. Numbers in square brackets refer to method number.

*Carbon to Nitrogen ratio (C/N) is calculated.

Client ID	Site ID	Mole Proximity	Depth (mm)	Lab ID	Organic Carbon (%) [114]	Total Nitrogen (%) [114]	C/N ratio [*]	Phosphate Retention (%) [132]	Cation Exchange Capacity (cmol(+)/kg) [144(i)]	Air-Dried Soil Water Content (%) [104(i)]
1808-50	dSS	Distal	110-185	M18/1588	2.93	0.28	10	34	15.0	2.0
1808-52	dSS	Distal	260-335	M18/1589	1.59	0.14	12	39	9.8	1.8
1808-54	dSS	Distal	410-485	M18/1590	0.87	0.09	10	39	9.1	1.8
1808-56	dSS	Distal	560-635	M18/1591	0.60	0.05	12	39	10.4	2.2
1808-68	dSS	Distal	810-885	M18/1592	0.20	0.03	7	38	10.8	2.2
1808-58	dSS	Proximal	110-185	M18/1593	3.21	0.30	11	32	15.8	2.6
1808-60	dSS	Proximal	260-335	M18/1594	1.55	0.13	12	38	10.4	1.7
1808-62	dSS	Proximal	410-485	M18/1595	0.87	0.08	11	40	10.2	1.8
1808-64	dSS	Proximal	560-635	M18/1596	0.63	0.06	11	44	11.8	2.2
1808-66	dSS	Proximal	810-885	M18/1597	0.18	0.03	7	37	10.1	2.1
1808-24	pSS	Distal	110-185	M18/1598	3.11	0.29	11	36	15.3	2.5
1808-28	pSS	Distal	260-335	M18/1599	1.79	0.15	12	42	11.4	1.9
1808-32	pSS	Distal	410-485	M18/1600	0.96	0.08	12	44	10.5	1.9
1808-42	pSS	Distal	560-635	M18/1601	0.31	0.04	8	40	10.4	2.1
1808-34	pSS	Distal	635-710	M18/1603	0.64	0.05	12	40	11.6	2.1
1808-48	pSS	Distal	710-785	M18/1602	0.59	0.05	11	33	9.3	1.6
1808-38	pSS	Distal	860-935	M18/1604	0.26	0.04	7	33	9.8	1.7
1808-22	pSS	Proximal	110-185	M18/1605	3.37	0.32	11	36	15.9	2.0
1808-26	pSS	Proximal	260-335	M18/1606	1.90	0.16	12	43	12.1	1.9
1808-30	pSS	Proximal	410-485	M18/1607	0.90	0.07	12	46	11.2	2.0
1808-44	pSS	Proximal	560-635	M18/1608	0.83	0.07	12	42	10.9	2.0
1808-36	pSS	Proximal	635-710	M18/1610	0.30	0.04	8	44	11.1	2.1
1808-46	pSS	Proximal	710-785	M18/1609	0.24	0.03	7	41	11.3	2.0
1808-40	pSS	Proximal	860-935	M18/1611	0.27	0.04	8	33	10.5	1.8
1808-08	NS	Distal	110-185	M18/1612	2.96	0.27	11	38	14.2	2.0
1808-10	NS	Distal	260-335	M18/1613	1.28	0.11	11	41	10.3	1.8
1808-12	NS	Distal	410-485	M18/1614	0.37	0.04	9	38	9.5	1.8
1808-14	NS	Distal	560-635	M18/1615	0.36	0.04	9	38	11.5	2.0
1808-16	NS	Distal	710-785	M18/1616	0.27	0.03	8	42	14.4	2.3
180814-02	NS	Proximal	110-185	M18/1617	2.90	0.27	11	36	14.3	1.9
180814-04	NS	Proximal	260-335	M18/1618	1.72	0.15	12	40	10.8	1.8
1808-06	NS	Proximal	410-485	M18/1619	0.29	0.03	8	38	11.2	1.8
1808-18	NS	Proximal	560-635	M18/1620	0.37	0.04	9	39	11.0	2.1
1808-20	NS	Proximal	710-785	M18/1621	0.23	0.03	8	41	15.6	2.2

Table B-2. *continued.* Soil Chemistry. Numbers in square brackets refer to method number.

*Carbon to Nitrogen ratio (C/N) is calculated.

Client ID	Site ID	Mole Proximity	Depth (mm)	Lab ID	Organic Carbon (%) [114]	Total Nitrogen (%) [114]	C/N ratio [*]	Phosphate Retention (%) [132]	Cation Exchange Capacity (cmol(+)/kg) [144(i)]	Air-Dried Soil Water Content (%) [104(i)]
1808-110	HS	Proximal	110-185	M18/1622	3.12	0.29	11	34	15.2	1.8
1808-112	HS	Proximal	260-335	M18/1623	1.74	0.14	12	40	11.7	1.6
1808-114	HS	Proximal	410-485	M18/1624	1.39	0.11	13	41	10.6	1.7
1808-116	HS	Proximal	560-635	M18/1625	0.86	0.07	13	33	11.3	1.7
1808-118	HS	Proximal	710-785	M18/1626	0.61	0.05	11	30	12.8	1.8
1808-120	HS	Distal	110-185	M18/1627	2.91	0.28	10	33	13.8	1.8
1808-122	HS	Distal	260-335	M18/1628	1.90	0.16	12	36	11.3	1.6
1808-124	HS	Distal	410-485	M18/1629	1.34	0.11	13	42	10.2	1.6
1808-126	HS	Distal	560-635	M18/1630	0.84	0.07	12	30	9.3	1.5
1808-128	HS	Distal	710-785	M18/1631	0.60	0.06	11	29	11.8	1.7
1808-70	IN1	Proximal	110-185	M18/1632	3.35	0.31	11	36	14.5	1.8
1808-72	IN1	Proximal	260-335	M18/1633	1.52	0.13	11	31	9.9	1.4
1808-74	IN1	Proximal	410-485	M18/1634	0.82	0.08	10	31	9.4	1.6
1808-76	IN1	Proximal	560-635	M18/1635	0.53	0.05	10	32	13.2	2.1
1808-78	IN1	Proximal	810-885	M18/1636	0.31	0.04	8	32	14.0	2.3
1808-80	IN1	Distal	110-185	M18/1637	3.58	0.33	11	38	15.2	2.3
1808-82	IN1	Distal	260-335	M18/1638	1.65	0.14	12	41	11.3	2.0
1808-84	IN1	Distal	410-485	M18/1639	0.93	0.09	11	37	11.7	2.2
1808-86	IN1	Distal	560-635	M18/1640	0.50	0.05	10	33	13.4	2.4
1808-88	IN1	Distal	810-885	M18/1641	0.26	0.04	7	32	14.1	2.5
1808-100	IN2	Proximal	110-185	M18/1642	3.17	0.28	11	36	15.0	2.2
1808-102	IN2	Proximal	260-335	M18/1643	1.32	0.12	11	39	10.0	1.8
1808-104	IN2	Proximal	410-485	M18/1644	0.62	0.06	10	35	11.5	2.4
1808-106	IN2	Proximal	560-635	M18/1645	0.43	0.05	9	32	12.5	2.0
1808-108	IN2	Proximal	710-785	M18/1646	0.28	0.04	7	31	13.6	2.0
1808-90	IN2	Distal	110-185	M18/1647	3.36	0.30	11	35	14.1	1.9
1808-92	IN2	Distal	260-335	M18/1648	1.35	0.12	11	38	9.2	1.5
1808-94	IN2	Distal	410-485	M18/1649	0.95	0.09	11	39	8.6	1.5
1808-96	IN2	Distal	560-635	M18/1650	0.43	0.05	9	31	13.3	2.0
1808-98	IN2	Distal	710-785	M18/1651	0.30	0.04	7	31	14.5	2.0
1808-01	lHO	NA	110-185	M18/1723	2.90	0.27	11	39	14.2	2.1
1808-03	lHO	NA	410-485	M18/1724	2.22	0.19	12	41	12.6	2.1
Test starting date					13 Nov '18	13 Nov '18	13 Nov '18	10 Dec '18	19 Mar '19	30 Oct '18
Testing completion date					14 Nov '18	14 Nov '18	14 Nov '18	13 Dec '18	30 May '19	13 Nov '18

*Many low level results for C & N

B.3 Soil Physics

Environmental Chemistry Laboratory
Manaaki Whenua – Landcare Research
Riddet Rd, Massey University Campus,
Private Bag 11052, Palmerston North 4442

Job number: PJ18015
Customer: Kirstin Deuss c/o Sam Carrick, Manaaki Whenua – Landcare Research PO Box 69040, Lincoln 7640
Date received: 24th October & 6th November 2018

B.3.1 Physical Properties

B.3.1.1 Large Cores

Table B-3.1.1. Soil Physical Properties – Large (7.5 cm depth x 10 cm diameter) Cores.

Client ID	Site ID	Mole Proximity	Depth (mm)	Lab ID	Particle Density ($g\ cm^{-3}$)	Dry Bulk Density ($g\ cm^{-3}$)	Porosity (%)	Macro-porosity (%)	Air Capacity (%)
2154	dSS	Distal	110-185	PP18-0602	2.63	1.25	52	6	7
2276	dSS	Distal	260-335	PP18-0603	2.67	1.33	50	9	10
2050	dSS	Distal	410-485	PP18-0604	2.71	1.36	50	8	9
2201	dSS	Distal	560-635	PP18-0605	2.72	1.37	50	6	7
2103	dSS	Distal	810-885	PP18-0606	2.73	1.35	51	4	4
2100	dSS	Proximal	110-185	PP18-0607	2.62	1.21	54	5	7
2142	dSS	Proximal	260-335	PP18-0608	2.69	1.35	50	9	10
2132	dSS	Proximal	410-485	PP18-0609	2.71	1.35	50	9	10
2133	dSS	Proximal	560-635	PP18-0610	2.75	1.34	51	6	7
2123	dSS	Proximal	810-885	PP18-0611	2.75	1.38	50	3	3
2325	pSS	Distal	110-185	PP18-0612	2.60	1.16	56	7	9
2078	pSS	Distal	260-335	PP18-0613	2.68	1.36	49	8	9
2204	pSS	Distal	410-485	PP18-0614	2.71	1.40	48	9	10
2012	pSS	Distal	560-635	PP18-0615	2.72	1.39	49	8	8
2077	pSS	Distal	635-710	PP18-0617	2.74	1.45	47	5	5
2019	pSS	Distal	710-785	PP18-0616	2.75	1.49	46	4	4
2216	pSS	Distal	860-935	PP18-0618	2.72	1.50	45	4	4
2185	pSS	Proximal	110-185	PP18-0619	2.61	1.22	53	6	8
2259	pSS	Proximal	260-335	PP18-0620	2.67	1.32	50	9	10
2122	pSS	Proximal	410-485	PP18-0621	2.72	1.35	50	9	10
2296	pSS	Proximal	560-635	PP18-0622	2.73	1.35	50	9	9
2198	pSS	Proximal	635-710	PP18-0624	2.74	1.43	48	6	6
2280	pSS	Proximal	710-785	PP18-0623	2.72	1.49	45	4	4
2285	pSS	Proximal	860-935	PP18-0625	2.72	1.46	46	6	6
2220	NS	Distal	110-185	PP18-0641	2.64	1.22	54	6	7
2173	NS	Distal	260-335	PP18-0642	2.71	1.38	49	8	9
2007	NS	Distal	410-485	PP18-0643	2.72	1.46	46	5	5
2221	NS	Distal	560-635	PP18-0644	2.74	1.25	54	12	13
2274	NS	Distal	710-785	PP18-0645	2.72	1.18	57	6	6
2275	NS	Proximal	110-185	PP18-0646	2.61	1.15	56	6	8
2150	NS	Proximal	260-335	PP18-0647	2.69	1.35	50	8	9
2114	NS	Proximal	410-485	PP18-0648	2.73	1.45	47	5	6
2260	NS	Proximal	560-635	PP18-0649	2.75	1.38	50	4	4
2040	NS	Proximal	710-785	PP18-0650	2.72	1.20	56	4	4

Table B-3.1.1. *continued*. Soil Physical Properties – Large (7.5 cm depth x 10 cm diameter) Cores.

Client ID	Site ID	Mole Proximity	Depth (mm)	Lab ID	Particle Density ($g\ cm^{-3}$)	Dry Bulk Density ($g\ cm^{-3}$)	Porosity (%)	Macro-porosity (%)	Air Capacity (%)
2088	HS	Distal	110-185	PP18-0651	2.60	1.19	54	7	9
2017	HS	Distal	260-335	PP18-0652	2.66	1.36	49	9	10
2091	HS	Distal	410-485	PP18-0653	2.65	1.43	46	7	7
2044	HS	Distal	560-635	PP18-0654	2.71	1.41	48	7	8
2347	HS	Distal	710-785	PP18-0655	2.72	1.40	49	5	5
2337	HS	Proximal	110-185	PP18-0656	2.58	1.17	55	6	7
2268	HS	Proximal	260-335	PP18-0657	2.68	1.34	50	9	10
2270	HS	Proximal	410-485	PP18-0658	2.67	1.37	49	9	10
2265	HS	Proximal	560-635	PP18-0659	2.72	1.39	49	8	8
2269	HS	Proximal	710-785	PP18-0660	2.72	1.36	50	6	7
2158	IN1	Distal	110-185	PP18-0661	2.62	1.17	55	7	10
2180	IN1	Distal	260-335	PP18-0662	2.68	1.36	49	8	10
2200	IN1	Distal	410-485	PP18-0663	2.69	1.40	48	7	8
2287	IN1	Distal	560-635	PP18-0664	2.73	1.38	50	7	8
2194	IN1	Distal	810-885	PP18-0665	2.72	1.38	49	4	5
2029	IN1	Proximal	110-185	PP18-0687	2.61	1.15	56	7	10
2148	IN1	Proximal	260-335	PP18-0688	2.67	1.32	51	9	10
2047	IN1	Proximal	410-485	PP18-0689	2.71	1.31	52	10	11
2167	IN1	Proximal	560-635	PP18-0690	2.73	1.39	49	7	8
2179	IN1	Proximal	810-885	PP18-0691	2.72	1.39	49	3	3
2116	IN2	Distal	110-185	PP18-0692	2.63	1.12	57	9	11
2037	IN2	Distal	260-335	PP18-0693	2.70	1.35	50	8	9
2186	IN2	Distal	410-485	PP18-0694	2.69	1.39	48	7	8
2060	IN2	Distal	560-635	PP18-0695	2.73	1.42	48	5	5
2147	IN2	Distal	710-785	PP18-0696	2.75	1.38	50	4	4
2303	IN2	Proximal	110-185	PP18-0697	2.61	1.15	56	5	7
2238	IN2	Proximal	260-335	PP18-0698	2.68	1.36	49	8	9
2136	IN2	Proximal	410-485	PP18-0699	2.70	1.36	50	9	10
2298	IN2	Proximal	560-635	PP18-0700	2.74	1.44	47	4	4
2144	IN2	Proximal	710-785	PP18-0701	2.73	1.43	48	3	3
2092	lHO	NA	110-185	PP18-0666	2.64	1.27	52	7	8
2170	lHO	NA	410-485	PP18-0667	2.66	1.28	52	8	9

B.3.1.2 Small Cores

Table B-3.1.2. Soil Physical Properties – Small (3 cm depth x 5 cm diameter) Cores.

Client ID	Site ID	Mole Proximity	Depth (mm)	Lab ID	Particle Density ($g\ cm^{-3}$)	Dry Bulk Density ($g\ cm^{-3}$)	Porosity (%)
172	dSS	Distal	135-165	PP18-0538	2.63	1.20	54
174	dSS	Distal	285-315	PP18-0539	2.67	1.35	50
57	dSS	Distal	435-465	PP18-0540	2.71	1.37	50
294	dSS	Distal	585-615	PP18-0541	2.72	1.43	48
91	dSS	Distal	835-865	PP18-0542	2.73	1.35	50
212	dSS	Proximal	135-165	PP18-0543	2.62	1.21	54
63	dSS	Proximal	285-315	PP18-0544	2.69	1.35	50
123	dSS	Proximal	435-465	PP18-0545	2.71	1.36	50
75	dSS	Proximal	585-615	PP18-0546	2.75	1.33	52
170	dSS	Proximal	835-865	PP18-0547	2.75	1.36	51
L251	pSS	Distal	135-165	PP18-0548	2.60	1.10	58
L15	pSS	Distal	285-315	PP18-0549	2.68	1.28	52
L262	pSS	Distal	435-465	PP18-0550	2.71	1.33	51
116	pSS	Distal	585-615	PP18-0551	2.72	1.39	49
L275	pSS	Distal	660-690	PP18-0553	2.74	1.40	49
8	pSS	Distal	735-765	PP18-0552	2.75	1.47	47
L7	pSS	Distal	885-915	PP18-0554	2.72	1.43	48
L255	pSS	Proximal	135-165	PP18-0555	2.61	1.17	55
L297	pSS	Proximal	285-315	PP18-0556	2.67	1.29	52
L300	pSS	Proximal	435-465	PP18-0557	2.72	1.33	51
218	pSS	Proximal	585-615	PP18-0558	2.73	1.33	51
L268	pSS	Proximal	660-690	PP18-0560	2.74	1.37	50
228	pSS	Proximal	735-765	PP18-0559	2.72	1.46	47
L269	pSS	Proximal	885-915	PP18-0561	2.72	1.46	46
215	NS	Distal	135-165	PP18-0562	2.64	1.27	52
105	NS	Distal	285-315	PP18-0563	2.71	1.41	48
184	NS	Distal	435-465	PP18-0564	2.72	1.45	47
227	NS	Distal	585-615	PP18-0565	2.74	1.28	53
181	NS	Distal	735-765	PP18-0566	2.72	1.23	55
L248	NS	Proximal	135-165	PP18-0567	2.61	1.16	55
L291	NS	Proximal	285-315	PP18-0568	2.69	1.35	50
L299	NS	Proximal	435-465	PP18-0569	2.73	1.42	48
L252	NS	Proximal	585-615	PP18-0570	2.75	1.39	49
L5	NS	Proximal	735-765	PP18-0571	2.72	1.09	60

Table B-3.1.2. *continued*. Soil Physical Properties – Small (3 cm depth x 5 cm diameter) Cores.

Client ID	Site ID	Mole Proximity	Depth (mm)	Lab ID	Particle Density ($g\ cm^{-3}$)	Dry Bulk Density ($g\ cm^{-3}$)	Porosity (%)
L293	HS	Distal	135-165	PP18-0572	2.60	1.14	56
L212	HS	Distal	285-315	PP18-0573	2.66	1.34	50
L244	HS	Distal	435-465	PP18-0574	2.65	1.39	48
5	HS	Distal	585-615	PP18-0575	2.71	1.39	49
L237	HS	Distal	735-765	PP18-0576	2.72	1.39	49
L286	HS	Proximal	135-165	PP18-0577	2.58	1.14	56
108	HS	Proximal	285-315	PP18-0578	2.68	1.33	50
78	HS	Proximal	435-465	PP18-0579	2.67	1.38	48
76	HS	Proximal	585-615	PP18-0580	2.72	1.42	48
285	HS	Proximal	735-765	PP18-0581	2.72	1.32	52
81	IN1	Distal	135-165	PP18-0582	2.62	1.19	55
L3	IN1	Distal	285-315	PP18-0583	2.68	1.26	53
L289	IN1	Distal	435-465	PP18-0584	2.69	1.40	48
153	IN1	Distal	585-615	PP18-0585	2.73	1.36	50
18	IN1	Distal	835-865	PP18-0586	2.72	1.40	49
L283	IN1	Proximal	135-165	PP18-0587	2.61	1.15	56
98	IN1	Proximal	285-315	PP18-0588	2.67	1.32	51
231	IN1	Proximal	435-465	PP18-0589	2.71	1.36	50
162	IN1	Proximal	585-615	PP18-0590	2.73	1.43	48
249	IN1	Proximal	835-865	PP18-0591	2.72	1.39	49
L18	IN2	Distal	135-165	PP18-0592	2.63	1.10	58
L277	IN2	Distal	285-315	PP18-0593	2.70	1.34	50
L24	IN2	Distal	435-465	PP18-0594	2.69	1.32	51
L279	IN2	Distal	585-615	PP18-0595	2.73	1.40	49
L260	IN2	Distal	735-765	PP18-0596	2.75	1.46	47
L261	IN2	Proximal	135-165	PP18-0597	2.61	1.06	59
23	IN2	Proximal	285-315	PP18-0598	2.68	1.36	49
L281	IN2	Proximal	435-465	PP18-0599	2.70	1.36	50
275	IN2	Proximal	585-615	PP18-0600	2.74	1.42	48
220	IN2	Proximal	735-765	PP18-0601	2.73	1.49	46
74	lHO	Distal	135-165	PP18-0668	2.64	1.22	54
166	lHO	Distal	435-465	PP18-0669	2.66	1.26	53

B.3.2 Unsaturated Hydraulic Conductivity

Large Core (7.5 cm depth x 10 cm diameter) Results*:
***No small core measurements**

Notes:
Note 1: Mass at 1 kPa not taken - sorry.
Note 2: K-100 too slow for measurement
Note 3: 2 mm gap around 1/2 core. Cause of K-10 v. high?
Note 4: Slightly short on top, filled in

Table B-3.2. Soil Unsaturated Hydraulic Conductivity.

Client ID	Site ID	Mole Proximity	Depth (mm)	Lab ID	Note	Unsaturated Hydraulic Conductivity K-10 (mm h^{-1})	Unsaturated Hydraulic Conductivity K-40 (mm h^{-1})	Unsaturated Hydraulic Conductivity K-70 (mm h^{-1})	Unsaturated Hydraulic Conductivity K-100 (mm h^{-1})
2154	dSS	Distal	110-185	PP18-0602		2.3	1.9	1.2	0.9
2276	dSS	Distal	260-335	PP18-0603		18.3	11.5	2.3	0.9
2050	dSS	Distal	410-485	PP18-0604		10.4	5.0	1.9	0.8
2201	dSS	Distal	560-635	PP18-0605		6.2	2.3	0.9	0.7
2103	dSS	Distal	810-885	PP18-0606	1	0.6	0.3	0.3	0.1
2100	dSS	Proximal	110-185	PP18-0607		4.8	2.4	1.3	0.7
2142	dSS	Proximal	260-335	PP18-0608		21.4	20.3	15.3	1.4
2132	dSS	Proximal	410-485	PP18-0609		18.9	4.7	1.5	0.6
2133	dSS	Proximal	560-635	PP18-0610		1.4	1.2	0.8	0.7
2123	dSS	Proximal	810-885	PP18-0611		0.6	0.4	0.4	0.3
2325	pSS	Distal	110-185	PP18-0612		42.0	8.1	3.2	1.8
2078	pSS	Distal	260-335	PP18-0613		11.3	3.1	1.2	0.6
2204	pSS	Distal	410-485	PP18-0614		73.9	4.8	1.1	0.4
2012	pSS	Distal	560-635	PP18-0615		6.4	2.4	0.9	0.5
2077	pSS	Distal	635-710	PP18-0617		2.8	0.9	0.5	0.4
2019	pSS	Distal	710-785	PP18-0616		0.3	0.3	0.2	0.2
2216	pSS	Distal	860-935	PP18-0618		4.5	0.3	0.3	0.1
2185	pSS	Proximal	110-185	PP18-0619		27.5	3.5	1.4	0.8
2259	pSS	Proximal	260-335	PP18-0620		30.1	9.0	2.0	0.7
2122	pSS	Proximal	410-485	PP18-0621		26.9	6.2	1.8	0.7
2296	pSS	Proximal	560-635	PP18-0622		7.8	2.9	1.1	0.5
2198	pSS	Proximal	635-710	PP18-0624		0.6	0.5	0.4	0.2
2280	pSS	Proximal	710-785	PP18-0623		0.5	0.5	0.3	0.3
2285	pSS	Proximal	860-935	PP18-0625	2	0.2	0.2	0.1	N/A
2220	NS	Distal	110-185	PP18-0641		18.8	3.2	1.8	1.1
2173	NS	Distal	260-335	PP18-0642		4.5	2.0	0.9	0.5
2007	NS	Distal	410-485	PP18-0643		0.6	0.3	0.2	0.2
2221	NS	Distal	560-635	PP18-0644	3	177.0	2.0	0.5	0.2
2274	NS	Distal	710-785	PP18-0645		0.3	0.1	0.1	0.1
2275	NS	Proximal	110-185	PP18-0646		10.3	4.4	2.7	1.2
2150	NS	Proximal	260-335	PP18-0647		18.0	4.4	1.5	0.6
2114	NS	Proximal	410-485	PP18-0648		0.3	0.2	0.1	0.1
2260	NS	Proximal	560-635	PP18-0649		0.6	0.5	0.3	0.2
2040	NS	Proximal	710-785	PP18-0650		0.2	0.2	0.2	0.1

Table B-3.2. *continued*. Soil Unsaturated Hydraulic Conductivity.

Client ID	Site ID	Mole Proximity	Depth (mm)	Lab ID	Note	Unsaturated Hydraulic Conductivity K-10 (mm h^{-1})	Unsaturated Hydraulic Conductivity K-40 (mm h^{-1})	Unsaturated Hydraulic Conductivity K-70 (mm h^{-1})	Unsaturated Hydraulic Conductivity K-100 (mm h^{-1})
2088	HS	Distal	110-185	PP18-0651		18.8	7.4	7.3	3.3
2017	HS	Distal	260-335	PP18-0652		18.5	6.7	2.0	0.8
2091	HS	Distal	410-485	PP18-0653		18.4	5.3	1.0	0.2
2044	HS	Distal	560-635	PP18-0654		4.9	2.1	0.8	0.4
2347	HS	Distal	710-785	PP18-0655		2.8	1.3	0.4	0.2
2337	HS	Proximal	110-185	PP18-0656		10.5	9.4	6.8	3.2
2268	HS	Proximal	260-335	PP18-0657		64.6	18.4	5.2	1.5
2270	HS	Proximal	410-485	PP18-0658		13.7	5.3	1.9	0.5
2265	HS	Proximal	560-635	PP18-0659		7.5	3.0	0.9	0.4
2269	HS	Proximal	710-785	PP18-0660		8.5	2.6	0.5	0.3
2158	IN1	Distal	110-185	PP18-0661		22.9	14.7	9.3	3.0
2180	IN1	Distal	260-335	PP18-0662		15.2	7.1	1.8	0.5
2200	IN1	Distal	410-485	PP18-0663		9.0	2.3	0.7	0.4
2287	IN1	Distal	560-635	PP18-0664		5.6	1.5	0.5	0.3
2194	IN1	Distal	810-885	PP18-0665	4	3.7	0.4	0.2	0.2
2029	IN1	Proximal	110-185	PP18-0687		15.2	9.2	5.0	2.4
2148	IN1	Proximal	260-335	PP18-0688		31.8	12.0	2.9	0.8
2047	IN1	Proximal	410-485	PP18-0689		36.6	6.0	1.2	0.2
2167	IN1	Proximal	560-635	PP18-0690		6.8	1.9	0.8	0.4
2179	IN1	Proximal	810-885	PP18-0691		2.8	1.1	0.6	0.4
2116	IN2	Distal	110-185	PP18-0692		72.7	9.8	5.0	2.3
2037	IN2	Distal	260-335	PP18-0693		22.6	9.0	3.8	1.3
2186	IN2	Distal	410-485	PP18-0694		5.6	2.6	1.4	0.7
2060	IN2	Distal	560-635	PP18-0695		19.5	4.9	0.9	0.5
2147	IN2	Distal	710-785	PP18-0696		2.3	0.6	0.4	0.2
2303	IN2	Proximal	110-185	PP18-0697		9.0	4.1	2.3	1.4
2238	IN2	Proximal	260-335	PP18-0698		22.6	9.7	3.2	0.9
2136	IN2	Proximal	410-485	PP18-0699		41.3	8.6	2.8	1.1
2298	IN2	Proximal	560-635	PP18-0700		14.8	1.4	0.8	0.5
2144	IN2	Proximal	710-785	PP18-0701		19.4	4.3	0.4	0.3
2092	lHO	NA	110-185	PP18-0666		12.4	6.4	2.8	1.2
2170	lHO	NA	410-485	PP18-0667		20.3	9.2	2.4	0.6

B.3.3 Gravimetric Water Content

Warning: The following samples have large differences between large and small cores, i.e., don't match well.

OTA18-03	02	5
OTA18-02	02	7
OTA18-02	01	5

B.3.3.1 Large Cores

Table B-3.3.1. Soil Gravimetric Water Content – Large (7.5 cm depth x 10 cm diameter) Cores.

Client ID	Site ID	Mole Proximity	Depth (mm)	Note	Lab ID	Field Moisture (%v/w)	Saturation (calc) (%v/w)	0.1 kPa (funnel) (%v/w)	0.4 kPa (funnel) (%v/w)	0.7 kPa (funnel) (%v/w)	1 kPa (funnel) (%v/w)	5 kPa (%v/w)	10 kPa (%v/w)	1500 kPa (%v/w)
2154	dSS	Distal	110-185		PP18-0602	36	42	39	38	38	38	37	36	16
2276	dSS	Distal	260-335		PP18-0603	31	38	34	34	34	33	31	30	14
2050	dSS	Distal	410-485		PP18-0604	31	37	33	33	33	32	31	30	15
2201	dSS	Distal	560-635		PP18-0605	32	36	33	33	33	33	32	31	17
2103	dSS	Distal	810-885	1	PP18-0606	35	37	36	35	35	N/A	35	35	23
2100	dSS	Proximal	110-185		PP18-0607	39	44	42	42	41	41	40	38	14
2142	dSS	Proximal	260-335		PP18-0608	29	37	33	32	32	32	30	29	12
2132	dSS	Proximal	410-485		PP18-0609	31	37	33	33	33	32	31	30	16
2133	dSS	Proximal	560-635		PP18-0610	34	38	36	35	35	35	34	33	20
2123	dSS	Proximal	810-885		PP18-0611	34	36	34	34	34	34	34	34	22
2325	pSS	Distal	110-185		PP18-0612	41	48	45	44	44	44	42	40	16
2078	pSS	Distal	260-335		PP18-0613	30	36	32	32	32	32	30	29	19
2204	pSS	Distal	410-485		PP18-0614	28	35	33	31	30	30	28	28	21
2012	pSS	Distal	560-635		PP18-0615	30	35	32	32	31	31	30	29	22
2077	pSS	Distal	635-710		PP18-0617	29	32	30	30	30	30	29	29	22
2019	pSS	Distal	710-785		PP18-0616	28	31	29	29	29	28	28	28	22
2216	pSS	Distal	860-935		PP18-0618	27	30	28	27	27	27	27	27	17
2185	pSS	Proximal	110-185		PP18-0619	39	44	42	42	41	41	39	37	17
2259	pSS	Proximal	260-335		PP18-0620	31	38	34	34	33	33	31	30	18
2122	pSS	Proximal	410-485		PP18-0621	30	37	34	33	33	32	31	30	20
2296	pSS	Proximal	560-635		PP18-0622	31	37	33	33	33	33	31	31	21
2198	pSS	Proximal	635-710		PP18-0624	29	33	30	30	30	30	29	29	18
2280	pSS	Proximal	710-785		PP18-0623	28	30	28	28	28	28	28	28	19
2285	pSS	Proximal	860-935	2	PP18-0625	28	32	29	29	28	N/A	28	28	16
2220	NS	Distal	110-185		PP18-0641	39	44	42	42	42	41	40	38	18
2173	NS	Distal	260-335		PP18-0642	30	35	32	32	31	31	30	29	17
2007	NS	Distal	410-485		PP18-0643	29	32	29	29	29	29	29	28	18
2221	NS	Distal	560-635	3	PP18-0644	34	44	36	35	34	34	34	33	20
2274	NS	Distal	710-785		PP18-0645	43	48	44	44	44	44	43	43	26
2275	NS	Proximal	110-185		PP18-0646	43	49	47	46	46	46	44	42	19
2150	NS	Proximal	260-335		PP18-0647	31	37	34	33	33	33	31	30	17
2114	NS	Proximal	410-485		PP18-0648	28	32	29	29	29	29	28	28	18
2260	NS	Proximal	560-635		PP18-0649	33	36	34	34	34	34	33	33	19
2040	NS	Proximal	710-785		PP18-0650	43	46	44	44	44	44	43	43	26

Table B-3.3.1.*continued*. Soil Gravimetric Water Content – Large (7.5 cm depth x 10 cm diameter) Cores.

Client ID	Site ID	Mole Proximity	Depth (mm)	Note	Lab ID	Field Moisture (%v/w)	Saturation (calc) (%v/w)	0.1 kPa (funnel) (%v/w)	0.4 kPa (funnel) (%v/w)	0.7 kPa (funnel) (%v/w)	1 kPa (funnel) (%v/w)	5 kPa (%v/w)	10 kPa (%v/w)	1500 kPa (%v/w)
2088	HS	Distal	110-185		PP18-0651	38	46	43	43	43	42	40	38	18
2017	HS	Distal	260-335		PP18-0652	29	36	32	32	32	32	30	29	16
2091	HS	Distal	410-485		PP18-0653	28	32	30	30	30	30	28	27	17
2044	HS	Distal	560-635		PP18-0654	29	34	31	30	30	30	29	29	18
2347	HS	Distal	710-785		PP18-0655	31	35	32	32	32	32	31	31	18
2337	HS	Proximal	110-185		PP18-0656	40	47	45	44	44	44	42	40	17
2268	HS	Proximal	260-335		PP18-0657	30	37	34	34	34	34	31	30	14
2270	HS	Proximal	410-485		PP18-0658	29	36	32	32	32	31	29	29	15
2265	HS	Proximal	560-635		PP18-0659	29	35	32	32	31	31	30	29	17
2269	HS	Proximal	710-785		PP18-0660	32	37	34	34	33	33	32	32	20
2158	IN1	Distal	110-185		PP18-0661	41	47	45	44	44	44	41	39	16
2180	IN1	Distal	260-335		PP18-0662	30	36	33	32	32	32	30	29	15
2200	IN1	Distal	410-485		PP18-0663	30	34	31	31	31	31	29	29	15
2287	IN1	Distal	560-635		PP18-0664	32	36	33	32	32	32	31	30	19
2194	IN1	Distal	810-885	4	PP18-0665	33	36	34	33	33	33	33	33	21
2029	IN1	Proximal	110-185		PP18-0687	41	49	45	45	45	44	42	40	17
2148	IN1	Proximal	260-335		PP18-0688	31	38	35	34	34	34	31	30	15
2047	IN1	Proximal	410-485		PP18-0689	32	39	35	34	34	33	32	31	18
2167	IN1	Proximal	560-635		PP18-0690	31	35	32	32	32	31	30	30	18
2179	IN1	Proximal	810-885		PP18-0691	33	35	34	33	33	33	33	33	19
2116	IN2	Distal	110-185		PP18-0692	42	51	48	48	48	47	43	41	17
2037	IN2	Distal	260-335		PP18-0693	31	37	33	33	33	33	31	30	15
2186	IN2	Distal	410-485		PP18-0694	30	35	32	32	31	31	30	29	16
2060	IN2	Distal	560-635		PP18-0695	31	34	31	31	31	31	30	30	18
2147	IN2	Distal	710-785		PP18-0696	34	36	34	34	34	34	33	33	19
2303	IN2	Proximal	110-185		PP18-0697	43	48	46	46	46	45	44	42	17
2238	IN2	Proximal	260-335		PP18-0698	31	36	33	33	33	33	31	30	16
2136	IN2	Proximal	410-485		PP18-0699	31	36	33	32	32	32	30	29	17
2298	IN2	Proximal	560-635		PP18-0700	30	33	31	31	31	31	30	30	19
2144	IN2	Proximal	710-785		PP18-0701	32	33	33	32	32	32	32	31	19
2092	lHO	NA	110-185		PP18-0666	34	41	38	38	38	38	36	35	17
2170	lHO	NA	410-485		PP18-0667	34	41	37	37	36	36	34	34	19

B.3.3.2 Small Cores

Table B-3.3.2. Soil Gravimetric Water Content – Small (3 cm depth x 5 cm diameter) Cores.

Client ID	Site ID	Mole Proximity	Depth (mm)	Lab ID	Field Moisture (%v/w)	Saturation (calc) (%v/w)	0.4 kPa (funnel) (%v/w)	0.7 kPa (funnel) (%v/w)	1 kPa (funnel) (%v/w)	5 kPa (%v/w)	10 kPa (%v/w)	20 kPa (%v/w)	40 kPa (%v/w)	100 kPa (%v/w)
172	dSS	Distal	135-165	PP18-0538	39	45	42	42	42	40	38	36	33	29
174	dSS	Distal	285-315	PP18-0539	31	37	33	33	33	32	31	29	27	24
57	dSS	Distal	435-465	PP18-0540	31	36	33	33	33	32	31	30	29	27
294	dSS	Distal	585-615	PP18-0541	31	33	31	31	31	31	30	30	30	29
91	dSS	Distal	835-865	PP18-0542	35	37	36	36	36	36	35	35	35	34
212	dSS	Proximal	135-165	PP18-0543	39	45	41	41	41	40	38	36	33	30
63	dSS	Proximal	285-315	PP18-0544	30	37	32	32	32	31	30	28	26	23
123	dSS	Proximal	435-465	PP18-0545	32	37	33	33	33	32	31	30	29	28
75	dSS	Proximal	585-615	PP18-0546	35	39	36	36	36	36	35	35	34	34
170	dSS	Proximal	835-865	PP18-0547	35	37	35	35	35	35	35	34	34	33
L251	pSS	Distal	135-165	PP18-0548	44	52	49	48	48	44	42	38	36	31
L15	pSS	Distal	285-315	PP18-0549	30	41	33	33	33	31	30	28	27	24
L262	pSS	Distal	435-465	PP18-0550	30	38	34	33	33	30	29	28	27	25
116	pSS	Distal	585-615	PP18-0551	31	35	33	33	33	32	31	30	29	27
L275	pSS	Distal	660-690	PP18-0553	29	35	30	29	29	29	29	28	28	27
8	pSS	Distal	735-765	PP18-0552	30	32	30	30	30	30	30	29	29	29
L7	pSS	Distal	885-915	PP18-0554	28	33	29	29	29	28	28	28	28	27
L255	pSS	Proximal	135-165	PP18-0555	41	47	44	44	43	41	40	37	34	30
L297	pSS	Proximal	285-315	PP18-0556	32	40	36	36	36	33	32	30	28	25
L300	pSS	Proximal	435-465	PP18-0557	32	38	34	34	34	33	32	31	30	28
218	pSS	Proximal	585-615	PP18-0558	32	39	34	34	34	32	32	31	30	28
L268	pSS	Proximal	660-690	PP18-0560	33	36	33	33	33	33	32	31	31	29
228	pSS	Proximal	735-765	PP18-0559	28	32	29	29	29	29	29	28	28	27
L269	pSS	Proximal	885-915	PP18-0561	30	32	30	30	30	30	30	30	29	29
215	NS	Distal	135-165	PP18-0562	36	41	39	39	38	37	35	32	30	26
105	NS	Distal	285-315	PP18-0563	30	34	32	32	32	31	30	29	27	25
184	NS	Distal	435-465	PP18-0564	28	32	29	29	29	28	28	27	26	23
227	NS	Distal	585-615	PP18-0565	36	42	37	37	37	36	35	34	34	32
181	NS	Distal	735-765	PP18-0566	41	45	42	42	42	42	41	41	41	40
L248	NS	Proximal	135-165	PP18-0567	41	48	44	44	44	42	40	36	33	28
L291	NS	Proximal	285-315	PP18-0568	31	37	33	33	33	31	30	29	27	25
L299	NS	Proximal	435-465	PP18-0569	29	34	30	30	30	30	29	28	27	24
L252	NS	Proximal	585-615	PP18-0570	31	36	32	32	32	31	30	30	29	28
L5	NS	Proximal	735-765	PP18-0571	50	55	50	50	50	50	49	49	49	47

Table B-3.3.2. *continued.* Soil Gravimetric Water Content – Small (3 cm depth x 5 cm diameter) Cores.

Client ID	Site ID	Mole Proximity	Depth (mm)	Lab ID	Field Moisture (%v/w)	Saturation (calc) (%v/w)	0.4 kPa (funnel) (%v/w)	0.7 kPa (funnel) (%v/w)	1 kPa (funnel) (%v/w)	5 kPa (%v/w)	10 kPa (%v/w)	20 kPa (%v/w)	40 kPa (%v/w)	100 kPa (%v/w)
L293	HS	Distal	135-165	PP18-0572	38	49	47	45	45	40	38	35	33	28
L212	HS	Distal	285-315	PP18-0573	30	37	34	34	34	31	30	28	27	24
L244	HS	Distal	435-465	PP18-0574	28	34	31	31	31	29	28	27	26	24
5	HS	Distal	585-615	PP18-0575	30	35	32	32	32	30	29	28	27	25
L237	HS	Distal	735-765	PP18-0576	32	35	33	33	33	32	31	31	30	28
L286	HS	Proximal	135-165	PP18-0577	41	49	47	46	46	42	40	37	35	30
108	HS	Proximal	285-315	PP18-0578	30	38	35	34	34	31	30	28	26	24
78	HS	Proximal	435-465	PP18-0579	29	35	32	32	32	30	29	28	26	24
76	HS	Proximal	585-615	PP18-0580	29	34	31	31	31	30	29	28	27	25
285	HS	Proximal	735-765	PP18-0581	33	39	36	35	35	34	33	32	31	30
81	IN1	Distal	135-165	PP18-0582	41	46	44	44	44	42	39	35	33	28
L3	IN1	Distal	285-315	PP18-0583	31	42	34	34	34	31	30	27	26	22
L289	IN1	Distal	435-465	PP18-0584	29	34	31	31	30	29	28	27	26	24
153	IN1	Distal	585-615	PP18-0585	32	37	33	33	33	31	31	29	28	26
18	IN1	Distal	835-865	PP18-0586	33	35	34	34	33	33	33	32	32	31
L283	IN1	Proximal	135-165	PP18-0587	40	49	46	46	46	42	39	36	33	28
98	IN1	Proximal	285-315	PP18-0588	31	38	35	35	35	32	30	28	27	24
231	IN1	Proximal	435-465	PP18-0589	31	37	33	33	33	31	30	29	28	26
162	IN1	Proximal	585-615	PP18-0590	30	33	31	31	31	30	29	29	27	25
249	IN1	Proximal	835-865	PP18-0591	33	35	33	33	33	33	33	33	32	32
L18	IN2	Distal	135-165	PP18-0592	39	53	46	46	46	41	39	36	33	29
L277	IN2	Distal	285-315	PP18-0593	31	38	34	34	34	31	30	29	28	24
L24	IN2	Distal	435-465	PP18-0594	30	38	32	32	32	30	29	28	27	25
L279	IN2	Distal	585-615	PP18-0595	32	35	33	33	33	32	31	30	29	28
L260	IN2	Distal	735-765	PP18-0596	30	32	30	30	30	30	30	29	29	28
L261	IN2	Proximal	135-165	PP18-0597	51	56	55	55	55	52	50	46	43	39
23	IN2	Proximal	285-315	PP18-0598	31	36	34	34	34	31	30	28	27	23
L281	IN2	Proximal	435-465	PP18-0599	31	36	33	33	33	31	30	28	27	24
275	IN2	Proximal	585-615	PP18-0600	31	34	32	32	32	31	30	29	28	26
220	IN2	Proximal	735-765	PP18-0601	29	31	29	29	29	29	29	29	28	28
74	lHO	Distal	135-165	PP18-0668	36	44	41	41	41	37	36	33	30	26
166	lHO	Distal	435-465	PP18-0669	33	42	37	36	36	34	33	31	29	26

B.3.4 Volumetric Water Content

Warning: The following samples have large differences between large and small cores, i.e., don't match well.

OTA18-03	02	5
OTA18-02	02	7
OTA18-02	01	5

B.3.4.1 Large Cores

Table B-3.4.1. Soil Volumetric Water Content – Large (7.5 cm depth x 10 cm diameter) Cores.

Client ID	Site ID	Mole Proximity	Depth (mm)	Note	Lab ID	Field Moisture (%v/v)	Saturation (calc) (%v/v)	0.1 kPa (funnel) (%v/v)	0.4 kPa (funnel) (%v/v)	0.7 kPa (funnel) (%v/v)	1 kPa (funnel) (%v/v)	5 kPa (%v/v)	10 kPa (%v/v)	1500 kPa (%v/v)	Field capacity (%)	RAWC (10-100) (%)	AWC (10-1500) (%)
2154	dSS	Distal	110-185		PP18-0602	45	52	48	48	48	48	46	45	20	45	11	27
2276	dSS	Distal	260-335		PP18-0603	41	50	45	45	45	44	41	40	19	40	9	22
2050	dSS	Distal	410-485		PP18-0604	42	50	45	44	44	44	42	41	21	41	6	21
2201	dSS	Distal	560-635		PP18-0605	44	50	46	45	45	45	43	43	24	43	2	18
2103	dSS	Distal	810-885	1	PP18-0606	47	51	49	48	47	N/A	47	47	31	47	1	17
2100	dSS	Proximal	110-185		PP18-0607	48	54	51	50	50	50	48	47	16	47	10	30
2142	dSS	Proximal	260-335		PP18-0608	40	50	44	44	43	43	40	39	17	39	9	23
2132	dSS	Proximal	410-485		PP18-0609	41	50	44	44	44	44	41	40	21	40	5	21
2133	dSS	Proximal	560-635		PP18-0610	45	51	48	47	47	47	45	45	26	45	2	21
2123	dSS	Proximal	810-885		PP18-0611	47	50	47	47	47	47	47	47	30	47	2	17
2325	pSS	Distal	110-185		PP18-0612	48	56	52	51	51	51	48	46	19	46	12	28
2078	pSS	Distal	260-335		PP18-0613	41	49	44	43	43	43	41	40	25	40	8	14
2204	pSS	Distal	410-485		PP18-0614	39	48	47	43	43	42	39	39	29	39	5	11
2012	pSS	Distal	560-635		PP18-0615	41	49	44	44	43	43	41	40	30	40	5	13
2077	pSS	Distal	635-710		PP18-0617	42	47	44	43	43	43	42	42	31	42	2	10
2019	pSS	Distal	710-785		PP18-0616	42	46	43	43	43	42	42	41	32	41	2	12
2216	pSS	Distal	860-935		PP18-0618	41	45	42	41	41	41	41	41	26	41	1	15
2185	pSS	Proximal	110-185		PP18-0619	47	53	51	51	50	50	47	46	21	46	11	27
2259	pSS	Proximal	260-335		PP18-0620	41	50	45	45	44	44	41	40	24	40	9	18
2122	pSS	Proximal	410-485		PP18-0621	41	50	46	45	44	44	41	40	26	40	5	16
2296	pSS	Proximal	560-635		PP18-0622	42	50	45	45	44	44	42	41	29	41	5	14
2198	pSS	Proximal	635-710		PP18-0624	42	48	43	43	43	43	42	42	26	42	4	19
2280	pSS	Proximal	710-785		PP18-0623	41	45	42	42	42	42	41	41	29	41	2	14
2285	pSS	Proximal	860-935	2	PP18-0625	41	46	42	42	41	N/A	41	41	23	41	1	21
2220	NS	Distal	110-185		PP18-0641	48	54	51	51	51	50	48	47	21	47	11	22
2173	NS	Distal	260-335		PP18-0642	41	49	44	44	43	43	41	40	24	40	7	18
2007	NS	Distal	410-485		PP18-0643	42	46	43	42	42	42	42	41	27	41	7	14
2221	NS	Distal	560-635	3	PP18-0644	42	54	45	44	43	43	42	42	25	42	5	20
2274	NS	Distal	710-785		PP18-0645	51	57	52	52	52	52	51	51	30	51	2	19
2275	NS	Proximal	110-185		PP18-0646	50	56	54	53	53	53	50	48	22	48	13	24
2150	NS	Proximal	260-335		PP18-0647	42	50	46	45	45	44	42	41	23	41	8	18
2114	NS	Proximal	410-485		PP18-0648	41	47	42	42	42	42	41	41	26	41	8	16
2260	NS	Proximal	560-635		PP18-0649	46	50	47	47	47	47	46	45	26	45	4	17
2040	NS	Proximal	710-785		PP18-0650	52	56	53	53	53	52	52	52	31	52	2	25

Table B-3.4.1. *continued*. Soil Volumetric Water Content – Large (7.5 cm depth x 10 cm diameter) Cores.

Client ID	Site ID	Mole Proximity	Depth (mm)	Note	Lab ID	Field Moisture (%v/v)	Saturation (calc) (%v/v)	0.1 kPa (funnel) (%v/v)	0.4 kPa (funnel) (%v/v)	0.7 kPa (funnel) (%v/v)	1 kPa (funnel) (%v/v)	5 kPa (%v/v)	10 kPa (%v/v)	1500 kPa (%v/v)	Field capacity (%)	RAWC (10-100) (%)	AWC (10-1500) (%)
2088	HS	Distal	110-185		PP18-0651	45	54	51	51	51	50	47	46	21	46	12	24
2017	HS	Distal	260-335		PP18-0652	39	49	44	44	44	43	40	39	22	39	9	19
2091	HS	Distal	410-485		PP18-0653	39	46	43	42	42	42	39	39	24	39	6	16
2044	HS	Distal	560-635		PP18-0654	40	48	43	43	42	42	41	40	25	40	6	16
2347	HS	Distal	710-785		PP18-0655	44	49	46	45	45	45	44	43	26	43	4	18
2337	HS	Proximal	110-185		PP18-0656	47	55	52	52	52	52	49	47	19	47	12	27
2268	HS	Proximal	260-335		PP18-0657	40	50	45	45	45	45	41	40	19	40	9	21
2270	HS	Proximal	410-485		PP18-0658	40	49	44	43	43	43	40	39	20	39	7	20
2265	HS	Proximal	560-635		PP18-0659	41	49	44	44	44	43	41	41	23	41	6	17
2269	HS	Proximal	710-785		PP18-0660	44	50	46	46	45	45	44	43	28	43	4	17
2158	IN1	Distal	110-185		PP18-0661	48	55	52	52	52	52	48	45	19	45	12	27
2180	IN1	Distal	260-335		PP18-0662	41	49	44	44	44	44	41	40	20	40	9	19
2200	IN1	Distal	410-485		PP18-0663	42	48	44	43	43	43	41	40	21	40	6	18
2287	IN1	Distal	560-635		PP18-0664	43	50	45	45	44	44	43	42	27	42	6	15
2194	IN1	Distal	810-885	4	PP18-0665	45	49	47	46	46	46	45	45	28	45	3	17
2029	IN1	Proximal	110-185		PP18-0687	48	56	52	51	51	51	49	46	20	46	13	25
2148	IN1	Proximal	260-335		PP18-0688	41	51	46	45	45	45	41	40	20	40	8	20
2047	IN1	Proximal	410-485		PP18-0689	42	52	46	45	44	44	42	41	24	41	6	16
2167	IN1	Proximal	560-635		PP18-0690	43	49	45	44	44	43	42	41	25	41	6	17
2179	IN1	Proximal	810-885		PP18-0691	46	49	47	47	46	46	46	46	26	46	2	20
2116	IN2	Distal	110-185		PP18-0692	47	57	54	54	53	53	48	46	19	46	12	24
2037	IN2	Distal	260-335		PP18-0693	41	50	45	45	45	45	42	41	21	41	8	20
2186	IN2	Distal	410-485		PP18-0694	42	48	44	44	43	43	42	41	22	41	6	18
2060	IN2	Distal	560-635		PP18-0695	44	48	45	44	44	44	43	42	26	42	5	19
2147	IN2	Distal	710-785		PP18-0696	46	50	47	47	47	47	46	46	26	46	3	15
2303	IN2	Proximal	110-185		PP18-0697	50	56	53	53	53	52	51	49	20	49	12	35
2238	IN2	Proximal	260-335		PP18-0698	42	49	45	45	45	45	42	40	21	40	9	20
2136	IN2	Proximal	410-485		PP18-0699	43	50	45	44	44	44	41	40	23	40	8	17
2298	IN2	Proximal	560-635		PP18-0700	44	47	45	45	45	45	43	43	28	43	6	16
2144	IN2	Proximal	710-785		PP18-0701	45	48	47	46	46	46	45	45	27	45	2	15
2092	lHO	NA	110-185		PP18-0666	43	52	49	48	48	48	45	44	22	44	12	22
2170	lHO	NA	410-485		PP18-0667	43	52	47	47	47	46	44	43	24	43	8	18

B.3.4.2 Small Cores

Table B-3.4.2. Soil Volumetric Water Content – Small (3 cm depth x 5 cm diameter) Cores.

Client ID	Site ID	Mole Proximity	Depth (mm)	Lab ID	Field Moisture (%v/v)	Saturation (calc) (%v/v)	0.4 kPa (funnel) (%v/v)	0.7 kPa (funnel) (%v/v)	1 kPa (funnel) (%v/v)	5 kPa (%v/v)	10 kPa (%v/v)	20 kPa (%v/v)	40 kPa (%v/v)	100 kPa (%v/v)	1500 kPa (%v/v)
172	dSS	Distal	135-165	PP18-0538	47	54	50	50	50	49	46	43	40	35	19
174	dSS	Distal	285-315	PP18-0539	42	50	44	44	44	43	41	39	37	32	19
57	dSS	Distal	435-465	PP18-0540	43	50	45	45	45	44	42	41	39	36	21
294	dSS	Distal	585-615	PP18-0541	44	48	44	44	44	44	43	43	42	41	25
91	dSS	Distal	835-865	PP18-0542	48	50	48	48	48	48	48	48	47	46	31
212	dSS	Proximal	135-165	PP18-0543	47	54	50	50	50	48	46	43	40	36	16
63	dSS	Proximal	285-315	PP18-0544	41	50	44	44	44	41	40	38	35	31	17
123	dSS	Proximal	435-465	PP18-0545	43	50	45	45	45	43	42	41	40	38	21
75	dSS	Proximal	585-615	PP18-0546	47	52	48	48	48	47	47	46	46	45	26
170	dSS	Proximal	835-865	PP18-0547	47	51	47	47	47	47	47	47	46	45	29
L251	pSS	Distal	135-165	PP18-0548	48	58	54	53	53	49	46	42	40	35	18
L15	pSS	Distal	285-315	PP18-0549	39	52	42	42	42	40	38	36	34	30	24
L262	pSS	Distal	435-465	PP18-0550	39	51	45	44	43	40	39	37	37	34	28
116	pSS	Distal	585-615	PP18-0551	43	49	46	46	46	44	43	41	41	38	30
L275	pSS	Distal	660-690	PP18-0553	41	49	41	41	41	41	40	39	39	38	30
8	pSS	Distal	735-765	PP18-0552	44	47	45	45	45	44	44	43	43	42	32
L7	pSS	Distal	885-915	PP18-0554	40	48	41	41	41	40	40	40	39	39	25
L255	pSS	Proximal	135-165	PP18-0555	48	55	51	51	51	49	47	43	40	35	20
L297	pSS	Proximal	285-315	PP18-0556	42	52	47	46	46	43	41	39	36	32	24
L300	pSS	Proximal	435-465	PP18-0557	43	51	46	46	45	43	42	41	40	38	26
218	pSS	Proximal	585-615	PP18-0558	43	51	45	45	45	43	42	41	39	37	28
L268	pSS	Proximal	660-690	PP18-0560	45	50	46	46	46	45	44	43	42	40	25
228	pSS	Proximal	735-765	PP18-0559	41	47	43	43	42	42	42	41	41	40	28
L269	pSS	Proximal	885-915	PP18-0561	44	46	44	44	44	44	43	43	43	42	23
215	NS	Distal	135-165	PP18-0562	46	52	49	49	49	47	45	41	38	34	22
105	NS	Distal	285-315	PP18-0563	42	48	45	45	45	43	42	40	39	35	24
184	NS	Distal	435-465	PP18-0564	41	47	42	42	42	41	41	40	38	34	26
227	NS	Distal	585-615	PP18-0565	46	53	48	48	47	46	45	44	43	40	25
181	NS	Distal	735-765	PP18-0566	51	55	51	51	51	51	51	50	50	49	32
L248	NS	Proximal	135-165	PP18-0567	47	55	51	51	51	49	46	42	39	33	22
L291	NS	Proximal	285-315	PP18-0568	41	50	44	44	44	42	41	39	37	33	23
L299	NS	Proximal	435-465	PP18-0569	42	48	43	43	43	42	42	40	39	34	26
L252	NS	Proximal	585-615	PP18-0570	43	49	44	44	44	43	42	41	41	38	26
L5	NS	Proximal	735-765	PP18-0571	54	60	54	54	54	54	54	53	53	51	28

Table B-3.4.2. *continued*. Soil Volumetric Water Content – Small (3 cm depth x 5 cm diameter) Cores.

Client ID	Site ID	Mole Proximity	Depth (mm)	Lab ID	Field Moisture (%v/v)	Saturation (calc) (%v/v)	0.4 kPa (funnel) (%v/v)	0.7 kPa (funnel) (%v/v)	1 kPa (funnel) (%v/v)	5 kPa (%v/v)	10 kPa (%v/v)	20 kPa (%v/v)	40 kPa (%v/v)	100 kPa (%v/v)	1500 kPa (%v/v)
L293	HS	Distal	135-165	PP18-0572	43	56	53	51	51	46	44	40	37	32	20
L212	HS	Distal	285-315	PP18-0573	41	50	45	45	45	42	40	38	36	32	22
L244	HS	Distal	435-465	PP18-0574	39	48	43	43	43	40	39	38	36	33	23
5	HS	Distal	585-615	PP18-0575	41	49	44	44	44	42	41	39	37	35	25
L237	HS	Distal	735-765	PP18-0576	44	49	46	45	45	44	44	43	42	39	25
L286	HS	Proximal	135-165	PP18-0577	46	56	53	53	53	49	46	43	40	35	19
108	HS	Proximal	285-315	PP18-0578	40	50	46	46	46	42	40	38	35	31	19
78	HS	Proximal	435-465	PP18-0579	41	48	44	44	44	42	40	39	37	33	20
76	HS	Proximal	585-615	PP18-0580	41	48	44	44	44	42	41	39	38	35	24
285	HS	Proximal	735-765	PP18-0581	43	52	47	46	46	44	44	43	42	40	27
81	IN1	Distal	135-165	PP18-0582	48	55	53	53	52	49	46	42	39	34	19
L3	IN1	Distal	285-315	PP18-0583	39	53	42	42	42	39	38	35	33	28	19
L289	IN1	Distal	435-465	PP18-0584	41	48	43	43	43	41	40	38	37	34	21
153	IN1	Distal	585-615	PP18-0585	43	50	45	45	45	43	42	40	38	35	26
18	IN1	Distal	835-865	PP18-0586	46	49	47	47	47	46	46	45	45	43	29
L283	IN1	Proximal	135-165	PP18-0587	46	56	53	53	53	48	45	41	37	32	20
98	IN1	Proximal	285-315	PP18-0588	41	51	46	46	46	42	40	37	35	31	20
231	IN1	Proximal	435-465	PP18-0589	42	50	44	44	44	42	41	39	38	35	25
162	IN1	Proximal	585-615	PP18-0590	43	48	45	45	44	43	42	41	39	36	25
249	IN1	Proximal	835-865	PP18-0591	46	49	46	46	46	46	46	45	45	44	26
L18	IN2	Distal	135-165	PP18-0592	43	58	51	50	50	45	43	40	37	31	19
L277	IN2	Distal	285-315	PP18-0593	41	50	46	46	46	42	41	39	37	33	20
L24	IN2	Distal	435-465	PP18-0594	40	51	42	42	42	40	39	38	36	33	21
L279	IN2	Distal	585-615	PP18-0595	45	49	47	47	46	45	44	42	41	39	25
L260	IN2	Distal	735-765	PP18-0596	44	47	44	44	44	44	43	43	42	41	28
L261	IN2	Proximal	135-165	PP18-0597	55	59	58	58	58	55	53	48	46	41	19
23	IN2	Proximal	285-315	PP18-0598	42	49	46	46	46	42	41	39	36	32	21
L281	IN2	Proximal	435-465	PP18-0599	42	50	45	45	45	42	40	38	36	32	23
275	IN2	Proximal	585-615	PP18-0600	44	48	45	45	45	44	43	41	40	37	27
220	IN2	Proximal	735-765	PP18-0601	43	46	43	43	43	43	43	43	42	41	28
74	lHO	Distal	135-165	PP18-0668	44	54	50	50	50	46	43	41	37	32	21
166	lHO	Distal	435-465	PP18-0669	42	53	46	46	46	43	42	39	37	33	24

Appendix C
Principal Component Scores

Table C-1. Principal component 1 – 4 scores for each collected sample. d = mole distal; p = mole proximal

Point ID	Landscape Element	Exposure	Depth (cm)	Principal Component Score			
	Divergent Side Slope (dSS)			PC1	PC2	PC3	PC4
1		d	15	3.59	2.09	1.03	1.28
2			30	1.40	-2.04	-0.84	0.31
3			45	-0.43	-1.50	-0.19	-0.42
4			60	-2.14	0.00	-1.70	0.94
5			85	-3.81	2.83	-0.51	-0.61
6		p	15	3.90	2.74	1.15	1.08
7			30	1.30	-2.32	-0.18	-0.42
8			45	-0.34	-1.51	-1.17	-0.83
9			60	-2.11	1.78	-3.29	0.91
10			85	-4.22	3.09	-0.91	0.46
	Planar Side Slope (pSS)			PC1	PC2	PC3	PC4
11		d	15	5.50	1.55	0.40	-0.99
12			30	0.94	-2.14	-0.61	0.08
13			45	-0.03	-3.44	-1.67	-2.41
14			60	-2.25	-0.41	-1.90	1.25
15			67	-3.00	-0.47	-0.95	1.28
16			75	-3.30	-0.81	1.22	1.71
17			90	-3.81	-0.22	2.17	-0.30
18		p	15	4.56	1.89	0.89	-0.08
19			30	1.92	-1.95	-1.30	-0.52
20			45	-0.27	-2.02	-1.78	-1.60
21			60	-0.94	-1.24	-2.07	0.10
22			67	-2.64	0.42	-1.05	0.47
23			75	-3.98	0.12	0.78	0.10
24			90	-3.05	-0.01	1.47	-0.30
	Nose Slope (NS)			PC1	PC2	PC3	PC4
25		d	15	3.06	1.65	-0.66	1.73
26			30	-0.45	-1.45	-0.99	1.03
27			45	-2.85	-0.60	0.17	1.81
28			60	-1.65	1.67	-2.37	-0.83
29			75	-2.32	4.72	-3.14	-1.68
30		p	15	4.18	2.06	0.29	0.52
31			30	0.67	-1.47	-1.14	0.62
32			45	-2.39	-0.15	0.15	1.40
33			60	-3.44	1.74	-1.03	0.58
34			75	-1.84	6.52	-2.73	-1.78
	Head Slope (HS)			PC1	PC2	PC3	PC4
35		d	15	4.33	1.19	1.13	-0.02
36			30	1.62	-2.17	0.46	0.41
37			45	0.03	-2.39	-0.54	1.62
38			60	-0.79	-2.04	1.58	0.37
39			75	-1.84	0.31	1.92	-0.09
40		p	15	4.65	2.42	1.08	0.76
41			30	2.19	-2.61	-0.32	-1.63
42			45	0.79	-2.45	-0.62	0.48
43			60	-0.67	-1.72	0.61	0.29
44			75	-1.29	0.36	1.18	-0.91
	Interfluve 1 (IN1)			PC1	PC2	PC3	PC4
45		d	15	5.23	1.17	0.43	-0.41
46			30	1.45	-2.12	-0.40	-0.03
47			45	-0.70	-1.31	0.57	-0.01
48			60	-1.37	-0.24	0.78	-0.85
49			85	-2.97	2.07	1.87	-1.31
50		p	15	5.03	1.37	0.36	0.02
51			30	1.47	-2.31	0.89	-0.94
52			45	0.14	-2.32	0.45	-1.76
53			60	-1.42	-0.61	1.22	-0.64
54			85	-2.73	2.20	2.50	-0.67
	Interfluve 2 (IN2)			PC1	PC2	PC3	PC4
55		d	15	5.88	0.12	-0.44	-2.02
56			30	0.91	-2.27	0.16	0.17
57			45	-0.30	-2.05	0.42	0.99
58			60	-1.82	0.46	1.82	-0.45
59			75	-2.97	1.50	2.57	-0.43
60		p	15	5.31	3.70	0.72	0.54
61			30	0.91	-2.14	0.52	0.12
62			45	-0.08	-1.79	-0.24	-1.13
63			60	-2.40	0.45	1.66	0.36
64			75	-3.35	1.20	2.92	-0.48
	Lower Hollow (IHO)			PC1	PC2	PC3	PC4
65		g	15	3.14	1.12	-0.74	1.59
66			45	1.85	-0.23	-2.08	1.19

Appendix D

S-Map fact sheet for soil sibling Pukemutu_6a.1

Manaaki Whenua
Landcare Research

S O I L R E P O R T

Environment Southland

Pukemutu_6a.1

Report generated: 2-Jan-2022 from https://smap.landcareresearch.co.nz

Pukem_6a.1 (100% of the mapunit at location (1229115, 4868617), Confidence: Low)

This information sheet describes the typical average properties of the specified soil to a depth of 1 metre, and should not be the primary source of data when making land use decisions on individual farms and paddocks. S-map correlates soils across New Zealand. Both the old soil name and the new correlated (soil family) name are listed below.

Capture of the base soil information in this region was funded by Environment Southland and MWLR.

Soil Classification

Soil Classification:
Argillic-fragic Perch-gley Pallic Soils (PPJX)

Family Name:
Pukemutu (Pukem)

Sibling Name:
Pukemutu_6a.1 (Pukem_6a.1)

Soil profile material
Stoneless soil

Depth class (diggability)
Moderately deep (40 - 80 cm)

Profile texture
silt over clay

Parent Material

Stones/rocks
not applicable

Soil material
tuffaceous sandstone rock

Origin
Loess

Soil Sibling Concept

This soil belongs to the Pallic soil order of the New Zealand soil classification. Pallic Soils have pale coloured subsoils, due to low contents of iron oxides, have weak soil structure and high density in subsurface horizons. Pallic Soils tend to be dry in summer and wet in winter. It is formed in a blanket deposit of silt sized windblown materials, from hard tuffaceous sandstone parent material.

The topsoil typically has silt texture and is stoneless. The subsoil has dominantly clay textures, with gravel content of less than 3%. The plant rooting depth is 40 - 80 (cm), due to a continuous hard pan that impedes root growth and oxygen supply.

Generally the soil is poorly drained with very high vulnerability of water logging in non-irrigated conditions, and has moderate soil water holding capacity. Inherently these soils have a high structural vulnerability and a moderate N leaching potential, which should be accounted for when making land management decisions.

Allan Hewitt ©

Perch-gley Pallic

About this publication

- This information sheet describes the *typical average properties* of the specified soil.
- For further information on individual soils, contact Landcare Research New Zealand Ltd: www.landcareresearch.co.nz
- Advice should be sought from soil and land use experts before making decisions on individual farms and paddocks.
- The information has been derived from numerous sources. It may not be complete, correct or up to date.
- This information sheet is licensed by Landcare Research on an "as is" and "as available" basis and without any warranty of any kind, either express or implied.
- Landcare Research shall not be liable on any legal basis (including without limitation negligence) and expressly excludes all liability for loss or damage howsoever and whenever caused to a user of this factsheet.

Manaaki Whenua
Landcare Research

environment SOUTHLAND
Te Taiao Tonga

Pukemutu_6a.1

Soil horizons

Characteristics of functional horizons in order from top to base of profile:

Functional Horizon	Thickness	Stones	Clay*	Sand*	Permeability
Loamy Weak	20 - 25 cm	0 %	20 - 35 %	3 - 15 %	rapid
Loamy Weak	10 - 20 cm	0 %	20 - 35 %	3 - 15 %	rapid
Loamy Coarse Slightly Firm	10 - 30 cm	0 %	25 - 35 %	3 - 15 %	moderately slow
Clayey Coarse	30 - 60 cm	0 %	35 - 40 %	3 - 15 %	slow

* clay and sand percent values are for the mineral fines (excludes stones). Silt = 100 - (clay + sand)

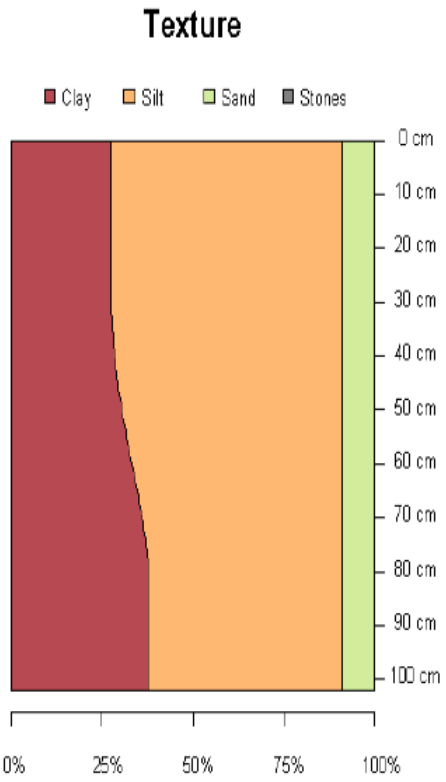

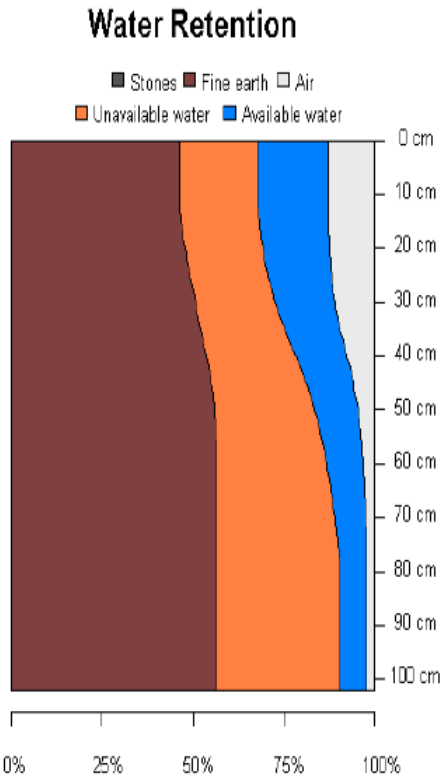

The values for the graphs above have been generated from horizon and pedotransfer data. These values have then been splined to create continuous estimates of soil water holding capacity and particle size distribution the soil profile. These curves express the particle size distribution and water retention of the soil however there may be barriers to rooting depth that are not necessarily represented in these properties directly. It is advisable to check the potential rooting depth and rooting barrier fields in the soil physical properties section on page three of this factsheet.

Pukemutu_6a.1

Soil physical properties

Depth class (diggability)
Moderately deep (40 - 80 cm)

Potential rooting depth
40 - 80 (cm)

Rooting barrier
Pan

Depth to hard rock
No hard rock within 1 m

Depth to soft rock
No soft rock within 1 m

Depth to stony layer class
No significant stony layer within

Texture profile
Silt over clay

Topsoil stoniness
Stoneless

Topsoil clay range
20 - 35 %

Drainage class
Poorly drained

Permeability profile
Moderate over slow

Depth to slowly permeable horizon
40 - 80 (cm)

Permeability of slowest horizon
Slow (< 4 mm/h)

Aeration in root zone
Very limited

Profile available water

(0 - 30cm or root barrier)	(0 - 60cm or root barrier)	(0 - 100cm or root barrier)
High (56 mm)	High (93 mm)	Moderate (93 mm)

Dry bulk density

topsoil	subsoil
1.22 g/cm³	1.22 g/cm³

Soil chemical properties

Topsoil P retention
Low (22%)

Soil management factors

Vulnerability classes relate to soil properties only and do not take into account climate or management

Soil structure integrity

Structural vulnerability
High (0.69)

Pugging vulnerability
not available yet

Septic tank installation category
A1 if slope > 15 deg otherwise A2

Contaminant management

N leaching vulnerability
Medium

P leaching vulnerability
not available yet

Dairy effluent (FDE) risk category
B

Water management

Water logging vulnerability
High

Drought vulnerability - if not irrigated
Moderate

Bypass flow
Medium

Hydrological soil group
D

Relative Runoff Potential

Slope	0-3°	4-7°	8-15°	16-25°	>25°
Risk	H	VH	VH	VH	VH

SINDI - Soil quality Indicators

SINDI - Soil Quality Indicators

A suite of soil quality indicators is available from http://sindi.landcareresearch.co.nz/

- Compare your soil with information from our soils databases.
- Assess the intrinsic resources and biological, chemical and physical quality of your soil
- See how your soil measures up against current understanding of optimal values.
- Learn about the effect each indicator has on soil quality and some general management practices that could be implemented to improve soil quality.

Pukemutu_6a.1

Soil information for OVERSEER

The following information can be entered in the OVERSEER® Nutrient Budget model. This information is derived from the S-map soil properties which are matched to the most appropriate OVERSEER categories. Please read the notes below for further information.

Soil description page

1. Select **Link to S-map**
2. Under S-map sibling data enter the S-map name/ref: **Pukem_6a.1**

Considerations when using Smap soil properties in OVERSEER

- The soil water values are estimated using a regression model based on soil order, parent rock, soil functional horizon information (stone content, soil density class), as well as texture (field estimates of sand, silt and clay percentages). The model is based on laboratory - measured water content data held in the National Soils Database and other Manaaki Whenua datasets. Most of this data comes from soils under long-term pasture and may vary from land under arable use, irrigation, etc.

- Each value is an estimate of the water content of the whole soil within the target depth range or to the depth of the root barrier (if this occurs above the base of the target depth). Where soil layers contain stones, the soil water content has been decreased according to the stone content.

- S-map only contains information on soils to a depth of 100 cm. The soil water estimates in the > 60 cm depth category assume that the bottom functional horizon that extends to 100 cm, continues down to a depth of 150cm. Where it is known by the user that there is an impermeable layer or non-fractured bedrock between 100 and 150 cm, this depth should be entered into OVERSEER. Where there is a change in the soil profile characteristics below 100 cm, the user should be aware that the values provided on this factsheet for the > 60 cm depth category will not reflect this change. For example, the presence of gravels at 120 cm would usually result in lower soil water estimates in the > 60 cm depth category. Note though that this assumption only impacts on a cropping block, as OVERSEER uses soil data from just the top 60 cm in pastoral blocks.

- OVERSEER requires the soil water values to be non-zero integers (even though zero is a valid value below a root barrier), and the wilting point value must be less than the field capacity value which must be less than the saturation value. The S-map water content estimates supplied by the S-map web service have been rounded to integers and may be assigned minimal values to meet these OVERSEER requirements. These modifications will result in a slightly less accurate estimate of Available Water to 60 cm (labelled PAW in OVERSEER) than that provided on the first page of this factsheet, but this is not expected to lead to any significant difference in outputs from OVERSEER .

Manaaki Whenua
Landcare Research

environment SOUTHLAND
Te Taiao Tonga

Appendix E
CS655 Calibration Procedure

The Campbell Scientific CS655 soil moisture sensor is a time domain reflectometer (TDR) sensor that indirectly measures the apparent dielectric permittivity (K_a) of its surrounding medium by sending a low voltage pulse down two 12 cm rods and measuring the time required for the pulse to return in the form of reflections generated at the beginning and ends of the rods (Campbell Scientific Inc., 2018). The K_a of the soil is a function of the velocity of the electromagnetic wave, and can be calculated from,

$$K_a = \left(\frac{c}{v}\right)^2 = \left(\frac{ct}{2L}\right)^2 \qquad \text{(Equation E} - 1\text{)}$$

where v is the velocity of the electromagnetic wave, c is the speed of light in a vacuum/ the velocity of electromagnetic waves in free space (3 x 10^8 ms^{-1}), t is the time required for the pulse to travel down the length of the rods and back, and L is the length of the rods. The K_a of the soil is principally dependent on the soil moisture content because the K_a of water is significantly greater than the K_a of any of the other soil constituents. Soil water content can therefore be determined from the measured K_a using a generic or, more accurate, soil-specific calibration model.

The soil moisture sensors were calibrated for the topsoil (0 – 30 cm; Ap horizon), the upper subsoil (30 – 60 cm; Bw horizon), and the fragipan (60 – 90 cm; Bx horizon), following the procedure outlined in the Campbell Scientific instruction manual (Campbell Scientific Inc., 2018). Bulk soil samples (~8 kg each) were collected from the field site and transported back to the workshop for sensor calibration. Each bulk soil sample soil was dried out in an oven to bring it close to 0 % water. The residual moisture content of each bulk soil sample was then determined by oven drying subsamples at 105 ˚C for 24 hours and comparing the before and after weight of the subsamples using the equation,

$$\theta_g = \frac{m_{water}}{m_{soil}} = \frac{m_{wet} - m_{dry}}{m_{dry}} \qquad \text{(Equation E} - 2\text{)}$$

where θ_g is the residual gravimetric moisture content (%w/w), m_{water} is the weight of the water in the sample, m_{soil} is the weight of the soil in the sample, m_{wet} is the weight of the pre-dried soil sample, and m_{dry} is the weight of the oven-dried soil sample. A known volume of water was then thoroughly mixed into the soil to ensure it was evenly distributed throughout the sample, increasing the soil up to a low, known θ_g. The soil was then packed into a PVC cylinder (186 mm diameter x

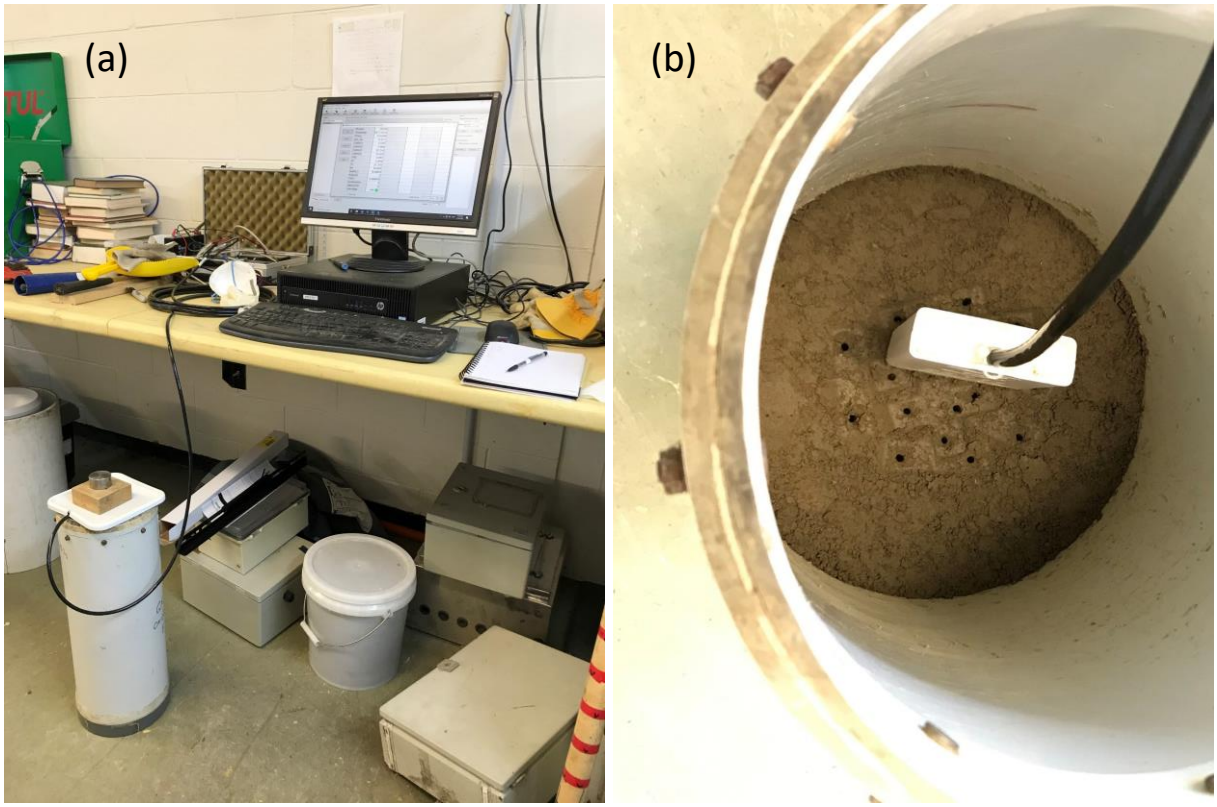

Plate E-1. The water content of bulk soil samples was modified to a known value before (a) being filled into a PVC cylinder and compacted to a bulk density representative of field conditions. To measure the dielectric permittivity at the known moisture content, (b) a CS655 soil moisture sensor was then inserted into the compacted soil and left until the value for dielectric permittivity had stabilised.

500 mm height; Plate E-1a) and compacted to a bulk density that was calculated as the average bulk density measured at that depth from previously collected soil cores (1.2 g cm^{-3} topsoil; 1.35 g cm^{-3} upper subsoil; 1.4 g cm^{-3} fragipan).

The measured θg of each sample was converted to a volumetric basis using the equation,

$$\theta_v = \theta_g \cdot \frac{\rho_b}{\rho_w} \qquad \text{(Equation E} - 3)$$

where θ_v is the volumetric moisture content (%v/v), ρ_b is the average dry bulk density (g cm^{-3}) at that depth, and ρ_w is the density of water (1.0 g cm^{-3}).

A CS655 sensor was then inserted into the repacked soil (Plate E-1b) and time was allowed for the K_a reading to settle, after which the K_a reading was recorded. The sensor was removed and reinserted at different angles and positions to obtain a total of 10 readings of K_a, and the average value was used to represent K_a at the respective gravimetric and volumetric water content. The soil

was then removed from the cylinder and loosened before adding a further known volume of water. The method was repeated a minimum of five times until the soil was saturated, to obtain a curve of the K_a -VWC relationship. After every second reading, a sample of the soil was removed for gravimetric water content analysis to verify the volume of water in the soil.

The topsoil (Ap) and upper subsoil (Bw) calibration points aligned well with one another, so they were combined to generate a Ka - θV relationship that was applied to all sensors installed at depths of 15, 30 and 45 cm, with the exception of the 45 cm deep sensor at the nose slope (because this sensor was installed into a shallow fragipan; Appendix A.2.4). The following regression equation was derived ($F(3,7) = 465$, $p < 0.001$), with an R2 of 0.995,

$$\theta_V = 2.91e^{-5} \cdot Ka^3 - 1.74e^{-3} \cdot Ka^2 + 4.33e^{-2} \cdot Ka - 6.85e^{-2} \qquad \text{(Equation D} - 4\text{)}$$

The calibration of the fragipan (Bx) sample was unable to achieve a Ka reading over approximately 29. Further addition of water beyond a Ka of 29 resulted in the soil becoming too sticky to evenly mix in additional water and effectively pack back into the column without creating large air gaps. Additional water moved quickly down the interfaces between the wetted clumps of soil and pooled in the base of the column. For this reason, the upper subsoil data points were combined with the fragipan data points to create a Ka - θV calibration curve that was applied to all sensors installed at depths of 60 cm and deeper (Figure D-1). It was also applied to the sensor installed at 45 cm at the nose slope. The following third-degree polynomial equation was derived ($F(3,4) = 2180$, $p < 0.001$) to determine θv, with an R2 of 0.999:

$$\theta_V = 1.06e^{-5} \cdot Ka^3 - 8.21e^{-4} \cdot Ka^2 + 3.05e^{-2} \cdot Ka - 2.2e^{-2} \qquad \text{(Equation D} - 5\text{)}$$

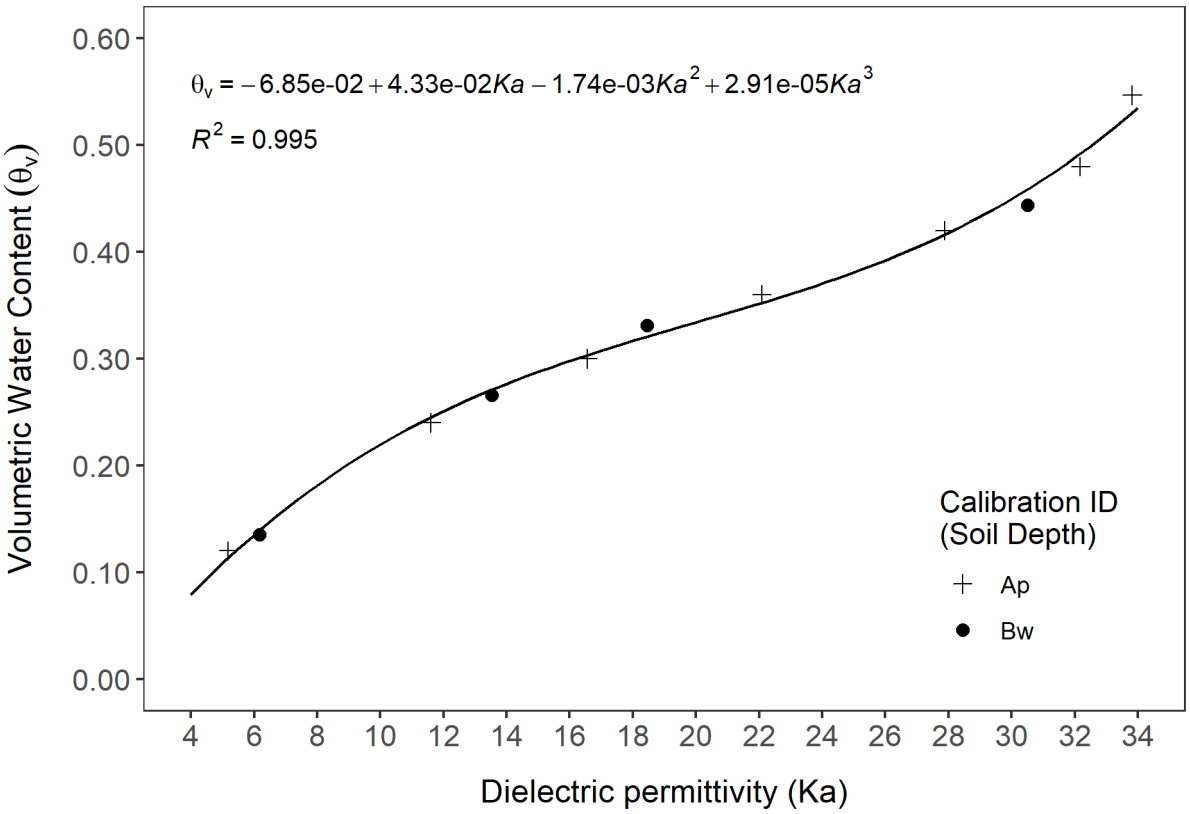

Figure D-1. Calibration equation used for CS655 TDR sensors installed at 15, 30 and 45 cm, with the exception of the 45 cm sensor at the nose slope.

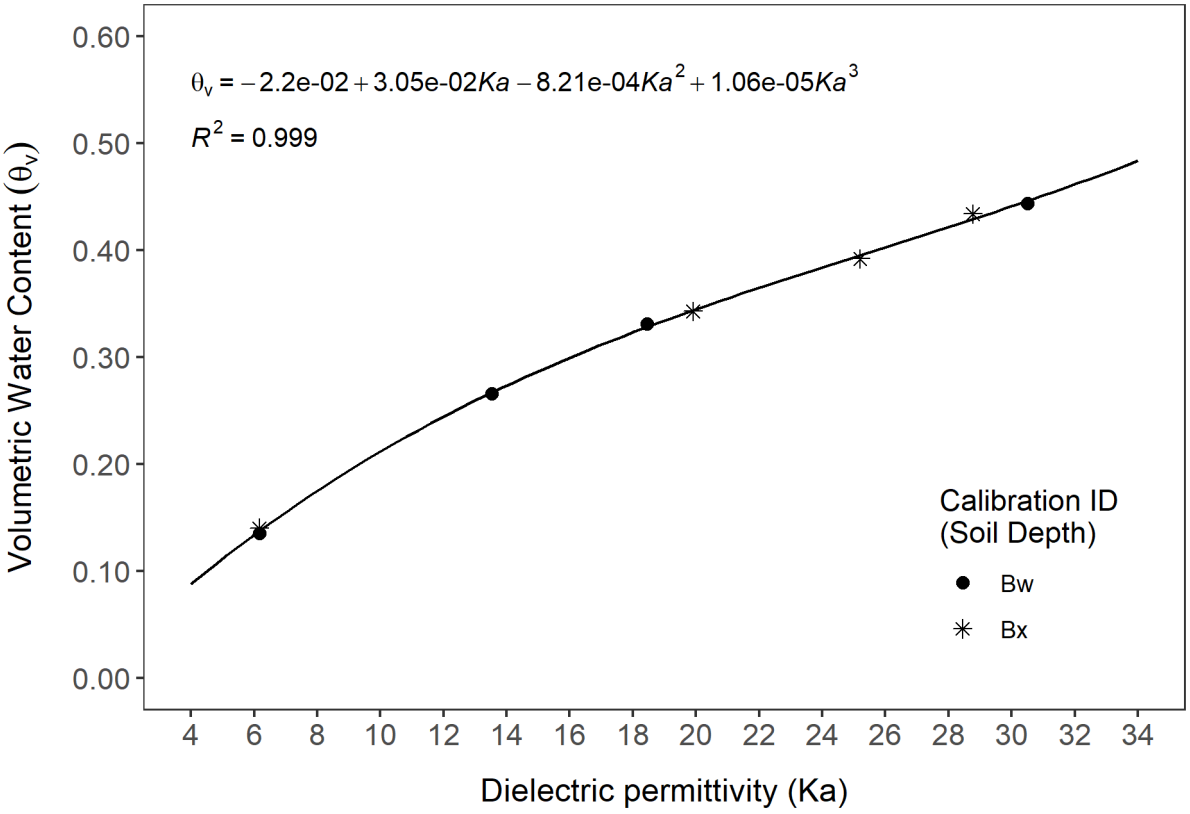

Figure D-2. Calibration equation used for CS655 TDR sensors installed at 60 cm and deeper, as well as the 45 cm sensor at the nose slope.